

**ADSORPTION OF HOMOISOFLAVONOID AND
EXTRACTED DYES FROM HEARTWOOD OF
CEASALPINIA SAPPAN LINN. ON SILK FIBERS
AND TREATMENT OF DYE EFFLUENT
BY ACTIVATED CARBONS**

Kamonchanok Wongsooksin

**A Thesis Submitted in Partial Fulfillment of the Requirements for the
Degree of Doctor of Philosophy in Chemistry
Suranaree University of Technology
Academic Year 2008**

การดูดซับสีไฮโมไอโซฟลาโวนอยด์และสีสกัดจากแก่นฝาง (*Ceasalpinia sappan* Linn.) บนเส้นไหมและการบำบัดน้ำทิ้งจากการย้อมด้วยถ่านกัมมันต์

นางสาวกมลชนก วงศ์สุขสิน

วิทยานิพนธ์นี้เป็นส่วนหนึ่งของการศึกษาตามหลักสูตรปริญญาวิทยาศาสตรดุษฎีบัณฑิต
สาขาวิชาเคมี
มหาวิทยาลัยเทคโนโลยีสุรนารี
ปีการศึกษา 2551

**ADSORPTION OF HOMOISOFLAVONOID AND EXTRACTED
DYES FROM HEARTWOOD OF *CEASALPINIA SAPPAN* LINN.
ON SILK FIBERS AND TREATMENT OF DYE EFFLUENT
BY ACTIVATED CARBONS**

Suranaree University of Technology has approved this thesis submitted in partial fulfillment of the requirements for the Degree of Doctor of Philosophy.

Thesis Examining Committee

(Prof. Dr. John Barnard Bremner)

Chairperson

(Assoc. Prof. Dr. Malee Tangsathitkulchai)

Member (Thesis Advisor)

(Assoc. Prof. Dr. Saowanee Rattanaphani)

Member

(Assoc. Prof. Dr. Vichitr Rattanaphani)

Member

(Assoc. Prof. Dr. Saisunee Liawruangrath)

Member

(Prof. Dr. Pairote Sattayatham)

Vice Rector for Academic Affairs

(Assoc. Prof. Dr. Prapan Manyum)

Dean of Institute of Science

กมลชนก วงศ์สุขสิน : การดูดซับสีโสมโอโซฟลาโวนอยด์และสีสกัดจากแก่นฝาง (*Ceasalpinia sappan* Linn.) บนเส้นไหมและการบำบัดน้ำทิ้งจากการย้อมด้วยถ่านกัมมันต์ (ADSORPTION OF HOMOISOFLAVONOID AND EXTRACTED DYES FROM HEARTWOOD OF *CEASALPINIA SAPPAN* LINN. ON SILK FIBERS AND TREATMENT OF DYE EFFLUENT BY ACTIVATED CARBONS. อาจารย์ที่ปรึกษา : รองศาสตราจารย์ ดร.มาลี ตั้งสติกข์กุลชัย, 242 หน้า.

งานวิจัยนี้เป็นการศึกษาอันตรกิริยาระหว่างบราซิลีน (BE) สีสกัดจากแก่นฝางและโลหะไอออนบางชนิด ($M = \text{Al(III)}$, Ga(III) and In(III)) จากการทดลองพบว่าปริมาณสัมพัทธ์ของการเกิดสารเชิงซ้อนของโลหะไอออนและบราซิลีนเป็น 1:2 ซึ่งหาโดยวิธีโมลาร์และวิธีของจ็อบ นอกจากนี้ยังได้ทำการศึกษาการเกิดสารประกอบเชิงซ้อนระหว่างโลหะไอออนและบราซิลีนด้วยเทคนิคอิเล็กโทรสเปกโตรสโคปี โดยเมื่อทำการเติมอะเซทิลเซอรินเมทิลเอสเทอร์ (Ser) ซึ่งเป็นตัวแทนขององค์ประกอบในเส้นไหมลงไปในการเกิดสารประกอบเชิงซ้อน M:BE พบว่า อัตราส่วนของ Ser:M:BE เป็น 1:1:1 อัตราส่วนโครงสร้างของสารประกอบเชิงซ้อนทั้งหมดที่ได้จากการทดลองนี้พบว่า ข้อมูลค่าความร้อนของการเกิดสารเชิงซ้อนทางทฤษฎีโดยวิธีเซมิเอมพิริคัล PM3 สนับสนุนโครงสร้างดังกล่าว

การศึกษาจลนพลศาสตร์และอุณหพลศาสตร์ของการดูดซับในการย้อมบราซิลีนและสีสกัดจากแก่นฝางบนเส้นไหม พบว่า ความสามารถในการดูดซับบราซิลีนบนเส้นไหมมีสภาวะที่เหมาะสมที่สุดคือ pH 4 อัตราส่วนของเส้นไหมต่อปริมาณของสารละลายสีย้อม 1:100 ใช้เวลา 120 นาที และความเข้มข้นเริ่มต้นของสารละลายบราซิลีน 14 มิลลิกรัมต่อลิตร และยังพบว่าวิธีการใส่สารช่วยติดสีลงไปพร้อมกันก่อนย้อม (simultaneous mordanting) เป็นวิธีการย้อมที่เหมาะสมที่สุด การศึกษาจลนพลศาสตร์พบว่า ก่อนเข้าสู่สมดุลของการดูดซับสีบนเส้นไหมเป็นกระบวนการที่ถูกควบคุมแบบจลนพลศาสตร์ (kinetically controlled process) และที่สมดุลสมการอัตราของการดูดซับบราซิลีนและสีสกัดจากแก่นฝางบนเส้นไหมที่ pH 4 จัดเป็นปฏิกิริยาอันดับสองเสมือน (pseudo second-order) โดยมีพลังงานก่อกัมมันต์ (E_a) เท่ากับ 41.57 กิโลจูลต่อโมล ซึ่งชี้ได้ว่าเป็นกระบวนการดูดซับทางเคมี การศึกษาผลของอุณหภูมิต่อการดูดซับและพารามิเตอร์ต่าง ๆ ทางอุณหพลศาสตร์ (พลังงานอิสระของกิบส์ (ΔG°) และค่าเอนทัลปี (ΔH°)) พบว่า การดูดซับบนเส้นไหมเป็นกระบวนการที่เกิดขึ้นเองได้และเป็นกระบวนการคายความร้อน

นอกจากนี้ งานวิจัยนี้ได้ทำการกำจัดสารเชิงซ้อนของบราซิลีน $[\text{Al}(\text{BE})_2]^+$ ที่เหลือจากกระบวนการย้อมสีบนเส้นไหม โดยใช้ถ่านกัมมันต์ที่ผลิตจากกะลามะพร้าวและไม่ยูคาลิปตัส

เป็นสารดูดซับสี ถ่านกัมมันต์ซึ่งมีโครงสร้างสมบัติรูพรุนที่แตกต่างกันได้มาจากการใช้วิธีการเตรียมและสารตั้งต้นที่แตกต่างกัน ส่วนถ่านกัมมันต์ซึ่งมีสมบัติเคมีพื้นผิวต่างกันได้มาจากการเพิ่มหมู่ฟังก์ชันที่เป็นออกซิเจนเข้าไป ในขณะที่วิธีการให้ความร้อนสามารถเลือกกำจัดหมู่ฟังก์ชันที่เป็นออกซิเจนบางหมู่ออกไปได้ จากการทดลองพบว่าการนำหมู่ฟังก์ชันที่เป็นออกซิเจนเข้าสู่พื้นผิวของถ่านกัมมันต์ได้มากสามารถเพิ่มประสิทธิภาพของการดูดซับสีได้มากขึ้นด้วย โดยกระบวนการดูดซับเกิดจากอันตรกิริยาแบบไฟฟ้าสถิต ส่วนอีกกระบวนการหนึ่งเป็นการดูดซับที่เกิดจากแรงการกระจายแบบไพ – ไพ (π - π dispersion) ซึ่งเป็นกลไกหลักของการดูดซับสำหรับถ่านกัมมันต์ที่มีอัตราส่วนปริมาตรของรูพรุนขนาดกลางสูง ทำให้สามารถสรุปได้ว่าการกำจัดสีที่มีประจุบวกให้มีประสิทธิภาพสูงนั้น ถ่านกัมมันต์ที่มีรูพรุนขนาดเล็กจะต้องทำการออกซิเดชันเพื่อเพิ่มหมู่ฟังก์ชันออกซิเจนบนพื้นผิวก่อนนำไปดูดซับสีข้อม ในขณะที่ถ่านกัมมันต์ที่มีรูพรุนขนาดกลางหรือใหญ่จะสามารถใช้ดูดซับสีข้อมได้โดยตรง

สาขาวิชาเคมี

ปีการศึกษา 2551

ลายมือชื่อนักศึกษา _____

ลายมือชื่ออาจารย์ที่ปรึกษา _____

ลายมือชื่ออาจารย์ที่ปรึกษาร่วม _____

KAMONCHANOK WONGSOOKSIN : ADSORPTION OF
HOMOISOFLAVONOID AND EXTRACTED DYES FROM
HEARTWOOD OF *CEASALPINIA SAPPAN* LINN. ON SILK FIBERS
AND TREATMENT OF DYE EFFLUENT BY ACTIVATED CARBONS.
THESIS ADVISOR : ASSOC. PROF. MALEE TANGSATHITKULCHAI,
Ph.D. 242 PP.

ADSORPTION/KINETICS/THERMODYNAMICS/BRAZILEIN/ALUMINIUM/
GALLIUM/INDIUM/(S)-N-ACETHYL SERINE METHYL ESTER

The interactions of brazilein (BE) as well as extracted dye from *C. Sappan*. with some metal ions (M = Al(III), Ga(III), and In(III)) were investigated. The structure of all complexes formed had a stoichiometric ratio M:BE of 1:2 as identified from the molar method and Job's method. This stoichiometric ratio was further confirmed by ES-MS spectra. When (S)-N-acetyl serine methyl ester (Ser), as a silk serine residue mimic, was added to M:BE complex, a new complex with a stoichiometric ratio for Ser:M:BE of 1:1:1, was formed. The structures of all complexes were proposed and supported by the calculated heat of formation obtained by the semiempirical PM 3 method.

The best conditions for kinetic and thermodynamic studies on the adsorption of dye onto silk were found to be pH = 4, MLR = 1:100, contact time 120 min and initial dye concentration 14 mg/L. Simultaneous mordanting was found to be the most suitable method for dyeing. Kinetics studies showed that, before equilibrium, the adsorption was a kinetically controlled process. In addition, the pseudo second-order

kinetic model with an activation energy (E_a) of 41.57 kJ/mol indicated that the adsorption was controlled by a chemical process. The study into the effect of temperature on equilibrium adsorption and all thermodynamic parameters (ΔG° , ΔH°) revealed that the dye adsorption was a spontaneous and an exothermic process.

In an attempt to remove residual dye complex, $[\text{Al}(\text{BE})_2]^+$, left from the effluent after the dyeing process, coconut shell-based and Eucalyptus wood based-activated carbon were investigated as dye adsorbents. Activated carbons having different porous textures were obtained through preparation with different activation methods and by using different precursors. The change in surface chemistry was achieved with oxidation treatment to introduce surface oxygen functional groups, while heat treatment selectively removed some of the oxygen functional groups (carboxylic acid groups). It was found that a high content of oxygen functional group introduced on the activated carbon surface significantly enhanced the dye adsorption by electrostatic interaction. On the other hand, the π - π dispersive interaction was the main mechanism responsible for the highest increases of dye uptake on the activated carbon containing a high proportion of mesopore volume. It can be concluded that for achieving the highest efficiency of cationic dye removal, the micropore activated carbon requires an oxidative surface treatment, whereas the activated carbon with high mesoporosity can be directly used.

School of Chemistry

Academic Year 2008

Student's Signature_____

Advisor's Signature_____

Co-advisor's Signature_____

ACKNOWLEDGEMENTS

I would like to express my deep gratitude to Assoc. Prof. Dr. Malee Tangsathitkulchai, Assoc. Prof. Dr. Saowanee Rattanaphani, Assoc. Prof. Dr. Vichitr Rattanaphani, for all of their supervisions and encouragements. Also my great appreciation goes to Prof. Dr. John B. Bremner, who advised me during my time at University of Wollongong, Australia. In addition, I would like to thank, Assoc. Prof. Dr. Saisunee Liawruangrath for her time, comments and suggestions.

The assistance from the following people are also appreciate Dr. Julie Lock for her guidance and help with modeling analyses. Larry Hick for his help with MS analyses. I would also like to thank all lectures at the School of Chemistry, SUT for their good attitude and advice. I would like to thank scientific equipment center F1, F2 and F5, SUT for providing all equipments and glassware.

I would also like to thank all of my good friends in the Saowanee group the School of Chemistry, Suranaree University of Technology and the Bremner lab at the University of Wollongong, Australia for their friendship and all the help they have provided.

I wish to thank Nakhon Ratchasima Rajabhat University, Nakhon Ratchasima, Thailand, for supporting my scholarship throughout my study. I also thank Suranaree University of Technology and the University of Wollongong for partial financial support.

Finally, I would like to express my deepest gratitude to my parents, my sister and my brothers for their unconditional love and continual encouragement during my education.

Kamonchanok Wongsooksin

CONTENTS

	Page
ABSTRACT IN THAI.....	I
ABSTRACT IN ENGLISH.....	III
ACKNOWLEDGEMENTS.....	V
CONTENTS.....	VII
LIST OF TABLES.....	XVII
LIST OF FIGURES.....	XXI
LIST OF ABBREVIATIONS.....	XXXII
CHAPTER	
I GENERAL INTRODUCTION.....	1
1.1 Introduction.....	1
1.2 Natural dyes.....	2
1.2.1 Flavonoids.....	2
1.2.2 Quinones.....	3
1.2.3 Carotenoids.....	4
1.2.4 Chlorophylls.....	5
1.3 Synthetic dyes.....	6
1.3.1 Chemical classification.....	6
1.3.2 Application classification.....	7
1.4 Textile fibers.....	9
1.4.1 Protein fibers.....	9

CONTENTS (Continued)

	Page
1.4.2 Cellulosic fibers.....	10
1.5 Natural dyes for protein fibers.....	11
1.5.1 Direct dyes.....	12
1.5.2 Vat dyes.....	12
1.5.3 Mordant dyes.....	13
1.6 Synthetic dyes for protein fibers.....	14
1.6.1 Acid dyes.....	15
1.6.2 Basic dyes.....	16
1.6.3 Disperse dyes.....	16
1.7 Natural organic dyes.....	17
1.8 Treatment of dye effluent.....	18
1.9 Activated carbon.....	19
1.9.1 Manufacture of activated carbon.....	21
1.9.1.1 Physical activation.....	22
1.9.1.2 Chemical activation.....	22
1.9.2 Classification of pores of activated carbon.....	23
1.9.3 Applications of activated carbon.....	23
1.9.3.1 Gas phase applications.....	24
1.9.3.2 Liquid phase applications.....	24
1.9.4 The surface chemistry of activated carbon.....	24
1.9.5 Method of analysis of surface oxygen functional groups.....	26

CONTENTS (Continued)

	Page
1.10 Adsorption.....	30
1.10.1 Type of adsorption.....	30
1.10.1.1 Physical adsorption.....	30
1.10.1.2 Chemical adsorption.....	30
1.10.2 Classification of adsorption isotherms.....	32
1.11 Research objectives.....	34
1.12 Scope and limitations of the study.....	34
1.13 References.....	35
II PREPARATION AND CHARACTERIZATION OF DYE-METAL	
COMPLEXES AND DYE-METAL-AMINO ACID COMPLEXES.....	43
2.1 Abstract.....	43
2.2 Introduction.....	44
2.3 Experimental.....	50
2.3.1 Chemicals.....	50
2.3.2 Instruments.....	50
2.3.3 Experimental methods.....	52
2.3.3.1 Extraction of dye.....	52
2.3.3.2 Separation of brazilin from crude extract of <i>C. sappan</i>	53
2.3.3.3 Oxidation of brazilin to brazilein.....	53

CONTENTS (Continued)

	Page
2.3.3.4 Determination of the stoichiometric ratio for brazilein with Al(III) ion.....	54
2.3.3.5 Effect of alum concentration on brazilein aqueous solution.....	54
2.3.3.6 Determination of the amount of brazilein dye in crude extracted dye.....	55
2.3.3.7 Sample preparation for ESI-MS.....	55
2.4 Results and discussion.....	56
2.4.1 Properties of brazilein.....	56
2.4.2 UV-Vis spectra of dyes in aqueous solution and at pH 4.5.....	59
2.4.3 Complex stoichiometry of brazilein and alum in aqueous solution and at pH 4.5.....	61
2.4.4 Effect of alum concentration on brazilein in aqueous solution.....	63
2.4.5 Determination of the amount of brazilein in crude extracted dye.....	65
2.4.6 Electrospray mass spectrometry analysis.....	67
2.4.6.1 Brazilin complexes.....	68
2.4.6.2 Brazilein complexes.....	79
2.4.7 High resolution mass spectrometry.....	87
2.4.8 Computational modeling.....	88

CONTENTS (Continued)

	Page
2.5 Conclusion.....	91
2.6 References.....	92
 III ADSORPTION OF Al-BRAZILEIN AND Al-EXTRACTED DYE	
COMPLEX ON SILK.....	98
3.1 Abstract.....	98
3.2 Introduction.....	99
3.2.1 Physical chemistry of dyeing process.....	103
3.2.2 Adsorption kinetics.....	108
3.2.2.1 Pseudo first-order equation.....	108
3.2.2.2 Pseudo second-order equation.....	109
3.2.3 Adsorption isotherms.....	112
3.2.3.1 Langmuir isotherm.....	113
3.2.3.2 Freundlich isotherm.....	114
3.2.4 Thermodynamic modeling of adsorption.....	115
3.3 Experimental.....	117
3.3.1 Chemicals.....	117
3.3.2 Instruments.....	117
3.3.3 Experimental methods.....	118
3.3.3.1 Silk yarn preparation (Chairat, 2004; Septhum, 2006)....	118
3.3.3.2 Stock solutions.....	118

CONTENTS (Continued)

	Page
3.3.3.3 Pre-, simultaneous and post-mordanting for brazilain dyeing onto silk.....	119
3.3.3.4 Effect of pH.....	121
3.3.3.5 Batch kinetics of the alum-brazilain experiments.....	121
3.3.3.6 Batch equilibrium of the alum-brazilain experiments.....	122
3.3.3.7 Adsorption and desorption studies of alum-brazilain and alum-extracted dye onto silk.....	123
3.3.3.8 Extraction of dye.....	123
3.3.3.9 Batch kinetic studies of alum-extracted dye onto silk.....	124
3.3.3.10 Batch equilibrium adsorption of alum-extracted dye onto silk.....	124
3.4 Results and discussion.....	125
3.4.1 Comparison of pre-, simultaneous and post-modanting for brazilain dyeing onto silk.....	125
3.4.2 Optimal conditions of silk dyeing with alum-brazilain.....	127
3.4.2.1 The effect of pH on the adsorption of alum-brazilain onto silk.....	127
3.4.2.2 The effect of material to liquor ratio (MLR) on the adsorption of alum-brazilain onto silk.....	130
3.4.2.3 The effect of contact time and initial dye concentration on the adsorption of alum-brazilain onto silk.....	133

CONTENTS (Continued)

	Page
3.4.2.4 The effect of temperature on the adsorption of alum-brazilein onto silk.....	136
3.4.2.5 Activation parameters for the adsorption of alum-brazilein on silk.....	140
3.4.2.6 Thermodynamic parameters for the adsorption of alum-brazilein onto silk.....	142
3.4.2.7 Adsorption isotherm for the adsorption of alum-brazilein on silk.....	143
3.4.2.8 Adsorption-desorption of alum-brazilein on silk.....	147
3.4.3 Optimal conditions of silk dyeing with alum-extracted dye.....	151
3.4.3.1 The effect of material to liquor ratio on the adsorption of alum-extracted dye onto silk.....	151
3.4.3.2 The effect of contact time and initial dye concentration on the adsorption of alum-extracted dye onto silk.....	154
3.4.3.3 The effect of temperature on the adsorption of alum-extracted dye onto silk.....	157
3.4.3.4 Activation parameters for the adsorption of alum-extracted dye on silk.....	161
3.4.3.5 Thermodynamic parameters for the adsorption of alum-extracted dye on silk.....	163

CONTENTS (Continued)

	Page
3.4.3.6 Adsorption isotherm for the adsorption of alum-extracted dye on silk.....	164
3.4.3.7 Adsorption-desorption of alum-extracted dye on silk.....	168
3.4.4 Comparison of activation, thermodynamic parameters and desorption between alum-brazilein and alum-extracted dye dyeing on silk.....	171
3.4.4.1 Comparison of activation parameters between alum-brazilein and alum-extracted dye dyeing on silk.....	171
3.4.4.2 Comparison of thermodynamics parameters between alum-brazilein and alum-extracted dye dyeing on silk.....	172
3.5 Conclusion.....	173
3.6 References.....	175
IV TREATMENT OF DYE EFFLUENT USING ACTIVATED CARBONS.....	182
4.1 Abstract.....	182
4.2 Surface modification of activated carbon	183
4.3 The treatment of dye effluent using activated carbons	185
4.4 Experimental.....	190
4.4.1 Materials and chemicals.....	190
4.4.2 Instruments.....	191

CONTENTS (Continued)

	Page
4.4.3 Methods.....	191
4.4.3.1 Surface modification of activated carbon.....	192
4.4.3.2 Preparation of activated carbon by chemical activation and surface modification.....	193
4.4.3.3 Characterization of activated carbons.....	196
4.4.3.4 Batch adsorption experiments.....	198
4.4.3.4.1 Preparation of natural dye extract and Al-extrctated dye complex.....	198
4.4.3.4.2 Batch contact time studies.....	199
4.4.3.4.3 Batch pH studies.....	199
4.4.3.4.4 Batch equilibrium studies.....	200
4.5 Results and discussion.....	201
4.5.1 Characterization of porosity and surface chemistry of activated carbons.....	201
4.5.2 Adsorption studies.....	217
4.5.2.1 Equilibrium adsorption time.....	217
4.5.2.2 Effect of pH.....	218
4.5.2.3 Effect of adsorbent dosage.....	220
4.5.2.4 Dependence of adsorption capacity of cationic dye on different surface characteristics of activated carbon.....	221
4.5.2.5 Adsorption of dye on mesoporous activated carbon.....	226

CONTENTS (Continued)

	Page
4.6 Conclusion.....	228
4.7 References.....	230
V CONCLUSION.....	238
CURRICULUM VITAE.....	242

LIST OF TABLES

Table	Page
1.1 The characteristics of the chemical classes of synthetic dyes (Christie <i>et al.</i> , 2000).....	8
1.2 The composition of fibroin and sericin (Karmakar, 1999).....	10
1.3 Some FT-IR assignments of functional groups on carbon surfaces (Fanning and Vannice, 1993 quoted in Figueiredo, Pereira, Freitas, and Orfao, 1999; Shen, Li, and Liu, 2008).....	29
1.4 General characteristics of physical and chemical adsorption (Ruthven, 1997).....	31
2.1 ¹ H-NMR data of brazilin and brazilein (500 MHz).....	57
2.2 ¹³ C-NMR data of brazilin and brazilein (125 MHz).....	58
2.3 Exact mass measurements and elemental compositions for ion derived from AlBE ₂ , GaBE ₂ , InBE ₂ , SerAlBE, SerGaBE, and SerInBE complexes.....	88
2.4 Calculated heats of formation of Al:BE ₂ , Ser:Al:BE, Ga:BE ₂ , Ser:Ga:BE, In:BE ₂ , and Ser:In:BE complexes.....	91
3.1 The amount of dye adsorbed per gram of silk at different pH values; dyeing at MLR 1:100, an initial dye concentration of 14 mg/L, 30°C and 1 hour of contact time.....	128

LIST OF TABLES (Continued)

Table	Page
3.2 Comparison of the pseudo first-order and pseudo second-order adsorption rate constants, calculated q_e and experimental q_e values for different MLR, initial dye concentrations and temperatures for alum-brazilein dyeing onto silk.....	139
3.3 Activation parameters for the adsorption of alum-brazilein onto silk at initial brazilein concentration 14 mg/L.....	140
3.4 Thermodynamic parameters for the adsorption of alum-brazilein dyeing at initial brazilein concentration 14 mg/L.....	143
3.5 Langmuir and Freundlich isotherm constants for the adsorption of alum-brazilein onto silk at different temperatures.....	145
3.6 R_L values at different temperatures relating to the initial dye concentrations for alum-brazilein dyeing of silk.....	146
3.7 Percentage of desorption analysis of alum-brazilein dye onto and off silk in different type of water and material to liquor ratios.....	150
3.8 Comparison of the pseudo first-order and pseudo second-order adsorption rate constants, calculated q_e and experimental q_e values for different MLR, initial dye concentrations and temperatures for adsorption of Al-extracted dye on silk.....	160
3.9 Activation parameters for the adsorption of alum-extracted dye onto silk at initial dye concentration 284 mg/L.....	162

LIST OF TABLES (Continued)

Table	Page
3.10 Thermodynamic parameters for the adsorption of alum-extracted dye onto silk.....	164
3.11 Langmuir and Freundlich isotherm constants for the adsorption of alum-extracted dye onto silk at 30 and 50°C.....	166
3.12 R_L values at different temperatures relating to the initial extracted dye concentrations.....	167
3.13 Percentage of desorption analysis of alum-extracted dye onto and off silk in different type of water and material to liquor ratios.....	170
3.14 Activation parameters for the adsorption of alum-brazilein and alum-extracted dye dyeing on silk.....	172
3.15 Thermodynamic parameters for the adsorption of alum-brazilein and alum-extracted dye dyeing on silk.....	173
4.1 Preparation conditions and sample code used in prepared original activated carbons.....	195
4.2 The experimental conditions for liquid phase oxidation.....	196
4.3 Textural characteristics obtained from N ₂ adsorption isotherm for various activated carbon (the value in the square bracket [] is the percentage changes with reference to the original carbon, where “+” denotes % increasing and “-” denotes % decreasing.....	204

LIST OF TABLES (Continued)

Table	Page
4.4 Boehm titration results of original and oxidized activated carbons (the value in the square bracket [] is the percentage changes with reference to the original carbon, where “+” denotes % increasing and “-” denotes % decreasing.....	205

LIST OF FIGURES

Figure	Page
1.1 Basic structure of flavonoid and example of flavonoid: morin (Lemmens and Wulijarni-Soetjipto, 1992).....	2
1.2 Chemical structure of brazilein and brazilin (Wongsooksin, Rattanaphani, S., Tangsathitkulchai, Rattanaphani, V., and Bremner, 2008).....	3
1.3 Structure of quinone and examples of a naphthaquinone (lawsone) and an anthraquinone dye (alizarin) (Lemmens and Wulijarni-Soetjipto, 1992).....	4
1.4 Structure of carotenoid and example of carotenoid: bixin (Lemmens and Wulijarni-Soetjipto, 1992).....	5
1.5 Chemical structure of chlorophyll.....	6
1.6 Examples of the structures of carbonyl dye, methine dye and nitro dye (a) C.I. Disperse Green 5, carbonyl dye; (b) C.I. Basic Yellow 11, methine dye and (c) C.I. Disperse Yellow 4, nitro dye (Christie <i>et al.</i> , 2000).....	7
1.7 General α -amino acid formula.....	9
1.8 General structure of silk.....	10
1.9 The structure of cellulose; (a) cellulose structure and (b) hydrogen bonding in cellulose structure.....	11
1.10 The interaction of direct dye with fiber.....	12
1.11 The reaction of indigo.....	13
1.12 Examples of acid dyes; (a) C.I. Acid Orange 6 and (b) C.I. Acid Green 25 (Christie <i>et al.</i> , 2000).....	15

LIST OF FIGURES (Continued)

Figure	Page
1.13 Examples of basic dyes; C.I. Basic Blue 41 (Christie, 2001).....	16
1.14 Examples of disperse dye; C.I. Disperse Orange 15 (Christie <i>et al.</i> , 2000).....	16
1.15 A schematic representation of the structure of activated carbon (Bansal <i>et al.</i> , 1988).....	21
1.16 Examples of (a) acidic and (b) basic oxygen functional groups.....	26
1.17 The influence of pH on surface charge: (a) $\text{pH} < \text{pH}_{\text{pzc}}$, (b) $\text{pH} = \text{pH}_{\text{pzc}}$, and (c) $\text{pH} > \text{pH}_{\text{pzc}}$ (Leon and Radovic, 1994 quoted in Rodríguez- Reinoso, 1998).....	28
1.18 Types of adsorption isotherms according to the IUPAC classification.....	32
2.1 Chemical structure of (a) brazilein and (b) brazilin (Wongsooksin <i>et al.</i> , 2008).....	44
2.2 Molecular models of Al(III) complexation with brazilein (P ⁻ and Q ⁻ represent anions such as NO ₃ ⁻ ions or brazilein molecules and X represents H) (Kanazawa, 1991).....	46
2.3 Chemical structure of (<i>S</i>)- <i>N</i> -acetylserine methyl ester (Ser).....	49
2.4 HMBC correlaions of brazilein.....	56
2.5 Electronic absorption spectra of brazilein (5.0×10^{-5} M) in aqueous solution in the absence and in presence of alum ($0-2.0 \times 10^{-4}$ M).....	60
2.6 Absorbance versus [alum]/[brazilein] molar ratios plots at 509 nm.....	62
2.7 Absorbance versus the mole fraction of brazilein at 509 nm.....	63

LIST OF FIGURES (Continued)

Figure	Page
2.8 The proposed structure of the $[\text{Al}(\text{brazilein})_2]^+$ complex.....	63
2.9 The effect of alum concentrations on brazilein in aqueous solution (pH 3.8-5.5). The dotted line is the $[\text{alum}]/[\text{brazilein}]$, 1:1 complex. The solid line is the $[\text{alum}]/[\text{brazilein}]$, 2:1 complex.....	64
2.10 UV-Vis spectra of crude extracted dye (100 mg/L), alum-extracted dye and alum-brazilein in water.....	66
2.11 Estimation of the amount of brazilein in the crude extracted dye.....	66
2.12 (a) Full scan mass spectrum of the Al:brazilin complex, (b) MS^2 spectrum of the m/z 593 ion in Figure 2.12(a).....	69
2.13 (a) Full scan mass spectrum of the Ser:Al:brazilin complex, (b) MS^2 spectrum of the m/z 470 ion in Figure 2.13(a).....	71
2.14 (a) Full scan mass spectrum of the Al:brazilin complex, (b) MS^2 spectrum of the m/z 593 ion in Figure 2.14(a).....	73
2.15 (a) Full scan mass spectrum of the Ser:Al:brazilin complex, (b) MS^2 spectrum of the m/z 470 ion in Figure 2.15(a).....	74
2.16 (a) Full scan mass spectrum of the Ga:brazilin complex, (b) MS^2 spectrum of the m/z 636 ion in Figure 2.16(a).....	75
2.17 (a) Full scan mass spectrum of the Ser:Ga:brazilin complex, (b) MS^2 spectrum of the m/z 513 ion in Figure 2.17(a).....	76

LIST OF FIGURES (Continued)

Figure	Page
2.18 (a) Full scan mass spectrum of the In:brazilin complex, (b) MS ² spectrum of the <i>m/z</i> 681 ion in Figure 2.18(a).....	77
2.19 (a) Full scan mass spectrum of the Ser:In:brazilin complex, (b) MS ² spectrum of the <i>m/z</i> 558 ion in Figure 2.19(a).....	78
2.20 (a) Full scan mass spectrum of the Al:brazilein complex, (b) MS ² spectrum of the <i>m/z</i> 593 ion in Figure 2.20(a).....	79
2.21 (a) Full scan mass spectrum of the Ser:Al:brazilein complex, (b) MS ² spectrum of the <i>m/z</i> 470 ion in Figure 2.21(a).....	80
2.22 (a) Full scan mass spectrum of the Al:brazilein complex, (b) MS ² spectrum of the <i>m/z</i> 593 ion in Figure 2.22(a).....	81
2.23 (a) Full scan mass spectrum of the Ser:Al:brazilein complex, (b) MS ² spectrum of the <i>m/z</i> 470 ion in Figure 2.23(a).....	82
2.24 (a) Full scan mass spectrum of the Ga:brazilein complex, (b) MS ² spectrum of the <i>m/z</i> 636 ion in Figure 2.24(a).....	83
2.25 (a) Full scan mass spectrum of the Ser:Ga:brazilein complex, (b) MS ² spectrum of the <i>m/z</i> 513 ion in Figure 2.25(a).....	84
2.26 (a) Full scan mass spectrum of the In:brazilein complex, (b) MS ² spectrum of the <i>m/z</i> 681 ion in Figure 2.26(a).....	85
2.27 (a) Full scan mass spectrum of the Ser:In:brazilein complex, (b) MS ² spectrum of the <i>m/z</i> 558 ion in Figure 2.27(a).....	86

LIST OF FIGURES (Continued)

Figure	Page
2.28 Proposed structure of the Ser:Al:brazilein 1:1:1 complex.....	87
2.29 General structure of M:brazilein 1:2 complex with (a) and without water (b) and the Ser:M:brazilein 1:1:1 complex with (c) and without water (d) (M) represent metal ions such as Al, Ga, and In) used for calculation of the heat of formation.....	90
3.1 Morphological illustration of <i>Ceasalpinia sappan</i> Linn. (top) and its heartwood (bottom) from Nakhon Ratchasima, Thailand.....	102
3.2 Graphical representation of a dyeing process: kinetics (left) and equilibrium (right) (Zollinger, 1991).....	104
3.3 Rate of dyeing isotherms (Perkins, 1996).....	105
3.4 Comparison of pre-, simultaneous and post-mordanting with alum for brazilein dyeing onto silk.....	126
3.5 The effect of pH on alum-brazilein dyeing onto silk.....	129
3.6 Electrostatic map of brazilein (left) and brazilein anion (right). (Spartan Program; AM1; Wavefunction Inc.; '02 Linux/Unix).....	129
3.7 The effect of material to liquor ratio on the adsorption of alum- brazilein onto silk.....	131
3.8 Pseudo first-order equation plots for the adsorption of alum-brazilein onto silk at different material to liquor ratios.....	132

LIST OF FIGURES (Continued)

Figure	Page
3.9 Pseudo second-order equation plots for the adsorption of alum-brazilein onto silk at different material to liquor ratios.....	132
3.10 The effect of contact time and initial dye concentration on the adsorption of alum-brazilein onto silk.....	134
3.11 Pseudo first-order equation plots for the adsorption of alum-brazilein onto silk at different initial dye concentrations.....	135
3.12 Pseudo second-order equation plots for the adsorption of alum-brazilein onto silk at different initial dye concentrations.....	135
3.13 The effect of temperature on the adsorption of alum-brazilein onto silk.....	137
3.14 Pseudo first-order equation plots for the adsorption of alum-brazilein onto silk at different temperatures.....	138
3.15 Pseudo second-order equation plots for the adsorption of alum-brazilein onto silk at different temperatures.....	138
3.16 Arrhenius plot for the adsorption of alum-brazilein onto silk.....	141
3.17 Plot of $\ln(k/T)$ against $1/T$ for the adsorption of alum-brazilein onto silk.....	142
3.18 Langmuir adsorption isotherms of alum-brazilein onto silk at 30, 50, and 70°C.....	144
3.19 A Langmuir plot of C_e/q_e against C_e for the adsorption of alum-brazilein onto silk at the initial dye concentration range 2.84-56.85 mg/L.....	145
3.20 Adsorption-desorption analysis of alum-brazilein dye onto and off silk in deionized water at different material to liquor ratios.....	148

LIST OF FIGURES (Continued)

Figure	Page
3.21 Adsorption-desorption analysis of alum-brazilein dye onto and off silk in distilled water at different material to liquor ratios.....	148
3.22 Adsorption-desorption analysis of alum-brazilein dye onto and off silk in tap water at different material to liquor ratios.....	149
3.23 The effect of material to liquor ratios on the adsorption of alum-extracted dye onto silk.....	152
3.24 Pseudo first-order equation plots for the adsorption of alum-extracted dye onto silk at different material to liquor ratios.....	153
3.25 Pseudo second-order equation plots for the adsorption of alum-extracted dye onto silk at different material to liquor ratios.....	153
3.26 The effect of contact time and initial dye concentrations on the adsorption of alum-extracted dye onto silk.....	155
3.27 Pseudo first-order equation plots for the adsorption of alum-extracted dye onto silk at different initial dye concentrations.....	156
3.28 Pseudo second-order equation plots for the adsorption of alum-extracted dye onto silk at different initial dye concentrations.....	156
3.29 The effect of temperature on the adsorption of alum-extracted dye onto silk.....	158
3.30 Pseudo first-order equation plots for the adsorption of alum-extracted dye onto silk at different temperatures.....	159

LIST OF FIGURES (Continued)

Figure	Page
3.31 Pseudo second-order equation plots for the adsorption of alum-extracted dye onto silk at different temperatures.....	159
3.32 Arrhenius plots for the adsorption of alum-extracted dye onto silk.....	161
3.33 Plot of $\ln(k/T)$ against $1/T$ for the adsorption of alum-extracted dye onto silk.....	162
3.34 Langmuir adsorption isotherms of alum-extracted dye onto silk at 30 and 50°C...	165
3.35 A Langmuir plot of C_e/q_e against C_e for the adsorption of alum-extracted dye onto silk at the initial dye concentration range 142-853 mg/L.....	166
3.36 Adsorption-desorption analysis of alum-extracted dye onto and off silk in deionized water at different material to liquor ratios.....	169
3.37 Adsorption-desorption analysis of alum-extracted dye onto and off silk in distilled water at different material to liquor ratios.....	169
3.38 Adsorption-desorption analysis of alum-extracted dye onto and off silk in tap water at different material to liquor ratios.....	170
4.1 Chemical structure of (a) brazilein and (b) brazilin (Wongsooksin <i>et al.</i> , 2008).....	188
4.2 The proposed structure of the $[Al(\text{brazilein})_2]^+$ complex (Wongsooksin <i>et al.</i> , 2008).....	189

LIST OF FIGURES (Continued)

Figure	Page
4.3 Adsorption (closed symbols) and desorption (open symbols) isotherms of N ₂ at -196°C for physically activated carbon (sample C) and chemically activated carbon (sample CZ).....	203
4.4 Adsorption (closed symbols) and desorption (open symbols) isotherms of N ₂ at -196°C for physically activated carbon (sample C) and their oxidized activated carbons (sample C1, C2, and C4).....	206
4.5 Adsorption (closed symbols) and desorption (open symbols) isotherms of N ₂ at -196°C for physically activated carbon (sample C), oxidized activated carbon (sample C4) and heat treatment activated carbons (sample C4-700 and C4-900).....	207
4.6 Adsorption (closed symbols) and desorption (open symbols) isotherms of N ₂ at -196°C for wood based-activated carbons prepared from chemical activation (sample W1 and W2).....	208
4.7 Content of surface functional groups of the physically activated carbon (sample C) and their oxidized activated carbons (sample C1, C2, C4, C8, C16, C24, and C48).....	209
4.8 Content of surface functional groups of the physically activated carbon (sample C), oxidized activated carbon (sample C4) and heat treatment activated carbons (sample C4-700 and C4-900).....	211

LIST OF FIGURES (Continued)

Figure	Page
4.9 Content of surface functional groups of the physically activated carbon (sample C), chemically activated carbon (sample CZ) and their oxidized activated carbons (sample C4 and CZ4).....	212
4.10 Content of surface functional groups of the wood based-activated carbons prepared from chemical activation (sample W1 and W2).....	213
4.11 FT-IR spectra of the physically activated carbon (sample C) and their oxidized activated carbons (sample C1, C2, C4, C8, C16, C24, and C48).....	215
4.12 FT-IR spectra of the chemically activated carbon (sample CZ) and oxidized activated carbon (sample CZ4).....	216
4.13 FT-IR spectra of the physically activated carbon (sample C), oxidized activated carbon (sample C4) and heat treatment activated carbons (sample C4-700 and C4-900).....	217
4.14 Effect of the contact time on the adsorption of dye effluent on unoxidized physically activated carbon (sample C), oxidized activated carbon (sample C4) and unoxidized chemically activated carbon (sample CZ).....	218
4.15 Effect of pH on the adsorption of dye effluent on oxidized activated carbon (sample C4).....	219
4.16 Effect of amount of activated carbon on the adsorption of dye effluent on oxidized activated carbon (sample C4).....	220

LIST OF FIGURES (Continued)

Figure	Page
4.17 Adsorption isotherms at 30°C of dye effluent on physically activated carbon (sample C) and their oxidized activated carbons (sample C1, C2, and C4).....	222
4.18 Adsorption isotherms at 30°C of dye effluent on physically activated carbon (sample C), oxidized activated carbon (sample C4) and heat treatment activated carbons (sample C4-700 and C4-900).....	223
4.19 Adsorption isotherms at 30°C of dye effluent on unoxidized chemically activated carbon (sample CZ), oxidized physically activated carbon (sample C4) and heat treated activated carbons (sample C4-700 and C4-900).....	225
4.20 Adsorption isotherms at 30°C of dye effluent on chemically activated carbon (sample CZ) and oxidized activated carbon (sample CZ4).....	226
4.21 Adsorption isotherms at 30°C of dye effluent on chemically activated carbon prepared from wood (sample W1 micropore and W2 mesopore) and oxidized activated carbon (sample C4).....	228

LIST OF ABBREVIATIONS

BE	Brazilein
BI	Brazilin
Al	Aluminium
Ga	Gallium
In	Indium
Ser	(<i>S</i>)- <i>N</i> -acetyl serine methyl ester
mL	Millitre
L	Litre
mg	Milligram
g	Gram
cm	Centimeter
nm	Nanometer
MS	Mass Spectrometry
HRMS	High Resolution Mass Spectroscopy
ESMS	Electrospray Mass Spectroscopy
FT-IR	Fourier Transform Infrared spectroscopy
NMR	Nuclear Magnetic Resonance
TLC	Thin Layer Chromatography
<i>m/z</i>	mass to charge value
mp.	Melting point

LIST OF ABBREVIATIONS (Continued)

k_1	Rate constant of pseudo first-order adsorption
q_e	The amount of dye adsorbed per gram fibers at equilibrium
q_t	The amount of dye adsorbed per gram fibers at time t
k_2	Rate constant of pseudo second-order adsorption
h_i	The initial dye adsorption rate
A	The pre-exponential factor
E_a	Activation energy
R	Gas constant
$\Delta H^\#$	Enthalpy of activation
$\Delta S^\#$	Entropy of activation
$\Delta G^\#$	Free energy of activation
k_b	Boltzmann's constant
h	Planck's constant
T	Temperature (K)
t	Time
Q	Adsorption capacity of the Langmuir isotherm
b	Langmuir constant
R_L	Dimensionless constant separation factor
Q_f	Adsorption capacity of the Freundlich isotherm
ΔG°	Gibbs free energy

LIST OF ABBREVIATIONS (Continued)

ΔH°	Enthalpy change
ΔS°	Entropy change
K_c	Equilibrium constant
$C_{ad,e}$	Concentration of the dye adsorbed at equilibrium
C_e	Concentration of dye left in the dye bath at equilibrium
w/w	Weight by weight
C_0	Initial dye concentration
C_t	Concentration of dye after dyeing time t
V	Volume of dye solution
W	Weight of fibre used
MLR	Material to Liquor Ratio
mg/L	Milligram per Litre
w/w	Weight by weight
v/v	Volume/volume
R^2	Correlation coefficient
Temp	Temperature
min	minute
q_{de}	The amount of dye desorbed from the fibres
λ_{max}	Maximum wavelength

CHAPTER I

GENERAL INTRODUCTION

1.1 Introduction

Since the earliest times, natural dyes have been used for many purposes such as the coloring of natural fibers wool, cotton and silk as well as fur and leather (Cristea and Vilarem, 2006). Natural coloring matters are dyes and pigments occurring in animals (birds, insects, bacteria) and in plant material including trees, leaves, grass and flowers (Christie, Mather, and Wardman, 2000). The use of natural dyes to color textiles declined rapidly after the discovery of synthetic dyes in 1856, until they were virtually unused by 1900. Recently a revival of interest in the use of natural dyes in textile coloration has been growing. This is a result of the stringent environmental standards imposed by many countries in response to the toxic and allergic reactions associated with synthetic dyes. Natural dyes are friendlier to the environment than synthetic dyes and can exhibit better biodegradability and generally have a higher compatibility with the environment (Kamel, El-Shishtawy, Yussef, and Mashaly, 2005; Nagia and EL-Mohamedy, 2007). The following sections discuss natural dyes and synthetic dyes including their classification, source and application.

1.2 Natural dyes

The dyes obtained from either plants material including trees, leaves, grass and flowers, or animal sources are referred to as natural dyes. Generally, the major natural dyes classes of plants material are flavonoids, quinones, carotenoids, and chlorophylls (Lemmens and Wulijarni-Soetjipto, 1992).

1.2.1 Flavonoids

Flavonoids are a group of polyphenolic compounds that are widely distributed in plants and are used as pigments (Doménech-Carbó, A., Doménech-Carbó, M., and Sauf-Peris, 2005). The flavonoids include the following subgroups namely chalcones, flavanones, flavones, flavonols, anthocyanins and isoflavonoids (Lemmens and Wulijarni-Soetjipto, 1992). The flavonoids are yellow in color. Example of flavonoid dye is morin as shown in Figure 1.1.

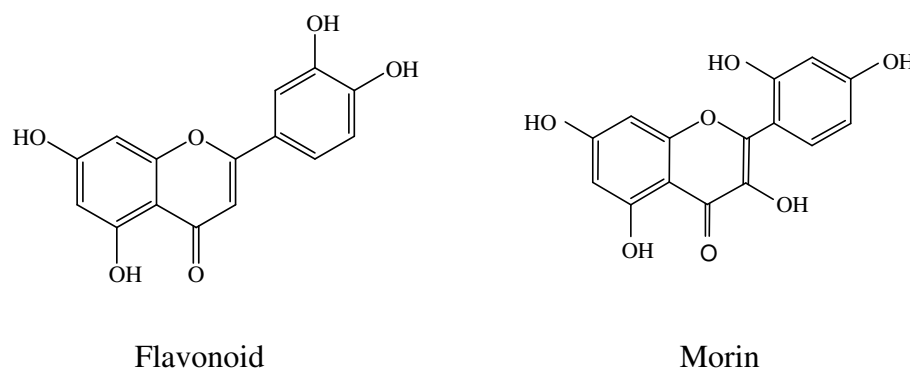


Figure 1.1 Basic structure of flavonoid and example of flavonoid: morin (Lemmens and Wulijarni-Soetjipto, 1992).

Homoisoflavonoids exhibit a flavonoid-like structure and can be classified as a sub-group of flavonoids. The homoisoflavonoids are pink-yellow in color, for examples: brazilein and brazilin (Figure 1.2).

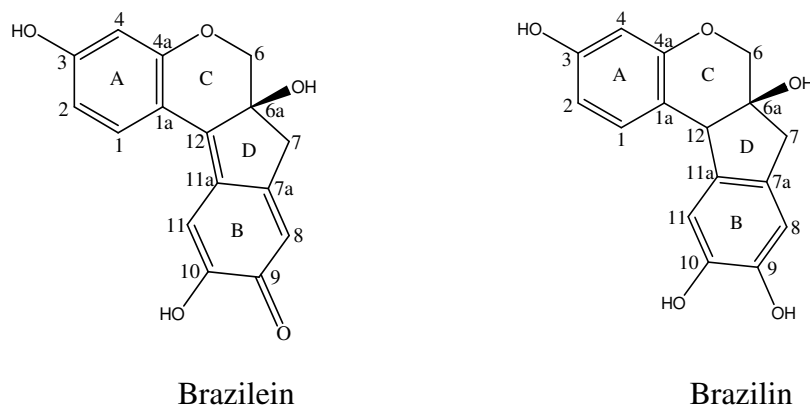


Figure 1.2 Chemical structure of brazilein and brazilin (Wongsooksin, Rattanaphani, S., Tangsathitkulchai, Rattanaphani, V., and Bremner, 2008).

1.2.2 Quinones

Quinones include various compounds containing a quinone structure. The color is usually yellow to red. The important subgroups are benzoquinones, naphthoquinones and anthraquinones (Lemmens and Wulijarni-Soetjipto, 1992). Examples of naphthoquinone and anthraquinone dyes are presented in Figure 1.3.

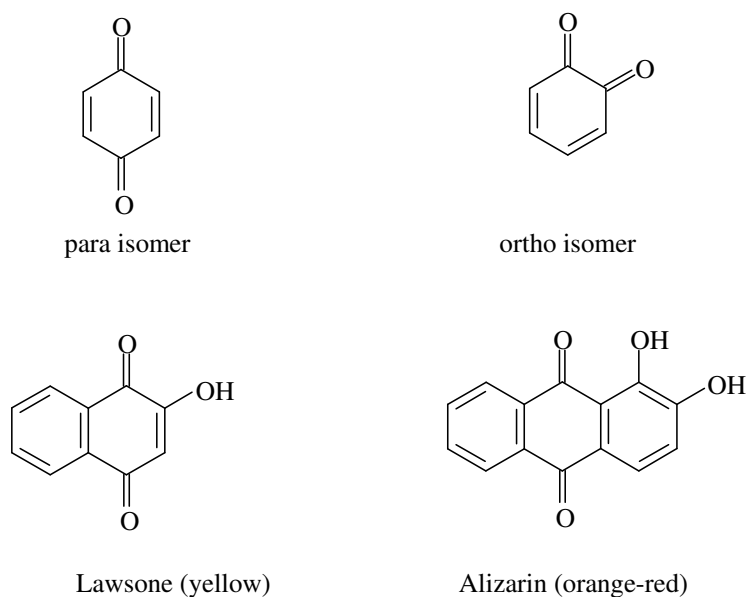


Figure 1.3 Structure of quinone and examples of a naphthoquinone (lawsone) and an anthraquinone (alizarin) (Lemmens and Wulijarni-Soetjipto, 1992).

1.2.3 Carotenoids

Carotenoids are a class of natural fat-soluble pigments found principally in plants. Carotenoids are polyene dyes which contain a long chain of conjugated double bonds. They have a variety of structures and intense characteristic colors: yellow, orange, red and purple (Lemmens and Wulijarni-Soetjipto, 1992). Example of carotenoid dye is bixin as shown in Figure 1.4.

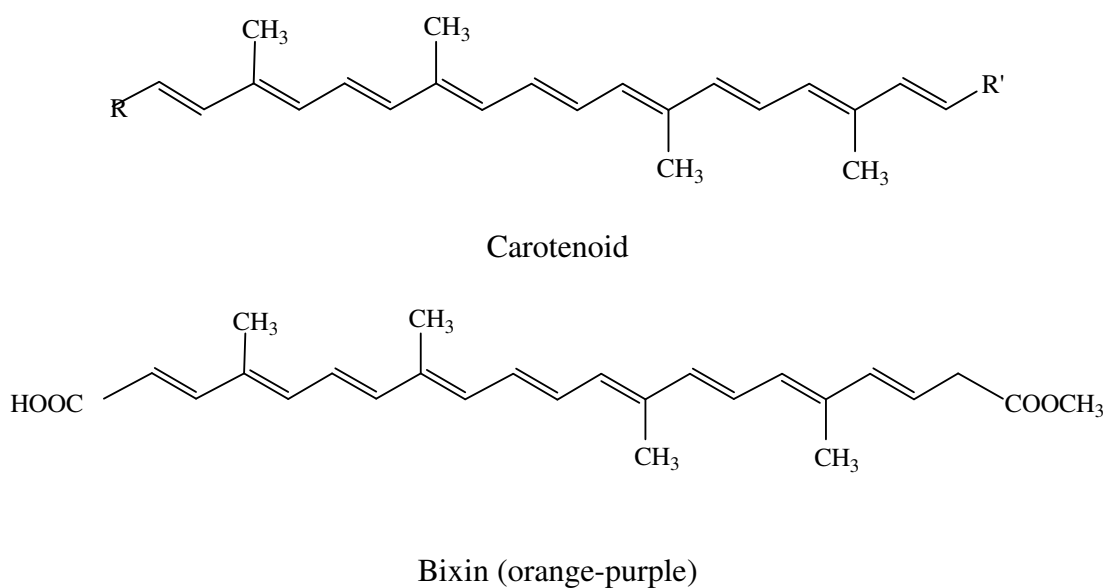
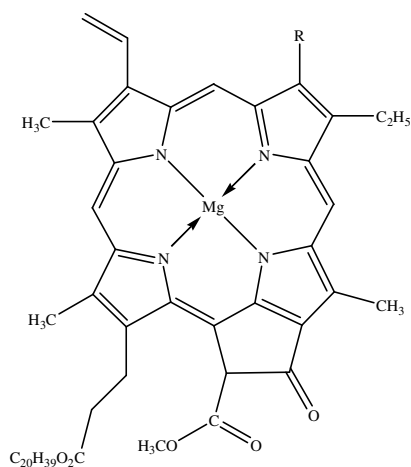


Figure 1.4 Structure of carotenoid and example of carotenoid: bixin (Lemmens and Wulijarni-Soetjipto, 1992).

1.2.4 Chlorophylls

Chlorophyll is a green pigment found in leaves and green stems of plants (Lemmens and Wulijarni-Soetjipto, 1992). In chlorophyll the central ion is magnesium, and the large organic molecule is a porphyrin. The porphyrin contains four nitrogen atoms that form bonds to magnesium in a square planar arrangement. Chemical structure of chlorophyll as shown in Figure 1.5.



Chlorophyll a: R = CH₃

Chlorophyll b: R = CHO

Figure 1.5 Chemical structure of chlorophyll.

1.3 Synthetic dyes

Synthetic dye is any of the organic dyes originally derived from coal-tar derivatives, but currently synthesized from benzene and its derivatives. Synthetic dyes for the dyeing process may be classified in two class according to their chemical structure or the method of application (Christie *et al.*, 2000).

1.3.1 Chemical classification

In the chemical classification method, the synthetic dyes can be grouped according to certain common chemical structural features as shown in Table 1.1 (Christie *et al.*, 2000). Examples of the structures of a carbonyl dye, methane dye and nitro dye are illustrated in Figure 1.6.

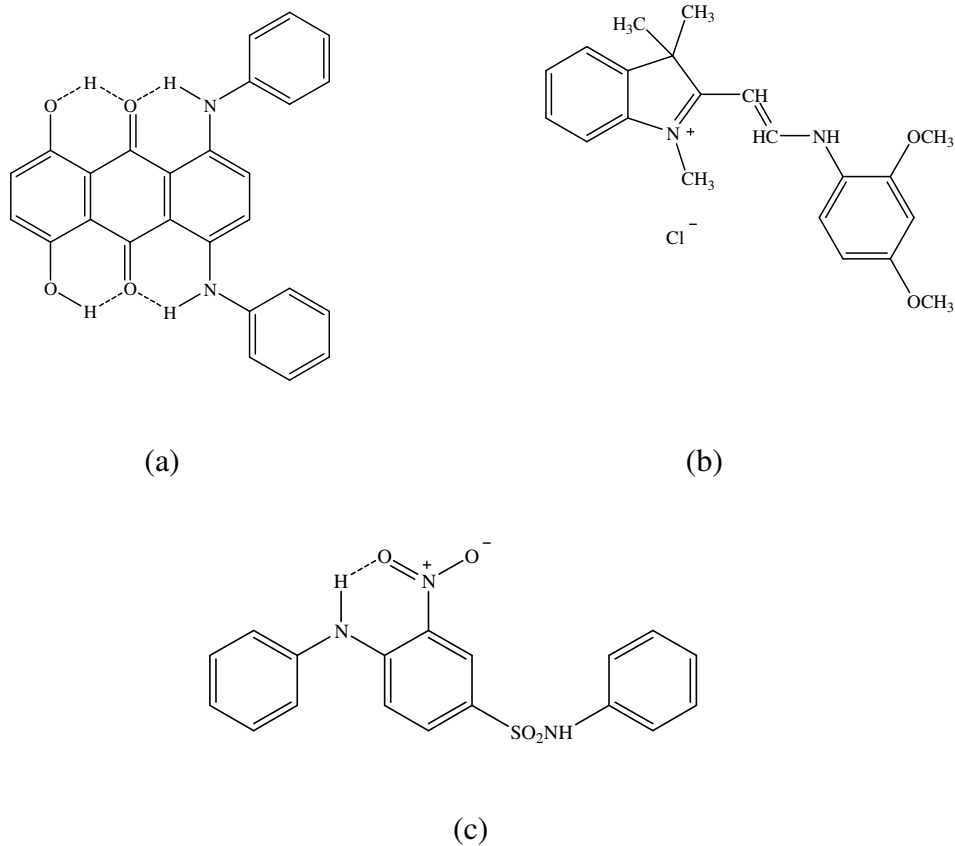


Figure 1.6 Examples of the structures of carbonyl dye, methine dye and nitro dye (a) C.I. Disperse Green 5, carbonyl dye; (b) C.I. Basic Yellow 11, methine dye and (c) C.I. Disperse Yellow 4, nitro dye (Christie *et al.*, 2000).

1.3.2 Application classification

There are eight major classes according to the method of application.

1. Three dye classes used mainly for protein and synthetic fibers are acid, basic and disperse dyes.
2. Five dye classes applied to dye on cellulose fibers are direct, azoic, sulphur, reactive and vat dyes.

Table 1.1 The characteristics of the chemical classes of synthetic dyes (Christie *et al.*, 2000).

Chemical class	Distinctive structural feature	General characteristics	Main application class(es)
Azo	-N=N-	All hues, but yellow to red most important	Dominate most, but not vat dyes
Carbonyl	C=O	All hues, but blue most important	Important in most applications
Phthalocyanine	16-membered heterocyclic ring, metal complex	Blue and green only	Most important in pigments
Triarycarbonium ion	Positively-charged carbon atom	All hues, but reds and blues most important	Cationic dyes and pigments
Sulfur dyes	Complex polymeric S-containing species	Mostly dull colors, such as blacks and browns	Often considered as an application class itself
Methine dyes	-C=	All hues, but yellows most important	Disperse, cationic
Nitro	-NO ₂	Mainly yellows	Disperse, hair dyes
Inorganic colorants	Range of inorganic types	All hues, white and metals	Exclusive pigments

1.4 Textile fibers

The classification of textile fibers for the application of dyes may be classified into three broad groups (Christie *et al.*, 2000):

- (a) protein fibers e.g. silk and wool
- (b) cellulosic fibers e.g. cotton, viscose rayon, and flax (linen)
- (c) synthetic and cellulose acetate fibers e.g. polyester, polyamide, acrylic and cellulose acetate.

1.4.1 Protein fibers

The most important of the protein textile fibers are silk and wool. Protein fibers are natural fibers derived from animal sources. The protein molecules consist of a long polypeptide chain constructed from different naturally occurring α -amino acids as seen in Figure 1.7.

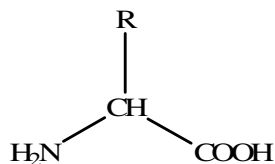


Figure 1.7 General α -amino acid formula.

Raw silk is a secretion of the silk-worm, *Bombyx mori* (Truter, 1973; Lewin and Pearce, 1998). The silk fiber is almost a pure protein fiber composed of two types of protein, namely, fibroin and sericin. It also contains small quantities of carbohydrate, wax and inorganic components which also play a significant role as structural elements during the formation of silk fibers (Hojo, 2000).

Both fibroin and sericin are protein substances built up from 18 amino acids out of which glycine, alanine, serine and tyrosine make up the largest part of the silk fiber (Hojo, 2000). The composition of fibroin and sericin with respect to the four main amino acids is shown in Table 1.2; the side groups R refer to the general structure in Figure 1.7 and general structure of silk (polypeptides) as shown in Figure 1.8.

Table 1.2 The composition of fibroin and sericin (Karmakar, 1999).

Amino acids	Side groups R	Fibroin (% mol)	Sericin (% mol)
Glycine	H –	45.21	14.75
Alanine	CH ₃ –	29.16	4.72
Serine	HOCH ₂ –	11.26	34.71
Tyrosine	<i>p</i> -OHPHCH ₂ –	5.14	3.35

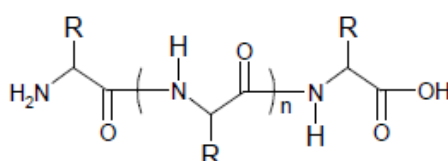


Figure 1.8 General structure of silk.

1.4.2 Cellulosic fibers

Cellulose fibers are natural fibers derived from plant sources. The most important cellulosic fibers are cotton, viscose, linen, jute, hemp, and flax (Christie, 2001). The major component of cellulose fibers is cellulose, an organic compound

with the formula $(C_6H_{10}O_5)_n$, a straight and long chain polymer with repeating units of β -D-glucose ($C_6H_{12}O_6$) linked through carbon atoms in the 1- and 4-positions (Figure 1.9). Each unit of the cellulose molecule has a number of hydroxyl (-OH) groups. These are the binding site for dyes (Christie, 2001).

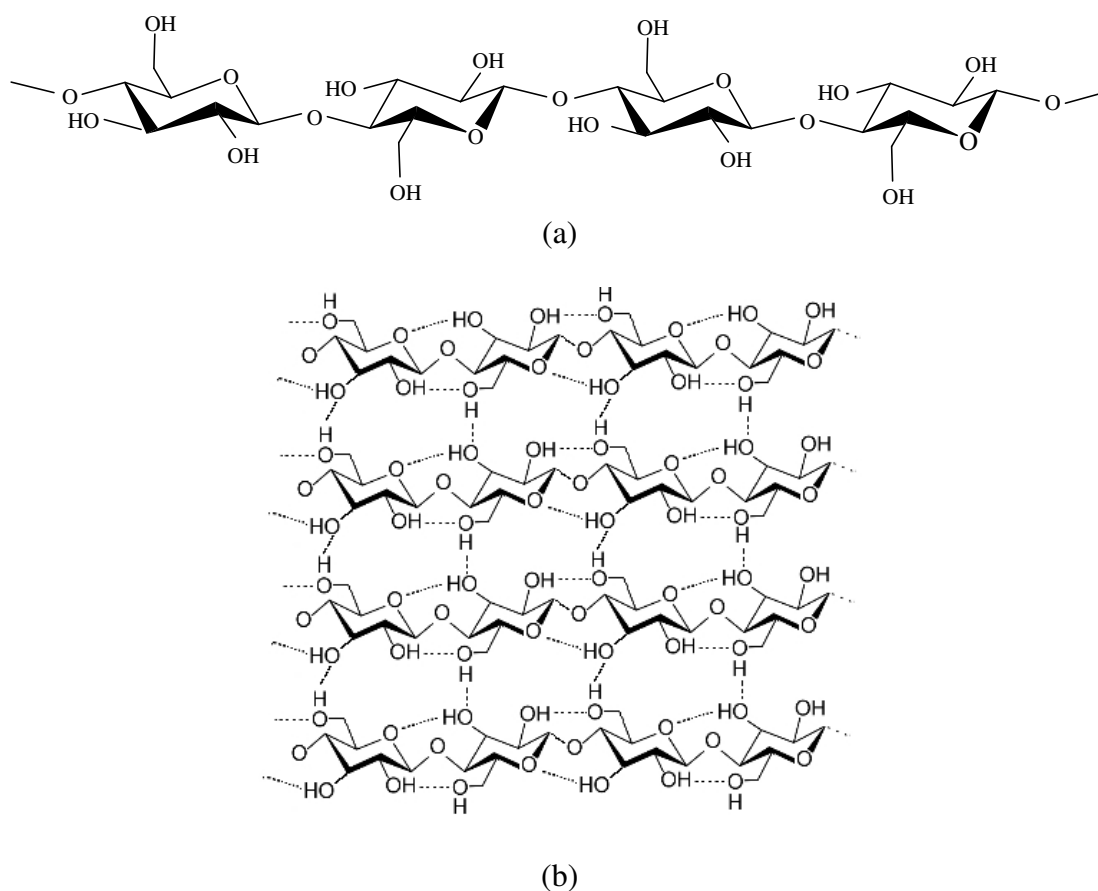


Figure 1.9 The structure of cellulose; (a) cellulose structure and (b) hydrogen bonding in cellulose structure.

1.5 Natural dyes for protein fibers

The use of natural dyes to color textiles declined rapidly after the discovery of synthetic dyes in 1856, until they were virtually unused by 1900. From the application

point of view these dyes are classified as: (i) direct dyes, (ii) vat dyes, or (iii) mordant dyes (Bhat, Nagasampagi, and Sivakumar, 2005).

1.5.1 Direct dyes

Direct dyes are applied to dye on cellulose directly without pretreatment being required either to the dyestuff or to the fabric. Generally, direct dyes contain amino or hydroxyl groups which can interact to fibers by forming hydrogen bonds or ionic bonds. For example, picric acid is a direct dye for silk or wool. Since it is a strong acid, it interacts with the basic end groups and side chains in silk and wool to form a salt linkage or electrostatic interaction between itself and the fiber. The picric acid gives its proton to some basic group on the fiber and becomes an anion, which strongly binds to a cationic group on the fiber by ionic interaction. This interaction is illustrated in Figure 1.10.

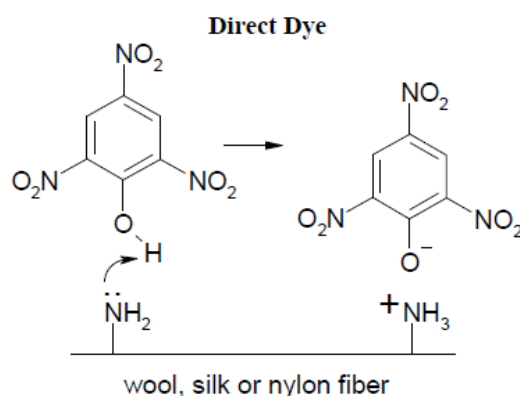


Figure 1.10 The interaction of direct dye with fiber.

1.5.2 Vat dyes

Vat dyes are essentially insoluble in water and incapable of dyeing fibers directly. However, reduction in alkaline liquor produces the water soluble alkali metal salt of the dye, which, in this leuco form, has an affinity for fiber. Subsequent

oxidation reforms the original insoluble dye. Usually, vat dyes are classified into three groups such as indigoid, anthraquinone, and fused ring polycyclic dyes. Vat dyes are used mainly on cellulosic fibers, but some can be applied to protein fibers (Perkins, 1996). The most famous vat dye is indigo and the reaction of indigo is illustrated below:

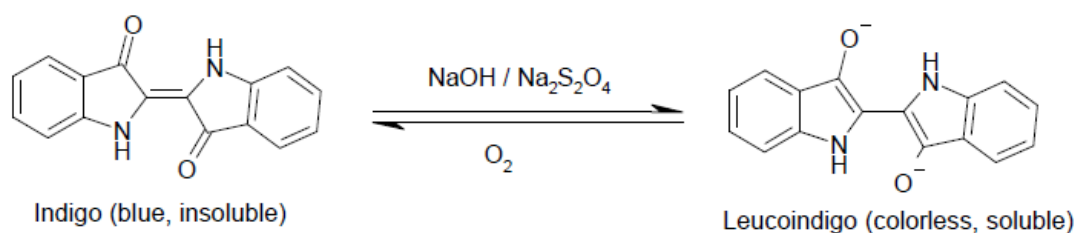


Figure 1.11 The reaction of indigo.

1.5.3 Mordant dyes

Most natural dyes need a mordant to fix the dye to the fiber and increase fastness property. The word mordant is derived from the Latin word *mordere*, which means “to bite”. The first reason for using a mordant in dyeing process is to make the dyestuff stick to the fiber. A second reason for using a mordant is that the mordant can affect the color of the dyestuff that is used. It can deepen and intensify the color, or it can lighten it, or it can completely change the color. Thirdly, use of a mordant can positively influence the fastness of the dye (Bechtold, Turcanu, Ganglberger, and Geissler, 2003; Moeyes, 1993). The basic principle of mordanting (with metal ions) is the formation of metal ion bonds with the electron donating chromophores of dyes.

Mordants are of two types: (i) Natural or organic and (ii) Inorganic (Kongkachuichay, Shitangkoon, and Chinwongamorn, 2002; Bhat *et al.*, 2005).

(i) Natural mordants consist of tannic acid, ellagic acid, tannins and sulfated and sulfonated oil obtained from vegetable oil.

(ii) Inorganic mordants include alum or potash alum ($\text{Al}_2\text{K}_2(\text{SO}_4)_4$), chrome alum ($\text{Cr}_2(\text{SO}_4)_4 \cdot 24\text{H}_2\text{O}$), ferric alum ($\text{Fe}_2(\text{NH}_4)_2(\text{SO}_4)_4 \cdot 24\text{H}_2\text{O}$), potassium dichromate ($\text{K}_2\text{Cr}_2\text{O}_7$), ferrous sulfate ($\text{FeSO}_4 \cdot 7\text{H}_2\text{O}$), Cupric sulfate ($\text{CuSO}_4 \cdot 5\text{H}_2\text{O}$), stannous chloride (SnCl_2).

There are four ways of using a mordant (Bechtold *et al.*, 2003; Moeyes, 1993) as follows:

- (a) Mordanting before dyeing, or pre-mordanting;
- (b) Mordanting and dyeing at the same time, called stuffing or simultaneous mordanting;
- (c) Mordanting after dyeing, or after-mordanting or post-mordanting;
- (d) A combination of pre-mordanting and after-mordanting.

The methods have different effects on the shade obtained after dyeing and also on the fastness properties. It also depends upon the dye and the fiber. It is therefore necessary to choose a proper method to get the required and fastness by optimization of parameters.

1.6 Synthetic dyes for protein fibers

Protein fibers mainly silk and wool may be dyed using synthetic dyes of various application classes, the most important of which are acid, basic and disperse dyes.

1.6.1 Acid dyes

Acid dyes are anionic in aqueous media, the anion being colored. Acid dyes contain one or more sulphonate ($-\text{SO}_3^-$) groups in their structure, usually as sodium (Na^+) salts, but some contain carboxyl and phenolic groups on the molecule making them soluble in water (Christie *et al.*, 2000; Christie, 2001). The most common structural types of acid dyes are monoazo and anthraquinone dyes as shown in Figure 1.12.

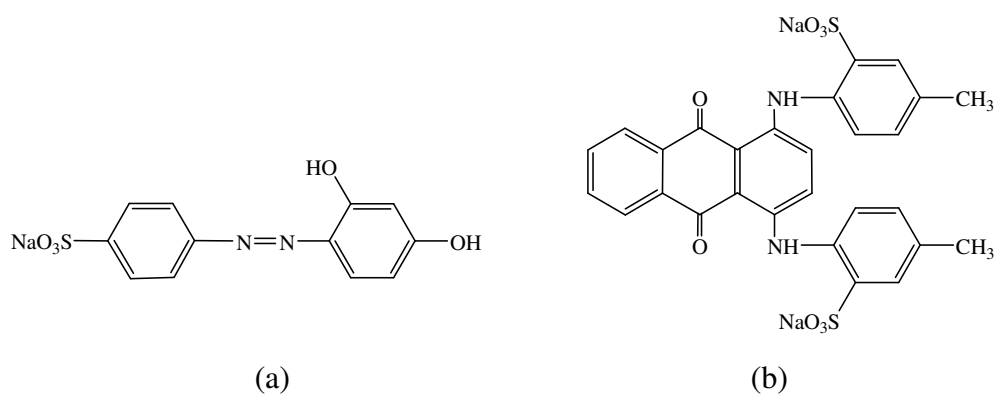


Figure 1.12 Examples of acid dyes; (a) C.I. Acid Orange 6 and (b) C.I. Acid Green 25 (Christie *et al.*, 2000).

They have been used to dye protein fibers such as wool and silk. Wool, silk and other protein-based natural fibers have amino groups that can interact with acid dyes. The protein molecules carry a positive charge (through amine group protonation) which attracts the acid dye anion by ionic forces as well as these ionic forces of attraction, Van der Waal's forces, dipolar forces and hydrogen bonding between appropriate functionality of the dye and fiber molecules may also play a part in the acid-dyeing of protein fibers. The strength of these bond is considered to be

responsible for the washfastness of good acid dyes (Perkins, 1996; Christie *et al.*, 2000).

1.5.2 Basic dyes

Basic dyes are water-soluble cationic dyes containing a positive charge in their structure (Horrocks and Anand, 2000). They have been used to dye on fibers containing acidic groups that can interact with these cationic groups on their chromophore. Example of basic dye is given in Figure 1.13.

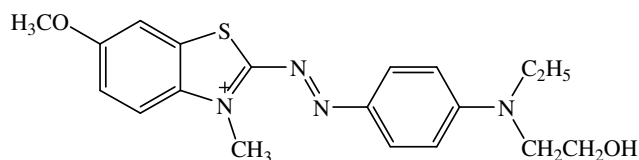


Figure 1.13 Example of basic dyes; C.I. Basic Blue 41 (Christie, 2001).

1.6.3 Disperse dyes

Disperse dyes are dyes of relatively low water-solubility applied as a fine dispersion in water. Three important types are azo, anthraquinone and nitrophenylamine dyes. They are applied to relatively non-polar (hydrophobic) fibers, especially to polyester (Christie *et al.*, 2000). An example of a disperse dye is represented in Figure 1.14.

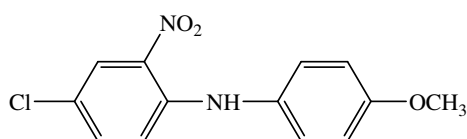


Figure 1.14 Example of disperse dye; C.I. Disperse Orange 15 (Christie *et al.*, 2000).

1.7 Natural organic dyes

The red color from the heartwood of the plant *Caesalpinia sappan* Linn. is used to dye textile fibers and it is used in mixtures of dyes. In addition, the wood has been used for coloring drinks pink. Moreover it has been used to treat fever, and a decoction of the bark and wood is used in the treatment of tuberculosis, diarrhea, and dysentery, as an astringent and as a vulnerary. The seeds serve as a sedative (Lemmens and Wulijarni-Soetjipto, 1992). The plant *C. sappan*, belongs to the Leguminosae family; its synonym is *Biancaea sappan* L. It is a small shrubby tree whose the origin is not certain, but it is thought to be in the region from central and southern India through Burma, Thailand, China, Malaysia, Indonesia, Philippines, Papua New Guinea, India, Sri Lanka, Taiwan, Solomon Islands, and Hawaii.

The red homoisoflavonoids, brazilin (6aS-*cis*)(7,11b-dihydrobenz[*b*]indeno[1,2-*d*]pyran-3,6a,9,10,(6*H*)-tetrol) and brazilein (6aS-(6a,7-dihydro-3,6a,10-tri-hydroxy-benz[*b*]indeno[1,2-*d*]pyran-9(6*H*)-one) (Figure 1.2), are components of the heartwood of the tree *Caesalpinia sappan* Linn. (family Leguminosae) (Ferreira, Hulme, McNab, and Quye, 2004). Homoisoflavonoids exhibit a flavonoid-like structure and can be classified as a sub-group of flavonoids. Flavonoids are a group of polyphenolic compounds that are widely distributed in plants and are used as pigments (Doménech-Carbó *et al.*, 2005). Brazilin is readily converted to brazilein by exposure to atmospheric oxygen and light. In Thailand, the aqueous extracts from the wood of *C. sappan* are generally used for the dyeing of silk, especially in the Northeast (Moeyes, 1993). The extracted dyes, which are mainly composed of brazilin and brazilein, give a beautiful red or pink color to silk. However, this natural dye has poor fastness properties, and in order to try and overcome this, metal ion-

based mordants are used (Lemmens and Wulijarni-Soetjipto, 1992; Yan, Wang, Xing, Zhao, and Du, 2005). One such mordant generally used by villagers in Northeast Thailand is alum, which provides a source of Al(III) ions. Alum ($KAl(SO_4)_2 \cdot 12H_2O$) is widely used as a mordant for dyeing keratin fibers with polyphenolic dyes to improve the fastness properties. The ability of metal ions to form very stable metal-dye complexes may be used to produce dyed protein fibers with superior fastness properties, especially towards washing and light (Christie, 2001).

1.8 Treatment of dye effluent

Dyeing is a fundamental operation during textile fiber processing. This operation causes the production of colored wastewater. Water from spent dyebaths and dye rinse operations contains unfixed dyes and may be highly colored. The persisting color and the non-biodegradable nature of the spent dyebaths cause serious problems to the environment. The presence of dye in water is highly visible and affects water transparency, resulting in reduction of light penetration, and gas solubility in water. Moreover, several commonly used dyes have been reported to be carcinogenic and mutagenic for aquatic organisms (Faria, Orfao, and Pereira, 2004; Gong, Sun, Chen, Liu, and Yang, 2005; Wang and Li, 2005; Wang, Zhu, Coomes, Haghseresht, and Lu, 2005; Demirbas, Kobya, and Sulak, 2008; Thinakaran, Baskaralingam, Pulikesi, Panneerselvam, and Sivanesan, 2008). The inorganic mordants used for the dyeing process contain toxic metal ions which also cause serious problems to the environment.

With the growing emphasis on environmentally friendly industry, it is important to use cheap and efficient methods for cleaning industrial wastewater. The

conventional methods for removal of dyes from wastewater include adsorption, coagulation and flocculation, oxidation or ozonation, membrane separation and precipitation. Among various treatment technologies, adsorption onto activated carbon has proven to be an effective and reliable physicochemical treatment methodology (Wang and Li, 2005; Choi, Shin, Kim, Jeon, and Baek, 2008). The large sorption capacity of activated carbon is linked to its well developed internal pore structure, surface area and the presence of a wide spectrum of surface functional groups (Chingombe, Saha, and Wakeman, 2005).

1.9 Activated carbon

Activated carbon is an amorphous carbon which has a highly developed internal surface area and porosity and exhibits various surface chemical properties. The performance of activated carbon is determined by its porous structure and surface chemistry (Bansal, Donnet, and Stoeckli, 1988). Activated carbon contains hydrophobic graphene layers and hydrophilic surface functional groups, therefore it can be used to remove a wide variety of organic and inorganic species from both the gas and liquid phase, for example, the separation of gases, colored wastewater treatment, removal of heavy metal ions from aqueous solution and purification of drinking water (Biniak, Pakula, Szymański, and Świątkowski, 1999; Jia and Thomas, 2000; Pereira, Soares, Órfão, and Figueiredo, 2003; Faria *et al.*, 2004; Wang *et al.*, 2005; Demirbas *et al.*, 2008; Karaca, Gürses, Açıkyıldız, and Ejder, 2008; Kavitha and Namasivayam, 2008; Tan, Ahmad, and Hameed, 2008; Thinakaran *et al.*, 2008). Activated carbon can be prepared from a large number of carbonaceous raw materials such as coconut shell, wood, agricultural by products, sawdust, peat, coal, petroleum

coke and fruit nuts. The criteria for selecting a carbonaceous raw material include: high carbon content, availability and low cost, but the manufacturing process and application of the product are also important considerations. Among a variety of carbonaceous sources, coconut shell is suitable for preparing microporous activated carbon due to its excellent natural structure: low ash content, hardness, and abrasion resistance, and it can be activated either chemically or physically. Coconut shell is composed mainly of lignin (around 35-45%) and cellulose (around 23-43%) (Carrijo, Liz, and Makishima, 2002 quoted in Pino, Mesquita, Torem, and Pinto, 2006; Wei, Li, and Ya-ping, 2006; Wei, Ya-ping, Liu-fang, Yan, and Li, 2007; Li, Peng, Zhang, L., Yang, Xia, Zhang, S., and Guo; 2008). Eucalyptus is a fast growing wood and some researchers have reported the potential use of this wood in the preparation of activated carbon (Tancredi, Cordero, Rodríguez-Mirasol, and Rodríguez, 1996; Arriagada, García, Molina-Sabio, and Rodríguez-Reinoso, 1997). Conversion of these biomass into activated carbons which can be used as adsorbents in water purification or the treatment of industrial and municipal effluents would add value to agricultural commodities, helping to reduce the cost of waste disposal, and provide a potentially cheap alternative to existing commercial carbon (Pino, Mesquita, Torem, and Pinto, 2006; Li *et al.*, 2008).

Figure 1.15 represents a schematic structure of activated carbon which consists of aromatic sheets and strips, often bent. Basically, the activated structure consists of the amorphous structure and the graphite-like microcrystalline structure. The graphite-like structure is dominant for the contribution of the porosity to accommodate the adsorbate molecules. This porosity originates from the free interstices between the graphene layers that are arranged in a disordered structure.

This disorganized structure means the pores cover a broad range of pore sizes. Besides the crystalline and porous structure, an activated carbon has a chemical structure as well. The chemical structure is related to the presence of functional groups, particularly oxygen functional groups, usually located at the edges of graphene layers (Boehm, 1994). The content and type of oxygen functional group in activated carbon can have a profound effect on the surface chemistry which may improve or hinder its ability to absorb certain species (El-Sheikh, 2008).

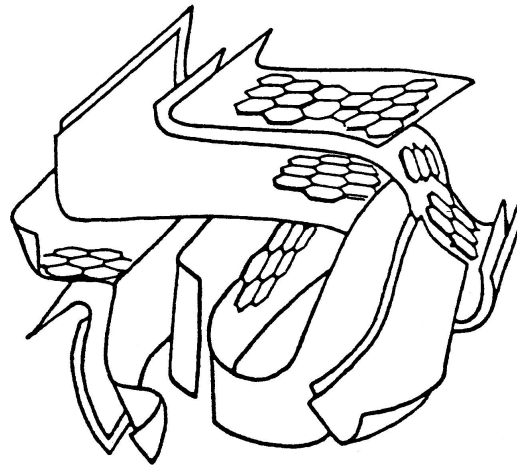


Figure 1.15 A schematic representation of the structure of activated carbon

(Bansal *et al.*, 1988).

1.9.1 Manufacture of activated carbon

The manufacture of activated carbon is divided into two main categories: physical activation and chemical activation.

1.9.1.1 Physical activation

In physical activation, carbonaceous raw material is carbonized under an inert gas atmosphere condition at a temperature between 400-800°C to produce char with a rudimentary pore structure. Then, the resulting char is activated at high temperatures (800-1100°C) with an activating gas (e.g. steam, CO₂, air, or a mixture of these gases, and flue gas) to further develop an extended porosity and internal surface area. During carbonization, the moisture and volatile matter are removed as CH₄, H₂, CO, CO₂, H₂O, and other hydrocarbons, and char with high carbon content is produced. In the manufacture of commercial activated carbon, the two steps (carbonization and activation) can be combined into a one-step procedure. The one-step activation is achieved by heating raw carbonaceous material at 600-900°C in the presence of the activating agent.

1.9.1.2 Chemical activation

Chemical activation proceeds by impregnation of the carbonaceous raw material with a chemical activating agent usually by mixing and kneading and then carbonization under an inert gas atmosphere at temperatures in the range from 400-800°C, depending on the carbonaceous raw material and activating agent used.

Chemical activating agents used in chemical activation are dehydrating agents that inhibit the formation of tar and other by-products, thus enhancing the yield of carbon (Howe-Grant, 1992). Moreover, the chemical activating agents help to degrade (pyrolyze) and/or dehydrate the cellulose materials and prevent shrinkage during carbonization. Examples of chemical activating agents are ZnCl₂, AlCl₃, KOH, K₂CO₃, NaOH, Na₂CO₃, KCl, NaCl, MgCl₂, H₃PO₄, and H₂SO₄

(Jagtøyen and Derbyshire, 1998 ; Hu and Srinivasan, 2001; Hu, Srinivasan, and Ni, 2001; Tsai, Chang, Lin, Chien, Sun, and Usieh, 2001; Mozammel, Masahiro, and Bhattacharya, 2002; Molina-Sabio and Rodríguez-Reinoso, 2004). The advantages of chemical activation over physical activation are lower temperature, one step, higher product yield, and high surface area product. However, the incorporation of impurities in the activated carbon due to the impregnation of a chemical activating agent necessitates several washing stages.

1.9.2 Classification of pores of activated carbon

The porosity of a solid is a measure of its volume accessible to the specific vapour under investigation and is usually classified according to the pore size. Pore size of activated carbon is classified by the International Union of Pure and Applied Chemistry (IUPAC) as micropore (pore width < 2 nm), mesopore (pore width 2-50 nm), and macropore (pore width > 50 nm) (Howe-Grant, 1992). Alternatively, activated carbon is classified on the basis of its particle size and particle shapes into two general forms i.e. powdered activated carbon (PAC) and granular activated carbon (GAC). PAC is made in particulate form as powders or fine granules less than 1.0 mm in size. GAC has a relatively larger particle size compared to PAC and consequently, presents a smaller external surface area per unit weight than PAC (Bansal *et al.*, 1988).

1.9.3 Applications of activated carbon

The applications can be classified into two categories: gas phase and liquid phase.

1.9.3.1 Gas phase applications

Activated carbon used in gas phase applications require smaller pore size than activated carbon for liquid phase application. Activated carbon for gas phase application is hard and dense granular material produced from high-density carbonaceous raw material such as coconut shell, palm kernel shell, coal, or coke (Bansal *et al.*, 1988). Gas phase application accounts for about 20% of the total use of activated carbon (Burchell, 1999). Examples of applications include solvent vapour recovery, gasoline emission control, adsorption of radionuclides, protection against atmospheric contaminants and process stream separations.

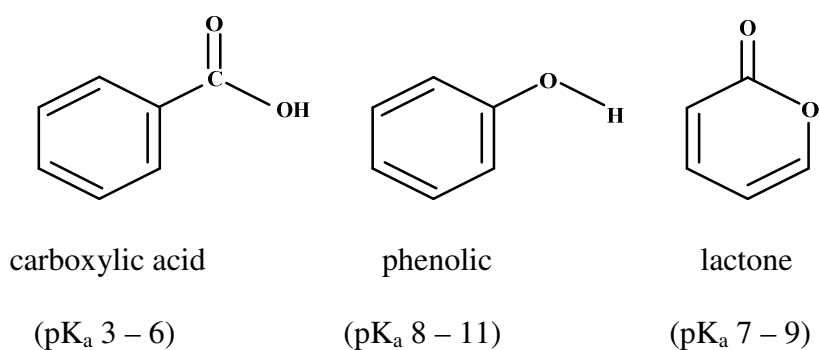
1.9.3.2 Liquid phase applications

Activated carbon used in liquid phase applications typically has a high fraction of macropores. This is to permit the liquid phase molecules to diffuse more rapidly into the rest of the pore structure. Activated carbon for liquid phase application is produced from low-density carbonaceous raw material such as sawdust, agricultural by products, and peat (Bansal *et al.*, 1988). Liquid phase application accounts for nearly 80% of the total use of activated carbon (Burchell, 1999). Examples of application include potable water treatment, groundwater remediation, industrial and municipal wastewater treatment, sweetener decolorization, chemical processing and food, beverage and cooking oil production.

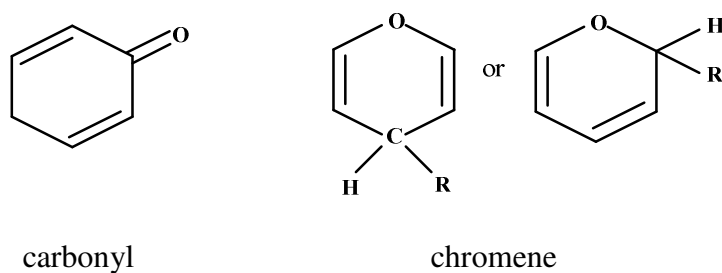
1.9.4 The surface chemistry of activated carbon

The surface chemistry of activated carbons determines their acid-base, adsorptive, hydrophilic-hydrophobic, and catalytic properties (Jankowska, Świątkowski, and Choma, 1991). It is related to the presence of surface functional groups, particularly oxygen functional groups, usually located at the edges of the

graphene layer. In addition to oxygen acidic functional groups (see Figure 1.16), the carbon surface is known to have some basic functional groups. However, some researchers (Jia and Thomas, 2000; Moreno-Castilla, López-Ramón, and Carrasco-Marín, 2000; Radovic, Silva, Ume, Menéndez, Leon, Y., Leon, C. A., and Scaroni, 1997) have reported that the basic characteristic of the carbon surface could be of an oxygen-free Lewis type associated with π electron density within the carbon plane. The content and types of oxygen functional groups incorporated on each activated carbon are different, depending on the precursors, activation method employed in the manufacturing processes and method of chemical surface modification. The activated carbon surface contains two types of surface sites: the hydrophobic sites of graphene basal plane layers and the hydrophilic functional group sites. The adsorption potential of a non-polar adsorbate is determined by both sites, whereas a polar adsorbate will preferentially adsorb initially, on the hydrophilic sites. Activated carbon, containing mainly a non-polar surface, is very useful for the adsorption of molecules of low polarity such as hydrocarbons, but generally is not adequate for the adsorption of polar molecules or inorganic charged species. However, the surface chemistry of an activated carbon can be modified, for example, by oxidation treatment in order to increase the concentration of oxygen functional groups. These groups are polar in nature and hence produce more hydrophilic or polar characteristics. This treatment will significantly enhance the adsorption capacity of activated carbon in the adsorption of polar molecules or inorganic charged species.



(a) Example of acidic oxygen functional groups



(b) Example of basic oxygen functional groups

Figure 1.16 Examples of (a) acidic and (b) basic oxygen functional groups.

1.9.5 Method of analysis of surface oxygen functional groups

Acid/base titration, pH at the point of zero charge (pH_{pzc}), and Fourier Transform Infrared spectroscopy (FT-IR) are commonly used experimental methods to characterize the surface functional groups of activated carbon.

Acid/base titration

The acid-base titration of the carbons based on Boehm's method is performed to measure the amount of oxygen functionalities of the samples. This method involves selective neutralization of acidic oxygen groups with bases of various strengths. This method assumes that the following groups become neutralized

as follows: carboxylic groups in a solution of sodium bicarbonate (NaHCO_3), carboxylic and lactonic groups in a solution of sodium carbonate (Na_2CO_3), carboxylic, lactonic, and phenolic groups in a solution of sodium hydroxide (NaOH), and carboxylic, lactonic, phenolic, and carbonyl groups in a solution of sodium ethoxide (NaOC_2H_5). Oppositely, the basic oxygen groups on activated carbon surface are determined based on reaction (protonation) with hydrochloric acid (HCl) (Boehm, 1994).

pH at the point of zero charge (pH_{pzc})

The pH_{pzc} is defined as the pH at which the activated carbon has an equal amount of positive and negative charges on the surface, resulting in a net zero charge. The pH_{pzc} is measured in order to know the surface charge on activated carbon which is a function of the pH of the solution. The activated carbon is positively charged at pH values of the solution containing activated carbon below the pH_{pzc} ($\text{pH} < \text{pH}_{\text{pzc}}$) and exhibits an anion exchange capacity (see Figure 1.17). This favors the adsorption of anionic species. If the pH of the solution equals to the pH_{pzc} ($\text{pH} = \text{pH}_{\text{pzc}}$), the surface charge of activated carbon contains a balance of positive and negative and exhibits no exchange capacity. At $\text{pH} > \text{pH}_{\text{pzc}}$, the activated carbon is negatively charged and prefers the adsorption of cationic species due to its large cation exchange capacity (Radovic *et al.*, 1997; Álvarez-Merino, Fontecha-Cámara, López-Ramón, and Moreno-Castilla, 2008).

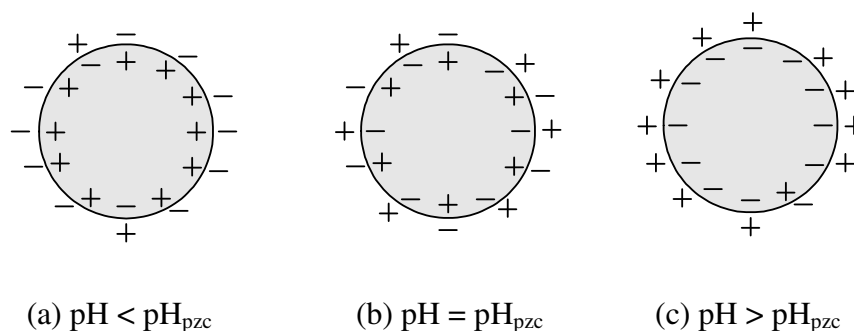


Figure 1.17 The influence of pH on surface charge: (a) $\text{pH} < \text{pH}_{\text{pzc}}$, (b) $\text{pH} = \text{pH}_{\text{pzc}}$, and (c) $\text{pH} > \text{pH}_{\text{pzc}}$ (Leon and Radovic, 1994 quoted in Rodríguez-Reinoso, 1998).

Fourier Transform Infrared spectroscopy (FT-IR)

The types of surface oxygen functional groups can be investigated by transmission infrared spectra obtained from a Fourier Transform Infrared Spectrophotometer. Fourier Transform Infrared Spectroscopy is a technique to measure the absorption of infrared light due to bond stretching or bending and thus it is able to identify various types of functional groups present on the surface of activated carbon. Some FT-IR assignments of chemical functional groups are listed in Table 1.3.

Table 1.3 Some FT-IR assignments of functional groups on carbon surfaces (Fanning and Vannice, 1993 quoted in Figueiredo, Pereira, Freitas, and Orfao, 1999; Shen, Li, and Liu, 2008).

Functional group	Assignment region (cm ⁻¹)		
	1000 – 1500	1500 – 2050	2050 – 3700
C–O in ethers (stretching)	1000 – 1300		
Alcohols	1049 – 1276		3200 – 3640
Phenolic groups:			
C–OH stretch	1000 – 1220		
O–H bend/stretch	1160 – 1200		2500 – 3620
Carbonates: carboxyl-carbonates	1100 – 1500	1590 – 1600	
aromatic C=C stretching		1585 – 1600	
Quinones		1550 – 1680	
Carboxylic acids (–COOH)	1120 – 1200	1665 – 1760	2500 – 3300
Lactones	1160 – 1370	1675 – 1790	
Carboxylic anhydrides	980 – 1300	1740 – 1880	
C–H stretch			2600 – 3000
N–H, C=N		1560 – 1570	
C–N aromatic ring	1000, 1250, 1355		
C–N	1190		
C=C=N			2040 – 2070
N–O-	1000 – 1300		

1.10 Adsorption

Adsorption is defined as the accumulation of a substance on the surface of a porous solid resulting from the interaction between the substance present in the fluid phase (gas or liquid phase) and the porous solid surface. This interaction gives rise to higher molecular density near the solid surface than in the bulk. The porous solid is called the adsorbent while adsorbate is the substance which is adsorbed.

1.10.1 Type of adsorption

There are two types of adsorption i.e. physical adsorption (physisorption) and chemical adsorption (chemisorption).

1.10.1.1 Physical adsorption

In physical adsorption, the interactions between adsorbate molecule and adsorbent surface result from the formation of relatively weak intermolecular forces such as London dispersion forces or Van der Waals's forces. There is no direct bonding and hence, physical adsorption is reversible and an exothermic process.

1.10.1.2 Chemical adsorption

Chemical adsorption is a stronger adsorption force than physical adsorption due to chemical interaction between adsorbate molecule and adsorbent surfaces. Chemical adsorption is less common than physical adsorption and, due to chemical bonds being formed, the regeneration of the adsorbent for subsequent re-use is often difficult. The general characteristics of physical adsorption and chemical adsorption are summarized in Table 1.4.

Table 1.4 General characteristics of physical and chemical adsorption (Ruthven, 1997).

Parameter	Physical adsorption	Chemical adsorption
Heat of adsorption (kJ mol^{-1})	20 - 40	> 80
Specificity	Non-specific	Very specific
Nature of adsorbed phase	Monolayer or multilayer depended on conditions	Monolayer only
Temperature range	Only significant at relative low temperatures	Possible over a wide range of temperature
Temperature dependence of uptake (with increasing temperature)	Decrease	Increase
Forces of adsorption	No electron transfer although polarization of adsorbate may occur	Electron transfer leading to bond formation between adsorbate and adsorbent
Rate of adsorption (at 273 K)	Fast	Slow
Desorption	Easy by reduced pressure or increased temperature	Difficult (high temperature required to break bonds)
Desorbed species	Adsorbate unchanged	May be different to original adsorptive
Reversibility	Rapid, nonactivated, reversible	Activated, may be slow irreversible

1.10.2 Classification of adsorption isotherms

The equilibrium relationship between the extent of adsorption (mmol/g) of adsorbent and the equilibrium partial pressure (P/P°) of adsorbate at constant temperature is usually defined in terms of an adsorption isotherm. The majority of the adsorption isotherms in physical adsorption may typically be grouped into six IUPAC classes as shown in Figure 1.18 (Rouquerol, F., Rouquerol, J., and Sing, 1999).

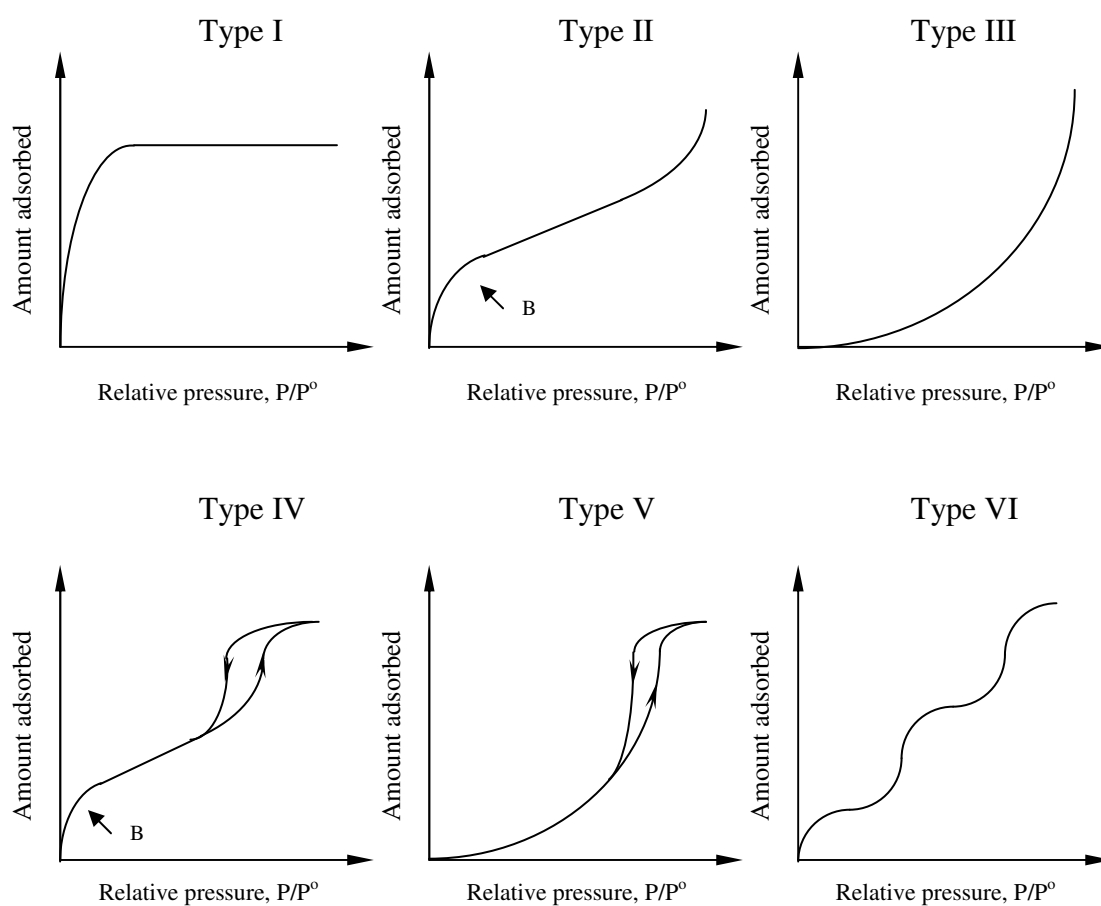


Figure 1.18 Types of adsorption isotherms according to the IUPAC classification.

Type I isotherm: This isotherm is the Langmuir Type, where only monolayer adsorption occurs and is characteristic of microporous adsorbents.

Type II isotherm: This isotherm involves the BET adsorption mechanism, that is, monolayer coverage (point B) is followed by multilayer at high relative pressures. This isotherm is characteristic of non-porous or macroporous adsorbents.

Type III isotherm: This isotherm is the result of weak adsorbent-adsorbate interactions which lead to low uptakes at low relative pressure. This type is most commonly associated with both non-porous and microporous adsorbents.

Type IV isotherm is closely related to the Type II isotherm at low relative pressure but exhibits a limit uptake and tends to level off at high relative pressure. This isotherm exhibits a hysteresis loop which is commonly associated with the presence of mesoporosity.

Type V isotherm is similar to Type III isotherm but exhibits a limit uptake at high relative pressure and there is a hysteresis loop. This isotherm associates with weak adsorbent-adsorbate interactions which is indicative of microporous or mesoporous adsorbents.

Type VI isotherm: This isotherm is associated with layer-by-layer adsorption on a highly uniform non-porous surface. The isotherm shape comes from the complete formation of monolayer before the progression to a subsequent layer. This type is relatively rare.

The aims of this research were thus to study the interaction of brazilin, brazilin with some metal ions and amino acid. The thermodynamics and kinetics of adsorption of Al-brazilin complex and Al-extracted dye complex onto silk were also

to be investigated in order to obtain the kinetic and thermodynamic parameters of dyeing. In addition, the treatment of dye effluent using activated carbons was also to be studied with a view to reducing environmental impacts.

1.11 Research objectives

- (a) To study the interaction of brazilein with some metal ions and amino acid.
- (b) To study the thermodynamics and kinetics of adsorption of Al-brazilein complex and Al-extracted dye complex onto silk.
- (c) To treat the dye effluent using activated carbons.

1.12 Scope and limitations of the study

Heartwood of *C. sappan* will be collected from Nakhon Ratchasima province, Thailand. The interaction of brazilein, brazilin with some metal ions and amino acid will be investigated by using UV-Visible spectroscopy, mass spectroscopy and then supported by computational modeling. The thermodynamics and kinetics of adsorption of Al-brazilein complex and Al-extracted dye complex onto silk will be performed using UV-Visible spectroscopy. The preparation and characterization of the original, oxidized and heat treatment activated carbons will be performed using various techniques such as the N₂ adsorption isotherm, Boehm titration, point of zero charge (pH_{PZC}) and Fourier transform infrared spectroscopy (FT-IR) and these activated carbons will also be used for the treatment of dye effluent.

1.13 References

- Álvarez-Merino, M. A., Fontecha-Cámara, M. A., López-Ramón, M. V., and Moreno-Castilla, C. (2008). Temperature dependence of the point of zero charge of oxidized and non-oxidized activated carbons. **Carbon** 46: 778-787.
- Arriagada, R., García, R., Molina-Sabio, M., and Rodríguez-Reinoso, F. (1997). Effect of steam activation on the porosity and chemical nature of activated carbons from *Eucalyptus globulus* and peach stones. **Microporous Materials** 8: 123-130.
- Bansal, R. C., Donnet, J. B., and Stoeckli, F. (1988). **Active Carbon**. New York: Marcel Dekker.
- Bechtold, T., Turcanu, A., Ganglberger, E., and Geissler, S. (2003). Natural dyes in modern textile dyehouses-how to combine experiences of two centuries to meet the demands of the future? **Journal of Cleaner Production** 11: 499-509.
- Bhat, S. V., Nagasampagi, B. A., and Sivakumar, M. (2005). **Chemistry of natural products**. New Delhi: Narosa Publishing House.
- Biniak, S., Pakula, M., Szymański, G. S., and Świątkowski, A. (1999). Effect of activated carbon surface oxygen-and/or nitrogen-containing groups on adsorption of copper (II) ions from aqueous solution. **Langmuir** 15: 6117-6122.
- Boehm, H. P. (1994). Some aspects of the surface chemistry of carbon blacks and other carbons. **Carbon** 32: 759-769.
- Burchell, T. D. (1999). **Carbon Materials for Advanced Technologies**. Netherland: Pergamon.

- Carrijo, O. A., Liz, R. S., and Makishima, N. (2002). Fiber of green coconut shell as agricultural substratum. **Brazilian Horticulture** 20: 533-535. Quoted in Pino, G. H., Mesquita, L. M. S., Torem, M. L., and Pinto, G. A. S. (2006). Biosorption of cadmium by green coconut shell powder. **Minerals Engineering** 19: 380-387.
- Chingombe, P., Saha, B., and Wakeman, R. J. (2005). Surface modification and characterization of a coal-based activated carbon. **Carbon** 43: 3132-3143.
- Choi, H. D., Shin, M. C., Kim, D. H., Jeon, C. S., and Baek, K. (2008). Removal characteristics of reactive black 5 using surfactant-modified activated carbon. **Desalination** 223: 290-298.
- Christie, R. M., Mather, M. M., and Wardman, R. H. (2000). **The Chemistry of Colour Application**. Oxford: Blackwell Science.
- Christie, R. M. (2001). **Colour Chemistry**. Cambridge: The Royal Society of Chemistry.
- Cristea, D. and Vilarem, G. (2006). Improving light fastness of natural dyes on cotton yarn. **Dyes and Pigments** 70: 238-245.
- Demirbas, E., Kobya, M., and Sulak, M. T. (2008). Adsorption kinetics of a basic dye from aqueous solutions onto apricot stone activated carbon. **Bioresource Technology** 99: 5368-5373.
- Doménech-Carbó, A., Doménech-Carbó, M. T., and Sauí-Peris, M. C. (2005). Electrochemical identification of flavonoid dyes in solid work of art samples by abrasive voltammetry at paraffin-impregnated graphite electrodes. **Talanta** 66: 769-782.

- El-Sheikh, A. H. (2008). Effect of oxidation of activated carbon on its enrichment efficiency of metal ions: Comparison with oxidized and non-oxidized multi-walled carbon nanotubes. **Talanta** 75(1): 127-134.
- Fanning, P. E. and Vannice, M. A. (1993). A DRIFTS study of the formation of surface groups on carbon by oxidation. **Carbon** 31: 721-730. Quoted in Figueiredo, J. L., Pereira, M. F. R., Freitas, M. M. A., and Orfao, J. J. M. (1999). Modification of the surface chemistry of activated carbons. **Carbon** 37: 1379-1389.
- Faria, P. C. C., Orfao, J. J. M., and Pereira, M. F. R. (2004). Adsorption of anionic and cationic dyes on activated carbons with different surface chemistries. **Water Research** 38: 2043-2052.
- Ferreira, E. S. B., Hulme, A. N., McNab, H., and Quye, A. (2004). The natural constituents of historical textile dyes. **Chemical Society Reviews** 33: 329-336.
- Gong, R., Sun, Y., Chen, J., Liu, H., and Yang, C. (2005). Effect of chemical modification on dye adsorption capacity of peanut hull. **Dyes and Pigments** 67: 175-181.
- Hojo, N. (2000). **Structure of silk yarn. Part A: Biological and physical aspects.** NH, USA: Science Publishers, Inc.
- Horrocks, A. R. and Anand, S. C. (2000). **Handbook of Technical Textiles.** Cambridge: Woodhead.
- Howe-Grant, M. (1992). **Encyclopedia of Chemical Technology.** New York: John Wiley & Sons.
- Hu, Z. and Srinivasan, M.P. (2001). Mesoporous high-surface-area activated carbon. **Microporous and Mesoporous Materials** 43: 267-275.

- Hu, Z., Srinivasan, M. P., and Ni, Y. (2001). Novel activation process for preparing highly microporous and mesoporous activated carbon. **Carbon** 39: 877-886.
- Jagtoyen, M. and Derbyshire, F. (1998). Activated carbons from yellow poplar and white oak by H₃PO₄ activation. **Carbon** 36: 1085-1097.
- Jankowska, H., Świątkowski, A., and Choma, J. (1991). **Active Carbon**. New York: Ellis Horwood.
- Jia, Y. F. and Thomas, K. M. (2000). Adsorption of cadmium ions on oxygen surface sites in activated carbon. **Langmuir** 16: 1114-1122.
- Kamel, M. M., El-Shishtawy, R. M., Yussef, B. M., and Mashaly, H. (2005). Ultrasonic assisted dyeing III. Dyeing of wool with lac as a natural dye. **Dyes and Pigments** 65: 103-110.
- Karaca, S., Gürses, A., Açıkyıldız, M., and Ejder, M. (2008). Adsorption of cationic dye from aqueous solution by activated carbon. **Microporous and Mesoporous Materials, In Press, Corrected Proof**.
- Karmakar, S. R. (1999). **Chemical technology in the pre-treatment processes of textiles**. Amsterdam: Elsevier Science B.V.
- Kavitha, D. and Namasivayam, C. (2008). Capacity of activated carbon in the removal of acid brilliant blue: Determination of equilibrium and kinetic model parameters. **Chemical Engineering Journal** 139: 453-461.
- Kongkachuichay, P., Shitangkoon, A., and Chinwongamorn, N. (2002). Studies on dyeing of silk yarn with lac dye: effects of mordants and dyeing conditions. **ScienceAsia** 28: 161-166.

- Lemmens, R. H. M. J. and Wulijarni-Soetjipto, N. (1992). **Plant Resources of South-East Asia 3: Dye and Tannin-Producing Plants**. Bogor Indonesia: Prosea.
- Leon, C. A. and Radovic, L. R. (1994). **Chemistry and Physics of Carbon**. New York: Marcel Dekker. Quoted in Rodríguez-Reinoso, F. (1998). The role of carbon materials in heterogeneous catalysis. **Carbon** 36: 159-175.
- Lewin, M. and Pearce, E. M. (1998). **Handbook of fiber chemistry**. New York: Marcel Dekker.
- Li, W., Peng J., Zhang, L., Yang, K., Xia, H., Zhang, S., and Guo, S. (2008). Preparation of activated carbon from coconut shell chars in pilot-scale microwave heating equipment at 60 kW. **Waste Management, In Press, Corrected Proof**.
- Moeyes, M. (1993). **Natural Dyeing in Thailand**. Bangkok: White Lotus.
- Molina-Sabio, M. and Rodríguez-Reinoso, F. (2004). Role of chemical activation in the development of carbon porosity. **Colloids and Surfaces A: Physicochemical and Engineering Aspects** 241: 15-25.
- Moreno-Castilla, C., López-Ramón, M. V., and Carrasco-Marín, F. (2000). Changes in surface chemistry of activated carbons by wet oxidation. **Carbon** 38: 1995-2001.
- Mozammel, H.M., Masahiro, O., and Bhattacharya, S.C. (2002). Activated charcoal from coconut shell using $ZnCl_2$ activation. **Biomass and Bioenergy** 22: 397-400.

- Nagia, F. A. and EL-Mohamedy, R. S. R. (2007). Dyeing of wool with natural anthraquinone dyes from *Fusarium oxysporum*. **Dyes and Pigments** 75: 550-555.
- Pereira, M. F. R., Soares, S. F., Órfão, J. J. M., and Figueiredo, J. L. (2003). Adsorption of dyes on activated carbons: influence of surface chemical groups. **Carbon** 41: 811-821.
- Perkins, W. S. (1996). **Textile coloration and finishing**. North Carolina: Carolina Academic Press.
- Pino, G. H., Mesquita, L. M. S., Torem, M. L., and Pinto, G. A. S. (2006). Biosorption of cadmium by green coconut shell powder. **Minerals Engineering** 19: 380-387.
- Radovic, L. R., Silva, I. F., Ume, J. I., Menéndez, J. A., Leon, Y., Leon, C. A., and Scaroni, A. W. (1997). An experimental and theoretical study of the adsorption of aromatics possessing electron-withdrawing and electron-donating functional groups by chemically modified activated carbons. **Carbon** 35: 1339-1348.
- Rouquerol, F., Rouquerol, J., and Sing, K. (1999). **Adsorption by Powders and Porous Solids**. London: Academic Press.
- Ruthven, D. M. (1997). **Encyclopedia of Separation Technology**. New York: John Wiley.
- Shen, W., Li, Z., and Liu, Y. (2008). Surface chemical functional groups modification of porous carbon. **Recent Patents on Chemical Engineering** 1: 27-40.

- Tan, I. A. W., Ahmad, A. L., and Hameed, B. H. (2008). Adsorption of basic dye on high-surface-area activated carbon prepared from coconut husk: Equilibrium, kinetic and thermodynamic studies. **Journal of Hazardous Materials** 154: 337-346.
- Tancredi, N., Cordero, T., Rodríguez-Mirasol, J., and Rodríguez, J. J. (1996). Activated carbons from Uruguayan eucalyptus wood. **Fuel** 75: 1701-1706.
- Thinakaran, N., Baskaralingam, P., Pulikesi, M., Panneerselvam, P., and Sivanesan, S. (2008). Removal of acid violet 17 from aqueous solutions by adsorption onto activated carbon prepared from sunflower seed hull. **Journal of Hazardous Materials** 151: 316-322.
- Truter, E. V. (1973). **Introduction to natural protein fibres: Basic chemistry**. London: Elek Science.
- Tsai, W. T., Chang, C. Y., Lin, M. C., Chien, S. F., Sun, H. F., and Usieh, M. F. (2001). Adsorption of acid dye onto activated carbons prepared from agricultural waste bagasse by $ZnCl_2$ activation. **Chemosphere** 45: 51-58.
- Wang, S. and Li, H. (2005). Dye adsorption on unburned carbon: Kinetics and equilibrium. **Journal of Hazardous Materials B126**: 71-77.
- Wang, S., Zhu, Z. H., Coomes, A., Haghseresht, F., and Lu, G. Q. (2005). The physical and surface chemical characteristics of activated carbons and the adsorption of methylene blue from wastewater. **Journal of Colloid and Interface Science** 284: 440-446.
- Wei, S., Li, Z., and Ya-ping, Z. (2006). Preparation of microporous activated carbon from raw coconut shell by two-step procedure. **Chinese Journal of Chemical Engineering** 14(2): 266-269.

- Wei, S., Ya-ping, Z., Liu-fang, W., Yan, S., and Li, Z. (2007). Effect of microstructure and surface modification on the hydrogen adsorption capacity of active carbons. **New Carbon Materials** 22(2): 135-140.
- Wongsooksin, K., Rattanaphani, S., Tangsathitkulchai, M., Rattanaphani, V., and Bremner, J. (2008). Study of an Al(III) complex with the plant dye brazilein from *Ceasalpinia sappan* Linn. **Suranaree Journal of Science and Technology** 15(2): 159-165.
- Yan, X., Wang, W., Xing, D., Zhao, Y., and Du, L. (2005). Development and optimization of a method for the analysis of brazilein by HPLC with electrochemical detection. **Journal of Chromatography A** 1077: 44-48.

CHAPTER II

PREPARATION AND CHARACTERIZATION OF DYE-METAL COMPLEXES AND DYE-METAL-AMINO ACID COMPLEXES

2.1 Abstract

The structure of the complex formed between Al(III) (alum) and brazilin in aqueous solution was investigated using UV-visible spectroscopy. The molar ratio method and Job's method of continuous variation were applied to ascertain the stoichiometric composition of the complex in aqueous solution. A 1:2 complex was indicated by both methods. A structure for $[Al(\text{brazilin})_2]^+$ was proposed and the calculated heat of formation of this complex, obtained by the semiempirical PM3 method, indicated that the proposed complex was a reasonable one energetically.

The structure of complexes formed between Al(III), Ga(III), and In(III) with brazilin (BE) in aqueous solution were investigated by means of electrospray mass spectrometry (ES-MS). In the full scan mass spectra, the main complex observed had a 1:2 stoichiometric ratio. When (*S*)-*N*-acetylserine methyl ester (Ser), as a partial mimic of the serine residue in silk, was added to Al:BE, Ga:BE, and In:BE complexes in aqueous solution, a new complex ion was observed in the mass spectrum corresponding to an Ser:Al:BE complex with a 1:1:1 ratio. The patterns of the mass spectra of Ga:BE, Ser:Ga:BE, In:BE, and Ser:In:BE complexes were similar to those

for the corresponding Al(III) complexes. Calculated heats of formation of potential structures of the complexes, with and without bound water, were obtained using semiempirical PM3 calculations.

2.2 Introduction

The red homoisoflavonoids, brazilin (6a*S-cis*)(7,11b-dihydrobenz[*b*]indeno-[1,2-*d*]pyran-3,6a,9,10,(6*H*)-tetrol) and brazilein (6a,7-dihydro-3,6a,10-trihydroxybenz[*b*]indeno[1,2-*d*]pyran-9(6*H*)-one) (Figure 2.1), are components of the heartwood of the tree *Ceasalpinia sappan* Linn. (family Leguminosae) (Kim, Baek, Oh, Jung, Lee, I. S., and Lee, H. K., 1997; Harborne, Baxter, and Moss, 1999; Ferreira *et al.*, 2004; Doménech-Carbó, A. *et al.*, 2005; Hulme, McNab, Peggie, and Quye, 2005; In-Kyung, Hye-Young, Ah-Reum, Eun-Kyoung, and Sang Kook, 2005). The homoisoflavonoids exhibit a flavonoid-like structure and can be classified as a subgroup of the flavonoids. Flavonoids are a group of polyphenolic compounds that are widely distributed in plants and are used as pigments (Harborne and Baxter, 1999; Doménech-Carbó, A. *et al.*, 2005).

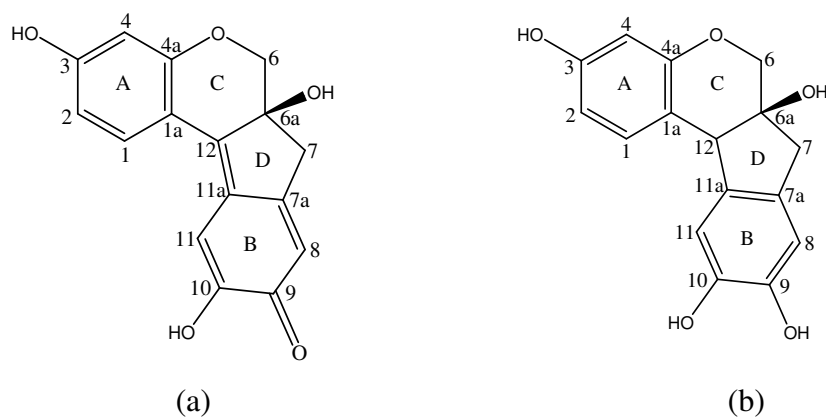


Figure 2.1 Chemical structure of (a) brazilein and (b) brazilin (Wongsooksin *et al.*, 2008).

In Thailand, especially in the Northeast, the aqueous extracts from the wood of *C. sappan* are used for the dyeing of silk (Moeyes, 1993). The extracted dyes, which are mainly composed of brazilin and brazilein, give a beautiful red or pink color to silk. However, this natural dye has poor fastness properties (wash and light fastness) and, in order to try and overcome this, metal ion-based mordants are used (Lemmens and Wulijarni-Soetjipto, 1992; Yan *et al.*, 2005). One such mordant generally used by villagers in Northeast Thailand is alum, which provide a source of Al(III) ions. Alum ($KAl(SO_4)_2 \cdot 12H_2O$) is widely used as a mordant for dyeing keratin fibers with polyphenolic dyes to improve the fastness properties (Ferreira *et al.*, 2004). The ability of metal ions to form very stable metal-dye complexes is used to produce dyed protein fibers with improved fastness properties, especially towards washing and light (Christie, 2001). However, problems with fastness in silk fabric dyed with vegetable dyes and metal ion mordant, including changed on UV light exposure still persist (Urabe and Yanagisawa, 1988). Therefore deeper studies on the molecular basis of the dye-mordant-silk interaction is required in order to help solve the fastness problems.

A number of studies have been reported on the dye-metal ion mordant interactions. These have included work on spectroscopic and structural analysis of complexes of some homoisoflavonoids and some flavonoids with metal ions (Kanazawa, 1991; Boudet, Cornard, and Merlin, 2000; Cornard, Boudet, and Merlin, 2001; Cornard and Merlin, 2001; Cornard and Merlin, 2002; Frenandez, Mira, Florêncio, and Jennings, 2002; Castro and Blanco, 2004; Souza and Giovani, 2005).

Kanazawa (1991) investigated conformational and spectroscopic properties of aluminium (III) complexes of extracted dyes from the heartwood of *Ceasalpinia sappan* Linn. and showed through spectrophotometric methods that the complex between aluminium (III) ion and brazilein had 1:1, 1:2, and 1:3 stoichiometries in ethanol-water solution. The main sites of Al (III) binding to brazilein are shown in Figure 2.2.

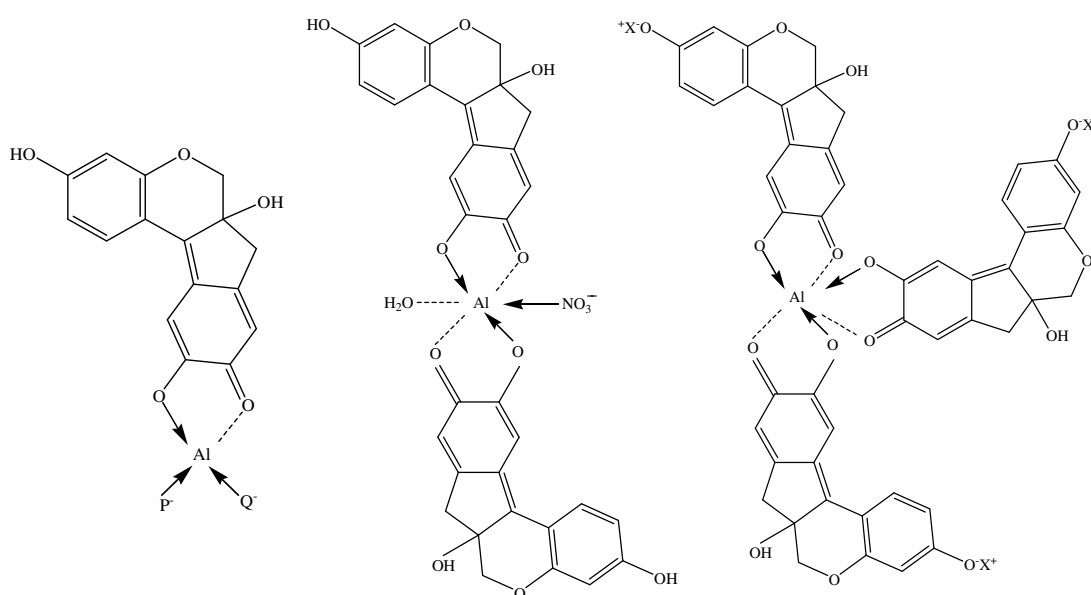


Figure 2.2 Molecular models of Al(III) complexation with brazilein (P^- and Q^- represent anions such as NO_3^- ions or brazilein molecules and X^- represents H) (Kanazawa, 1991).

Boudet *et al.* (2000) studied conformational and spectroscopic aspects of 3-hydroxyflavone (3HF)-aluminium chelates and showed that the 3-hydroxyflavone molecule formed an $Al(3HF)_2$ complex in pure methanol.

The complex formation between aluminium chloride and 3'4'-dihydroxyflavone (3'4'diOHF) in methanol was studied using UV-Vis and Raman spectroscopies combined with quantum chemical calculations (Cornard *et al.*, 2001). Job's method of continuous variation and the molar ratio method were applied to ascertain the stoichiometric composition of the chelate in pure methanol. A 1:1 complex was indicated by both the methods.

Cornard and Merlin (2001) reported a structural and spectroscopic investigation of 5-hydroxyflavone (5HF) and its complex with aluminium. The complex in methanol with a stoichiometry of 1:1 of 5HF with Al(III) was reported.

The complex formation between Al (III) and quercetin (Q) in methanol was studied by a combination of spectroscopic measurements and quantum chemical calculations (Cornard and Merlin, 2002). Quercetin presented in its structure three possible competitive chelating sites. UV-Vis spectroscopy showed the successive formation of two complexes of stoichiometry Al(III):Q of 1:2 and 2:1.

An electrospray mass spectrometric study of iron and copper ion complexing with flavonoids was also investigated (Frenandez *et al.*, 2002). It was found that complexes with a range of stoichiometries of metal:flavonoid of 1:1, 1:2, 2:2, and 2:3 were observed. This mass spectrometric technique together with collisionally activated dissociation (tandem mass spectrometry) was also used to characterize aluminium (III) complexes with a series of flavonoid glycosides. In these cases the preferred aluminium complexation resulted in a 1:2 aluminium (III) :flavonoid stoichiometry (Zhang, Wang, and Brodbelt, 2005). In addition, electrospray ionization mass spectrometry was also successfully used to detect aluminium and gallium

complexes of the flavonoid plant dye, morin (Septhum, Morgan, Hick, Bremner, Rattanaphani, S., and Rattanaphani, V., 2007).

The structure, stability and molar absorptivity of the complex formed between aluminium chloride and 5,7-dihydroxyflavone in methanol was investigated using UV-Vis spectroscopy and the semi-empirical AM1 method (Castro and Blanco, 2004). The molar ratio method and Job's method of continuous variation were applied to ascertain the stoichiometric composition of the complex in methanol at constant ionic strength. A 1:2 complex was indicated by both methods.

The synthesis, electrochemical and spectral (UV-Vis, $^1\text{H-NMR}$, IR, and fluorescence) properties as well as thermal behaviour of Al(III) and Zn(II) complexes with the flavonoids quercetin (H_2L^1), rutin (H_2L^2), and galangin (HL^3) was reported by Souza and Giovani (Souza and Giovani, 2005). These studies indicated that the complexes may be formulated as the following six forms: $[\text{Al}_2(\text{L}^1)(\text{H}_2\text{O})_8]\text{Cl}_4$, $[\text{Al}_3(\text{L}^2)_2(\text{H}_2\text{O})_{12}]\text{Cl}_5$, $[\text{Al}(\text{L}^3)(\text{H}_2\text{O})_4]\text{Cl}_2$, $[\text{Zn}_2(\text{L}^1)(\text{H}_2\text{O})_4]\text{Cl}_2$, $[\text{Zn}_3(\text{L}^2)_2(\text{H}_2\text{O})_6]\text{Cl}_2$, and $[\text{Zn}(\text{L}^3)(\text{H}_2\text{O})_2]\text{Cl}$.

As noted earlier, studies on the interaction between the crude dye extracted from *C. sappan* and various metallic ions, together with potential structures of the complex between the dye and Al(III) in ethanol-water solution have been previously described. However, the stoichiometry of the complex formed between Al(III) ion from alum with pure brazilein and Al(III) ion with extracted dye in aqueous solution have not been determined. As part of our studies aimed at a better molecular understanding of mordant-natural dye interactions in this study, we prepared pure brazilein by separate oxidation of extracted brazilin and then investigated the stoichiometric composition of the complex formed between brazilein and alum in

aqueous solution with and without pH control. The molar ratio method was used for the spectrophotometric determination of the complex composition and Job's method was applied to confirm the results obtained with the molar ratio method. Together with this, comparative studies with the related Ga(III) and In(III) ions were also undertaken.

Another aspect of this investigation involved the use of positive ion electrospray mass spectrometry (ESI-MS) in order to gain further information on metal ion-brazilein complexing. This involved Al(III) and comparative studies with the related Ga(III) ion with similar complexing ability. The two stable isotopes of Ga [^{71}Ga (39.9%) and ^{69}Ga (60.1%)] were anticipated to assist with the specification of metal ion-containing complex peaks by ESI-MS. This study was also extended to a preliminary exploration of potential interactions of the metal ion-homoisoflavonoid complexes with the silk protein fibers, the study of complexing of a serine analog with the complexes by ESI-MS, and associated molecular modeling. Serine is a significant component of silk protein (Kaplan, Adam, Farmer, and Viney, 1994; Karmakar, 1999) and is a possible site for Al(III) mordant complexing through the primary hydroxyl group in its side chain. A semi-mimic of the serine residue, (*S*)-*N*-acetylserine methyl ester (Ser) (Figure 2.3), was thus used in these initial complexing studies by ESI-MS, the results of which are presented in this chapter.

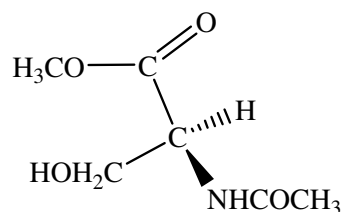


Figure 2.3 Chemical structure of (*S*)-*N*-acetylserine methyl ester (Ser).

2.3 Experimental

2.3.1 Chemicals

- (a) Brazilein (prepared by oxidation of brazilin using iodine solution)
- (b) Brazilin (separated from the crude aqueous extract from heartwood of *C. sappan*)
- (c) Aluminium potassium sulfate; alum ($\text{KAl}(\text{SO}_4)_2 \cdot 12\text{H}_2\text{O}$) (MW 474.38), UNIVAR
- (d) Aluminium nitrate ($\text{Al}(\text{NO}_3)_3 \cdot 9\text{H}_2\text{O}$) (MW 375.14) 99.997%, Aldrich
- (e) Gallium nitrate ($\text{Ga}(\text{NO}_3)_3 \cdot x\text{H}_2\text{O}$) (MW 255.74) 99.999%, Aldrich
- (f) Indium nitrate ($\text{In}(\text{NO}_3)_3 \cdot 5\text{H}_2\text{O}$) (MW 390.92) 99.99%, Aldrich
- (g) (*S*)-*N*-acetylserine methyl ester (MW 161.16) Purity > 99%, BACHEM
- (h) Methanol HPLC grade, UNICHROM

2.3.2 Instruments

- (a) Analytical Thin Layer Chromatography (TLC) and Column Chromatography

Analytical (TLC) was performed by using aluminium backed sheets of Merck Silica Gel 60 F₂₅₄ containing a fluorescent indicator and a UV lamp (254 nm) to identify compounds on the plate. Column chromatography was performed using Merck Kiesel Gel 60 F₂₅₄ (230-400 mesh) silica gel, with all solvent mixtures quoted as volume ratios.

(b) ^1H - and ^{13}C -Nuclear Magnetic Resonance (NMR) Spectra

All nuclear magnetic resonance (NMR) spectroscopy was performed on a Varian Unity 500 MHz spectrometer. Proton NMR (^1H -NMR) spectra and carbon NMR (^{13}C -NMR) spectra were acquired at 500 and 125 MHz respectively. Spectra for brazilin was recorded in ^6d -acetone (CD_3COCD_3) with 0.05% tetramethylsilane (TMS) and for brazilein was recorded in ^6d -dimethyl sulfoxide (CD_3SOCD_3), obtained from Cambridge Isotope Laboratories Inc., TMS was used as the internal standard.

(c) An Agilent 8453 UV-Vis spectrophotometer was employed for absorbance measurements using quartz cells of path length 1 cm.

(d) A pH meter (Schott) was used to measure the pH values of dye solutions.

(e) A Reichert melting point apparatus was used to determine melting points. Temperatures are expressed in degrees Celsius ($^{\circ}\text{C}$) and melting points are uncorrected.

(f) A Jasco digital polarimeter DIP-370 was used to determined optical rotations.

(g) Electrospray mass spectrometry

A Thermo Finnigan LTQ quadrupole ion trap (QIT) instrument equipped with an electrospray ionization (ESI) source was used. The flow-rate of the solutions was set at $10\ \mu\text{L}\ \text{min}^{-1}$. The heated capillary temperature was kept at 275°C . The ESI spray voltage was set at +4.5 kV. The injection time was set at 50 ms. The other instrumental parameters were tuned to optimize the relative abundance of the aluminium-brazilein, gallium-brazilein or indium-brazilein complex. All spectra were

obtained in the positive mode. The scan mode was positive and the isolation width for MS^n was 1.0-6.0 Da.

(h) High-resolution mass spectrometry

High-resolution mass spectrometry for the determination of the accurate masses of the complexes was performed on QTOF Ultima fitted with a lockspray source. Samples were loop injected (10 μ L) using 50% aqueous acetonitrile (v/v). The mass scale was calibrated with polyethylene glycol (PEG) and masses compared with a leucine enkephalin lock mass (m/z 566.2771).

(i) Computational modeling

Computational modeling was performed on a Silicon Graphics Fuel processor using PC Spartan Pro software (Wavefunction, Irvine, Ca). Lowest energy conformers were determined by molecular modeling using MMFF94 force fields. The equilibrium geometries of the lowest energy conformers were then optimized using semiempirical PM3 calculations.

2.3.3 Experimental methods

2.3.3.1 Extraction of dye

The heartwood of *C. sappan* was obtained from a plantation area in Nakhon Ratchasima province, Thailand; a herbarium specimen No. KW001 (SUT) of the plant is lodged in the Chemistry Laboratory, Suranaree University of Technology, Nakhon Ratchasima. The dried heartwood (200 g) of *C. sappan* was chopped into small pieces (0.3 x 3 cm), and extracted with boiling deionized water (2 L). In the standard procedure the ratio of mass of material (gram) to the volume (milliliter) of liquid was 1:10; extraction was performed for 60 minutes at 80-95°C. The aqueous extract was removed by filtration and was concentrated using a vacuum

rotary evaporator and then freeze-dried in a vacuum freeze-dryer to give crude extracted dye powder (13% w/w) which was then used without further treatment.

2.3.3.2 Separation of Brazilin from Crude Extract of *C. sappan*

The crude dye extract (500 mg) was dissolved in methanol and pre-adsorbed on silica gel. Column chromatography on silica gel using volume ratio of CHCl_3 :MeOH (15:1 to 7:1) as eluant gave brazilin as a crystalline reddish solid (100 mg; 20% based on the crude extract) (Kim *et al.*, 1997; Oliveira, Edwards, Velozo, and Nesbitt, 2002). The results from characterization of brazilin using mass spectroscopy, melting point and polarimetry were: **LRMS (EI)** : m/z 286 [M^+], **LRMS (ES)** : m/z 285 [MH^+ for brazilein], **HRMS (EI)** : 286.0839, Calc for $\text{C}_{16}\text{H}_{14}\text{O}_5$, 286.0841, **mp.** : 127-131°C (Lit. 145-149°C, Kim *et al.*, 1997), $[\alpha]_D^{23}$: +69.8 (c 2.65 x 10⁻³, DMSO).

2.3.3.3 Oxidation of Brazilin to Brazilein

Brazilin (100 mg) was dissolved in the minimum quantity of warm ethanol (*ca* 0.5 mL), mixed with hot deionized water (8 mL), and the clear solution was cooled down to 60-70°C. A solution (1.6 mL) of iodine (33.8 g of iodine in 42.5 mL of ethanol) was added, and the mixture allowed to remain overnight at room temperature. The brazilein precipitated as a dark colored powder. The precipitate was collected by filtration, washed with cold deionized water and then warm ethanol, and finally dried at room temperature as a deep reddish-black solid of brazilein (42 mg; 42% based on brazilin and 8.4% based on the crude extract) (Engels, Perkin, and Robinson, 1908).

2.3.3.4 Determination of the stoichiometric ratio for brazilein with Al(III) ion

The molar ratio method and Job's method were used to determine the composition of the Al(III) complex in solution by spectrophotometric means. For the molar ratio method, the brazilein stock solution (2.5×10^{-4} M) was prepared in methanol. Alum stock solution (2.5×10^{-4} M) was prepared in deionized water. A concentration of 5.0×10^{-5} M of brazilein in water was diluted from the stock solution and kept constant, while the alum concentration was varied from 0 to 2.0×10^{-4} M. In order to verify the results obtained from the molar ratio method, the complex stoichiometry was also determined by Job's method. A series of solutions was prepared by keeping constant the total concentration of brazilein and alum, but their proportions were continuously varied by using the different volumes of brazilein (5.0×10^{-5} M) and alum (5.0×10^{-5} M) solutions. After initial mixing of the solutions, the time of 30 minutes was necessary to reach the complexation equilibrium. After this time, the absorption spectrum of each solution was recorded on an Agilent 8453 UV-Vis spectrophotometer with quartz cells of 1 cm path length. For the experiments involving pH control of the solution, an acetic acid-acetate buffer was used as a buffer solution.

2.3.3.5 Effect of alum concentration on brazilein in aqueous solution

A concentration of 2.5×10^{-5} M, 5.0×10^{-5} M, 7.5×10^{-5} M of brazilein was diluted from stock solution and kept constant whereas alum was varied from 0 to 30.0×10^{-5} M of each concentration of brazilein. In order to reach the complexation equilibrium, the solution was allowed to stand at room temperature for

30 minutes. The absorbance of each solution was then recorded at 509 nm using an Agilent 8453 UV-Vis spectrophotometer.

2.3.3.6 Determination of the amount of brazilein dye in crude extracted dye

Stock extracted dye (1000 mg/L) was prepared in deionized water. In order to estimate the amount of brazilein dye in crude extracted dye, crude extracted dye 100 mg/L from the stock solution was mixed with alum (100 mg/L). The alum-extracted dye mixture was analysed by measurement of the λ_{\max} using Agilent 8453 UV-Vis spectrophotometer. The amount of brazilein dye in crude extracted dye was determined by using an alum-brazilein calibration curve.

2.3.3.7 Sample preparation for ESI-MS

The stock solutions were prepared as follows: 1.0×10^{-3} M brazilein and 1.0×10^{-3} M (*S*)-*N*-acetylserine methyl ester in methanol, 1.0×10^{-3} M alum, aluminium nitrate, gallium nitrate and indium nitrate in water. The solution of brazilein was mixed with separate solutions of alum, aluminium nitrate, gallium nitrate and indium nitrate in 10 mL volumetric flasks and the volume adjusted with 50% methanol/water in each case to give a 2:1 mole ratio; the final concentration of the sample was 300 μ M. Pre-mixed solutions of brazilein-alum, brazilein-aluminium nitrate, brazilein-gallium nitrate, or brazilein-indium nitrate were each added to separate solutions of (*S*)-*N*-acetylserine methyl ester in 10 mL volumetric flasks and the volume adjusted with 50% methanol/water in each case to give a 2:1:2 mole ratio of components.

2.4 Results and discussion

2.4.1 Properties of Brazilein

The EI mass spectrum of brazilein showed an $[M]^+$ ion at m/z 284 (HRMS (EI): 284.0678, Calc for $C_{16}H_{12}O_5$, 284.0685). The UV-visible spectrum showed prominent maximum absorptions at 446 and 541 nm (DMSO). The melting point was 249-253°C (dec.) (Lit. 260-265°C (dec.), Kim *et al.*, 1997) and the specific optical rotation value was $[\alpha]_D^{23} -1,126$ (c 2.90 x 10⁻³, DMSO). The ¹H- and ¹³C-NMR spectroscopic data (Table 2.1 and 2.2; comparative data for brazilin is also given in these Tables) and HMBC correlations (Figure 2.4) confirmed the structure and were in good agreement with the literature data (Kim *et al.*, 1997).

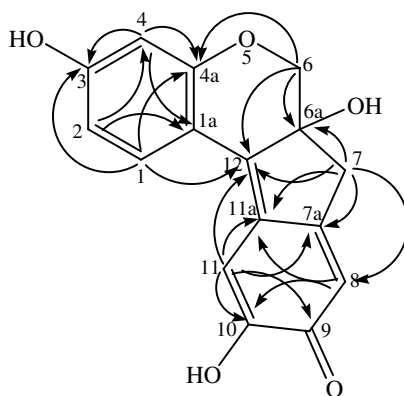


Figure 2.4 HMBC correlations of brazilein.

Table 2.1 ^1H -NMR data of brazilin and brazilein (500 MHz).

^1H	Brazilin	Brazilein
	(δ , acetone- d_6)	(δ , DMSO- d_6)
1	7.17, 1H, d, $J = 8.3$	7.79, 1H, d, $J = 8.5$
2	6.47, 1H, d, $J = 8.3$	6.54, 1H, d, $J = 8.5, 2.1$
4	6.28, 1H, s	6.34, 1H, d, $J = 2.1$
6	3.92, 1H, d, $J = 11.2$	3.99, 1H, d, $J = 11.7$
	3.70, 1H, d, $J = 11.2$	4.45, 1H, d, $J = 11.7$
7	2.98, 1H, d, $J = 15.6$	2.84, 2H, s
	2.80, 1H, d, $J = 15.6$	
8	6.63, 1H, s	6.31, 1H, s
11	6.76, 1H, s	7.09, 1H, s
12	3.95, 1H, s	

Table 2.2 ^{13}C -NMR data of brazilin and brazilein (125 MHz).

^{13}C	Brazilin	Brazilein
	(δ , acetone-d ₆)	(δ , DMSO-d ₆)
1	131.3	130.6
1a	114.8	111.0
2	109.1	110.9
3	154.7	162.3
4	103.2	102.9
4a	157.0	157.8
6	70.0	73.0
6a	77.0	74.3
7	42.1	39.7
7a	130.7	159.1
8	111.9	117.6
9	144.5	179.5
10	144.2	152.4
11	111.6	104.2
11a	136.5	126.1
12	50.4	151.7

2.4.2 UV-Visible spectra of dyes in aqueous solution and at pH 4.5

The UV-Vis spectrum of brazilein in aqueous solution (Figure 2.5) showed three major absorption bands with wavelength maxima at 446 nm (band I), 541 nm (band II) and 276 nm (band III) respectively. Band I is considered to be associated with the absorption due to the B-ring in the cinnamoyl system, and band III with the absorption involving the A ring system. It was found that increasing the alum concentration decreased the absorbance of band I (446 nm) and also resulted in the appearance of a new band at 509 nm.

The effect of alum concentration on the visible spectra (λ_{max}) of brazilein without pH control is shown in Figure 2.5 and indicated a large bathochromic shift of 63 nm in band I of brazilein; the intensity of this new band at 509 nm increased with increasing concentration of alum. The bathochromic shift occurs on complexing to the aluminium ion through the lone pair of electrons present on the O donor atom. This electron pair donation stabilizes the excited state relative to the ground state leading to longer wavelength absorption maxima (Christie, 2001; Zollinger, 2003). Absorption spectra of brazilein in aqueous solution at pH 4.5 with different concentrations of alum were similar to absorption spectra of brazilein and alum in aqueous solution without pH control and are not shown in this thesis.

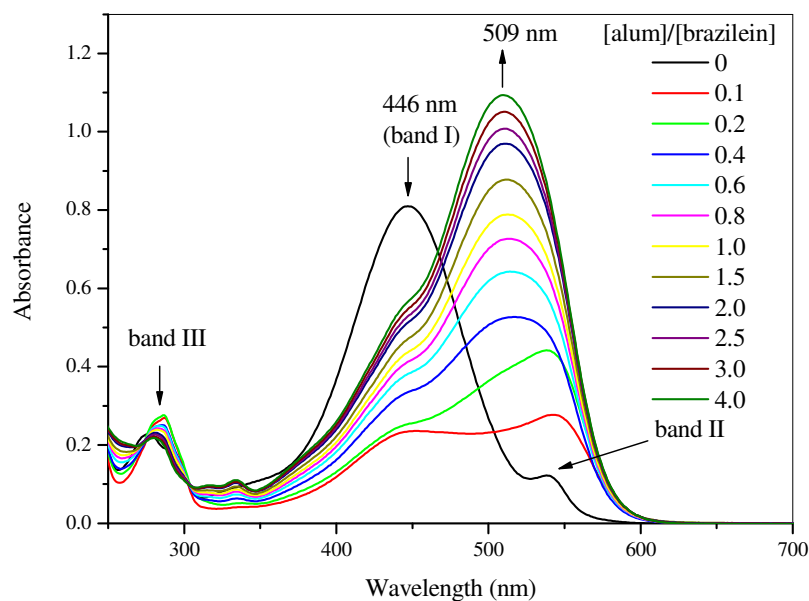


Figure 2.5 Electronic absorption spectra of brazilin (5.0×10^{-5} M) in aqueous solution in the absence and in presence of alum (0 - 2.0×10^{-4} M).

There are a number of particular technical advantages associated with the formation of colored metal complexes. Generally, the metal complexes of organic ligands exhibit light fastness properties better than those of the free ligands. This is due to the effect of coordination with a metal ion reducing the electron density at the chromophore, which in turn leads to improved resistance to photochemical oxidation. In addition, the larger size of the metal ion complex molecules compared with the free ligand generally gives rise to better wash fastness properties through stronger interactions with the fibers (Christie, 2001).

2.4.3 Complex stoichiometry of brazilein and alum in aqueous solution and at pH 4.5

In this study, the stoichiometry of the complex was determined by using the molar ratio and Job's methods. The molar ratio plots at 509 nm (λ_{\max} of complex) is shown in Figure 2.6. An inflection in the molar ratio was observed at 0.50, indicating a stoichiometric ratio of 1:2 for the Al:brazilein complex. The Job plot at 509 nm (Figure 2.7) showed an inflection at 0.66 mole fraction of brazilein, indicative of a 1:2 Al:brazilein complex in agreement with the determination from the molar ratio method, which high molar absorptivity ($14,343.7 \text{ L mol}^{-1} \text{ cm}^{-1}$). From this stoichiometric ratio, a possible structure for the complex between brazilein and Al(III) ion is proposed, with an oxygen atom of the 9-carbonyl group and the anion produced by deprotonation of the 10-hydroxyl group, forming a chelate compound with the Al(III) ion as illustrated in Figure 2.8. Kanazawa (1991) also suggested a 1:2 Al:brazilein chelate (with water and nitrate ion as co-ligands) as one of three possible complexes from the crude aqueous extract of *C. sappan* heartwood with Al(III).

Kanazawa (1991) investigated conformational and spectroscopic properties of aluminium (III) complexes of extracted dyes from the heartwood of *Ceasalpinia sappan* Linn. He found that, the complex between aluminium (III) ion (from aluminium(III) nitrate) and brazilein had 1:1, 1:2, and 1:3 stoichiometries in ethanol-water solution, but from above mentioned, showed only 1:2 stoichiometric in water solution. This might be due to the solvent effect and source of aluminium (III) ion.

When the pH of Al(III)/brazilein solution was maintained at 4.5, it was found that the stoichiometric composition of the complex could not be determined

from the molar ratio method. This might be due to the fact the constant H^+ concentration at the buffered pH of 4.5 suppresses the coordination properties of brazilein.

Al(III) ion has a coordination number of six and forms a complex with an octahedral configuration. In the case of brazilein, we propose that it coordinates as two bidentate ligands via the ionized 10-hydroxyl group and 9-carbonyl oxygen to Al(III), with two water molecules acting as co-ligands to complete the octahedral arrangement. The proposed structure of the Al-brazilein complex is shown in Figure 2.8. Computer-based molecular modeling was also carried out on this proposed structure of the complex by semiempirical PM3 calculations. Water molecules were added to maintain an octahedral environment for the complex ion. A heat of formation of $-1,545.7 \text{ kJ mol}^{-1}$ for the complex with H_2O molecules as co-ligands was found, consistent with a stable complex.

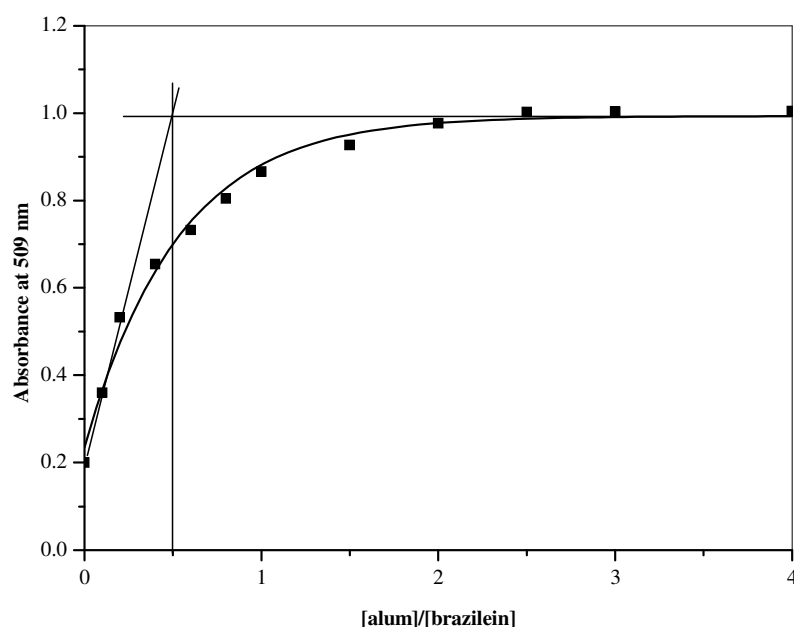


Figure 2.6 Absorbance versus [alum]/[brazilein] molar ratios plots at 509 nm.

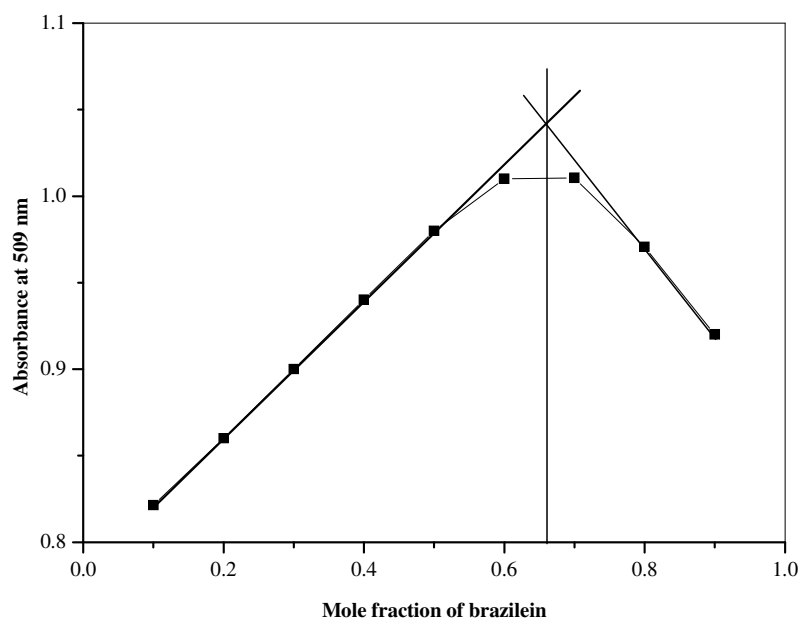


Figure 2.7 Absorbance versus the mole fraction of brazilin at 509 nm.

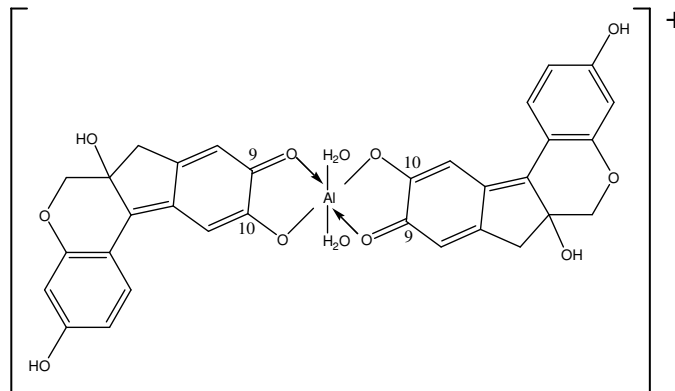


Figure 2.8 The proposed structure of the $[\text{Al}(\text{brazilin})_2]^+$ complex.

2.4.4 Effect of alum concentration on brazilin in aqueous solution

Brazilin and brazilin are components of the heartwood of the tree *C. sappan* but brazilin is readily converted to brazilin by exposure to atmospheric oxygen and light. An adsorption study on silk of brazilin and extracted dye from heartwood of *C. sappan* will be discussed in Chapter III. In order to minimize the

ratio of alum-brazilein, optimization of the amount of alum used for dyeing was studied. Alum was mixed with brazilein solutions at different brazilein concentrations ($2.5\text{-}7.5 \times 10^{-5}$ M). It was found that the absorbance of the alum-brazilein complex at a wavelength of 509 nm still kept increasing with increased alum concentration at the ratio $[\text{alum}]/[\text{brazilein}]$, 1:1 (dotted line in Figure 2.9) and started to plateau at $[\text{alum}]/[\text{brazilein}]$ 2:1 stoichiometry in $2.5\text{-}7.5 \times 10^{-5}$ M brazilein concentrations (solid line in Figure 2.9). Therefore, the alum-brazilein complex at $[\text{alum}]/[\text{brazilein}]$ 2:1 stoichiometry was then used to study the kinetics and thermodynamics of the adsorption process (Chapter III).

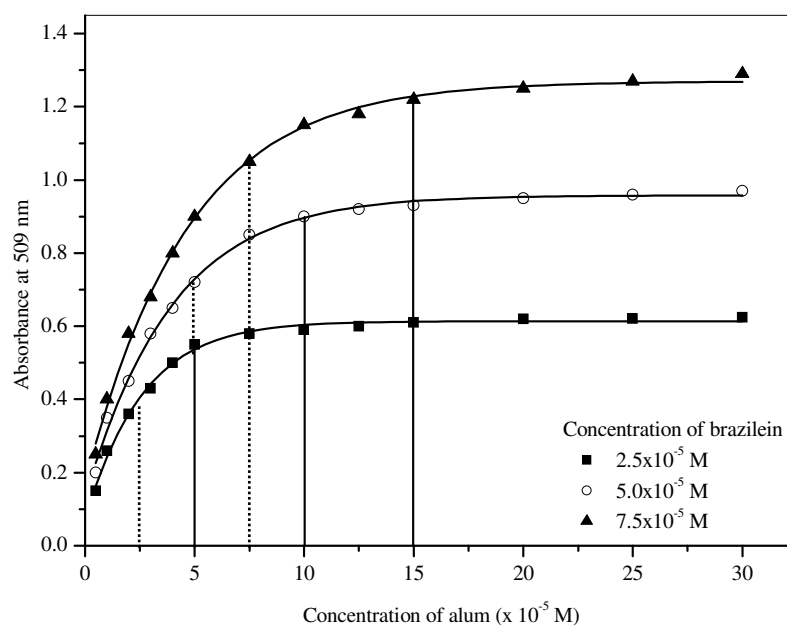


Figure 2.9 The effect of alum concentrations on brazilein in aqueous solution (pH 3.8-5.5). The dotted line is the $[\text{alum}]/[\text{brazilein}]$, 1:1 complex. The solid line is the $[\text{alum}]/[\text{brazilein}]$, 2:1 complex.

2.4.5 Determination of the amount of brazilein in crude extracted dye

As a prelude to later studies it was necessary to determine the amount of brazilein in the crude extracted dye. This was done on the basis of Al(III) ion complex formation. Several techniques have been employed to determine aluminium in complexes in water samples such as UV-Vis spectrophotometry, atomic spectrometry, inductively coupled plasma/mass spectrometry (ICP/MS), flow injection with spectrofluorimetric detector, voltammetry, potentiometry and fluorometry. (Wang, Lei, Bi, Gan, and Wei, 2001; Arancibia and Muñoz, 2007; Fernández, Villanueva, Diego, Arana, and Madariaga, 2008; Arvand and Asadollahzadeh, 2008; Kara, Fisher, and Hill, 2008; Sang, Liang, and Du, 2008). Flavonoids such as morin and quercetin can also be used to selectively form a complex with Al(III) and have been widely used as reagents for both fluorometric, spectrophotometric and chromatographic determinations (Ahmed and Hossan, 1995; Lian, Kang, Bi, Arkin, Shao, Li, Chen, Dai, Gan, and Tian, 2004). As mentioned in Chapter I, *C. sappan* contain mainly brazilein dye, and estimation of the amount of brazilein in the crude extracted dye from *C. sappan*, was undertaken via UV-vis spectrophotometric determination of the alum-brazilein complex.

Crude extracted dye 100 mg/L alone and the alum-extracted dye mixture were analysed by measurement of the appropriate λ_{\max} values by UV-Vis spectrophotometry. It was found that the λ_{\max} values of extracted dye alone and alum-extracted dye were 446 and 509 nm (Figure 2.10), respectively. In addition, the absorbance at 509 nm of 100 mg/L of alum-extracted dye was 0.47052, which indicated about 9% brazilein in this extract (Figure 2.11), assuming Beer's Law was followed and no other interfering absorbing species at this wavelength were present.

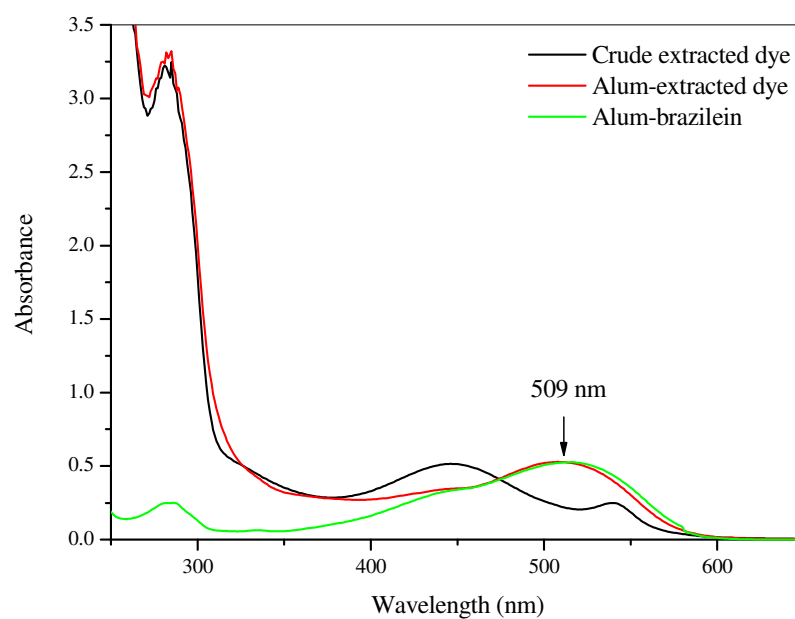


Figure 2.10 UV-Vis spectra of crude extracted dye (100 mg/L), alum-extracted dye and alum-brazilein in water.

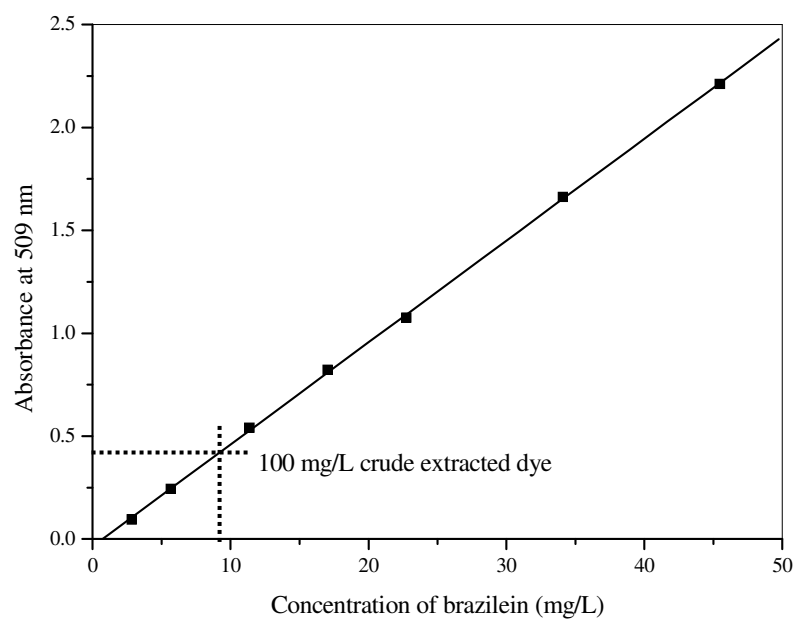


Figure 2.11 Estimation of the amount of brazilein in the crude extracted dye.

2.4.6 Electrospray mass spectrometry analysis

In the context of attempting to gain further molecular information on possible complexing modes of brazilin and brazilein with metal ion mordants, analysis of the solutions of the complexes by positive ion ESI-MS was undertaken. Even though this give a information on complex species in the gas phase and without solvent ligands attached, possible inferences on solution phase speciation may still be realized. Aluminium (III), gallium (III) and indium (III) were used to form complexes with brazilein and brazilin (Figure 2.1) in methanolic aqueous solution. (*S*)-*N*-acetylserine methyl ester was mixed with aluminium-, gallium-, indium-brazilin, and aluminium-, gallium-, and indium-brazilein solution. The chemical structure of brazilin, brazilein and (*S*)-*N*-acetylserine methyl ester can be found in Figure 2.3 The positive scan mode was used throughout the mass spectrometric experiments. In order to elucidate the structure of the complexes and the fragmentation mechanism of aluminium-, gallium-, indium-brazilin, aluminium-, gallium-, and indium-brazilein complexes, multistage tandem mass spectrometry was performed to produce abundant fragments. As well as this high resolution ESI-MS was utilized to determine molecular formulae for the complex ions in the gas phase.

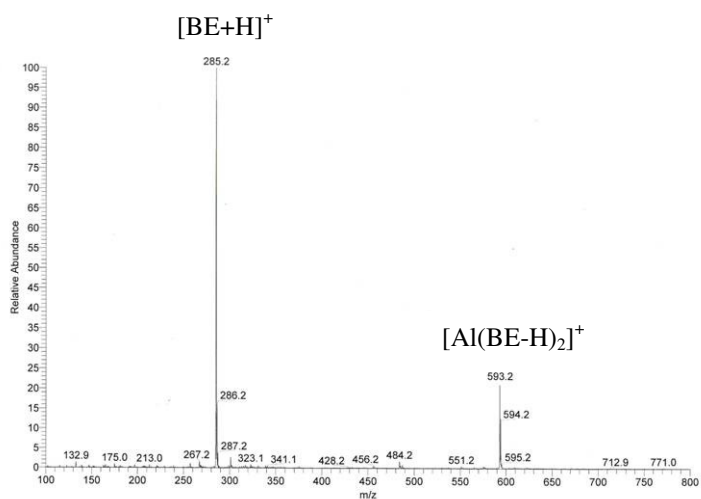
Throughout this section, brazilin, brazilein, aluminium(III), gallium (III) and indium(III) ions are referred to as BI, BE, Al, Ga, and In respectively, and (*S*)-*N*-acetylserine methyl ester is referred to as Ser for simplicity.

2.4.6.1 Brazilin complexes

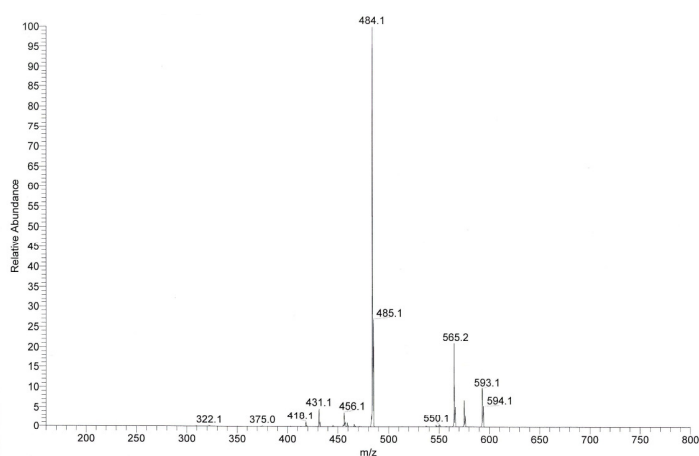
2.4.6.1.1 Al:BI and Ser:Al:BI complexes (Source of the

Al(III) ion: alum)

The full-scan ESI-MS of the Al and BI solution is shown in Figure 2.12(a). A peak was observed at m/z 593 and this was ascribed to the ion $[\text{Al}(\text{BE}-\text{H})_2]^+$ (BI being oxidized *in situ* to BE) for the complex. In order to obtain more structural information on the Al:BI complexes further analysis using multistage mass spectrometry (MS^n) was performed. Two ions at m/z 565 and 484 were present in the MS^2 spectrum of m/z 593 (Figure 2.12(b)). The ion at m/z 565 is most likely from the neutral loss of CO (-28 Da) and the ion at m/z 484 from the loss of $\text{C}_6\text{H}_5\text{O}_2$ (-109 Da) from the brazilein component.



(a)

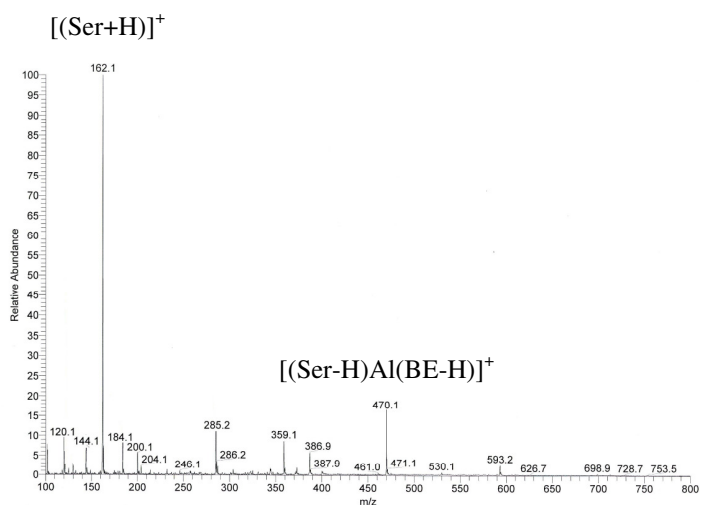


(b)

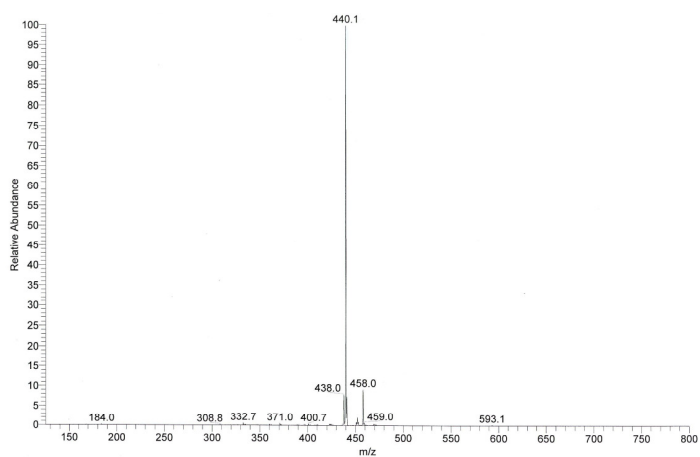
Figure 2.12 (a) Full scan mass spectrum of the Al:brazilin complex, (b) MS² spectrum of the m/z 593 ion in Figure 2.12(a).

The full-scan ESI mass spectrum of the Ser, Al and BI solution is shown in Figure 2.13(a). A peak was observed at m/z 470 and this was ascribed to the ion $[(\text{Ser-H})\text{Al}(\text{BE-H})]^+$ from the complex (with BI oxidation in Al(III) to BE). Multistage tandem mass spectrometry (MSⁿ) was also used to study these complexes.

Two daughter ions at m/z 458 and 440 were present in the MS^2 spectrum of m/z 470 (Figure 2.13(b)). The ion at m/z 458 is of some interest. Loss of a 12 Da fragment from m/z 470 is highly doubtful, and it is more likely that this ion arises from addition of water (18 Da) to the daughter ion at m/z 440 prior to electronic detection. Such addition of water to a precursor ion has been observed previously, for example, in the ESI-MS and MS/MS of dimethyl methylphosphonate ester (Bell, Despeyroux, Murrell, and Watts, 1997; Barr, Bell, Konn, Murrell, Timperley, Waters, and Watts, 2002). The ion at m/z 440 is from the neutral loss of CH_2O (-30 Da) from the methyl ester, and the small peak at m/z 438 corresponds to a loss of CH_3OH (-32 Da) from this serine ester.



(a)



(b)

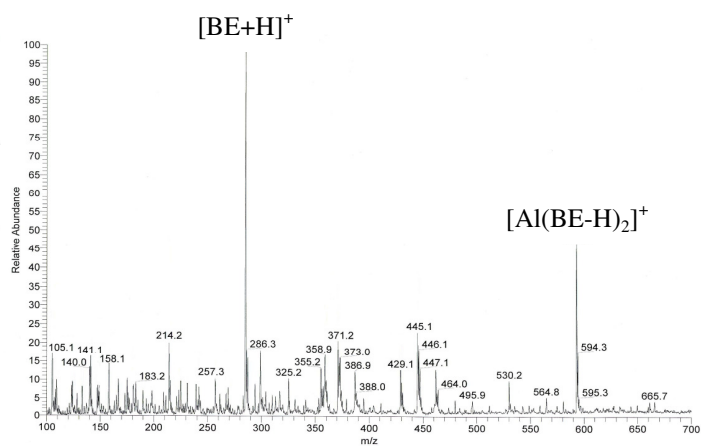
Figure 2.13 (a) Full scan mass spectrum of the Ser:Al:brazilin complex, (b) MS² spectrum of the m/z 470 ion in Figure 2.13(a).

2.4.6.1.2 Al:BI and Ser:Al:BI complexes (Source of the Al(III) ion: aluminium (III) nitrate nanohydrate)

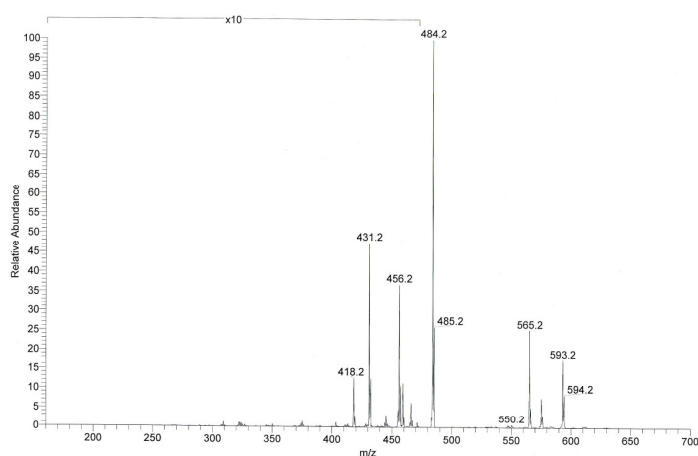
In an effort to determine if the other ions apart from Al(III) present in alum might be having an effect on complexes observed with brazilin in ESI-MS, and to enable a better comparison with the corresponding Ga(III) and In(III) complexes for which the precursor salts were available commercially as nitrates, the use of aluminium (III) nitrate was investigated. In the event, the same ESI-MS results (Figure 2.14(a), (b), and 2.15(a) and (b)) were obtained using aluminium (III) nitrate as were seen with alum.

2.4.6.1.3 Ga:BI and Ser:Ga:BI complexes

In order to seek further information on the Al:BI and Ser:Al:BI complexes, the related but larger Ga(III) and In(III) ions were also employed in the ESI-MS complexing studies. The full-scan ESI of the Ga and BI solution is shown in Figure 2.16(a). A peak was observed at m/z 636 (isotopic peaks at m/z 635, 637) and this was ascribed to the ion $[\text{Ga}(\text{BE-H})_2]^+$ from the complex. Analogous to the case with the corresponding Al(III) complex, the MS^2 spectrum of the ion at m/z 636 (Figure 2.16(b)) showed a neutral loss of CO (-28 Da) and $\text{C}_6\text{H}_5\text{O}_2$ (-109 Da) to afford daughter at m/z 607, 609 and 526, 528.

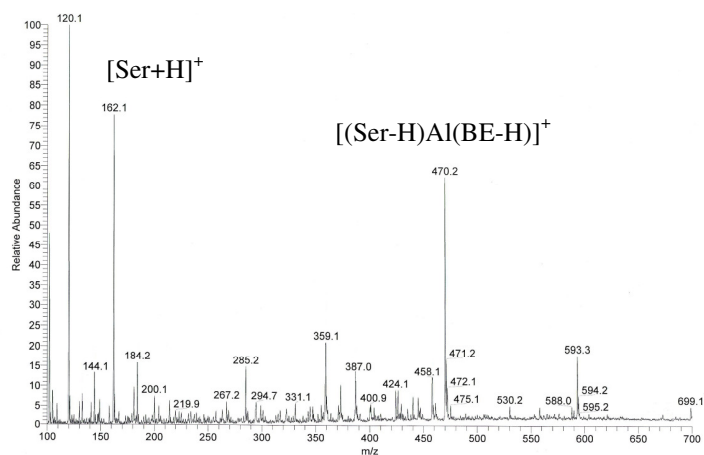


(a)

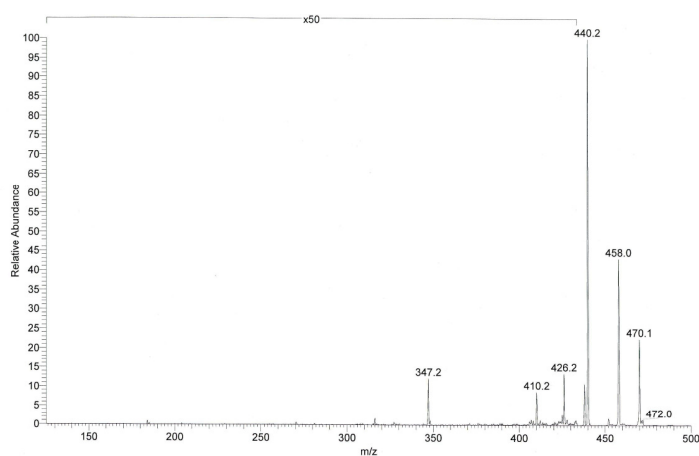


(b)

Figure 2.14 (a) Full scan mass spectrum of the Al:razilin complex, (b) MS² spectrum of the m/z 593 ion in Figure 2.14(a).

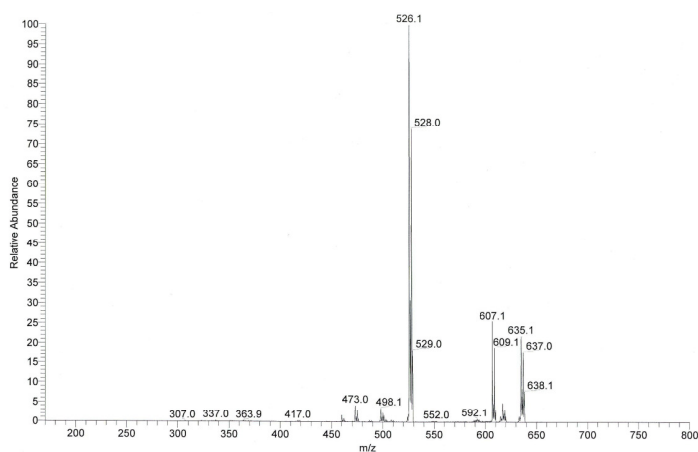
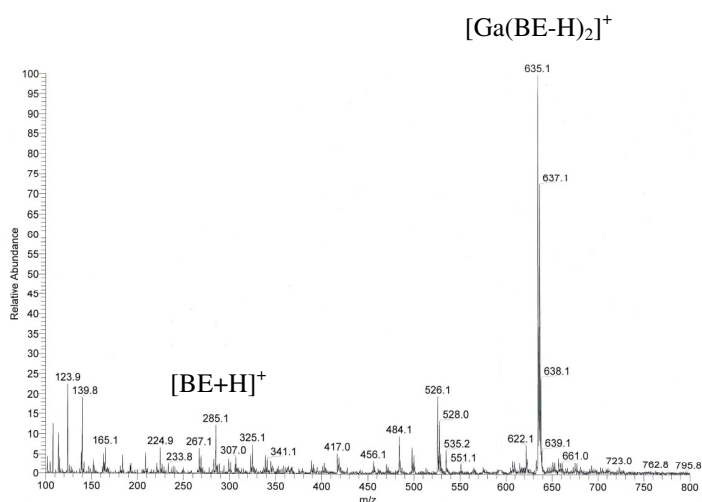


(a)



(b)

Figure 2.15 (a) Full scan mass spectrum of the Ser:Al:brazilin complex, (b) MS^2 spectrum of the m/z 470 ion in Figure 2.15(a).

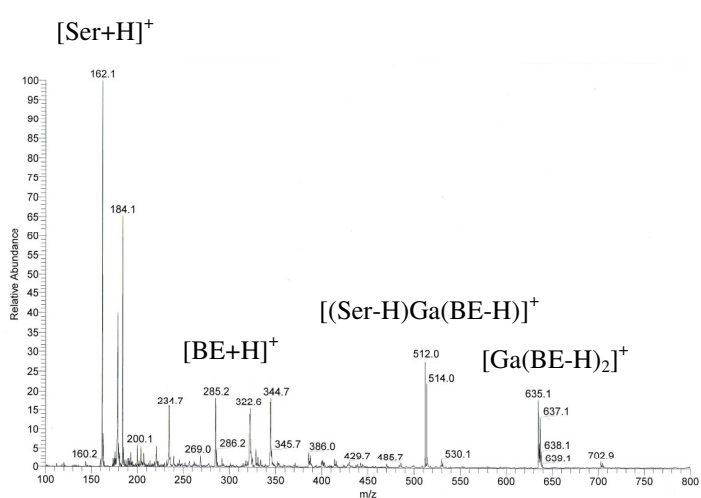


(b)

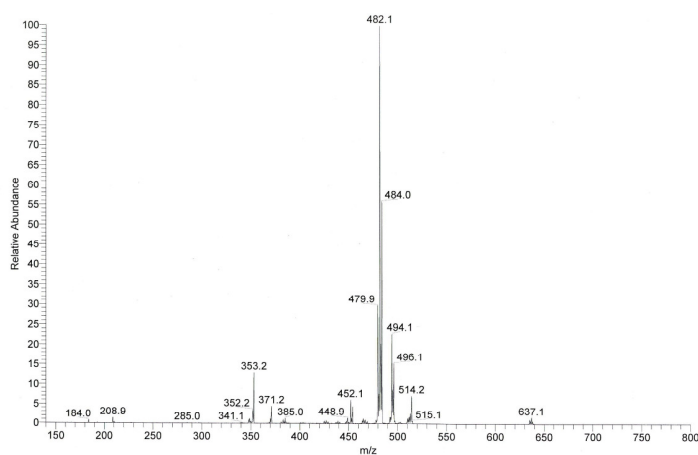
Figure 2.16 (a) Full scan mass spectrum of the Ga:brazilín complex, (b) MS^2 spectrum of the m/z 636 ion in Figure 2.16(a).

The full-scan ESI-MS of the Ser, Ga and BI solution is shown in Figure 2.17(a). A peak was observed at m/z 513 and this was ascribed to the ion $[(Ser-H)Ga(BE-H)]^+$ from the complex. Fragment ions at m/z 494, 496 and 482, 484 were present in the MS^2 spectrum of m/z 512, 514 (Figure 2.17(b)). The ion at m/z 494, 496 are from the neutral loss of H_2O (-18 Da) and those at m/z 482, 484 is from

the neutral loss of CH_2O (-30 Da); the ions observed at m/z 480, 482 probably arise from the neutral loss of CH_3OH from the serine methyl ester. Interestingly, in the case of the Ga(III) complex, no apparent addition of water to the ion at m/z 482, 484 was observed, in contrast to the MS^2 spectrum with the corresponding Al(III) complex ion. The reason for this is not clear.



(a)



(b)

Figure 2.17 (a) Full scan mass spectrum of the Ser:Ga:brazilin complex, (b) MS^2 spectrum of the m/z 513 ion in Figure 2.17(a).

2.4.6.1.4 In:BI and Ser:In:BI complexes

The full-scan ESI mass spectrum of the related In and BI solution is shown in Figure 2.18(a). A peak was observed at m/z 681 and this was ascribed to the ion $[\text{In}(\text{BE-H})_2]^+$ for the complex. The MS^2 spectrum of m/z 681 (Figure 2.18(b)) indicated that neutral loss of CO (-28 Da) to give the peak at m/z 653 had occurred and the ion at m/z 572 is again from the neutral loss of $\text{C}_6\text{H}_5\text{O}_2$ (-109 Da).

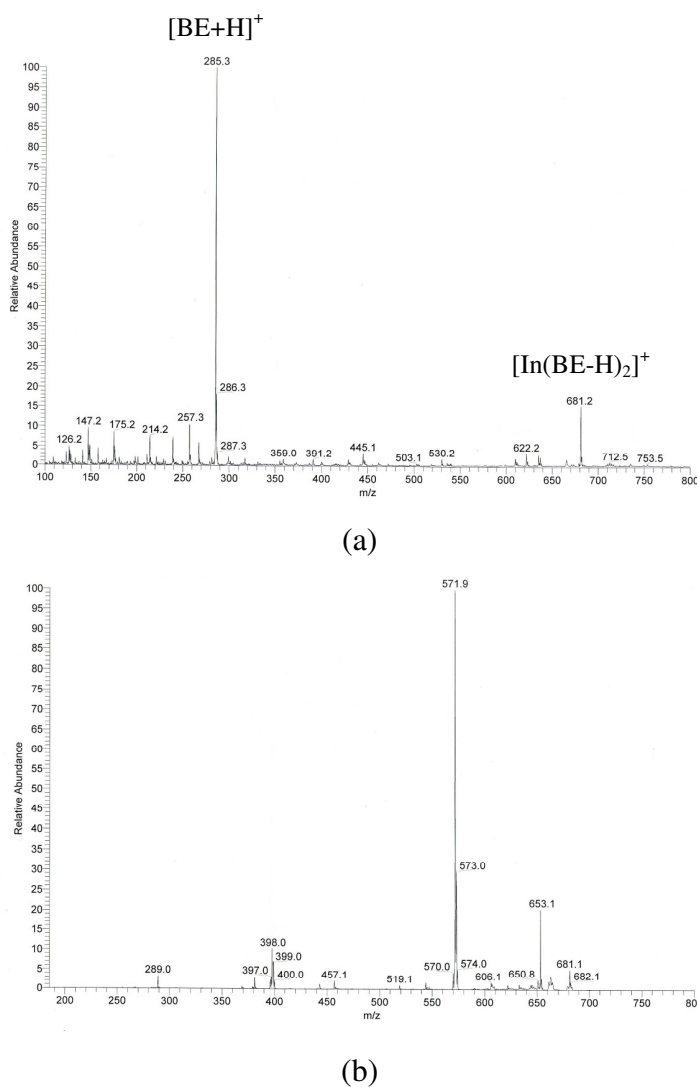
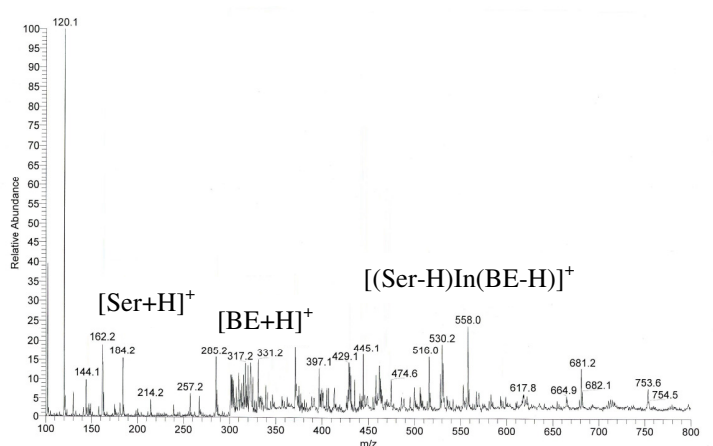
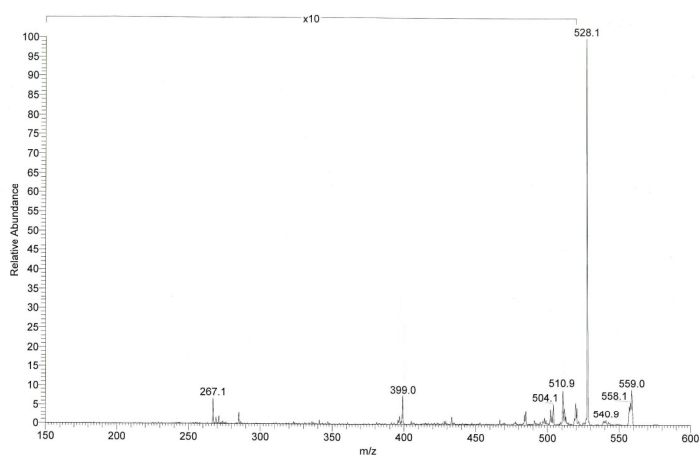


Figure 2.18 (a) Full scan mass spectrum of the In:brazilin complex, (b) MS^2 spectrum of the m/z 681 ion in Figure 2.18(a).

The full-scan ESI-MS of the Ser, In and BI solution is shown in Figure 2.19(a). A weak peak was observed at m/z 558 and this was ascribed to the ion $[(\text{Ser-H})\text{In}(\text{BE-H})]^+$ from the complex. The ion at m/z 528 was present in the MS² spectrum of m/z 558 (Figure 2.19(b)). The ion at m/z 528 is from the neutral loss of CH₂O (-30 Da).



(a)



(b)

Figure 2.19 (a) Full scan mass spectrum of the Ser:In:brazilin complex, (b) MS² spectrum of the m/z 558 ion in Figure 2.19(a).

2.4.6.2 Brazilein complexes

2.4.6.2.1 Al:BE and Ser:Al:BE complexes (Source of the Al(III) ion: alum)

The full-scan ESI-MS of the Al and BE solution is shown in Figure 2.20(a). A peak was observed at m/z 593 for the ion $[\text{Al}(\text{BE-H})_2]^+$ from the complex. The MS^2 spectrum of m/z 593 (Figure 2.20(b)) has shown neutral loss of CO (-28 Da) and $\text{C}_6\text{H}_5\text{O}_2$ (-109 Da) with peaks at m/z 565 and 484 respectively.

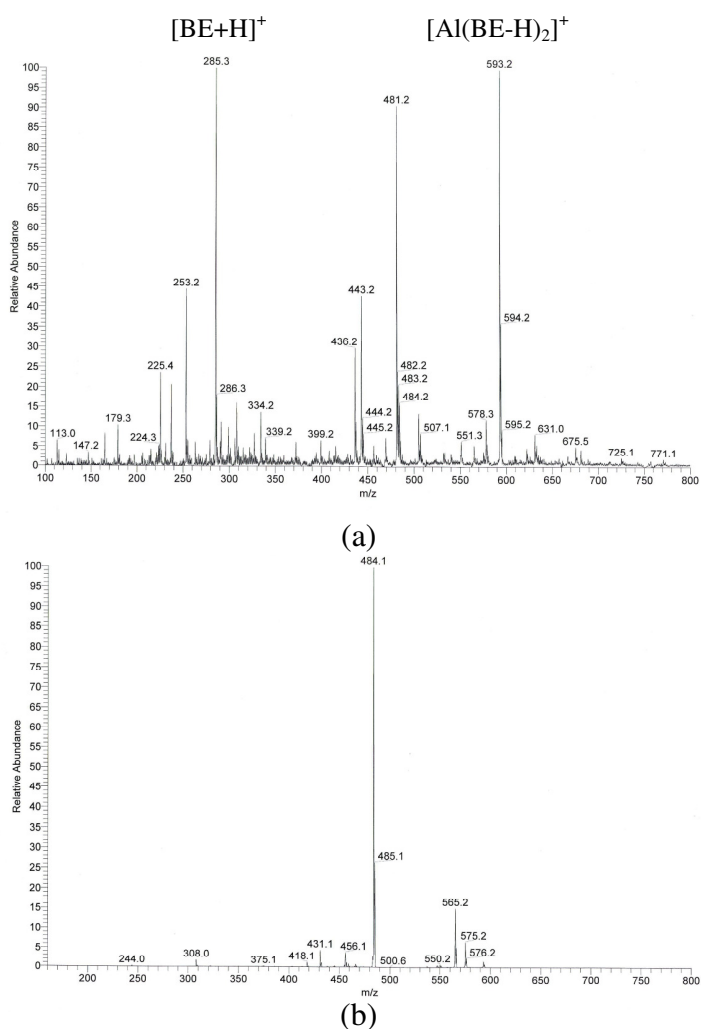
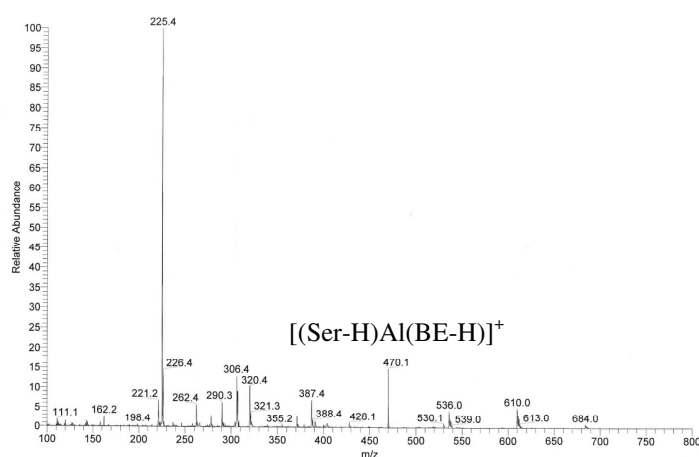
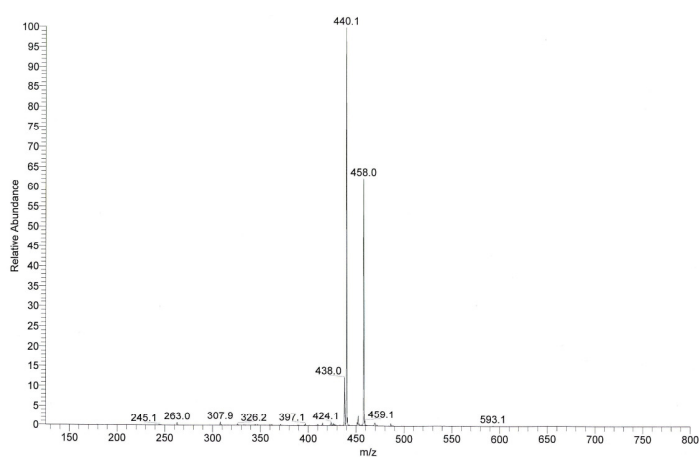


Figure 2.20 (a) Full scan mass spectrum of the Al:brazilein complex, (b) MS^2 spectrum of the m/z 593 ion in Figure 2.20(a).

The full-scan ESI mass spectrum of the Ser, Al and BE solution is shown in Figure 2.21(a). A peak was observed at m/z 470 and this was ascribed to the ion $[(\text{Ser-H})\text{Al}(\text{BE-H})]^+$ from the complex. Two main fragment ions at m/z 440 and m/z 458 were present in the MS^2 spectrum of m/z 470 (Figure 2.21(b)), as observed previously for the Ser, Al, BI solution.



(a)



(b)

Figure 2.21 (a) Full scan mass spectrum of the Ser:Al:brazilein complex, (b) MS^2 spectrum of the m/z 470 ion in Figure 2.21(a).

2.4.6.2.2 Al:BE and Ser:Al:BE complexes (Source of the Al(III) ion: aluminium (III) nitrate nanohydrate)

The same ESI-MS results (Figure 2.22(a), (b), and 2.23(a) and (b)) were obtained using aluminium (III) nitrate as were seen with alum on mixing with BE or BE and Ser.

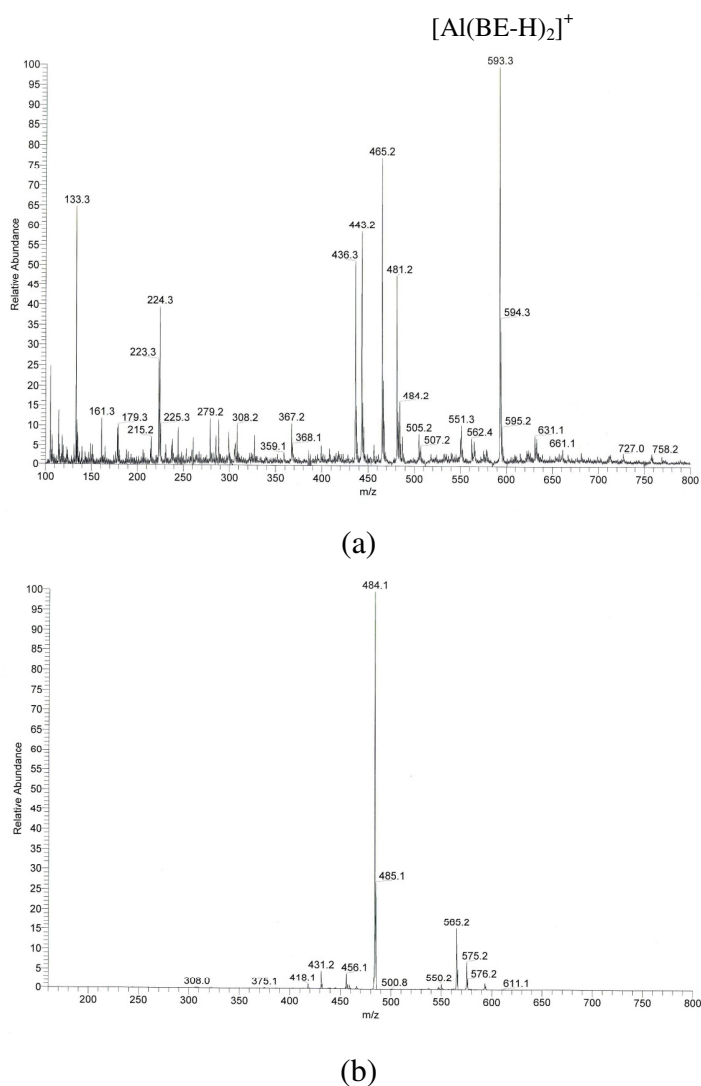


Figure 2.22 (a) Full scan mass spectrum of the Al:brazilein complex, (b) MS² spectrum of the m/z 593 ion in Figure 2.22(a).

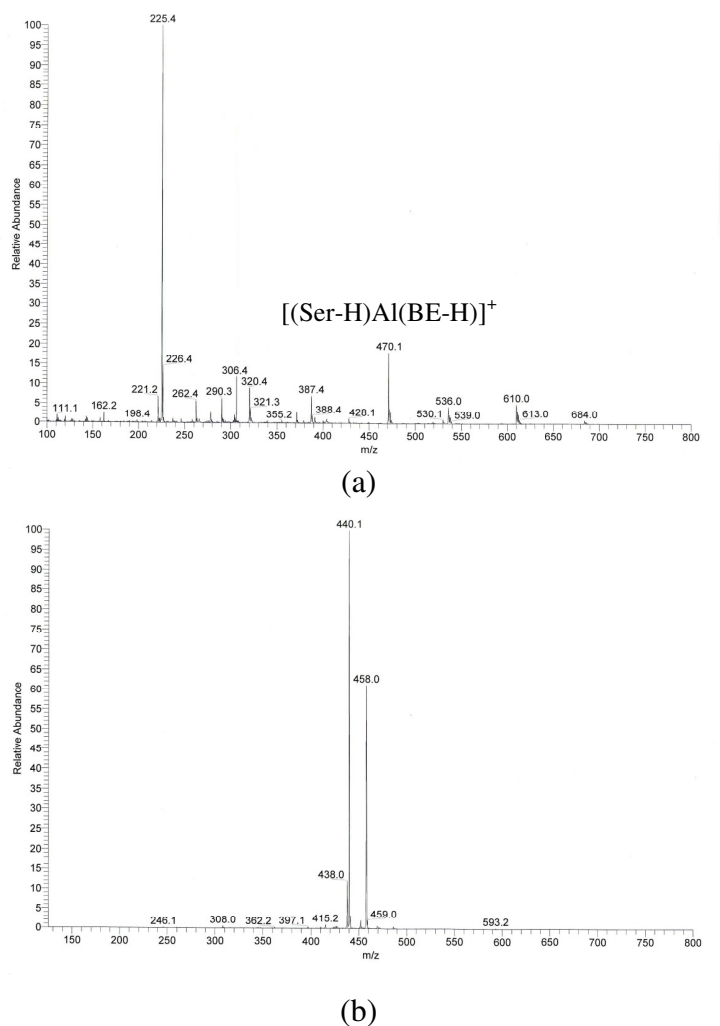


Figure 2.23 (a) Full scan mass spectrum of the Ser:Al:brazilein complex, (b) MS² spectrum of the m/z 470 ion in Figure 2.23(a).

2.4.6.2.3 Ga:BE and Ser:Ga:BE complexes

The full-scan ESI mass spectrum of the Ga and BE solution is shown in Figure 2.24(a). A peak was observed at m/z 636 and this was ascribed to the ion $[\text{Ga}(\text{BE-H})_2]^+$ from the complex. The MS² spectrum of m/z 636 (Figure 2.24(b)) showed the neutral loss of CO (-28 Da) and C₆H₅O₂ (-109 Da) to give daughter ions at m/z 607, 609 and 526, 528 respectively.

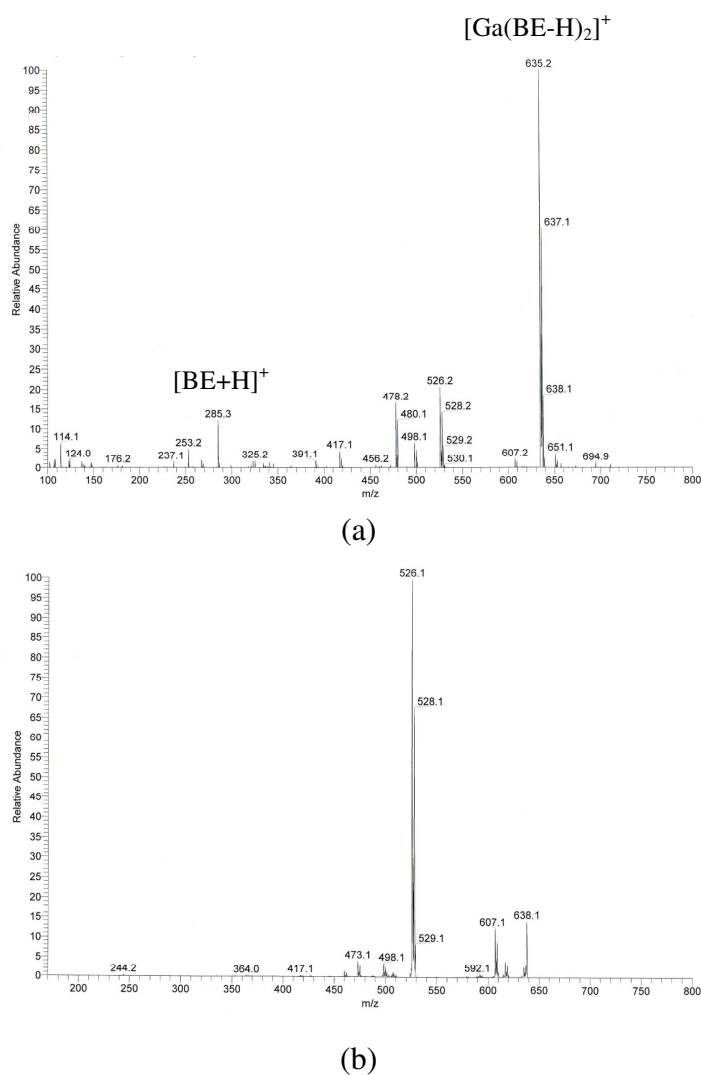
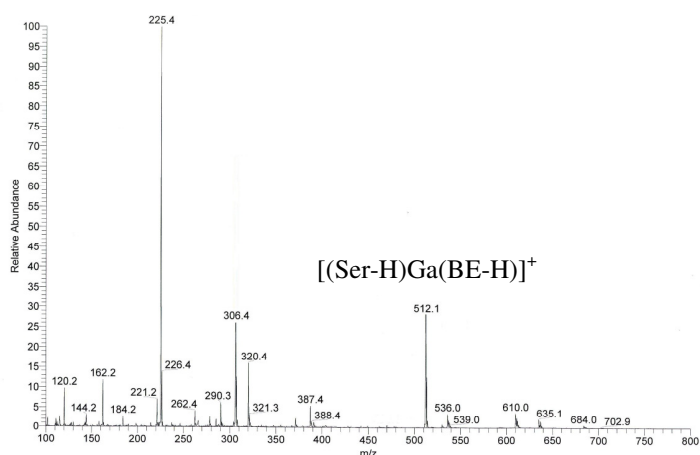
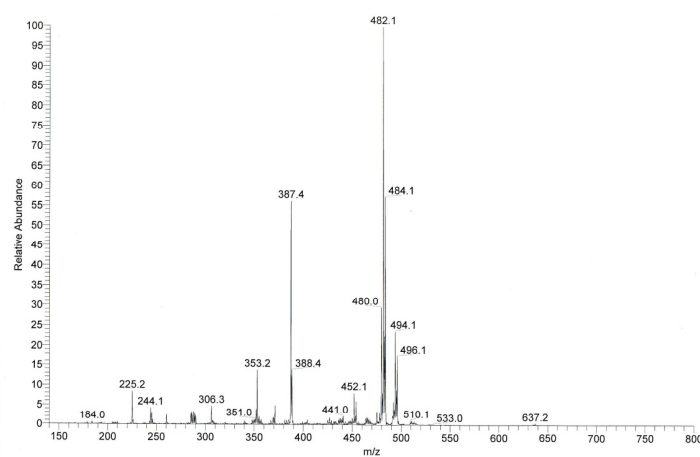


Figure 2.24 (a) Full scan mass spectrum of the Ga:brazilein complex, (b) MS² spectrum of the m/z 636 ion in Figure 2.24(a).

The full-scan ESI-MS of the Ser, Ga and BE solution is shown in Figure 2.25(a). A peak was observed at m/z 513 and this was ascribed to the ion $[(\text{Ser-H})\text{Ga}(\text{BE-H})]^+$ from the complex. The ions at m/z 494, 496 and 482, 484 were present in the MS² spectrum of m/z 512, 514 (Figure 2.25(b)). The ion at m/z 494, 496 are from the neutral loss of H₂O (-18 Da) and those at m/z 482, 484 from the neutral loss of CH₂O (-30 Da).



(a)

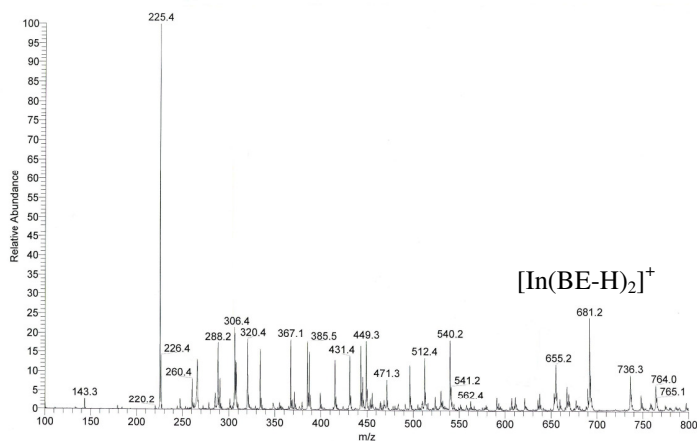


(b)

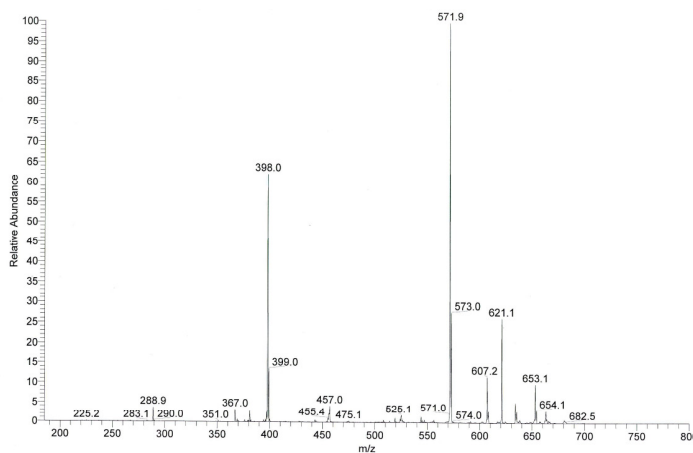
Figure 2.25 (a) Full scan mass spectrum of the Ser:Ga:brazilein complex, (b) MS^2 spectrum of the m/z 513 ion in Figure 2.25(a).

2.4.6.2.4 In:BE and Ser:In:BE complexes

The full-scan ESI mass spectrum of the In and BE solution is shown in Figure 2.26(a). A peak was observed at m/z 681 and this was ascribed to the ion $[\text{In}(\text{BE-H})_2]^+$ from the complex. The MS^2 spectrum of m/z 681 (Figure 2.26(b)) indicated the neutral loss of CO (-28 Da) had occurred resulting in the daughter ion at m/z 653, while the ion at m/z 572 is from the neutral loss of $\text{C}_6\text{H}_5\text{O}_2$ (-109 Da).



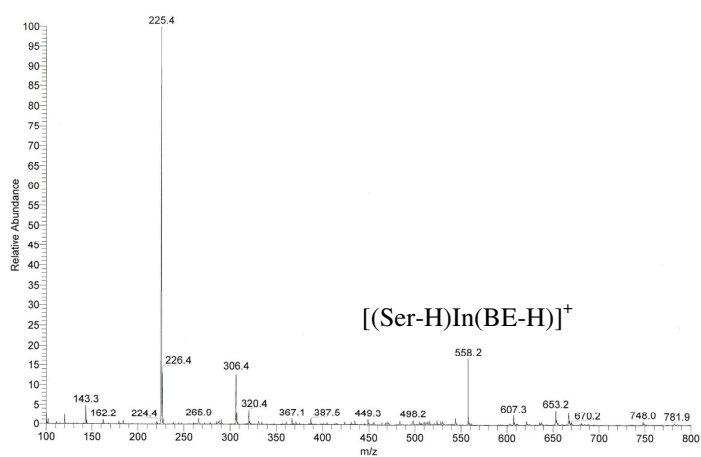
(a)



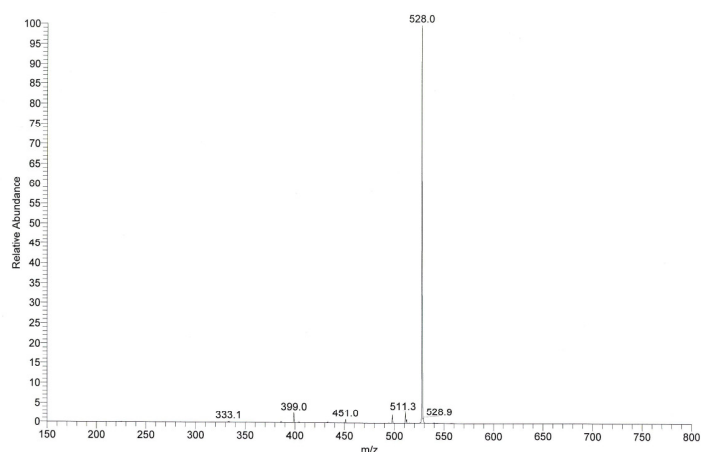
(b)

Figure 2.26 (a) Full scan mass spectrum of the In:brazilein complex, (b) MS² spectrum of the m/z 681 ion in Figure 2.26(a).

The full-scan ESI-MS of the Ser, In and BE solution is shown in Figure 2.27(a). A peak was observed at m/z 558 and this was ascribed to the ion $[(\text{Ser-H})\text{In}(\text{BE-H})]^+$ from the complex. The ion at m/z 528 was present in the MS² spectrum of m/z 558 (Figure 2.27(b)). The ion at m/z 528 is from the neutral loss of CH_2O (-30 Da).



(a)



(b)

Figure 2.27 (a) Full scan mass spectrum of the Ser:In:brazilein complex, (b) MS² spectrum of the m/z 558 ion in Figure 2.27(a).

From the full-scan ESI-MS for brazilin and brazilein complexes, it was shown that complexes of brazilein only were formed in the gas phase, due to brazilin being pre-oxidised to brazilein at low pH when mixed with the metal ion solutions (Kanazawa, 1991). This was then reflected in the fact that only complex

ions with brazilin were detected in the ESI mass spectra. Our results demonstrated that the preferred chelates formed for aluminium, gallium, indium with brazilin and brazilin are of stoichiometries 1:2. and the corresponding stoichiometries with Ser were 1:1:1.

Possible structures of the 1:2 complex of Al:BE and 1:1:1 of Ser:Al:BE are shown in Figure 2.8 (section 2.4.3) and Figure 2.28. The proposed structures, which have one positive charge, are based on the observed m/z ratios of the ions in the mass spectra and associated high resolution MS data as noted in the following section. The related Ga(III) and In(III) ions formed analogous complexes in aqueous solution.

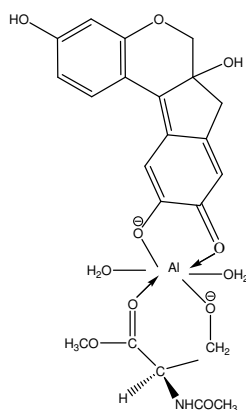


Figure 2.28 Proposed structure of the Ser:Al:brazilin 1:1:1 complex.

2.4.7 High resolution mass spectrometry

High-resolution ESI mass spectrometry for the determination of the accurate masses of AlBE₂, GaBE₂, InBE₂, SerAlBE, SerGaBE, and SerInBE complexes was performed on a QTOF Ultima mass spectrometer fitted with a lockspray source. The obtained exact mass measurements for these complexes,

presented in Table 2.3. It was found that the error value between the theoretical and experimental value was between -1.5 to 3.4 ppm, well within the commonly accepted 5 ppm error limit.

Table 2.3 Exact mass measurements and elemental compositions for ions derived from AlBE₂, GaBE₂, InBE₂, SerAlBE, SerGaBE, and SerInBE₂ complexes.

Complex	Ion	<i>m/z</i>	Elemental composition	Theoretical value	Experimental value	Δ (ppm)
AlBE ₂	[Al(BE-H) ₂] ⁺	593	C ₃₂ H ₂₂ O ₁₀ Al	593.0681	593.0675	3.2
GaBE ₂	[Ga(BE-H) ₂] ⁺	636	C ₃₂ H ₂₂ O ₁₀ Ga	635.9983	635.9985	-0.3
InBE ₂	[In(BE-H) ₂] ⁺	681	C ₃₂ H ₂₂ O ₁₀ In	681.0685	681.0678	2.5
SerAlBE	[(Ser-H)Al(BE-H)] ⁺	470	C ₂₂ H ₂₁ O ₉ NAl	470.0885	470.0895	3.4
SerGaBE	[(Ser-H)Ga(BE-H)] ⁺	513	C ₂₂ H ₂₁ O ₉ NGa	513.0529	513.0514	1.8
SerInBE	[(Ser-H)Ga(BE-H)] ⁺	558	C ₂₂ H ₂₁ O ₉ NIn	558.0680	558.0696	-1.5

2.4.8 Computational modeling

Molecular modeling was also carried out on the Al:BE, Ga:BE, In:BE, Ser:Al:BE, Ser:Ga:BE, and Ser:In:BE complexes by semiempirical PM3 calculations to determine the most probable structure of the complexes (Figure 2.8 in section 2.4.3 and 2.29). Water molecules have been added to obtain an octahedral environment of the complex ions, since such an environment is most likely structure for Al(III), Ga(III), and In(III) complexes. General structures of the metal ion:brazilein 1:2 complex and the Ser:metal ion:brazilein 1:1:1 complex, with and without water, and used for calculation of the heat of formation are shown in Figure 2.29 (a)-(d). Table 2.4 shows the heats of formation values for the proposed Al:BE, Ga:BE, In:BE,

Ser:Al:BE, Ser:Ga:BE, and Ser:In:BE complexes with and without H₂O molecules as ligands. All the proposed complexes have an overall single positive charge.

Lowest energy conformers of brazilein and (*S*)-*N*-acetyl serine methyl ester were ascertained through molecular modeling using the MMFF94 force fields (Halgren, 1996) and the resulting conformer structures were then used for the respective Al(III), Ga(III), and In(III) complex minimum energy structures using the semiempirical PM3 program (Stewart, 1989). Application of this latter program also enabled calculation of the estimated heats of formation of the probable structures of the metal ion complexes. These calculations refer to complexes in a vacuum and do not take account of any possible solvent effect. A range of possible binding modes in the complexes were considered and modeled but with the known binding to the metal ion through oxygen being a dominant consideration. The probable structures shown for the complexes are those with the largest negative heats of formation within comparable groups. Significant reduction in the calculated heats of formation were seen in the case without water as a binding ligand, although the complexes still had negative heats of formation consistent with their detection in the ESI-MS. The indium (III) complexes had the lowest heats of formation reflecting the known decreased stability of the +3 oxidation state in indium relative to gallium and the aluminium, which has the most stable +3 state (Greenwood and Earnshaw, 1984a). The large ionic radius of the indium (III) ion (Greenwood and Earnshaw, 1984b) also would be a factor since in the complex it has to be accommodated in two small 5-membered rings.

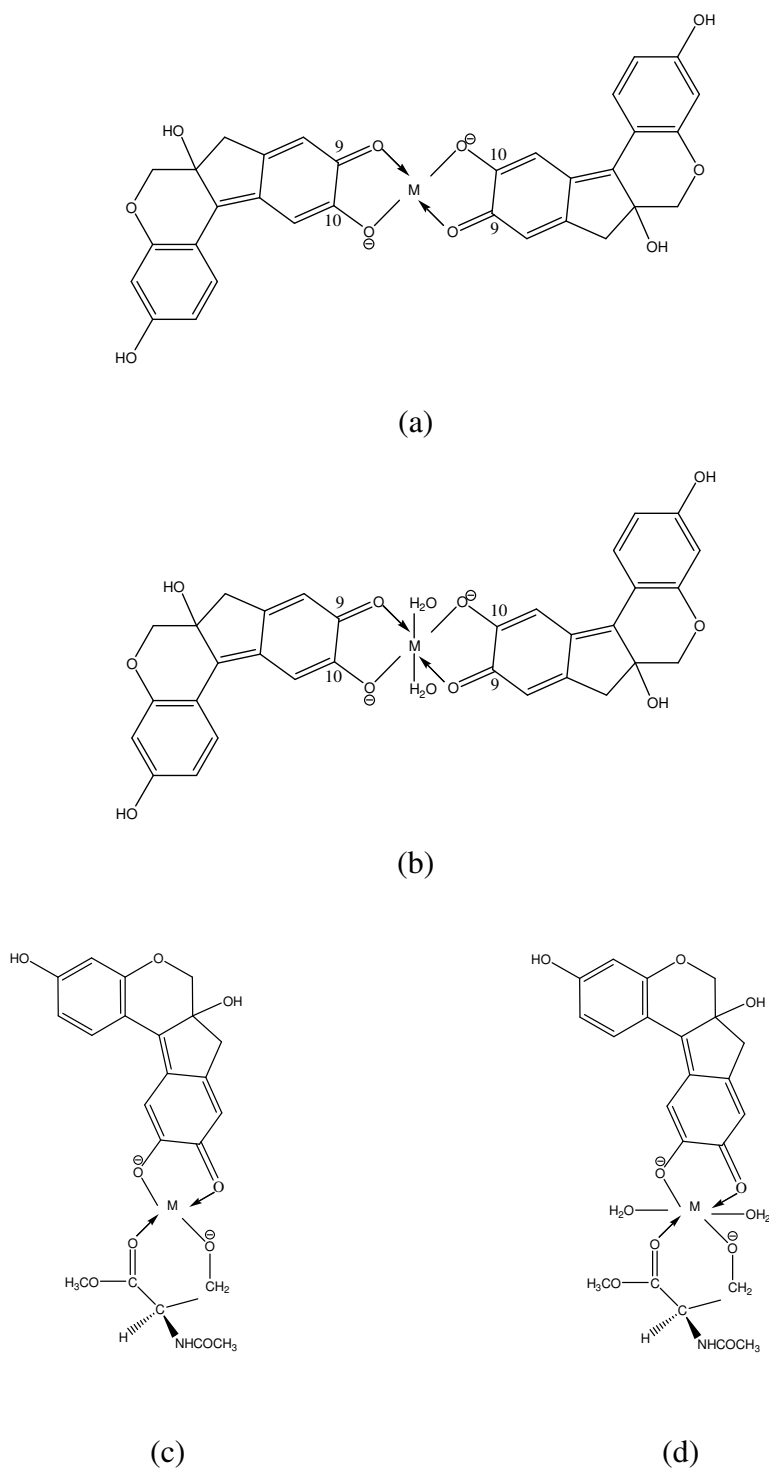


Figure 2.29 General structure of the M:brazilein 1:2 complex with (a) and without water (b) and the Ser:M:brazilein 1:1:1 complex with (c) and without water (d) (M represent metal ions such as Al, Ga, and In) used for calculation of the heat of formation.

Table 2.4 Calculated heats of formation of Al:BE₂, Ser:Al:BE, Ga:BE₂, Ser:Ga:Be, In:BE₂, and Ser:In:BE complexes.

Complex	Molecular weight		Ratio	Heat of formation (kJ/mol)	
	With H ₂ O	Without H ₂ O		With H ₂ O	Without H ₂ O
Al:BE	629.5300	593.5000	1:2	1,545.7	982.8
Ser:Al:BE	506.4200	470.3900	1:1:1	1,630.6	1,057.0
Ga:BE	686.3032	650.2732	1:2	1,570.9	860.4
Ser:Ga:BE	549.1580	513.1280	1:1:1	1,801.5	1,158.2
In:BE	717.3680	681.3380	1:2	939.4	366.4
Ser:In:BE	594.2580	558.2280	1:1:1	1,062.0	473.0

2.5 Conclusion

The interaction of brazilein and Al(III) (from alum) was studied by UV-Vis spectroscopy and the significant bathochromic shift observed for absorption band I in brazilein was consistent with complexation to the aluminium (III) ion. Using the molar ratio and Job's method, it was shown that the stoichiometric composition of the complex in aqueous solution was Al(brazilein)₂. The calculated negative heat of formation of the proposed complex indicated it was likely to be reasonably stable in aqueous solution.

From positive ion electrospray ionization mass spectra on aqueous methanolic solutions, the complexes of Al:BE, Ga:BE, and In:BE also showed 1:2 stoichiometry for the major complex formed in each case. Calculated heats of formation of complexes were reasonable for these complexes and indicated possible structures. The stoichiometries of the Ser:Al:BE 1:1:1 was also the same ratio with Ser:Ga:BE and

Ser:In:BE. It is possible, based on these results, that serine residues in the silk protein could be involved in binding of the complex to the silk

2.6 References

- Ahmed, M. J. and Hossain, J. (1995). Spectrophotometric determination of aluminium by morin. **Talanta** 42: 1135-1142.
- Arancibia, V. and Muñoz, C. (2007). Determination of aluminium in water samples by adsorptive cathodic stripping voltammetry in the presence of pyrogallol red and a quaternary ammonium salt. **Talanta** 73: 546-552.
- Arvand, M. and Asadollahzadeh, S. A. (2008). Ion-selective electrode for aluminum determination in pharmaceutical substances, tea leaves and water samples. **Talanta** 75: 1046-1054.
- Barr, J. D., Bell, A. J., Konn, D. O., Murrell, J., Timperley, C. M., Waters, M. J., and Watts, P. (2002). Fragmentations and reactions of three isotopically labeled methyl dimethylphosphonate ions produced by electrospray ionization in an ion trap mass spectrometer. **Physical Chemistry Chemical Physics** 4:2200-2205.
- Bell, A. J., Despeyroux, D., Murrell, J., and Watts, P. (1997). Fragmentation and reactions of organophosphate ions produced by electrospray ionization. **International Journal of Mass Spectrometry and Ion Processes** 165/166: 533-550.

- Boudet, A. C., Cornard, J. P., and Merlin, J. C. (2000). Conformational and spectroscopic investigation of 3-hydroxyflavone-aluminium chelates. **Spectrochimica Acta Part A: Molecular and Biomolecular Spectroscopy** 56: 829-839.
- Castro, G. T. and Blanco, S. E. (2004). Structural and spectroscopic study of 5,7-dihydroxy-flavone and its complex with aluminum. **Spectrochimica Acta Part A: Molecular and Biomolecular Spectroscopy** 60: 2235-2241.
- Christie, R. M. (2001). **Colour Chemistry**. Cambridge: .The Royal Society of Chemistry.
- Cornard, J. P., Boudet, A. C., and Merlin, J. C. (2001). Complexes of Al(III) with 3'4'-dihydroxy-flavone: characterization, theoretical and spectroscopic study. **Spectrochimica Acta Part A: Molecular and Biomolecular Spectroscopy** 57: 591-602.
- Cornard, J. P. and Merlin, J. C. (2001). Structural and spectroscopic investigation of 5-hydroxyflavone and its complex with aluminium. **Journal of Molecular Structure** 569: 129-138.
- Cornard, J. P. and Merlin, J. C. (2002). Spectroscopic and structural study of complexes of quercetin with Al(III). **Journal of Inorganic Biochemistry** 92: 19-27.
- Doménech-Carbó, A., Doménech-Carbó, M. T., and Sauí-Peris, M. C. (2005). Electrochemical identification of flavonoid dyes in solid work of art samples by abrasive voltammetry at paraffin-impregnated graphite electrodes. **Talanta** 66: 769-782.

- Engels, P., Perkin, W. H., and Robinson, R. (1908). CXI. Brazilin, haematoxylin, and their derivatives. Part IX. On brazilein, haematein and their derivatives. **Journal of Chemical Society** 93: 1115-1162.
- Fernández, S., Villanueva, U., Diego, A., Arana, G., and Madariaga, J. M. (2008). Monitoring trace elements (Al, As, Cr, Cu, Fe, Mn, Ni, and Zn) in deep and surface waters of the estuary of the Nerbioi-Ibaizabal River (Bay of Biscay, Basque Country). **Journal of Marine Systems** 72: 332-341.
- Ferreira, E. S. B., Hulme, A. N., McNab, H., and Quye, A. (2004). The natural constituents of historical textile dyes. **Chemical Society Reviews** 33: 329-336.
- Frenandez, M. T., Mira, M. L., Florêncio, M. H., and Jennings, K. R. (2002). Iron and copper chelation by flavonoids: an electrospray mass spectrometry study. **Journal of Inorganic Biochemistry** 92: 105-111.
- Greenwood, N. N. and Earnshaw, A(1984a,b). **Chemistry of the Elements**. Pergamon Press: Oxford a) p.252. b) p.250.
- Halgren, T. A. (1996). Merck molecular force field. I. Basis, form, scope, parameterization, and performance of MMFF94. **Journal of Computational Chemistry** 17: 490-519.
- Harborne, J. B., Baxter, H., and Moss, G. P. (1999). **Phytochemical dictionary a handbook of bioactive compounds from plants** (2nd ed.). United Kingdom. Taylor & Francis.
- Hulme, A. N., McNab, H., Peggie, D. A., and Quye, A. (2005). Negative ion electrospray mass spectrometry of neoflavonoids. **Phytochemistry** 66: 2766-2770.

- In-Kyung, B., Hye-Young, M., Ah-Reum, H., Eun-Kyoung, S., and Sang Kook, L. (2005). Suppression of lipopolysaccharide-induced expression of inducible nitric oxide synthase by brazilin in RAW 264.7 macrophage cells. **European Journal of Pharmacology** 513: 237-242.
- Kanazawa, H. (1991). Interaction between metallic ions and dyes. I. Effect of various metallic salts on dyeing of silk and cotton fabrics with dye extracted from *Ceasalpinia Sappan L.* **Rika Hokoku** 47: 19-34.
- Kaplan, D., Adam, W. W., Farmer, B., and Viney, C. (1994). **Silk polymers: Materials science and Biotechnology**. Washington: American Chemical Society.
- Kara, D., Fisher, A., and Hill, S. J. (2008). Flow injection determination of aluminium by spectrofluorimetric detection after complexation with N-*o*-vanillidine-2-amino-*p*-cresol: The application to natural waters. **Analytica Chimica Acta** 611: 62-67.
- Karmakar, S. R. (1999). **Chemical technology in the pre-treatment processes of textiles**. Amsterdam: Elsevier Science B.V. Hall.
- Kim, D. S., Baek, N. I., Oh, S. R., Jung, K. Y., Lee, I. S., and Lee, H. K. (1997). NMR assignment of brazilein. **Phytochemistry** 46(1): 177-178.
- Lemmens, R. H. M. J. and Wulijarni-Soetjipto, N. (1992). **Plant resources of South-East Asia³: Dye and tannin-producing plants**. Prosea, Bogor Indonesia, p. 60-62.
- Lian, H., Kang, Y., Bi, S., Arkin, Y., Shao, D., Li, D., Chen, Y., Dai, L., Gan, N., and Tian, L. (2004). Direct determination of trace aluminum with quercetin by reversed-phase high performance liquid chromatography. **Talanta** 62: 43-50.

- Moeyes, M. (1993). **Natural dyeing in Thailand**. Bangkok: White Lotus.
- Oliveira, L. F. C., Edwards, H. G. M., Velozo, E. S., and Nesbitt, M. (2002). Vibrational . spectroscopic study of brazilin and brazilein, the main constituents of brazilwood from Brazil. **Vibrational Spectroscopy** 28: 243-249.
- Sang, H., Liang, P., and Du, D. (2008). Determination of trace aluminum in biological and water samples by cloud point extraction preconcentration and graphite furnace atomic absorption spectrometry detection. **Journal of Hazardous Materials** 154: 1127-1132.
- Septum C., Morgan, J., Hick, L., Bremner, J. B., Rattanaphani, S., and Rattanaphani, V. (2007) Detection of Al(III) and Ga(III) complexes of the plant dye, morin, by electrospray ionization mass spectrometry. **Analytical Sciences** 23: 1209-1214.
- Stewart, J. J. P. (1989). Optimization of parameters for semiempirical methods. 1. Method. **Journal of Computational Chemistry** 10: 209-220.
- Souza, E. S. B. and Giovani, W. F. D. (2005). Synthesis, spectral and electrochemical properties of Al(III) and Zn(II) complexes with flavonoids. **Spectrochimica Acta Part A** 61: 1985-1990.
- Urabe, S. and Yanagisawa, M. (1988). Effect of several mordants on the deterioration of dyed silk fabrics. **Kobunkazai no Kagaku** 33: 10-17 (Chem. Abstr., 1990, 112, 22238).

- Wang, X., Lei, J., Bi, S., Gan, N., and Wei, Z. (2001). Determination of the speciation of aluminum(III) in natural waters by adsorption stripping voltammetry and complexation with Al^{III} - solochrome violet RS. **Analytica Chimica Acta** 449: 35-44.
- Yan, X., Wang, W., Xing, D., Zhao, Y., and Du, L. (2005). Development and optimization of a method for the analysis of brazilein by HPLC with electrochemical detection. **Journal of Chromatography A** 1077: 44-48.
- Zhang, J., Wang, J., and Brodbelt, J. S. (2005). Characterization of flavonoids by aluminium complexation and collisionally activated dissociation. **Journal of Mass Spectrometry** 40: 350-363.
- Zollinger, H. (2003). **Colour Chemistry**. Weinheim. Wiley-VCH.

CHAPTER III

ADSORPTION OF Al-BRAZILEIN COMPLEX AND Al-EXTRACTED DYE COMPLEX ON SILK

3.1 Abstract

Kinetic and thermodynamic studies on the adsorption of alum-brazilein and alum-extracted dye from *Ceasalpinia sappan* Linn. onto silk fibers indicated that the adsorption capacities were dependent on the pH of the dye solution, the material to liquor ratio (MLR), the initial dye concentration, and temperature. The initial dye adsorption rates of alum-brazilein and alum-extracted dye on silk before the time of equilibrium was reached increased at higher dyeing temperatures which indicated a kinetically controlled process. The pseudo second-order kinetic model was indicated for both alum-brazilein and alum-extracted dye adsorption on silk at pH 4.0 with activation energies (E_a) of 41.57 and 21.20 kJ/mol respectively. The corresponding values of the enthalpy of adsorption (ΔH) on silk at pH 4.0 were -25.32 and -32.63 kJ/mol, respectively. Moreover, the free energy (ΔG°) and entropy changes (ΔS°) for the adsorption on silk of alum-brazilein (ΔG° -14.11 to -12.52 kJ/mol, ΔS° -36.64 kJ/mol) and alum-extracted dye (ΔG° -18.22 to -16.15 kJ/mol, ΔS° -47.87 kJ/mol) were also determined. The experimental isotherm data were analyzed using the Langmuir and Freundlich equations. Additionally, the adsorption-desorption of alum-brazilein and alum-extracted dye with silk were investigated.

3.2 Introduction

Since the earliest times, natural dyes have been used for many purposes such as the coloring of natural fibers wool, cotton and silk as well as fur and leather (Cristea and Vilarem, 2006). Natural coloring matters are dyes and pigments occurring in animals (birds, insects, bacteria) and in plant material including trees, leaves, grass and flowers (Christie *et al.*, 2000). Amongst the components of some natural plant pigments are the flavonoids and homoisoflavonoids. Flavonoids are a group of polyphenolic compounds and the homoisoflavonoids are a sub-group of this general class with one extra carbon in the overall structural framework (Doménech-Carbó, A. *et al.*, 2005). Apart from their dyeing properties, homoisoflavonoids also display a range of useful biological activities including anti-tuberculosis and anti-diarrheal activity (Lemmens and Wulijarni-Soetjipto, 1992), as well as immunosuppressive (Ye, Xie, Lei, Meng, Zhao, Su, and Du, 2006) and cardiogenic effects (Zhao, Pan, Tao, Xing, and Du, 2006).

As mentioned previously, the red homoisoflavonoids, brazilin (6a*S-cis*)(7,11b-dihydrobenz[*b*]indeno[1,2-*d*]pyran-3,6a,9,10,(6*H*)-tetrol) and brazilein (6a*S*-(6a,7-dihydro-3,6a,10-trihydroxy-benz[*b*]indeno[1,2-*d*]pyran-9(6*H*)-one), are the major components of the heartwood of *Ceasalpinia sappan* Linn. but brazilin is readily converted to brazilein by exposure to atmospheric oxygen and light (Kim *et al.*, 1997; Harborne *et al.*, 1999; Ferreira *et al.*, 2004; Doménech-Carbó, A. *et al.*, 2005; Hulme *et al.*, 2005; In-Kyung *et al.*, 2005).

Silk is a protein-based fiber produced by the silkworm, *Bombyx mori* for the construction of its cocoon (Hojo, 2000; Horrocks and Anand, 2000). Silk fibers are made up of a protein called fibroin. This protein is constructed from layers of anti-

parallel beta pleated sheets which run parallel to the silk fiber axis. The highly repetitive sections are composed of glycine (45%), alanine (30%), and serine (12%) in a roughly 3:2:1 ratio and dominated by [Gly-Ala-Gly-Ala-Gly-Ser]_n sequences, where Gly, Ala and Ser refer to glycine, alanine and serine respectively (Khan, Morikawa, Gotoh, Miura, Ming, Sato, and Iwasa, 2008; Kaplan *et al.*, 1994). Like wool, silk fibers contain carboxyl acid and protonated amino groups which result in its amphoteric characteristics (Carr, 1995). Under acid conditions the carboxyl groups are unionized, leaving a net positive charge which enables dye anions to be adsorbed (Carr, 1995). Many studies have been undertaken to investigate silk dyeing. For instance, the two step ultrasonic dyeing of cotton and silk fabrics with natural dyes has been developed in which an enzyme is complexed with tannic acid first as a pretreatment (Vankar, Shanker, and Verma, 2006). It was found that the enzymatic treatment gave cotton and silk fabrics rapid dye adsorption kinetics and total higher adsorption than untreated samples for all dyes. The sonicator dyeing of modified cotton, wool and silk with *Mahonia napaulensis* DC. and identification of the colorant in *Mahonia* has been reported by Vankar *et al.* (Vankar, Shanker, Dixit, Mahanta, and Tiwari, 2008). It was found that sonicator dyeing with *Mahonia napaulensis* showed a significant improvement in dye uptake and showed that pretreatment with a metal ion mordant substantially improved the fastness properties for dyed cotton, silk fabrics and wool yarn. In addition, extracted dye obtained from *Hibiscus mutabilis* (Gulzuba) has been used for the dyeing of cotton, wool and silk (Shanker and Vankar, 2006). It was found that pretreatment with a metal mordant showed very good fastness properties for cotton, silk and wool dyed fabrics.

To understand the silk dyeing process, the adsorption kinetics and thermodynamics of dyeing have been studied. For example, adsorption and kinetic studies of lac dyeing on silk were investigated (Chairat, Rattanaphani, S., Bremner and Rattanaphani, V., 2005). It was found that the experimental data fitted well to the Langmuir and Freundlich isotherms with a high correlation coefficient (R^2). The pseudo second-order kinetic model was indicated for the adsorption process with an activation energy of 47.5 kJ/mol. It was suggested that the overall rate of lac dye adsorption was likely to be controlled by the chemical process. The kinetics of wool dyeing with acid dye has also been studied (Bruce and Broadwood, 2000). They found that the uptake rate of the acid dye was likely to be a second order reaction. The kinetics could be explained in terms of the rate controlling step, which in this case is the reaction between the dye anion and the attachment site, rather than diffusion of the dye to the attachment site. In addition, the influence of nonionic surfactant on the thermodynamic and kinetic parameters for wool fiber dyeing has investigated (Treigine and Musnickas, 2003). It was found that the favorable effects of nonionic surfactant on dyeing thermodynamics are related to the screening of hydrophobic sites on the wool fiber surface, thus improving dye migration into the fiber and its subsequent fixation.

In the north and the northeast of Thailand, extracted dye from *Ceasalpinia sappan* Linn. (Figure 3.1) is used as a natural red or pink dyestuff for silk dyeing but the fastness properties and reproducibility to give consistency in production are still problems to be solved. As part of the approach to tackle these problems, fundamental physical studies on the dyeing process are important.



Figure 3.1 Morphological illustration of *Ceasalpinia sappan* Linn. (top) and its heartwood (bottom) from Nakhon Ratchasima, Thailand.

From Chapter II, brazilin and brazilein, are the major components of the heartwood of *Ceasalpinia sappan* Linn. but brazilin is readily converted to brazilein by exposure to atmospheric oxygen and light. Aqueous extracts of the wood of this plant are used for the dyeing of silk. However, the use of this natural dye mixture is often linked to poor fastness properties and thus metal-based mordants are used to increase fastness (e.g. wash fastness) properties. In the current study, the use of aluminium (III)-brazilein complexes and of aluminium (III)-extracted dye mixtures have been investigated in the dye adsorption process. The adsorption of brazilein and

extracted dye from *C. sappan* Linn. onto silk yarn was measured and determined quantitatively in relation to dye solution pH values, contact time, initial dye concentration, and material to liquor ratio (MLR) in this research. In addition, the Langmuir and Freundlich equations were used to fit the equilibria of dyeing onto silk yarn. The overall aim of this aspect of the research was to attempt to gain a better understanding of the adsorption mechanism in this dyeing process.

3.2.1 Physical chemistry of dyeing process

The scientific investigation of the process of dyeing involves two experimental methods which can be explained by kinetics and equilibria of dyeing (Zollinger, 2003). The process of dyeing involves the distribution of a dye between at least two phases, namely the dye bath and the substrate. The distribution process is called adsorption if the substance which is to be distributed is retained by a surface (e.g. gas on a solid). If the substance does not stay at the surface but enters the interior of a body (e.g. gas in liquid), the process is termed sorption. Dyeing processes of water soluble dyes in aqueous dye baths with any substrate always requires a distribution process between two phases (dye bath and substrate) (Perkins, 1996). The kinetic aspects of dyeing are represented by dye uptake curves which give the rate of transfer of dye in solution from the dye bath to the substrate. The position of sorption versus desorption after infinite time is represented by the dyeing equilibria of the dyeing process. In Figure 3.2 the graphical representations of a dyeing process was shown, by the dye uptake curves (left hand side) and dyeing isotherms (right hand side).

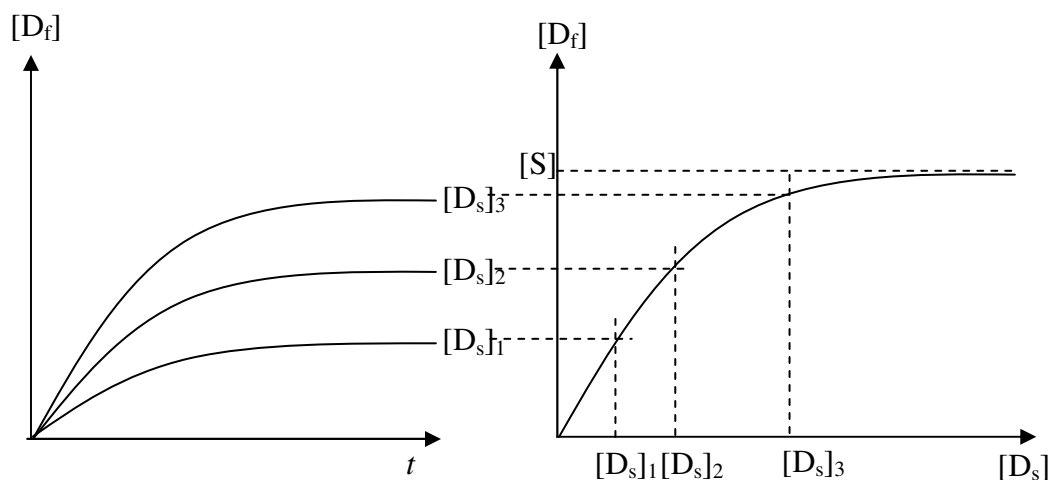


Figure 3.2 Graphical representation of a dyeing process: kinetics (left) and equilibrium (right) (Zollinger, 1991).

$[D_s]$: concentration of dye in solution $[D_f]$: concentration of dye in substrate

t : time

$[S]$: saturation value

If the process of dyeing is done under different isothermal conditions, a series of curves (Perkins, 1996) are given, as shown in Figure 3.3. The initial adsorption rate increases with an increase in temperature of dyeing. This can be described by the fact that the dye adsorption by fibers at higher temperature is faster than that at lower temperature and then leads to an increase in the initial rate constant. The slope of curve varies depending on the temperature, type of dye, type of fiber, amount of agitation of the dye bath, amount and type of dyeing auxiliaries used and other factors. As the amount of dye on the fiber increases, the sites being covered, and as a result the dye must leave the surface and diffuse toward the interior of the fiber before further additional dye molecules can be adsorbed from the dye bath.

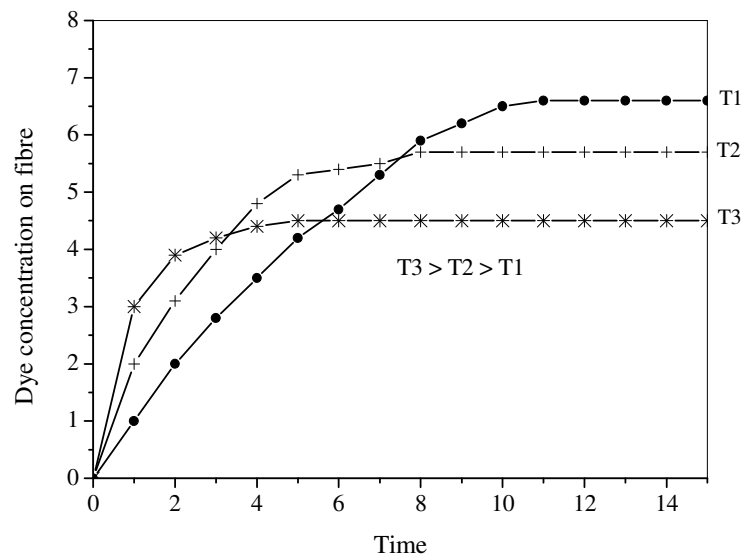


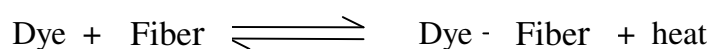
Figure 3.3 Rate of dyeing isotherms (Perkins, 1996).

The kinetic behaviour of a dye in the dyeing of a textile fiber comprises at least four stages (Zollinger, 2003) as follows:

- (a) convectonal diffusion to the fiber surface, occurring in the dye bath;
- (b) molecular diffusion through the hydrodynamic boundary layer;
- (c) adsorption at the outer surface;
- (d) molecular diffusion into the fiber (sorption).

The stages (a), (c), and (d) are important for the kinetics of the overall dyeing process. After some period of time, the slope of the isotherm becomes flat indicating that the system has reached equilibrium. The time required to reach equilibrium is always shorter at higher dyeing temperatures, mainly due to the fibers containing more dye at higher temperatures in the early stages but less dye in the latter stages of dyeing. Therefore, an increase in the temperature leads to an increase in the dyeing rate but a decrease in the ultimate exhaustion after the equilibrium time, as shown in

Figure 3.3. This shows that dye molecules can adsorb to a greater degree at a lower temperature because the dyeing reaction is exothermic.



Desorption of dye molecules from fibers to the dye bath takes place at higher dyeing temperatures because of more heat in the dyeing process. Thus, the equilibrium position of this process is shifted to the left hand side.

There are several different intermolecular and intramolecular interactions that are essential for understanding the chemistry of dyeing of a textile fiber. The four main types of interactions are Van der Waal's forces, Dipole-dipole interactions, covalent forces, ionic forces and hydrogen bonds (Christie *et al.*, 2000; Zollinger, 2003) and will be described below:

Van der Waal's forces

Van der Waal's forces or dispersion forces are the attractive force between non-polar molecules, which is caused by the induced temporary polarization of molecule by the dipole moments of molecules. The distances between molecules have an important effect on the strength of van der Waals forces. They are the weakest intermolecular forces and easily broken, but they can be important in dyeing. Although in a non-polar molecule there is no overall charge distribution, the electrons are in constant motion so that at any instant, small dipoles will be present. These instantaneous dipoles in turn induce oppositely-oriented dipoles in neighbouring molecules and a weak attraction between the molecules results. Van der Waals forces are therefore only effective for sorption of dyes to fiber molecules if the distance

between the dye and the fiber molecules is small. The influence of Van der Waal's forces particularly important in dyeing of cellulosic fibers.

Dipole-dipole interactions

Dipole-dipole interactions may make a contribution to the forces of attraction between dye and fiber molecules (Christie *et al.*, 2000). Dipole-dipole interactions are the forces that occur between two molecules with permanent dipoles. They result from the dipole-dipole interaction between two molecules. The strength of these interaction depends on the distance and relative orientation of the dipoles. Dipole-dipole interactions are weaker than ionic forces.

Covalent forces

Covalent bond is a chemical bond where a pair of electrons is shared relatively equally between two atoms in the compound. Covalent bonds are formed between the fibers and reactive dyes. These are the strongest type of chemical bond, and are responsible for the excellent wash fastness of reactive dyes.

Ionic forces

Ionic bond is a chemical bond as a result of electrical attraction between positive and negative ions. In ionic bonding, typically an electron transfer from one atom to another, leaving one with a positive charge and one with a negative charge. These electrical charge produce strong attraction between the differently charged ions. Ionic bonds are strong, but not generally as strong as covalent bonds. Such bonds are important with acid dyes and basic (cationic) dyes. Wool, silk, and polyamides contain amino and carboxylic acid groups and their state of ionization depends on the pH of the dyeing solution. At acidic pH values these fibers have an overall positive charge (NH_3^+ groups present) and the acidic carboxyl acid groups in the side chains

are hardly ionized. Therefore, under these conditions, anionic dyes for example, will be attracted towards the positively charged amino groups by ionic forces (Chairat *et al.*, 2005).

Hydrogen bonding

Hydrogen bond is a chemical bond in which hydrogen that already covalently bonded to one atom is electrically attracted to a lone pair of electrons on another atom. Some atoms such as oxygen are said to be very electronegative, which mean that they strongly draw bonding electrons toward themselves. If hydrogen is bonded to such an atom, the hydrogen “appears” to have some positive charge. Lone pair of electronegative atoms tend to attract hydrogen from other molecule. Hydrogen bonds are weak to moderate in strength. Hydrogen bonds play a role in dyeing with direct dyes.

3.2.2 Adsorption kinetics

In order to investigate the adsorption mechanism and potential rate controlling steps such as chemical reaction, diffusion control and mass transfer processes, kinetic models have been used to test experimental data. These kinetic models included the pseudo first-order equation and the pseudo second-order equation, that are describes as follows.

3.2.2.1 Pseudo first-order equation

The adsorption kinetic data were described by the Lagergren pseudo-first-order model, which is the earliest known equation describing the adsorption rate based on the adsorption capacity. The differential equation is generally expressed as follows (Purkait, DasGupta, and De, 2005; Septhum, Rattanaphani, S., Bremner, and Rattanaphani, V., 2007; Chairat, Rattanaphani, S., Bremner, and

Rattanaphani, V., 2008; Hameed and Daud, 2008; Kavitha and Namasivayam, 2008; Tan, Ahmad, and Hameed, 2008):

$$\frac{dq_t}{dt} = k_1(q_e - q_t) \quad (3.1)$$

where q_e and q_t are the amounts of dye adsorbed per gram silk (mg/g silk) at equilibrium and time t , respectively, and k_1 is the rate constant of pseudo first-order adsorption (min^{-1}). Integrating equation (3.1) with respect to the boundary conditions $q_t = 0$ at $t = 0$ and $q = q_t$ at $t = t$, then equation (3.1) becomes:

$$\ln (q_e - q_t) = \ln q_e - k_1 t \quad (3.2)$$

In order to confirm the applicability of the pseudo-first order kinetics model, a plot $\ln (q_e - q_t)$ against t should yield a straight line. The pseudo first-order rate constant k_1 and equilibrium adsorption density q_e were calculated from the slope and intercept of this line.

3.2.2.2 Pseudo second-order equation

If the rate of adsorption has a second-order mechanism, the pseudo second-order chemisorption kinetic rate equation of Ho and McKay is expressed as (Önal, 2006; Chairat *et al.*, 2005; Septhum *et al.*, 2007; Chairat *et al.*, 2008; Kavitha and Namasivayam, 2008):

$$\frac{dq_t}{dt} = k_2(q_e - q_t)^2 \quad (3.3)$$

where k_2 is the rate constant of pseudo second-order adsorption (g silk/mg min). Integrating equation (3.3) for the boundary conditions $q_t = 0$ at $t = 0$ and $q = q_t$ at $t = t$, gives (Ho and McKay, 1999):

$$\frac{1}{(q_e - q_t)} = \frac{1}{q_t} + k_2 t \quad (3.4)$$

Equation (3.4) can be rearranged to obtain a linear form:

$$\frac{t}{q_t} = \frac{1}{k_2 q_e^2} + \frac{1}{q_e} t \quad (3.5)$$

and

$$h_i = k_2 q_e^2 \quad (3.6)$$

where h_i is the initial dye adsorption rate (mg/g silk min) (Chiou and Li, 2003; Chairat *et al.*, 2005; Chairat *et al.*, 2008). If the pseudo second-order kinetic equation is applicable to fit the experimental data, the plot of (t/q_t) against t of equation (3.5) should give a linear relationship. The pseudo second-order rate constant k_2 and equilibrium adsorption density q_e were calculated from the intercept and slope of this line. This model is based on the assumption that the rate-limiting step may be chemisorption involving electrostatic forces through the sharing or exchange of electrons between adsorbent and adsorbate (Chiou and Li, 2002; Tan *et al.*, 2008).

Basically, the values of the rate constant, the adsorption capacity at equilibrium, and the initial adsorption rate increase with increasing solution temperature. The dependence of rate constants on temperature over a limited range

can usually be represented by an empirical equation proposed by van't Hoff and Arrhenius in 1884 (Laidler, Meiser, and Sanctuary, 2003):

$$k = Ae^{-E_a/RT} \quad (3.7)$$

where A is the pre-exponential factor, E_a is the activation energy of adsorption (kJ/mol), representing the minimum energy that reactants must have for the reaction to proceed, R is the gas constant, equal to 8.3145 J/mol K and T is the solution temperature in K. The pre-exponential factor A has the same units as the rate constant. An alternative form is obtained by taking the logarithm of each side.

$$\ln k = \ln A - \frac{E_a}{RT} \quad (3.8)$$

The activation energy was calculated from the slope of a straight line plots of $\ln k$ is plotted against $1/T$. The magnitude of the activation energy gives an idea about the adsorption type which is mainly physical or chemical. In the physical adsorption or *physisorption* which usually has low activation energies (5-40 kJ/mol) because the forces involved in physical adsorption are normally weak, the reaction is easily reversible and equilibrium is rapidly attained. While higher activation energies (40-800 kJ/mol) involved stronger forces (eg. covalent bonds), suggest chemisorption process or *chemisorption* (Aksu, 2002; Özcan, A. S. and Özcan, A., 2005; Uçun, Bayhan, and Kaya, 2008).

The enthalpy ($\Delta H^\#$), entropy ($\Delta S^\#$) and free energy ($\Delta G^\#$) of activation can be also calculated using the Eyring equation (House, 1997; Laidler *et al.*, 2003; Anirudhan and Radhakrishnan, 2008) as follows:

$$\ln\left(\frac{k}{T}\right) = \ln\left(\frac{k_b}{h}\right) + \frac{\Delta S^\#}{R} - \frac{\Delta H^\#}{RT} \quad (3.9)$$

where k_b and h refer to Boltzmann's constant and Planck's constant, equal to 1.38×10^{-23} J/K and 6.626×10^{-34} J.s respectively. The enthalpy ($\Delta H^\#$) and entropy ($\Delta S^\#$) of activation were calculated from the slope and intercept of a plot of $\ln(k/T)$ versus $1/T$. Gibbs energy of activation ($\Delta G^\#$) can be written in terms of enthalpy and entropy of activation (House, 1997; Laidler *et al.*, 2003; Anirudhan and Radhakrishnan, 2008):

$$\Delta G^\# = \Delta H^\# - T\Delta S^\# \quad (3.10)$$

3.2.3 Adsorption isotherms

The adsorption isotherm is basically importance to describe how adsorbates interact with adsorbents, and is critical in optimizing the use of adsorbents (Tan, Hameed, and Ahmad, 2007; Thinakaran *et al.*, 2008). The adsorption isotherm data was fitted to well-known and widely applied isotherm models of Langmuir and Freundlich. The applicability of the isotherm models to the adsorption study done was compared by judging the correlation coefficients, R^2 values.

3.2.3.1 Langmuir isotherm

The Langmuir isotherm is the most frequently used model for the real adsorption. This isotherm is based on the ideal assumption of a totally homogeneous adsorption surface. It is assumed that once a dye molecule occupies a site, no further adsorption can take place at that site. As a result, a saturation value is reached and no further adsorption can take place. (Chairat *et al.*, 2005; Septhum *et al.*, 2007; Hameed and Daud 2008; Thinakaran *et al.*, 2008). It is expressed by the following equation:

$$q_e = \frac{QbC_e}{1 + bC_e} \quad (3.11)$$

where q_e is the amount of dye adsorbed per units weight of silk at equilibrium (mg/g silk), Q (mg/g silk) is maximum amount of dye to form a complete monolayer on the surface, b is the adsorption equilibrium constant (L/mg) and C_e is the equilibrium dye concentration (mg/L) A linear form of this expression is given as:

$$\frac{C_e}{q_e} = \frac{1}{Qb} + \left(\frac{1}{Q}\right)C_e \quad (3.12)$$

For lower concentrations, the following form of Langmuir equation is found to be more satisfactory (Bhattacharyya and Sarma, 2003; Rattanaphani, S., Chairat, Bremner, and Rattanaphani, V., 2007):

$$\frac{1}{q_e} = \frac{1}{Q} + \frac{1}{QbC_e} \quad (3.13)$$

The straight line plots of $1/q_e$ against $1/C_e$ is obtained from this model and the values of Q and b are calculated from the intercepts and slopes of the straight lines.

To determine if the process of adsorption is favorable or unfavorable, for the Langmuir type adsorption process, isotherm can be classified by a term ' R_L ' a dimensionless constant separation factor, also called equilibrium parameter (Bulut, Özacar, and Şengil, 2008; Chairat *et al.*, 2005; Anirudhan and Radhakrishnan, 2008; Tan *et al.*, 2008; Uçun *et al.*, 2008), which is defined by Hall *et al.* (Hall, Eagleton, Acrivos, and Vermeulen, 1966) as:

$$R_L = \frac{1}{1+bC_0} \quad (3.14)$$

where C_0 is the initial concentration of dye (mg/L) and b is the Langmuir constant (L/mg). The value of R_L indicates the type of the isotherms to be either irreversible ($R_L = 0$), favorable ($0 < R_L < 1$), linear ($R_L = 1$) or unfavorable ($R_L > 1$).

3.2.3.2 Freundlich isotherm

The Freundlich isotherm can be applied to non-ideal adsorption on heterogeneous surfaces as well as multilayer adsorption. This isotherm is derived by assuming a heterogeneous surface with non-uniform distribution of energy of adsorption over the surface. This isotherm is suitable for the highly heterogeneous surface and the application of this isotherm suggests that energy of adsorption

exponentially decreases on completion of the adsorptional centers of an adsorbent (Chiou and Li, 2002; Chairat *et al.*, 2005; Hameed and Daud, 2008; Hameed and El-Khaiary, 2008; Vasanth Kumar and Sivanesan, 2007). It is expressed by the following equation:

$$q_e = Q_f C_e^{1/n} \quad (3.15)$$

where Q_f is the Freundlich adsorption constant related to the adsorption capacity and $1/n$ is the Freundlich adsorption constant related to the adsorption. A linear form of equation (3.15) is:

$$\ln q_e = \ln Q_f + \frac{1}{n} \ln C_e \quad (3.16)$$

When $\ln q_e$ is plotted against $\ln C_e$ and the data are treated by linear regression analysis, Q_f and $1/n$ can be calculated from the intercept and slope. The values of $1/n$ were found to be between 0 and 1 indicating favorable adsorption (Thinnakaran *et al.*, 2008).

3.2.4 Thermodynamic modeling of adsorption

The concept of thermodynamics assumed that in an isolated system where energy cannot be gained or lost, the entropy change is the only driving force. The thermodynamic parameters reflect the feasibility and spontaneous nature of the adsorption process. Thermodynamic parameters that must be considered to determine the process are changes in standard Gibbs free energy (ΔG°), enthalpy (ΔH°) and

entropy (ΔS°) of adsorption were calculated from the following equation (Chiou and Li, 2003; Chairat *et al.*, 2005; Anirudhan and Radhakrishnan, 2008; Uzun *et al.*, 2008; Nuhoglu and Malkoc, 2009):

$$\Delta G^\circ = -RT \ln K_c \quad (3.17)$$

where R is the gas constant, K_c is the equilibrium constant and T is the solution temperature in K . The K_c value is calculated from equation (3.18):

$$K_c = \frac{C_{ad,e}}{C_e} \quad (3.18)$$

where $C_{ad,e}$ and C_e are the dye concentrations adsorbed at equilibrium (mg/L) and the concentration of dye left in the dye bath at equilibrium (mg/L), respectively.

According to van't Hoff equation:

$$\ln K_c = \frac{\Delta S^\circ}{R} - \frac{\Delta H^\circ}{RT} \quad (3.19)$$

The values of ΔH° and ΔS° were calculated from the slope and intercept of van't Hoff plots of $\ln K_c$ against $1/T$.

The negative value ΔG° indicated the feasibility of the adsorption process and the spontaneous nature of the adsorption. The positive value of ΔH° indicated the endothermic nature of the adsorption process, whereas the negative

value of ΔH° indicated the exothermic nature of the adsorption process. The negative values of ΔS° suggest decreased randomness at the solid/solution interface and no significant changes occur in the internal structure of the adsorbent through the adsorption of the adsorbate onto the adsorbent, whereas the positive value of ΔS° suggests increased randomness at the solid/solution interface with some structural changes in the adsorbent and the adsorbate and an affinity of the adsorbate.

3.3 Experimental

3.3.1 Chemicals

- (a) Silk yarn from Pungthungchai, Nakhon Ratchasima
- (b) Brazilein (prepared by oxidation of brazilin using iodine solution)
- (c) Soap, commercial grade
- (d) Sodium silicate, commercial grade
- (e) Sodium hydroxide, NaOH, Aldrich
- (f) Sodium carbonate, Merck
- (g) Hydrogen peroxide 40% (w/v), commercial grade
- (h) Hydrochloric acid 37% (w/v), HCl, Merck
- (i) Glacial acetic acid, CH₃COOH, Merck
- (j) Alum, KAl(SO₄)₂·12H₂O, Merck

3.3.2 Instruments

- (a) An Agilent 8453 UV-Visible spectrophotometer was employed for absorbance measurements using quartz cells of path length 1 cm.
- (b) A pH meter (Schott) was used to measure the pH values of dye solutions.

(c) A thermostatted shaker bath (Type SBD-50 cold Heto-Holten A/S, Denmark), operated at 150 strokes/min, was used to study the adsorption kinetics and thermodynamics of dyeing on silk.

(d) A Freeze dryer (Heto FD3 model S/N 492497-B, Cat No. 837107, Denmark) was used to dry the crude extract.

3.3.3 Experimental methods

3.3.3.1 Silk yarn preparation (Chairat, 2004; Septhum, 2006)

The silk yarn for this study was purchased from villagers living in Nakhon Ratchasima, Thailand. To remove the sericin gum, the silk yarn (1 kg) was added to boiling water (5 L), to which had been added soap flakes (*ca* 100 g), sodium silicate (10 g), sodium carbonate (50 g) and 40% hydrogen peroxide (100 mL). The mixture was then boiled for 2 hours. The silk was then removed, washed with water, squeezed to remove excess liquor and air dried. Finally, it was treated with 0.5 M HCl (*ca* 3 L) at room temperature for 30 minutes and then removed and washed with deionized water until the rinsed water was neutral. The silk yarn was then dried at room temperature.

3.3.3.2 Stock solutions

Brazilein stock solution (5.0×10^{-4} M) was prepared in deionized water. Alum, $\text{KAl}(\text{SO}_4)_2 \cdot 12\text{H}_2\text{O}$, stock solution (5.0×10^{-4} M) was prepared in deionized water. These solutions were diluted with deionized water further as required. Alum-brazilein stock solution (2:1 molar ratio) for dyeing on silk yarn were prepared by mixing appropriate volumes of the initial alum and brazilein stock solutions and diluting to 1000 mL (volumetric flask) with deionized water.

3.3.3.3 Pre-, simultaneous and post-mordanting for brazilein dyeing onto silk

Pre-mordanting: Silk yarn was first immersed in alum solutions of 47 mg/L and 94 mg/L, material to liquor ratio (MLR) 1:100 in a thermostatted shaker bath at 30°C for 120 minutes and then the silks yarn was dried at room temperature. Brazilein solution (14 mg/L) was prepared by dissolving brazilein in deionized water. Adsorption experiments were carried out by shaking the dye solution (50 mL; brazilein concentration 14 mg/L) in each conical flask (125 mL) in a thermostatted shaker bath at 30°C. After 30 minutes, the silk yarn (0.50 g), which had been pre-warmed in the thermostatted shaker bath for 30 minutes, was immersed in the dye solution. The silk yarn samples were then rapidly withdrawn after different immersion times. Dye concentrations were determined at time zero and at subsequent times using a calibration curve based on absorbance at λ_{\max} 446 nm (an Agilent 8453 UV-Visible spectrophotometer) versus dye concentration. The amount of dye adsorbed onto silk, q_t (mg/g silk), at any time t was calculated by the mass balance relationship (equation (3.20)) as follows:

$$q_t = (C_0 - C_t) \frac{V}{W} \quad (3.20)$$

where C_0 and C_t are the dye concentration (mg/L) at time zero and after dyeing time t , respectively, V is the volume of the dye solution (L), and W is the weight of the silk used (g).

Simultaneous mordanting: Alum-brazilein (2:1) solutions were prepared in deionized water at the desired concentrations. Adsorption experiments were carried out by shaking the mordant-dye solution (50 mL) of each concentration in each conical flask (125 mL) in a thermostatted shaker bath at 30°C. After 30 minutes, the silk yarn (0.50 g), which had been pre-warmed in the thermostatted shaker bath for 30 minutes, was immersed in the dye solution. The silk yarn samples were then rapidly withdrawn after different immersion times. Dye concentrations were determined at time zero and at subsequent times using calibration curve based on absorbance at λ_{\max} 509 nm (an Agilent 8453 UV-Visible spectrophotometer) versus dye concentrations. The amount of dye adsorbed onto silk, q_t (mg/g silk), at any time t was calculated by the mass balance relationship (equation (3.20)).

Post-mordanting: The brazilein solution (14 mg/L) was prepared by dissolving brazilein in deionized water to give the desired concentration. Adsorption experiments were carried out by shaking the brazilein dye solution (50 mL) at the desired concentration in each conical flask (125 mL) in a thermostatted shaker bath at 30°C. After 30 minutes, the silk yarn (0.50 g), which had been pre-warmed in the thermostatted shaker bath for 30 minutes, was immersed in the dye solution. The silk yarn samples were then rapidly withdrawn after different immersion times and then immersed in the alum solution (50 mL; alum concentration 47 mg/L) for 120 minutes. Dye concentrations were determined at time zero and at subsequent times using a calibration curve based on absorbance at λ_{\max} 446 nm (Agilent 8453 UV-Visible spectrophotometer) versus dye concentration. The amount of dye adsorbed onto silk, q_t (mg/g silk), at any time t was calculated by the mass balance relationship (equation (3.20)).

3.3.3.4 Effect of pH

Alum-brazilein (2:1) solutions were made up in deionized water at the desired concentrations. The pH of the aqueous solutions was adjusted by using 0.1 M NaOH or 0.1 M CH₃COOH. Adsorption experiments were carried out by shaking the dye solution (50 mL) in each conical flask (125 mL) in a thermostatted shaker bath at 30°C. After 30 minutes, the silk yarn (0.50 g), which had been pre-warmed in the thermostatted shaker bath for 30 minutes, was immersed in the dye solution. The silk yarn samples were then rapidly withdrawn at 60 minutes. Dye concentrations were determined at time zero and at 60 minutes using a calibration curve based on absorbance at λ_{\max} 509 nm (Agilent 8453 UV-Visible spectrophotometer) versus dye concentration. The amount of dye adsorbed onto silk, q_t (mg/g silk), at any time t was calculated by the mass balance relationship (equation (3.20))

3.3.3.5 Batch kinetics of the alum-brazilein experiments

Alum-brazilein (2:1) solutions were prepared by dissolving the components in deionized water at the desired concentration. Adsorption experiments were carried out by shaking the dye solution (50 mL) in each conical flask (125 mL) in a thermostatted shaker bath at 30°C. After 30 minutes, the silk yarn (0.50 g), which had been pre-warmed in the thermostatted shaker bath for 30 minutes, was immersed in the dye solution. The silk yarn samples were then rapidly withdrawn after different immersion times. Dye concentrations were determined at time zero and at subsequent times using a calibration curve based on absorbance at λ_{\max} 509 nm (Agilent 8453 UV-Visible spectrophotometer) versus dye concentration. The amount of dye adsorbed onto silk, q_t (mg/g silk), at any time t was calculated by the mass balance

relationship (equation (3.20)). Kinetic experiments on alum-brazilein dyeing of silk were repeated three times.

3.3.3.6 Batch equilibrium of the alum-brazilein experiments

The alum-brazilein complexes were diluted in deionized water to the required concentrations. In experiments on the equilibrium adsorption isotherm, silk (0.5 g) and the alum-brazilein complex solutions (50 mL each) were put in a 125 mL conical flask and were shaken for 120 minutes using a thermostated shaker bath to control the temperature. The initial and equilibrium alum-brazilein complex concentrations were estimated by measuring absorbance at maximum wavelength (λ_{\max} 509 nm) by an Agilent 8453 UV-Visible spectrophotometer and computing concentration from the calibration curve based on absorbance at λ_{\max} 509 nm versus dye concentrations. The amount of dye adsorbed onto silk at equilibrium, q_e (mg/g silk) was calculated by the mass balance relationship (equation (3.21)) as follows:

$$q_e = (C_0 - C_e) \frac{V}{W} \quad (3.21)$$

where C_0 and C_e are the initial and equilibrium concentration of dye (mg/L), respectively, V is the volume of the dye solution (L), and W is the weight of the silk used (g). Equilibrium experiments for the adsorption of alum-brazilein dyeing onto silk were repeated three times.

3.3.3.7 Adsorption and desorption studies of alum-brazilein and alum-extracted dye onto silk

The silk yarn, prepared as noted in section 3.3.3.1, was dyed with an initial dye concentration of 14 mg/L in a thermostatted shaker bath. The adsorption conditions were MLR of 1:100 and 30°C. The absorbance of the dye solutions was monitored until constant absorbance values were obtained. The silk samples were then taken out and dried at room temperature. To study desorption of alum-brazilein and alum-extracted dye at 30°C, deionized water 50 mL in each conical flask (125 mL) was shaken in a thermostatted shaker bath. After 30 min, the dried silk sample (0.50 g), which had been pre-warmed in the thermostatted shaker bath at 30°C for 30 min, was immersed in deionized water. The silk samples were then rapidly withdrawn after different immersion times. The desorbed dye concentrations (q_{de}) were determined using a calibration curve based on absorbance at λ_{max} 509 (alum-brazilein) and 507 (alum-extracted dye) nm versus dye concentration. The amount of dye adsorbed on silk after desorption was calculated by subtraction. Studies of the dye-mordant desorption desorption at MLR 1:150, 1:200 in deionized water and at MLR 1:100, 1:150, 1:200 in distilled water and tap water were carried out in the same manner as for those in deionized water.

3.3.3.8 Extraction of dye

The extracted dye was, prepared as noted in section 2.3.3.1 in Chapter 2.

3.3.3.9 Batch kinetic studies of alum-extracted dye onto silk

Extracted dye stock solution (1000 mg/L) was prepared in deionized water. This solution was diluted further as required. Alum-extracted dye complex solutions were prepared by dissolving the components in deionized water to give the desired concentration. Sorption experiments were carried out by shaking the dye solution (50 mL) in the desired concentration in each conical flask (125 mL) in a thermostatted shaker bath at 30°C. After 30 minutes, the silk yarn (0.50 g), which had been pre-warmed in the thermostatted shaker bath for 30 minutes, was immersed in the dye solution. The silk yarn samples were then rapidly withdrawn after different immersion times. Dye concentrations were determined at time zero and at subsequent times using calibration curve based on absorbance at λ_{\max} 507 nm (Agilent UV-Visible spectrophotometer) versus dye concentration. The amount of dye adsorbed onto silk, q_t (mg/g silk), at any time t was calculated by the mass balance relationship (equation (3.20)). Kinetic experiments for alum-extracted dye adsorption onto silk were repeated three times.

3.3.3.10 Batch equilibrium adsorption of alum-extracted dye onto silk

Alum-extracted dye complexes were diluted in deionized water to the required concentrations. In experiments of equilibrium adsorption isotherm, 0.50 g silk and 50 mL alum-extracted dye solutions were put in a 125 mL conical flask and were shaken for 120 minutes by using a thermostated shaker bath to control the temperature. The initial and equilibrium alum-extracted dye complex concentrations were determined by measuring absorbance at maximum wavelength (λ_{\max} 507 nm) with an Agilent UV-Visible spectrophotometer and computing

concentration from the calibration curve based on absorbance at λ_{\max} 507 nm versus dye concentration. The amount of dyed adsorbed onto silk at equilibrium, q_e (mg/g silk) was calculated by the mass balance relationship (equation (3.21)). Equilibrium experiments for the adsorption of alum-extracted dye adsorption on silk were repeated three times.

3.4 Results and discussion

3.4.1 Comparison of pre-, simultaneous and post-mordanting for brazilain dyeing onto silk

Dyeing is a manifold phenomenon, and the precise nature of dye-fiber interactions still remains a matter of debate. The great variety of chemical and physical interactions possible between the dye molecules, fiber, and metal ions in mordant dyeing suggest that a number of different products can be formed in the fibers (Raisanen, Nousiainen, and Hynninen, 2001). The mordant is a metal salt or tannin and tannic acid used to fix the dye to the fiber, mordants work by forming chemical bonds or interactions between the dye molecules and the proteins of the silk fibre. There are three opportunities for immersion mordanting to fibers covering pre-mordanting, simultaneous mordanting and post-mordanting. For the effective dyeing of silk with brazilain, it was considered that mordanting was essential.

Figure 3.4 shows a comparison of pre-, simultaneous, and post-mordanting with alum for brazilain dyeing onto silk. Adsorption experiments carried out under the conditions of an initial concentration of brazilain of 14 mg/L, an MLR of 1:100, at pH 4.0, and a temperature of 30°C. It was found that the amount of dye adsorbed per gram of silk (q_t) of post-mordant alum (or brazilain alone) was lower

than for pre-mordant and alum-brazilein (simultaneous mordanting). When pre-mordanting with 94 mg/L of alum, the amount of dye adsorbed of alum-brazilein was close to that using only 47 mg/L of alum in alum-brazilein dyeing onto silk. Therefore, the dyeing of silk with alum-brazilein (simultaneous mordanting) was chosen throughout this study because the least amount of alum was used. Similar observation was reported for alum-morin dyeing onto silk (Septum, 2006).

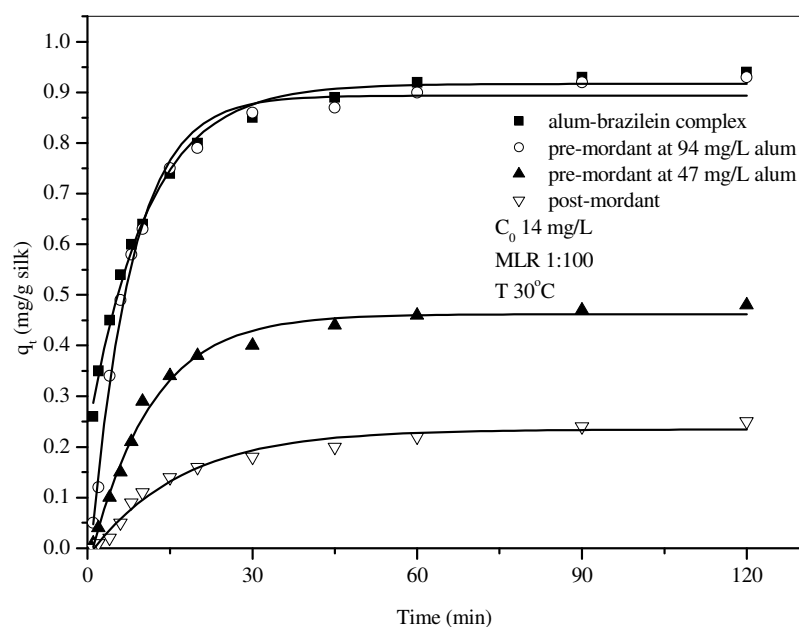


Figure 3.4 Comparison of pre-, simultaneous and post-mordanting with alum for brazilein dyeing onto silk.

3.4.2 Optimal conditions of silk dyeing with alum-brazilein

In order to investigate the adsorption of alum-brazilein on silk (simultaneous mordanting), the experimental parameters including pH, material to liquor ratio (MLR), contact time, initial dye concentration and temperature were determined to find the optimal conditions for adsorption. The mechanism of adsorption of alum-brazilein dyeing onto silk was investigated by using the pseudo first-order and pseudo second-order models. In addition, activation parameters and thermodynamic parameters of adsorption were calculated.

3.4.2.1 The effect of pH on the adsorption of alum-brazilein onto silk

The pH of the dye solution is one of the most important parameters controlling the adsorption capacity of dyes onto silk (Christie *et al.*, 2000; Chairat, 2004; Chairat *et al.*, 2005). As part of the studies on the pH effect, the influence of pH on the UV-visible absorption spectra of the alum-brazilein complex in the absence of silk was assessed. Subsequently, silk was included and the amount of alum-brazilein complex adsorbed was found to vary with pH. The adsorption data of alum-brazilein dyeing onto silk at different pH values are shown in Table 3.1. The effect of pH on the adsorption of alum-brazilein dyeing onto silk at an initial dye concentration of 14 mg/L, MLR 1:100 and 30°C are shown in Figure 3.5. It was found that the adsorption capacity decreased with increasing pH over the pH range 3.9-2.2, and remained constant in the pH range 3.9-4.5, but dropped gradually at pH values higher than 4.5. The maximum adsorption capacity was observed to occur at pH 3.9. At pH 3.9-4.5, if the coordination linkages between the silk, alum and brazilein were the major form of intermolecular interaction, then alum-brazilein

would be expected to form quite strong bonds with the silk fiber (Raisanen *et al.*, 2001; Septhum, 2006). Therefore, the alum-brazilein complex at pH 4.0 was used to study the kinetic and thermodynamic aspects of the adsorption process throughout this study.

Table 3.1 The amount of dye adsorbed per gram of silk at different pH values; dyeing at MLR 1:100, an initial dye concentration of 14 mg/L, 30°C and 1 hour of contact time.

pH of dye solution	Weight silk (g)	A_0	$A_{t = 1 \text{ hr}}$	q_e (mg/g silk)
2.28	0.5019	0.36957	0.32070	0.18
2.88	0.5008	0.25892	0.20405	0.29
3.29	0.5013	0.26616	0.19613	0.34
3.65	0.5008	0.62043	0.18634	0.70
3.90	0.5015	0.72846	0.16899	0.90
4.51	0.5029	0.71718	0.20801	0.88
4.95	0.5029	0.56233	0.15712	0.80

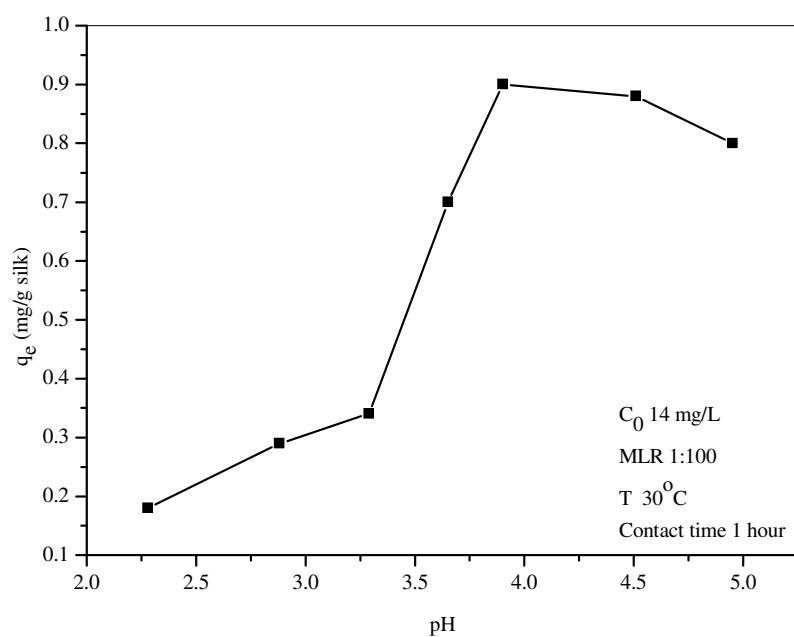


Figure 3.5 The effect of pH on alum-brazilein dyeing onto silk.

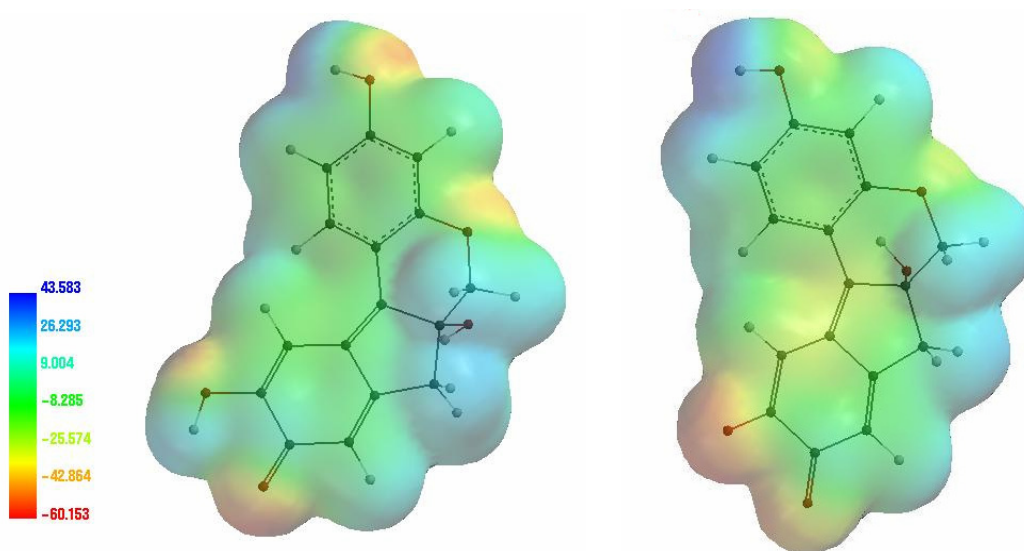


Figure 3.6 Electrostatic map of brazilein (left) and brazilein anion (right). (Spartan Program; AM1; Wavefunction Inc.; '02 Linux/Unix).

3.4.2.2 The effect of material to liquor ratio (MLR) on the adsorption of alum-brazilein onto silk

Material to liquor ratio is another important parameter which influences the exhaustion of dye and the establishment of an equilibrium between the concentration of dye on the fiber and the dye in the dye bath. The effect of the material liquor ratio on the adsorption of alum-brazilein onto silk was investigated under the dyeing condition of an initial dye concentration of 14 mg/L at pH 4.0 and temperature 30°C are shown in Figure 3.7. It was found that an increase in volume of the dye solution resulted in an increase of dye adsorbed onto silk. It indicated that silk yarn is loosely packed in the higher volume of dye solution and the dye solution readily moves past any surface transferring dye molecules to the silk surface in the process. On reaching the silk surface the dye molecules will be adsorbed onto the surface and then diffuse into the interior of the silk yarn. The amount of dye adsorbed at an MLR of 1:150 showed the highest values when compared with MLR values of 1:100 and 1:50 (Figure 3.7) but at MLR of 1:100 and 1:150 showed only a small difference in the amount of the dye adsorbed onto the silk. In order to minimize waste from the dyeing process, the MLR of 1:100 was then used for all the kinetic experiments.

The kinetic parameters from linear plots of pseudo first-order (Figure 3.8) and pseudo second-order (Figure 3.9) models are given in Table 3.2. The data indicated that a good compliance with the pseudo second-order equation and the regression coefficients (R^2) for the linear plot were all high (> 0.99). The equilibrium sorption capacity ($q_{e,cal}$) for the second-order process is more reasonable than for the

first-order process when comparing predicted results with experimental data ($q_{e,exp}$) because the equilibrium sorption capacities are higher than the experimental results.

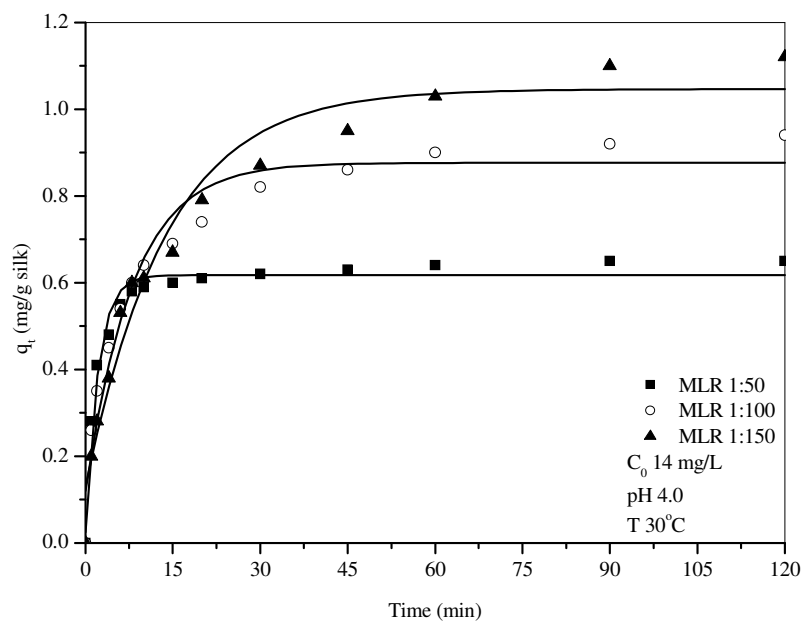


Figure 3.7 The effect of material to liquor ratio on the adsorption of alum-brazilein onto silk.

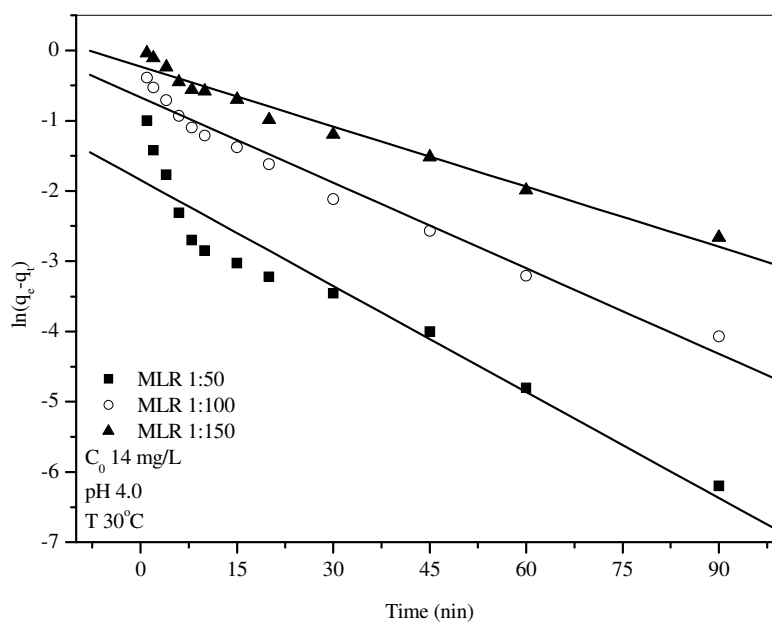


Figure 3.8 Pseudo first-order equation plots for the adsorption of alum-brazilein onto silk at different material to liquor ratios.

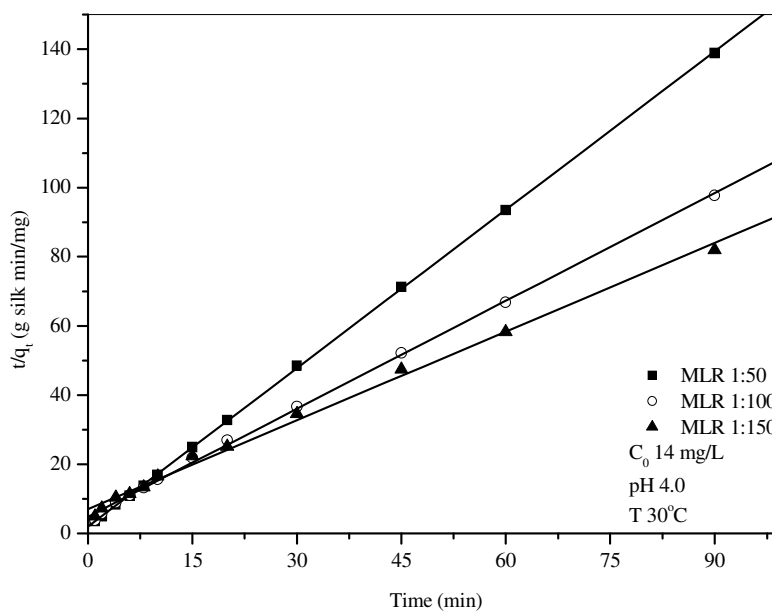


Figure 3.9 Pseudo second-order equation plots for the adsorption of alum-brazilein onto silk at different material to liquor ratios.

3.4.2.3 The effect of contact time and initial dye concentration on the adsorption of alum-brazilein onto silk

The adsorption capacity of alum-brazilein onto silk was a function of the initial dye concentration. The effect of contact time and initial dye concentration on adsorption of alum-brazilein onto silk was investigated with an MLR of 1:100 at pH 4.0 and a temperature of 30°C and the results are presented in Figure 3.10. It was found that the amount of dye adsorbed on silk increased with an increase in the initial concentration of the dye solution. This is due to the increase in the driving force of the concentration gradient with the higher initial dye concentration (Chiou and Li, 2002; Chairat *et al.*, 2005). This indicated that the initial dye concentration plays an important role in the adsorption capacity of alum-brazilein onto silk. The equilibrium time was found to be about 60 minutes for initial dye concentrations of 14, 21, and 28 mg/L at pH 4.0 and 30°C. The adsorption was very fast at the initial stages of the contact time and gradually decreased with time until it remained constant.

The results of the rate constant studies for different initial concentrations using the pseudo-first and pseudo-second order models and correlation coefficients are listed in Table 3.2, and in Figure 3.11 and Figure 3.12, pseudo-first and pseudo-second order plots, respectively, are presented. It was found that the pseudo-second order model well described the adsorption of alum-brazilein onto silk with a higher correlation coefficient ($R^2 > 0.99$) than the pseudo-first order model and the calculated equilibrium sorption capacities fitted well with the experimental data. These suggest that the pseudo-second order adsorption mechanism is predominant and that the overall alum-brazilein adsorption process on silk appears to be controlled by

the chemical process. The results in Table 3.2 also show k_2 , h_i , and q_e as a function of initial dye concentration. The rate constant (k_2) for the pseudo-second order decreases with an increasing of initial dye concentration, while the initial dye adsorption rate(h_i) increases with an increasing initial dye concentration. An increase in initial dye concentration results in a significant increase in $q_{e,cal}$.

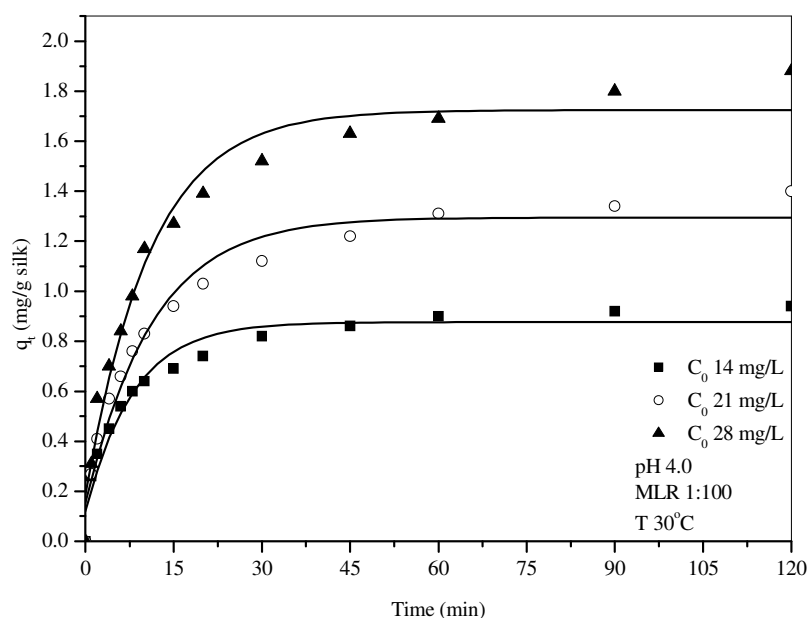


Figure 3.10 The effect of contact time and initial dye concentration on the adsorption of alum-brazilein onto silk.

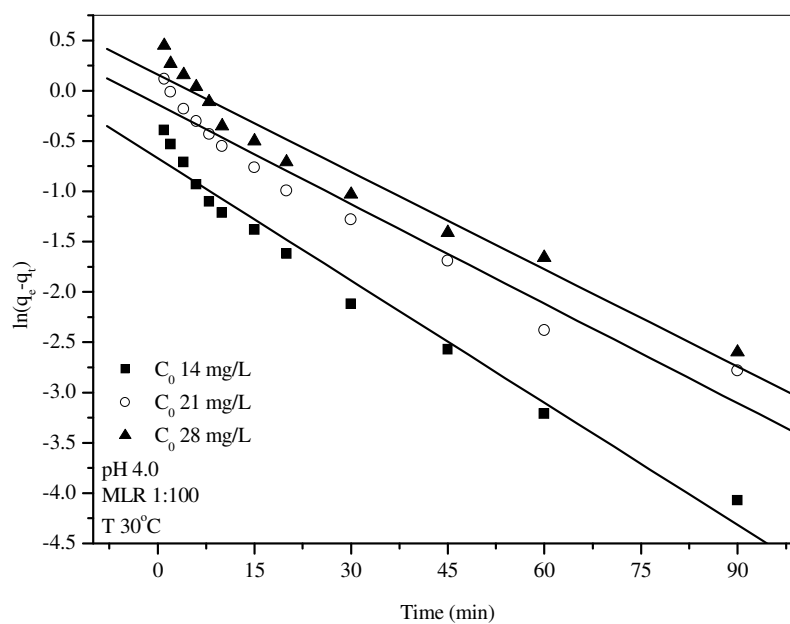


Figure 3.11 Pseudo first-order equation plots for the adsorption of alum-brazilein onto silk at different initial dye concentrations.

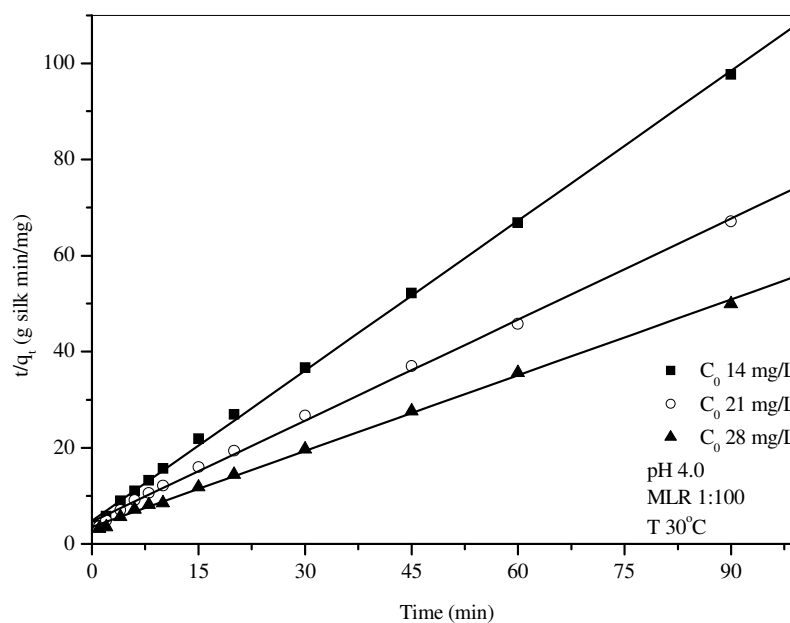


Figure 3.12 Pseudo second-order equation plots for the adsorption of alum-brazilein onto silk at different initial dye concentrations.

3.4.2.4 The effect of temperature on the adsorption of alum-brazilein onto silk

The results of the studies on the influence of temperature on the adsorption of alum-brazilein dye onto silk, under the optimal conditions of an initial dye concentration of 14 mg/L at pH 4.0 and an MLR of 1:100, are shown in Figure 3.13. A study of the temperature dependence of adsorptions gives valuable information about the enthalpy change during adsorption. The effect of temperature on the adsorption rate was studied by carrying out a series of experiments at 30, 50 and 70°C. An increase in the temperature lead to an increase in initial adsorption rate. Before and after the equilibrium time, the adsorption capacities showed different trends at different temperatures (Figure 3.13). Before equilibrium was attained, an increase in the temperature lead to an increase in the dye adsorption rate (h_i) which indicated a kinetically controlled process as shown in Table 3.2. After the equilibrium was reached, the decrease in the amount of dye adsorbed onto silk with increasing temperature suggested that the adsorption of the alum-brazilein was controlled by an exothermic process. Similar temperature effect trends on adsorption have also been shown in the case of adsorption of lac dye onto silk (Chairat *et al.*, 2005) as well as the adsorption of alum-morin onto silk (Septum, 2006). Our data showed that the equilibrium time for alum-brazilein dyeing process was shifted to the left-hand side. Then, the dye uptake at high temperature was lower than that at low temperature, i.e. 60, 20, and 10 min at 30, 50, and 70°C, respectively. This is probably due to more rapid diffusion of alum-brazilein dye complex to the silk surface at higher temperatures.

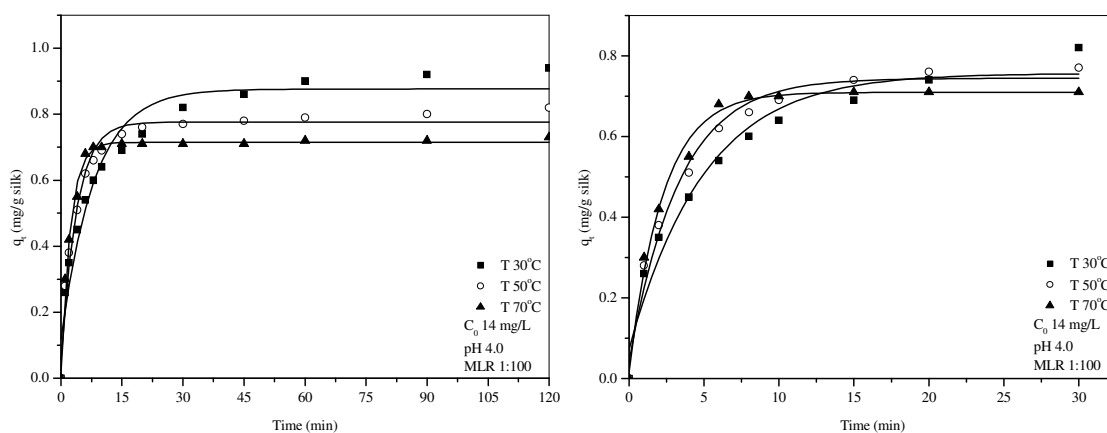


Figure 3.13 The effect of temperature on the adsorption of alum-brazilein onto silk.

The rate constant and other kinetic parameter studies for different temperatures calculated by the pseudo first-order (Figure 3.14) and pseudo-second order (Figure 3.15) models are listed in Table 3.2. It was found that the pseudo second-order adsorption model showed a correlation coefficient (R^2) higher than the pseudo first-order adsorption model. This is consistent with the dye adsorption occurs process occurring predominantly by the pseudo second-order adsorption mechanism.

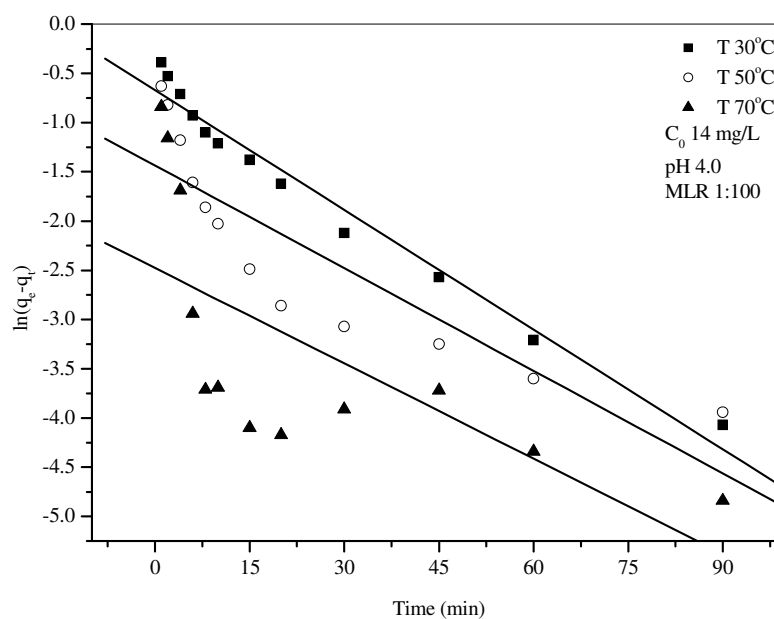


Figure 3.14 Pseudo first-order equation plots for the adsorption of alum-brazilein onto silk at different temperatures.

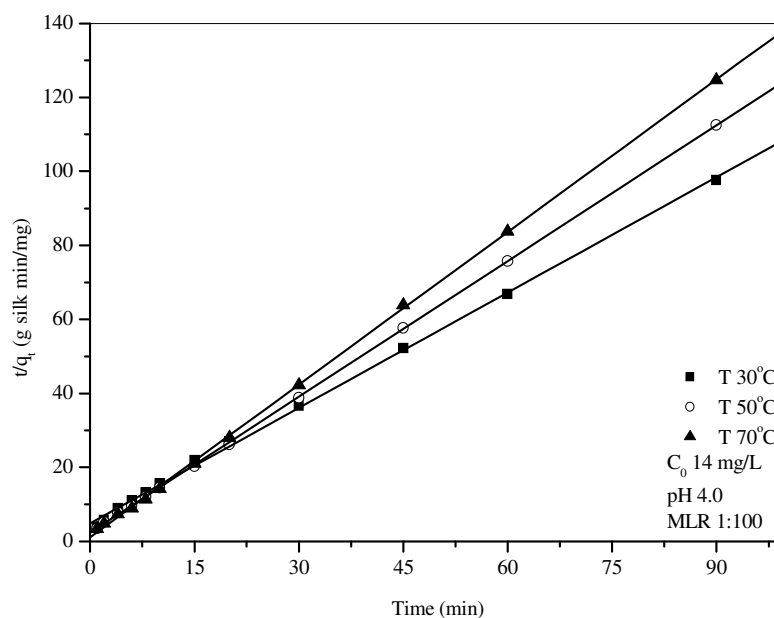


Figure 3.15 Pseudo second-order equation plots for the adsorption of alum-brazilein onto silk at different temperatures.

Table 3.2 Comparison of the pseudo first-order and pseudo second-order adsorption rate constants, calculated q_e and experimental q_e values for different MLR, initial dye concentrations and temperatures for alum-brazilein dyeing onto silk.

Parameters	$q_{e,exp}$ (mg/g silk)	First-order kinetic model			Second-order kinetic model			
		k_1	$q_{e,cal}$ (mg/g silk)	R^2	k_2	h_i	$q_{e,cal}$ (mg/g silk)	R^2
<i>MLR: initial dye concentration (C_0) 14 mg/L, pH4.0, temp. 30°C</i>								
1:50	0.65	0.0503	0.16	0.95575	1.1392	0.50	0.66	0.99996
1:100	0.94	0.0405	0.51	0.98723	0.2236	0.21	0.96	0.99940
1:150	1.17	0.0285	0.80	0.98719	0.1034	0.14	1.17	0.99744
<i>Initial dye concentration; (mg/L) : pH 4.0, MLR 1:100, temp. 30°C</i>								
14	0.94	0.0405	0.51	0.98723	0.2236	0.21	0.96	0.99940
21	1.40	0.0330	0.87	0.97907	0.1132	0.23	1.43	0.99894
28	1.88	0.0323	0.85	0.97950	0.0778	0.28	1.90	0.99914
<i>Temperature (°C): initial dye concentration (C_0)14 mg/L ,pH 4.0, MLR 1:100</i>								
30	0.94	0.0405	0.51	0.98723	0.2236	0.21	0.96	0.99940
50	0.82	0.0347	0.24	0.87733	0.6260	0.42	0.82	0.99995
70	0.73	0.0322	0.08	0.67766	1.6618	0.89	0.73	0.99984

3.4.2.5 Activation parameters for the adsorption of alum-brazilein on silk

Table 3.2 shows the rate constants k_2 obtained for the pseudo-second-order reaction at different temperatures, and these constants were then used to estimate the activation energy of the adsorption of alum-brazilein onto silk by the Arrhenius equation (equation (3.8)). The slope of the plot of $\ln k_2$ versus $1/T$ (Figure 3.16) was used to evaluate E_a as listed in Table 3.3.

Table 3.3 Activation parameters for the adsorption of alum-brazilein onto silk at initial brazilein concentration 14 mg/L.

Temp (°C)	k_2 (g silk/mg second)	E_a (kJ/mol)	R^2	$\Delta H^\#$ (kJ/mol)	$\Delta S^\#$ (J/mol K)	$\Delta G^\#$ (kJ/mol)	R^2
30	3.73×10^{-3}					88.36	
50	1.04×10^{-2}	41.57	0.99993	39.08	-162.54	91.61	0.99983
70	2.54×10^{-2}					94.86	

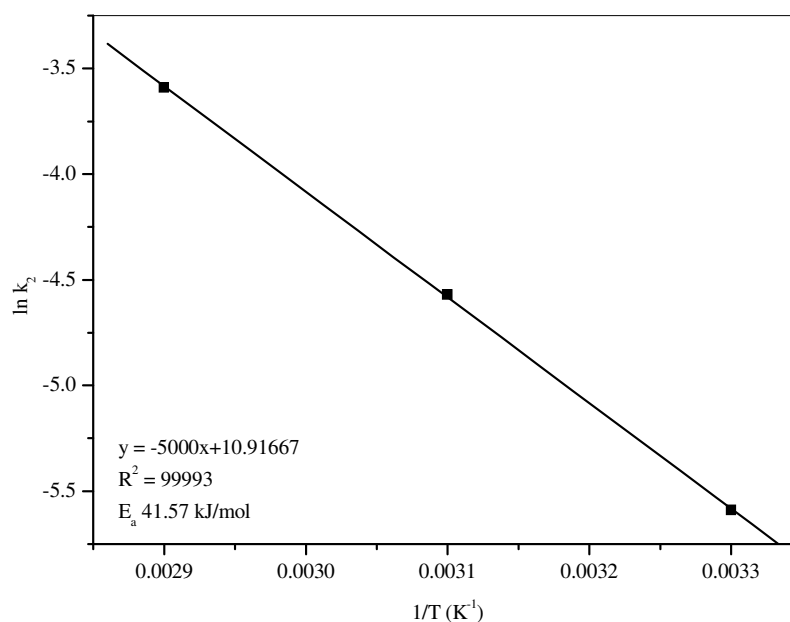


Figure 3.16 Arrhenius plot for the adsorption of alum-brazilein onto silk.

Table 3.3 shows the observed activation energy (E_a) and enthalpy of activation (ΔH^\ddagger) for alum-brazilein onto silk. As noted previously, physisorption adsorption processes usually have low activation energies (5-40 kJ/mol), while higher activation energies (40-800 kJ/mol) suggest chemical adsorption (Özcan, A.S. and A. Özcan, A., 2005). For the E_a of 41.57 kJ/mol observed we can infer that the adsorption of alum-brazilein onto silk yarn is most likely by a chemisorption process. Some other adsorption processes that have been found to be chemisorption-controlled include the sorption of the dye methylene blue onto palm kernel fiber with an E_a of 39.57 kJ/mol (Ofomaja, 2007) and methylene blue onto modified diatomite with an E_a of 99.80 kJ/mol (Al-Ghouti, Khraisheh, Allen, and Ahmad, 2005).

From the Eyring equation, the enthalpy (ΔH^\ddagger) and entropy (ΔS^\ddagger) of activation were calculated from the slope and intercept of a plot of $\ln(k/T)$ versus $1/T$ (Figure

3.17) as listed in Table 3.3. The value of ΔG^\ddagger was calculated at 303, 323, and 343 K by using equation (3.10) and these values are listed in Table 3.3, while the negative entropy value (ΔS^\ddagger) reflects more aggregation occurring on adsorption consistent with interaction between the alum-brazilein dye and the silk yarn.

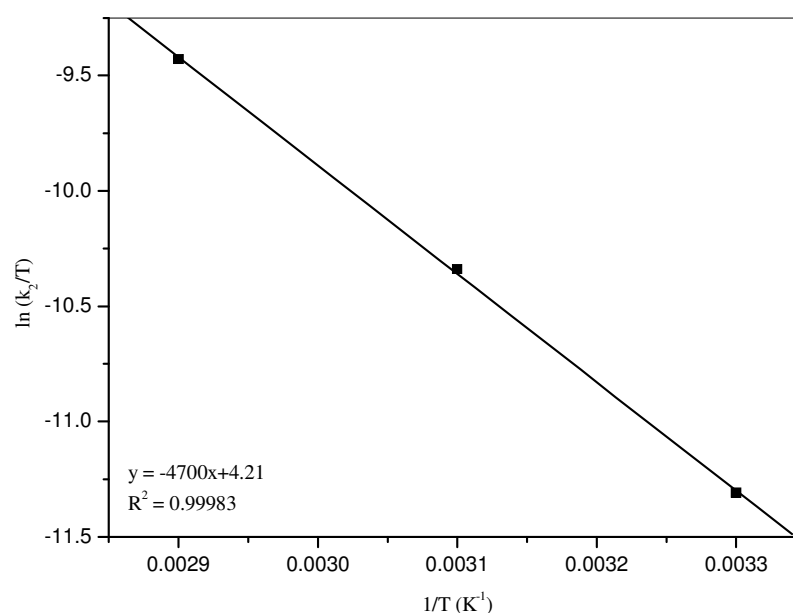


Figure 3.17 Plot of $\ln(k_2/T)$ against $1/T$ for the adsorption of alum-brazilein onto silk.

3.4.2.6 Thermodynamic parameters for the adsorption of alum-brazilein onto silk

In order to support the exothermic behaviour of alum-brazilein onto silk, the thermodynamic parameters ΔG° , ΔH° , and ΔS° of alum-brazilein adsorption after reaching equilibrium were calculated using the equations (3.17)-(3.19). Table 3.4 shows the thermodynamic parameters. The negative values of ΔG° indicate that the adsorption of alum-brazilein onto silk is spontaneous, while the negative value of ΔH° confirms that the adsorption process is an exothermic one. The

negative value of ΔS° indicates that adsorbed alum-brazilein dye becomes more restrained within the silk fiber molecules than in the dyeing solution as would be expected from other interactions of the complex with the amino acid residues or the amide backbone in the silk protein (Kim, Son, and Lim 2005).

Table 3.4 Thermodynamic parameters for the adsorption of alum-brazilein dyeing at initial brazilein concentration 14 mg/L.

Temperature (°C)	$\ln K_c$	ΔG° (kJ/mol)	ΔH° (kJ/mol)	ΔS° (J/mol K)	R^2
30	5.60	-14.11			
50	4.92	-13.22	-25.32	-36.64	0.99745
70	4.39	-12.52			

3.4.2.7 Adsorption isotherm for the adsorption of alum-brazilein on silk

The isothermal equilibrium data of alum-brazilein dye on silk under the dyeing conditions of the dye concentration range 2.84-56.85 mg/L at pH 4.0, MLR 1:100 and temperature 30, 50, and 70°C were described employing the Langmuir isotherm equation as shown in Figure 3.18. It was found that the dye uptake decreased with increasing temperature, thereby indicating that the process is exothermic.

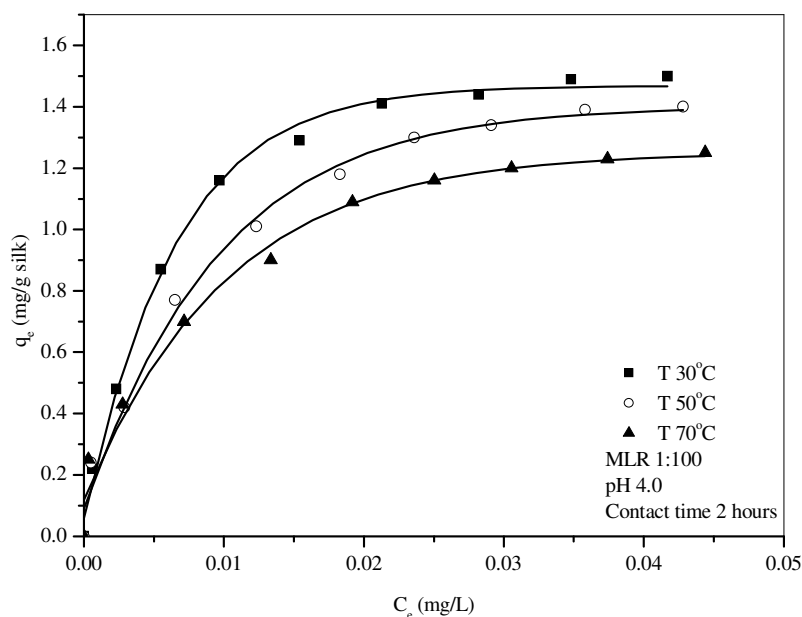


Figure 3.18 Langmuir adsorption isotherms of alum-brazilein onto silk at 30, 50, and 70°C.

When C_e/q_e was plotted against C_e according to the equation (3.12), the Langmuir model fitted the experimental data very well with high correlation coefficients ($R^2 > 0.99$) (Figure 3.19). The values of the Langmuir constants Q and b were calculated from the slopes and intercepts of the different straight lines respectively at different temperatures. The calculated results are listed in Table 3.5. It was indicated that Q values decreased with increasing temperature. Similar observations were reported for the adsorption of lac dye on silk (Kongkachuichay, Shitangkoon, and Chinwongamorn, 2002; Chairat *et al.*, 2005) and the adsorption of alum-morin onto silk (Septum, 2006). The values of b confirmed that the silk yarn has a maximum affinity for alum-brazilein dye at lower temperature (Chairat *et al.*, 2005).

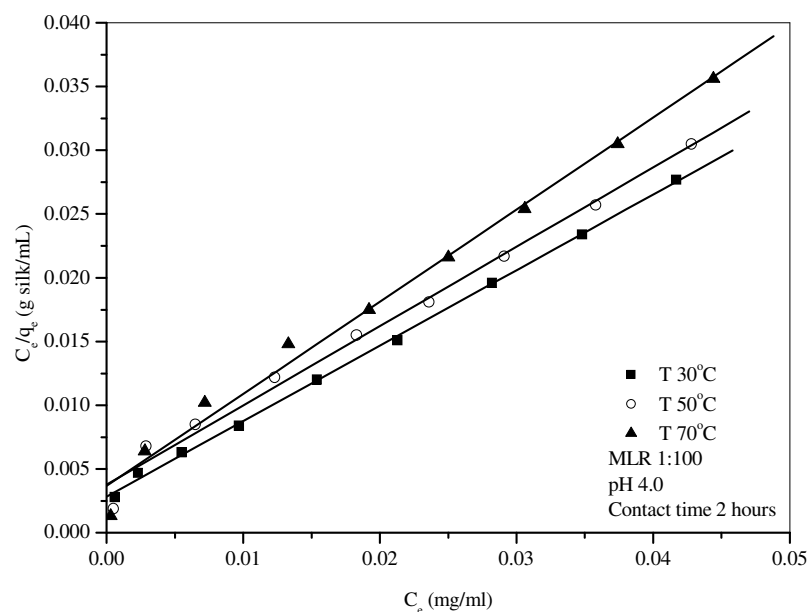


Figure 3.19 A Langmuir plot of C_e/q_e against C_e for the adsorption of alum-brazilein onto silk at the initial dye concentration range 2.84-56.85 mg/L.

Table 3.5 Langmuir and Freundlich isotherm constants for the adsorption of alum-brazilein onto silk at different temperatures.

Temp (°C)	Langmuir			Freundlich		
	Q (mg/g silk)	b (mL/mg)	R^2	Q_f (mg/g silk)	n	R^2
30	1.69	209.09	0.99948	7.82	2.18	0.97334
50	1.61	164.32	0.99442	5.90	2.38	0.98869
70	1.38	196.91	0.99434	4.08	2.81	0.99104

The equilibrium parameter values (R_L) for the adsorption of alum-brazilein dyeing on silk were calculated by using equation (3.14). It was found

that the values of R_L (Table 3.6) were in the range of 0-1, indicating that the adsorption of alum-brazilein onto silk was favourable for this study. Similar observations were again reported for the lac dyeing of silk (Chairat *et al.*, 2005) and the adsorption of alum-morin onto silk (Sephthum, 2006)

Table 3.6 R_L values at different temperatures relating to the initial dye concentrations for alum-brazilein dyeing of silk.

Temp (°C)	b (L/mg)	Initial dye concentration, C_0 (mg/L)	R_L
30	0.2091	2.84	0.6274
		7.10	0.4025
		14.21	0.2518
		21.32	0.2832
		28.42	0.1440
		35.53	0.1186
		42.64	0.1008
		49.74	0.0877
		56.85	0.0776
		50	0.1643
7.10	0.4616		
14.21	0.2999		
21.32	0.2221		
28.42	0.1764		
35.53	0.1462		
42.64	0.1249		
49.74	0.1090		
56.85	0.0967		
70	0.1969		
		7.10	0.4170
		14.21	0.2633
		21.32	0.1924
		28.42	0.1516
		35.53	0.1251
		42.64	0.1064
		49.74	0.0926
		56.85	0.0820

The Freundlich equation (Eq. (3.16)) was also applied to the data of the adsorption of alum-brazilein onto silk. The Q_f and $1/n$ values can be calculated from the linear plot of $\ln q_e$ versus $\ln C_e$. The magnitude of the exponent $1/n$ gives an indication of the favourability of adsorption. The values of $n > 1$ obtained represent favourable adsorption conditions (Chiou and Li, 2002; Chairat *et al.*, 2005; Septhum, 2006).

3.4.2.8 Adsorption-desorption of alum-brazilein on silk

After the adsorption of alum-brazilein dye onto silk was equilibrated desorption was then carried out in deionized, distilled and tap water at different MLR values (1:100, 1:150, and 1:200). After 120 minutes, the dye bath was replaced with deionized, distilled and tap water and desorption of the alum-brazilein complex was observed over a time range of 150-420 min. The amount of dye desorbed from the silk (q_{de}) was calculated and then subtracted from the amount of the dye adsorbed at the equilibrium time (q_e). The amount of dye adsorbed on silk after desorption over the time range 150-420 minutes is shown in Figure 3.20-3.22 and Table 3.7. It was found that the adsorption capacity of alum-brazilein at 120 minutes was 0.94 mg/g silk and after desorption, the amount of alum-brazilein adsorbed on silk was still close to this value irrespective of the type of water and MLRs used.

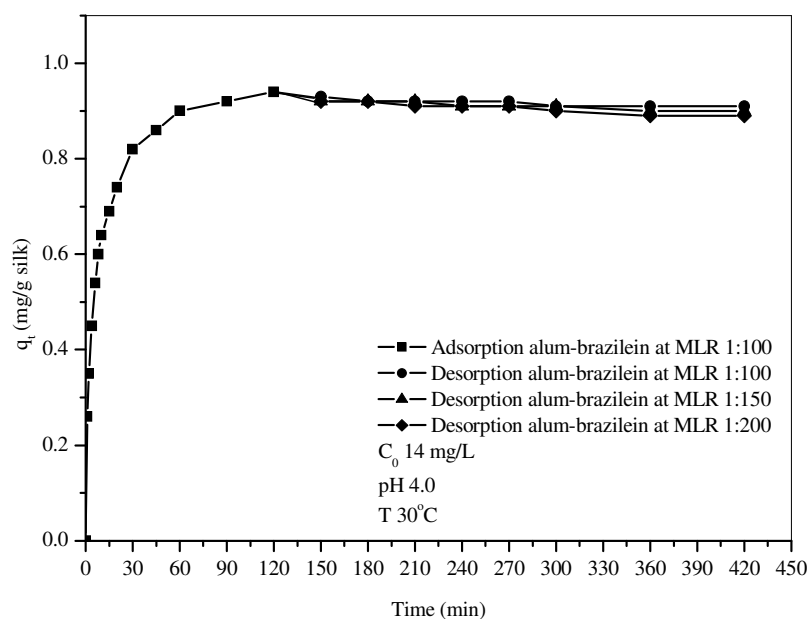


Figure 3.20 Adsorption-desorption analysis of alum-brazilein dye onto and off silk in deionized water at different material to liquor ratios.

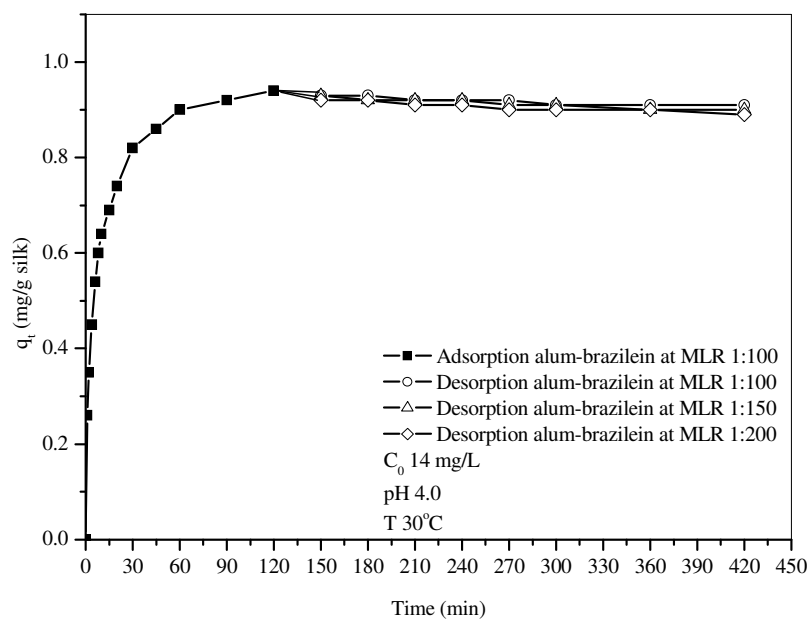


Figure 3.21 Adsorption-desorption analysis of alum-brazilein dye onto and off silk in distilled water at different material to liquor ratios.

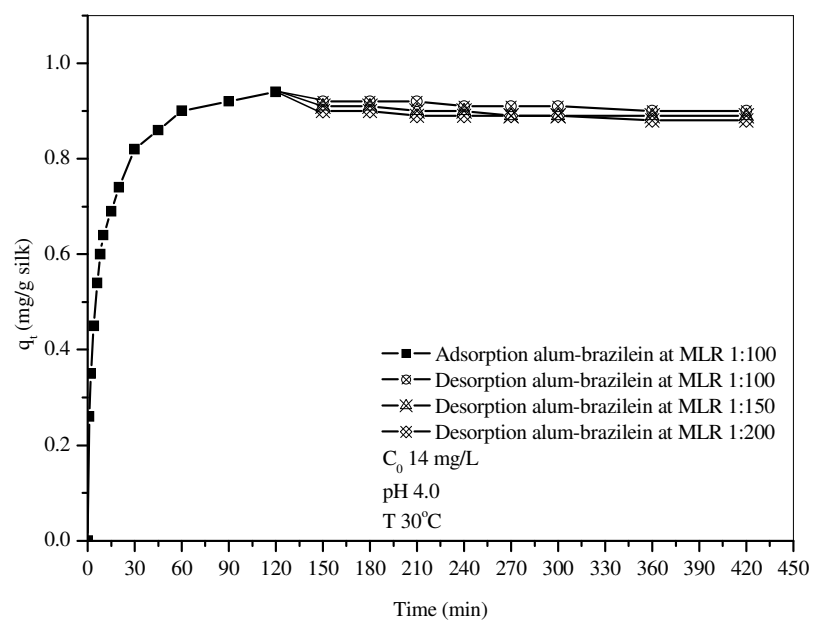


Figure 3.22 Adsorption-desorption analysis of alum-brazilein dye onto and off silk in tap water at different material to liquor ratios.

Table 3.7 Percentage of desorption analysis of alum-brazilein dye onto and off silk in different type of water and material to liquor ratios.

Time (min)	Deionized water			Distilled water			Tap water		
	1:100	1:150	1:200	1:100	1:150	1:200	1:100	1:150	1:200
150	20.00	40.00	40.00	25.00	25.00	50.00	22.22	33.33	44.44
180	33.33	33.33	33.33	20.00	40.00	40.00	22.22	33.33	44.44
210	28.57	28.57	42.86	28.57	28.57	42.86	18.18	36.36	45.45
240	25.00	37.50	37.50	28.57	28.57	42.86	25.00	33.33	41.67
270	25.00	37.50	37.50	22.22	33.33	44.44	23.08	38.46	38.46
300	30.00	30.00	40.00	30.00	30.00	40.00	23.08	38.46	38.46
360	25.00	33.33	41.67	27.27	36.36	36.36	26.67	33.33	40.00
420	25.00	33.33	41.67	25.00	33.33	41.67	26.67	33.33	40.00
Average	26.49	34.20	39.32	25.83	31.9	42.27	23.39	34.99	41.62

3.4.3 Optimal conditions of silk dyeing with alum-extracted dye

In order to compare the dyeing characteristics on silk of pure brazilein-alum complex with those of the aqueous extracted dye from *C. sappan*, optimum dyeing conditions for the alum-extracted dye were investigated. The initial aqueous extracted dye contained mainly brazilin and brazilein dye but brazilin is readily converted to brazilein by exposure to atmospheric oxygen and light. The amount of brazilein in the crude extracted dye was estimated as 9% (Chapter II section 2.4.5). The experimental parameters including material to liquor ratio (MLR), contact time, initial dye concentration, and temperature were determined to find the optimal conditions for adsorption. The mechanism of adsorption of alum-extracted dye onto silk was then investigated by using the pseudo first-order and pseudo second-order models. In addition, activation parameters and thermodynamic parameters of adsorption were determined.

3.4.3.1 The effect of material to liquor ratio on the adsorption of alum-extracted dye onto silk

The effect of the material liquor ratio on the adsorption of alum-extracted dye onto silk was studied with an alum-extracted dye concentration of 284 mg/L (contained ~ 25.56 mg/L brazilein) at pH 4.0 and temperature 30°C and the results are shown in Figure 3.23. It was found that an increase in volume of the dye solution resulted in an increase of dye adsorbed on the silk. Again it indicated that silk yarn is more loosely packed in the higher volume of dye solution and the dye solution readily moves past any surface transferring dye molecules to the silk surface in the process (Chairat *et al.*, 2005). The largest amount of dye was adsorbed at an MLR of

1:150 (Figure 3.23). However, in order to minimize waste from dyeing process, an MLR of 1:100 was adopted for all the kinetic experiments.

The kinetic parameters from linear plots of pseudo first-order (Figure 3.24) and pseudo second-order (Figure 3.25) models are given in Table 3.8. The data indicated a good compliance with the pseudo second-order equation and the regression coefficients (R^2) for the linear plot were all high (> 0.99). The calculated equilibrium sorption capacity values ($q_{e,cal}$) for the second-order model are more reasonable than the first-order model when comparing predicted results with experimental data ($q_{e,exp}$), with the calculated equilibrium sorption capacities being higher than the experimental values in the latter model.

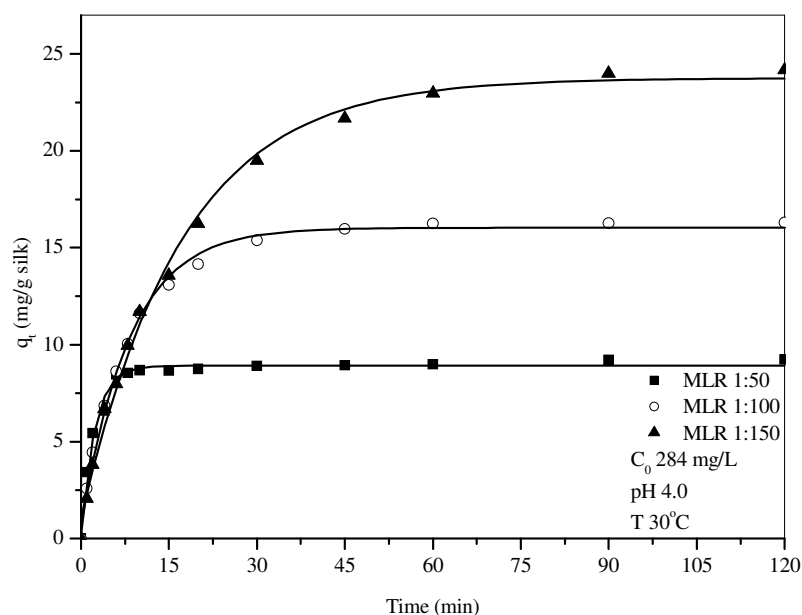


Figure 3.23 The effect of material to liquor ratios on the adsorption of alum-extracted dye onto silk.

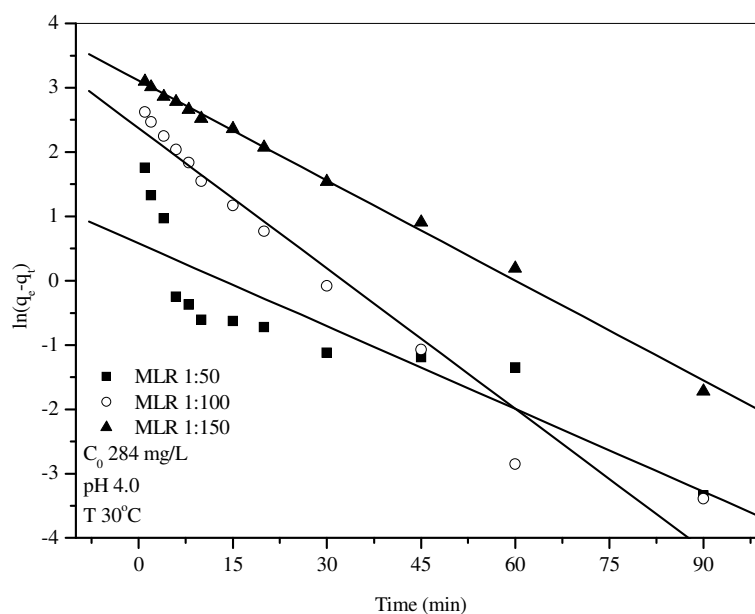


Figure 3.24 Pseudo first-order equation plots for the adsorption of alum-extracted dye onto silk at different material to liquor ratios.

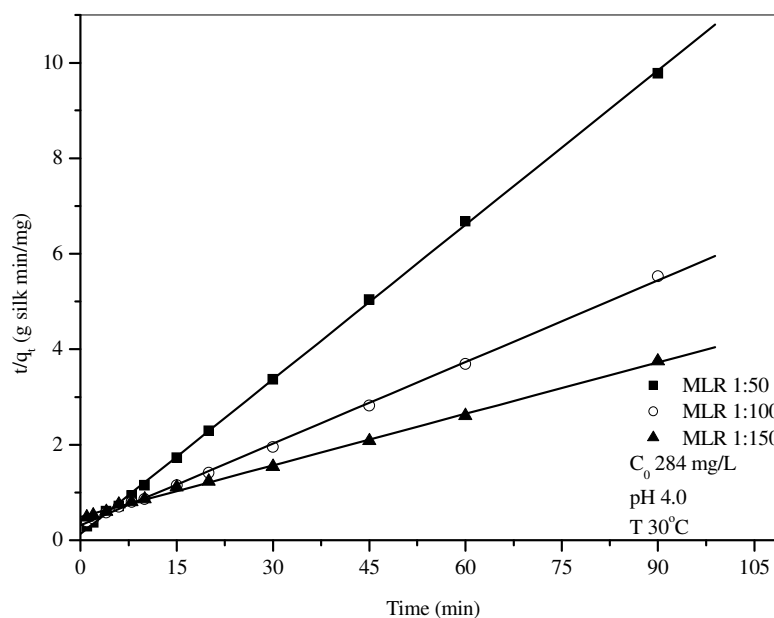


Figure 3.25 Pseudo second-order equation plots for the adsorption of alum-extracted dye onto silk at different material to liquor ratios.

3.4.3.2 The effect of contact time and initial dye concentration on the adsorption of alum-extracted dye onto silk

The adsorption capacity of alum-extracted dye onto silk was a function of the initial dye concentration. The effect of contact time and initial dye concentration on adsorption of alum-extracted dye onto silk was studied under dyeing conditions of an MLR of 1:100 at pH 4.0 and a temperature of 30°C, and the results are presented in Figure 3.26. It was found that the amount of dye adsorbed on silk increased with an increase in the initial concentration of dye solution. This is due to the increase in the driving force of the concentration gradient with the higher initial dye concentration (Chiou and Li, 2002; Chairat *et al.*, 2005). This indicated that the initial dye concentration plays an important role in the adsorption capacity of alum-extracted dye onto silk. The equilibrium time was found to be about 60 minutes for initial dye concentration of 284, 426, and 568 mg/L at pH 4.0 and 30°C. The adsorption was very fast at the initial stages of contact with the silk and gradually decreased with time until it remained constant; this was similar to the results obtained with the adsorption of alum-brazilein on silk.

The results of rate constant studies for different initial concentrations using the pseudo-first and pseudo-second order models and correlation coefficients are listed in Table 3.8 and in Figure 3.27, while Figure 3.28 presents pseudo-first and pseudo-second order plots, respectively. It was found that the pseudo-second order model closely matched the adsorption of alum-brazilein onto silk with a higher correlation coefficient ($R^2 > 0.99$) than that for the pseudo-first order model. The calculated equilibrium sorption capacities also fitted well with the experimental data in the pseudo-second order case. These results suggest that the

pseudo-second order adsorption mechanism is predominant and that the overall alum-extracted adsorption process appears to be controlled by the chemical process. The results in Table 3.8 also show k_2 , h_i and q_e as a function of initial dye concentration. The rate constant (k_2) for the pseudo-second order decreases with increases in the initial dye concentration, while the initial dye adsorption rate (h_i) increases with an increasing initial dye concentration. An increase in initial dye concentration resulted in a significant increase in $q_{e,cal}$.

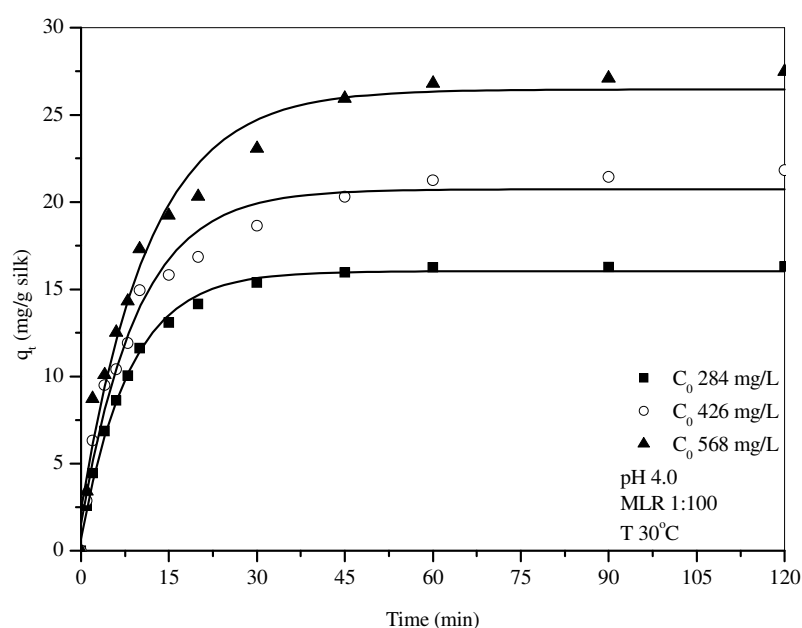


Figure 3.26 The effect of contact time and initial dye concentrations on the adsorption of alum-extracted dye onto silk.

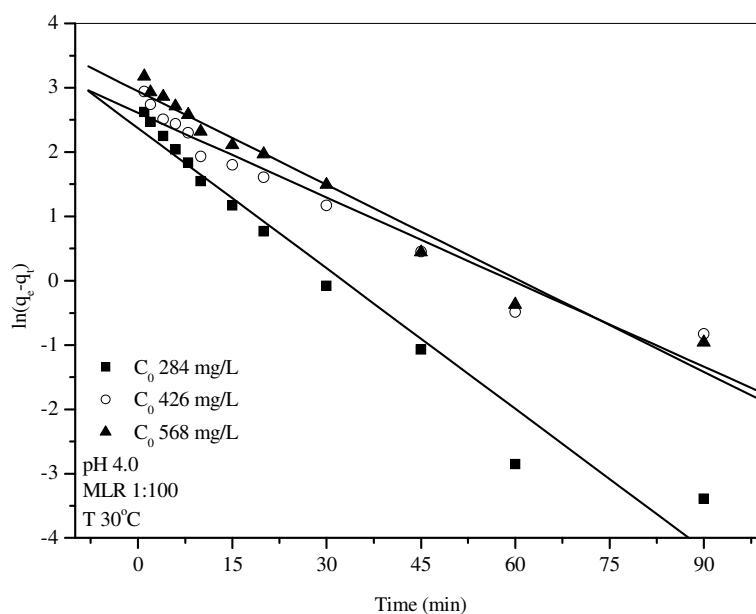


Figure 3.27 Pseudo first-order equation plots for the adsorption of alum-extracted dye onto silk at different initial dye concentrations.

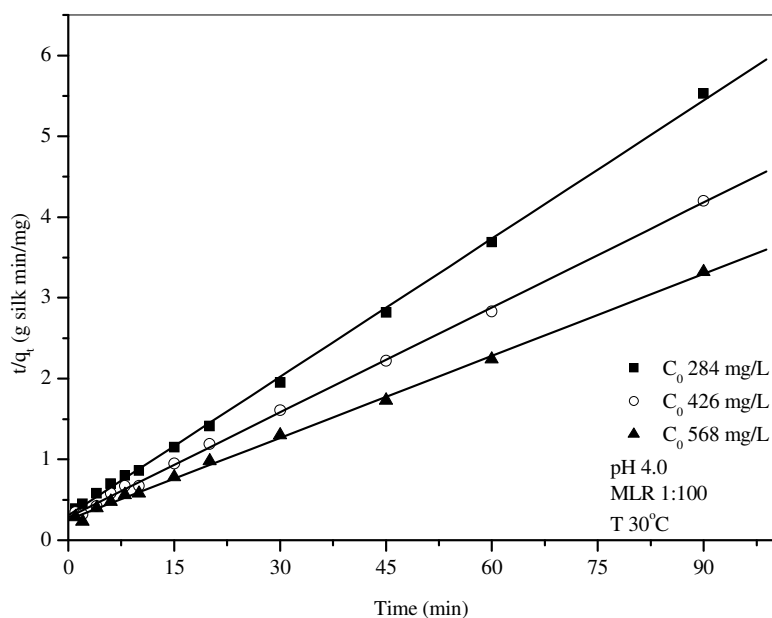


Figure 3.28 Pseudo second-order equation plots for the adsorption of alum-extracted dye onto silk at different initial dye concentrations.

3.4.3.3 The effect of temperature on the adsorption of alum-extracted dye onto silk

The results of the studies on the influence of temperature on the adsorption of alum-extracted dye onto silk are shown in Figure 3.29. These studies were undertaken under the optimal conditions with an initial dye concentration of 284 mg/L at pH 4.0 and an MLR of 1:100. A study of the temperature dependence of adsorption gives valuable information about the enthalpy change during the adsorption process. The effect of temperature on the adsorption rate was studied by carrying out a series of experiments at 30, 50, and 70°C. An increase in the temperature lead to an increase in initial adsorption rate. Before and after the equilibrium time was reached, the adsorption capacities (Figure 3.29) showed different trends at different temperatures. Before equilibrium was attained, an increase in the temperature lead to an increase the dye adsorption rate (h_i) (Table 3.8) which indicated a kinetically controlled process. After the equilibrium was reached, the decrease in the amount of dye adsorbed onto silk with increasing temperature suggested that the adsorption of the alum-extracted dye onto silk was controlled by an exothermic process. Similar temperature effect trends on adsorption have also been shown in the case of the adsorption of lac dye onto silk (Chairat *et al.*, 2005) as well as the adsorption of alum-morin onto silk (Septum, 2006). Our data showed that the equilibrium time for the alum-extracted dye adsorption process was shifted to the left-hand side, and the dye uptake at high temperature was lower than that at low temperature, i.e. 60, 20, and 10 min at 30, 50, and 70°C, respectively. This was most likely due to more rapid diffusion to the silk surface at higher temperatures.

The results of the rate constant and other kinetic parameter studies for different temperatures calculated by the pseudo first-order (Figure 3.30) and pseudo-second order (Figure 3.31) models are listed in Table 3.8. It was found that the pseudo second-order adsorption model showed correlation coefficient (R^2) higher than those for the pseudo first-order adsorption model, indicating that the dye adsorption process occurs predominantly by the pseudo second-order adsorption mechanism.

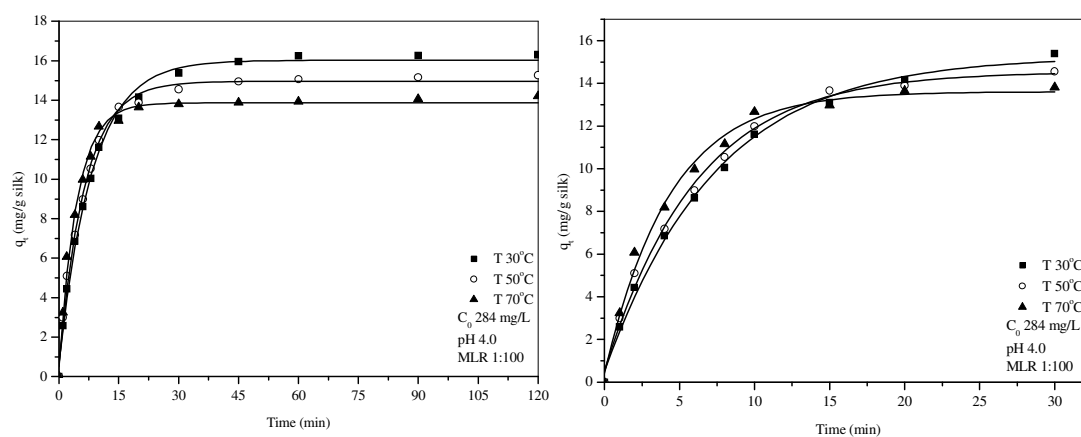


Figure 3.29 The effect of temperature on the adsorption of alum-extracted dye onto silk.

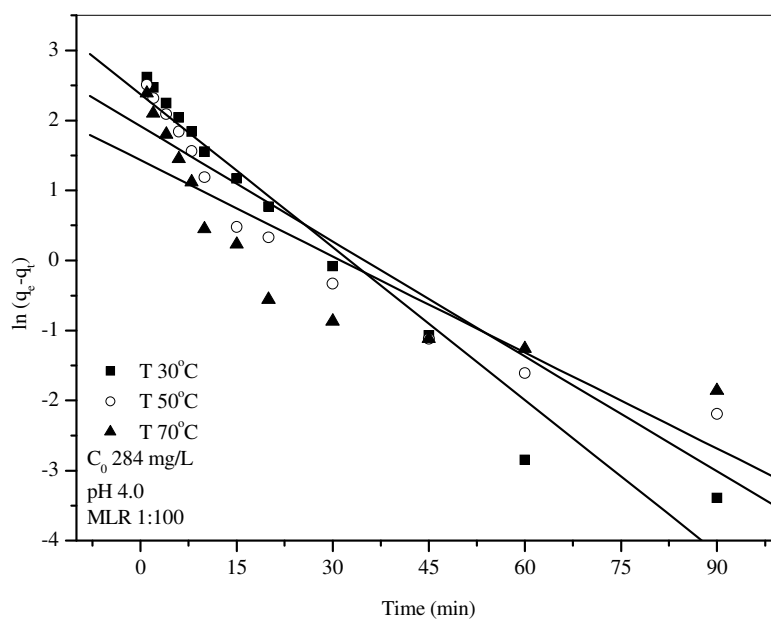


Figure 3.30 Pseudo first-order equation plots for the adsorption of alum-extracted dye onto silk at different temperatures.

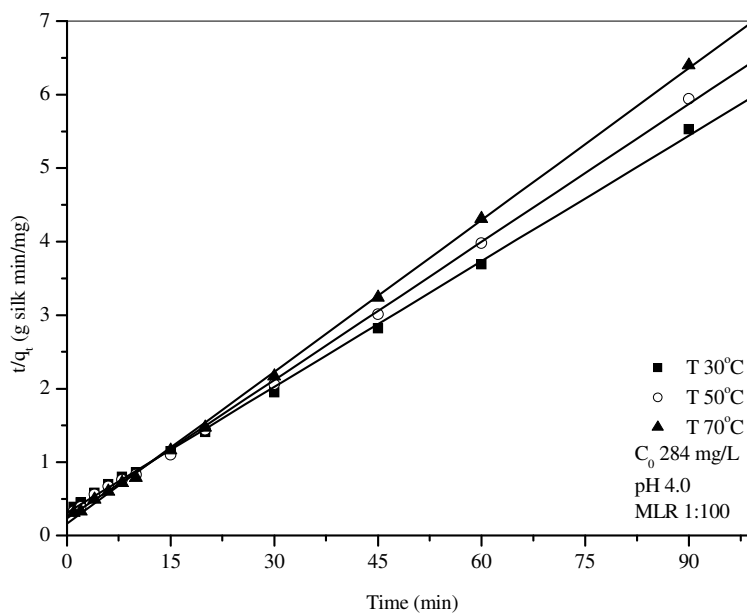


Figure 3.31 Pseudo second-order equation plots for the adsorption of alum-extracted dye onto silk at different temperatures.

Table 3.8 Comparison of the pseudo first-order and pseudo second-order adsorption rate constants, calculated q_e and experimental q_e values for different MLR, initial dye concentrations and temperatures for adsorption of alum-extracted dye on silk.

Parameters	$q_{e,exp}$ (mg/g silk)	First-order kinetic model			Second-order kinetic model			
		k_1	$q_{e,cal}$ (mg/g silk)	R^2	k_2	h_i	$q_{e,cal}$ (mg/g silk)	R^2
<i>MLR: initial dye concentration (C_0) 284 mg/L, pH4.0, temp. 30°C</i>								
1:50	9.23	0.0429	1.78	0.87126	0.0901	7.72	9.26	0.99985
1:100	16.31	0.0728	10.74	0.98145	0.0104	3.20	17.53	0.99952
1:150	24.17	0.0518	22.49	0.99797	0.0026	2.01	27.80	0.99917
<i>Initial dye concentration; (mg/L) : pH 4.0, MLR 1:100, temp. 30°C</i>								
284	16.31	0.0728	10.74	0.98145	0.0104	3.20	17.53	0.99952
426	21.85	0.0439	13.61	0.97541	0.0066	3.52	23.11	0.99951
568	27.49	0.0485	19.06	0.98485	0.0045	3.94	29.59	0.99903
<i>Temperature (°C): initial dye concentration (C_0)284 mg/L, pH 4.0, MLR 1:100</i>								
30	16.31	0.0728	10.74	0.98145	0.0104	3.20	17.53	0.99952
50	15.27	0.0548	6.80	0.94562	0.0165	4.21	15.97	0.99955
70	14.22	0.0458	4.19	0.87363	0.0290	6.12	14.53	0.99967

3.4.3.4 Activation parameters for the adsorption of alum-extracted dye on silk

The activation energy of the adsorption process can be calculated using Arrhenius equation (equation (3.8)). This parameter describes the dependence of the diffusion coefficient on the dyeing temperature and also represents the energy barrier that the dye molecule should overcome to diffuse into the fiber molecules (Kim *et al.*, 2005). The activation energy of the diffusion can be calculated from the slope in the linear relationship between $\ln k_2$ and $1/T$ shown in Figure 3.32. The calculated activation energy is listed in Table 3.9.

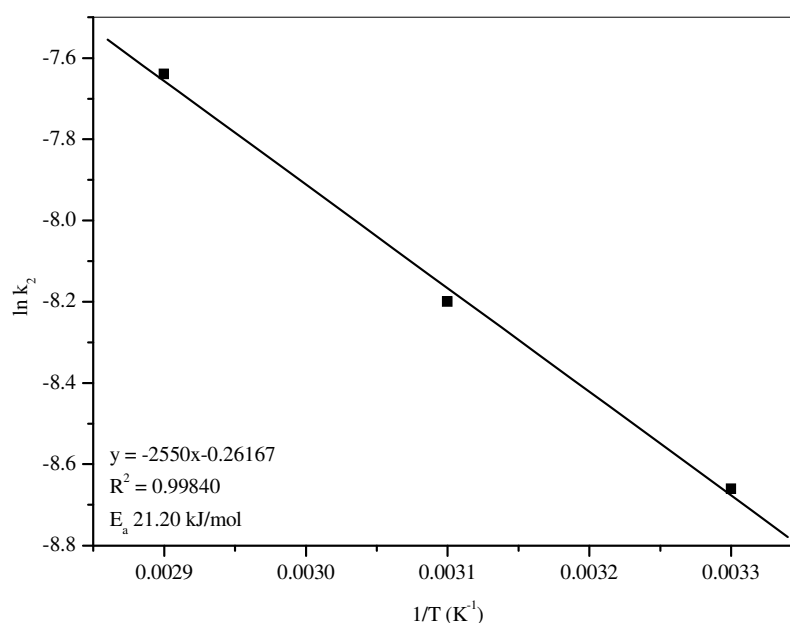


Figure 3.32 Arrhenius plots for the adsorption of alum-extracted dye onto silk.

From the Eyring equation, the enthalpy (ΔH^\ddagger) and entropy (ΔS^\ddagger) of activation were calculated from the slope and intercept of a plot of $\ln(kT)$ versus $1/T$ (Figure 3.33) as listed in Table 3.9. The value of ΔG^\ddagger was calculated at 303, 323,

and 343 K by using equation (3.10) and these values are listed in Table 3.9, while the negative entropy value (ΔS^\ddagger) reflects more aggregation and the interaction between alum-extracted dye and the silk yarn.

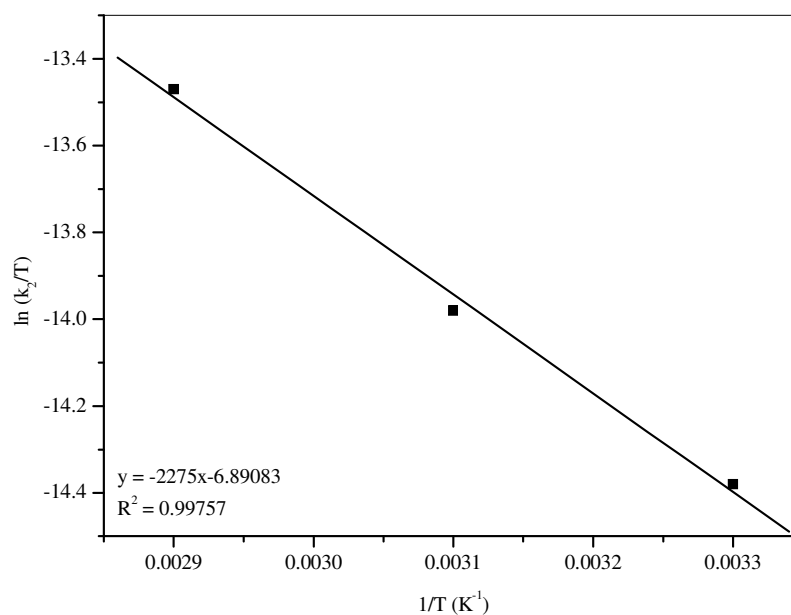


Figure 3.33 Plot of $\ln(k_2/T)$ against $1/T$ for the adsorption of alum-extracted dye onto silk.

Table 3.9 Activation parameters for the adsorption of alum-extracted dye onto silk at initial dye concentration 284 mg/L.

Temp (°C)	k_2 (g silk/mg second)	E_a (kJ/mol)	R^2	ΔH^\ddagger (kJ/mol)	ΔS^\ddagger (J/mol K)	ΔG^\ddagger (kJ/mol)	R^2
30	1.73×10^{-4}					96.16	
50	2.75×10^{-4}	21.20	0.99840	18.91	-254.83	101.26	0.99757
70	4.83×10^{-4}					106.36	

The value of E_a of adsorption of alum-extracted dye onto silk was 21.20 kJ/mol (Table 3.9). This E_a is low when compared with other dye-silk values (for example, an E_a of 18.73 kJ/mol for morin extract on silk in the presence of Al(III), (Septum *et al.*, 2006), and was lower than the E_a (41.57 kJ/mol) for alum-brazilein adsorption on silk. It is possible the crude extracted dye contained other components which could act to assist the adsorption of the alum-extracted dye on silk.

3.4.3.5 Thermodynamic parameters for the adsorption of alum-extracted dye onto silk

In order to quantify the exothermic adsorption behavior of alum-brazilein onto silk, the thermodynamic parameters ΔG° , ΔH° , and ΔS° of alum-extracted dye adsorption after reaching equilibrium were calculated using the equations (3.17)-(3.19). Table 3.10 shows the thermodynamic parameters obtained. The negative values of ΔG° indicated that the adsorption of alum-extracted dye onto silk was spontaneous, while the negative value of ΔH° confirmed the exothermic nature of the adsorption process. The negative value of ΔS° indicated that adsorbed alum-extracted dye become more restrained within the silk fiber molecules through further non-covalent interactions than in the dyeing solution.

Table 3.10 Thermodynamic parameters for the adsorption of alum-extracted dye onto silk.

Temp. (°C)	$\ln k_c$	ΔG° (kJ/mol)	ΔH° (kJ/mol)	ΔS° (J/mol K)	R^2
30	7.23	-18.22			
50	6.34	-17.03	-32.63	-47.87	0.99703
70	5.66	-16.15			

3.4.3.6 Adsorption isotherms for the adsorption of alum-extracted dye on silk

The isothermal equilibrium data of alum-brazilein dye on silk with a dye concentration range of 142-853 mg/L at pH 4.0, MLR 1:100 and 30°C and 50°C were analyzed employing the Langmuir and Freundlich isotherm equations as shown in Figure 3.34. The adsorption constants of alum-extracted dye onto silk are given in Table 3.11. The experimental data were found to fit well to the Langmuir isotherm, with this isotherm being slightly better as indicated by the higher correlation coefficient (R^2) values compared with those from the Freundlich isotherm equation (Figure 3.35). The applicability of the Langmuir isotherm suggested monolayer coverage of the dye on the surface of the silk.

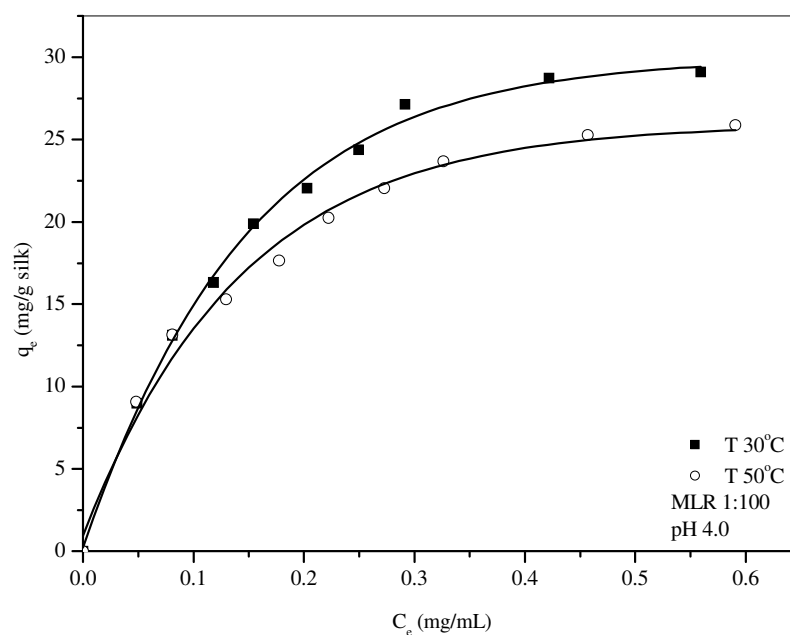


Figure 3.34 Langmuir adsorption isotherms of alum-extracted dye onto silk at 30 and 50°C.

When C_e/q_e was plotted against C_e according to the equation (3.12), the Langmuir model fitted the experimental data very well with high correlation coefficients ($R^2 > 0.99$) (Figure 3.35). The values of the Langmuir constants Q and b were calculated from the slopes and intercepts of the different straight lines respectively at different temperatures. The calculated results are listed in Table 3.11. It was indicated that Q values decreased with increasing temperature.

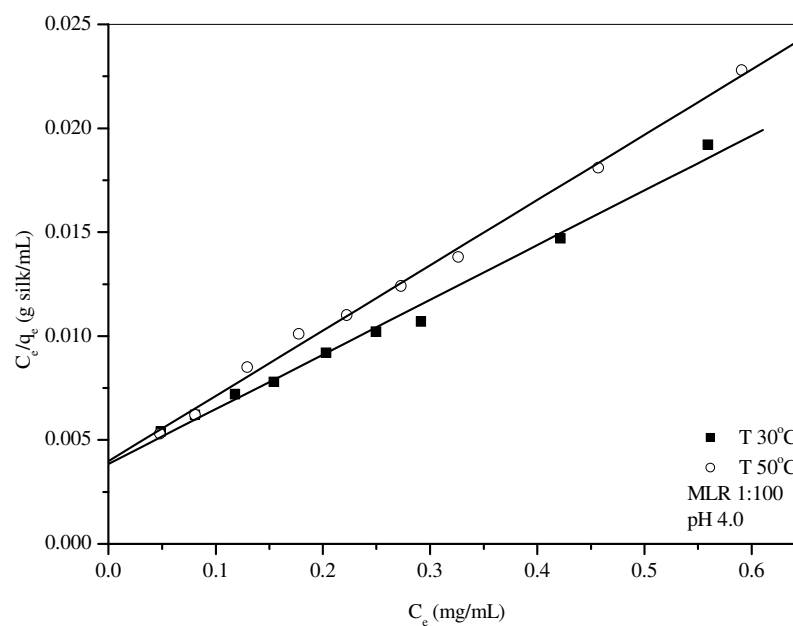


Figure 3.35 A Langmuir plot of C_e/q_e against C_e for the adsorption of alum-extracted dye onto silk at the initial dye concentration range 142-853 mg/L.

Table 3.11 Langmuir and Freundlich isotherm constants for the adsorption of alum-extracted dye onto silk at 30 and 50°C.

Temp (°C)	Langmuir			Freundlich		
	Q (mg/g silk)	b (mL/mg)	R^2	Q_f (mg/g silk)	n	R^2
30	37.95	6.86	0.99562	45.72	2.01	0.97226
50	31.82	7.92	0.99808	36.01	2.37	0.98096

The effect of isotherm shape can be used to predict whether a sorption system is “favourable” or “unfavourable”. The essential features of the Langmuir isotherm of alum-extracted dye on silk can be expressed in terms of a dimensionless constant separation factor or equilibrium parameter (R_L) which is defined by the equation (3.14). The R_L values at 30 and 50°C relating to the initial dye concentrations are found in the range of 0.5051-0.1452 and 0.4713-0.1292, respectively (Table 3.12), showing favourable adsorption.

Table 3.12 R_L values at different temperatures relating to the initial extracted dye concentrations.

Temp. (°C)	b (L/mg)	Initial extracted dye concentration, C_0 (mg/L)	R_L
30	0.0069	142	0.5051
		213	0.4049
		284	0.3379
		355	0.2899
		426	0.2538
		497	0.2258
		568	0.2033
		711	0.1693
		853	0.1452
		50	0.0079
213	0.3728		
284	0.3083		
355	0.2628		
426	0.2538		
497	0.2030		
568	0.1822		
711	0.1511		
		853	0.1292

The Freundlich equation describes heterogeneous systems and reversible adsorption and is not limited to the formation of a complete monolayer. It can be seen from the results in Table 3.11 that the correlation coefficients for the Freundlich isotherms are only slightly less than those obtained for the Langmuir expression. Thus, the Freundlich isotherm cannot be totally rejected in these equilibrium studies. Also the values of n more than 1 (Table 3.11) again indicate favourable adsorption.

3.4.3.7 Adsorption-desorption of alum-extracted dye on silk

After the adsorption of alum-extracted dye onto silk was equilibrated, desorption was then carried out in deionized, distilled and tap water at different MLRs (1:100, 1:150, and 1:200). After 120 minutes, the dye bath was replaced with deionized, distilled and tap water and the desorption of alum-extracted dye was observed over a time range of 150-420 minutes. The amount of dye desorbed from the silk (q_{de}) was calculated and then subtracted from the amount of the dye adsorbed at the equilibrium time (q_e). The amount of dye still adsorbed on the silk after desorption over the time range 150-420 minutes is shown in Figures 3.36-3.38 and Table 3.13. It was found that little dye was desorbed from the silk under any conditions; a similar finding was obtained in the alum-brazilein dye desorption studies (section 3.4.2.8) although the amount desorbed was a little higher in the former case. It is not clear why this should be the case although presumably the other components present in the extracted dye play a part.

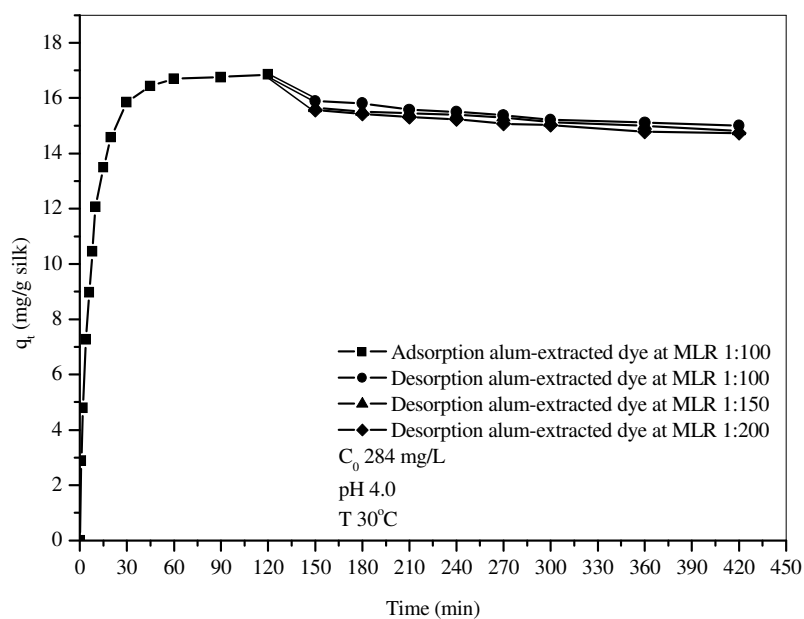


Figure 3.36 Adsorption-desorption analysis of alum-extracted dye onto and off silk in deionized water at different material to liquor ratios.

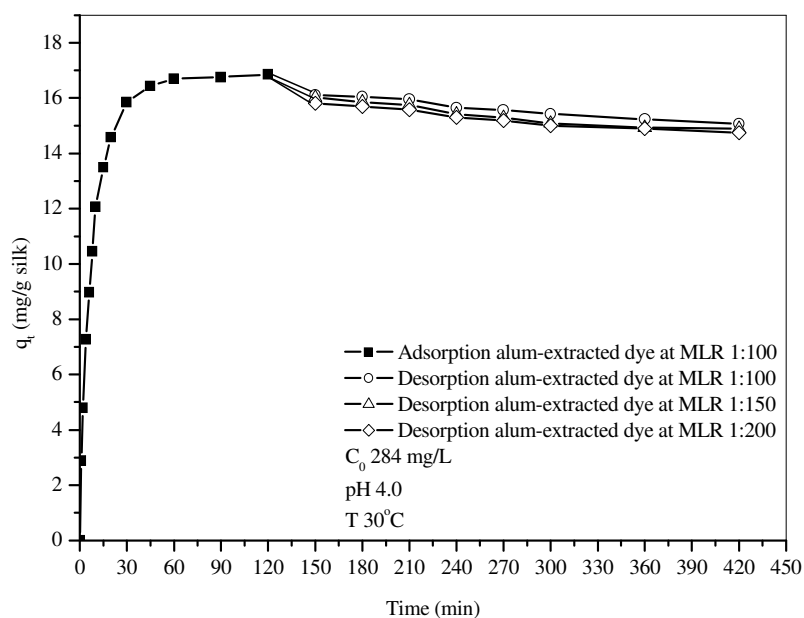


Figure 3.37 Adsorption-desorption analysis of alum-extracted dye onto and off silk in distilled water at different material to liquor ratios.

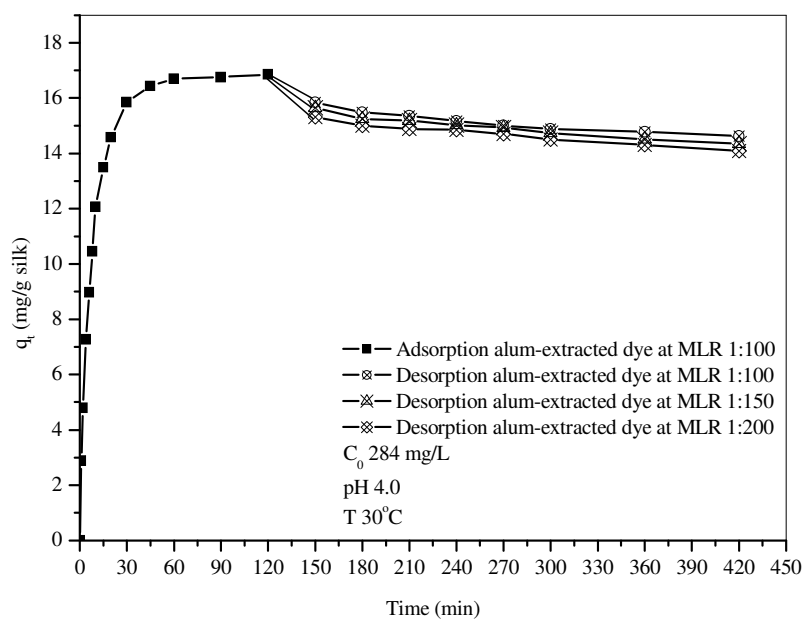


Figure 3.38 Adsorption-desorption analysis of alum-extracted dye onto and off silk in tap water at different material to liquor ratios.

Table 3.13 Percentage of desorption analysis of alum-extracted dye onto and off silk in different type of water and material to liquor ratios.

Time (min)	Deionized water			Distilled water			Tap water		
	1:100	1:150	1:200	1:100	1:150	1:200	1:100	1:150	1:200
150	27.95	34.87	37.18	28.3	32.08	39.62	26.79	32.10	41.11
180	27.42	35.25	37.34	27.18	33.56	39.26	28.51	33.26	38.22
210	30.19	33.25	36.56	27.36	33.74	38.91	29.07	32.56	38.37
240	30.56	33.03	36.40	28.67	34.36	36.97	30.56	33.09	36.35
270	30.64	32.3	37.06	28.41	34.58	37.00	31.20	32.55	36.26
300	31.54	33.27	35.19	28.26	35.18	36.56	30.65	32.82	36.53
360	30.69	32.63	36.68	29.35	34.96	35.69	29.80	33.67	36.53
420	30.79	34.11	35.10	30.49	33.56	35.95	29.65	33.38	36.97
Average	29.97	33.59	36.44	28.50	34.01	37.49	29.53	32.93	37.54

3.4.4 Comparison of activation, thermodynamic parameter and desorption between alum-brazilein and alum-extracted dye dyeing on silk

Crude extracted dye (hot water) from *C. sappan* is composed of 9% brazilein dye. For the dyeing with extracted dye by villagers in the northeast of Thailand, the dye is usually used without purification. Kinetics and thermodynamics parameters for alum-brazilein and alum-extracted dye dyeing onto silk are given in Tables 3.14 and 3.15, respectively.

3.4.4.1 Comparison of activation parameters between alum-brazilein and alum-extracted dye dyeing on silk

The activation parameters of alum-brazilein and alum-extracted dye are listed in Table 3.14. It was found that the activation energy for extracted dye was smaller than for alum-brazilein dye indicating that the former may contain others substances that could help binding of the extracted dye dyeing onto silk. The entropic values obtained in this investigation of alum-brazilein and alum-extracted complexes are both negative, indicating an increase in the order of the system in each case.

A value of the activation energy for alum-brazilein dyeing onto silk was > 40 kJ/mol (41.57 kJ/mol), and it is thus concluded that the adsorption kinetic of alum-brazilein onto silk involved a chemisorption while the activation energy of alum-extracted dye was lower than that of alum-brazilein dye onto silk. It is possible that crude extracted dye contained other components which can act as a catalyst for alum-extracted dye adsorbed on silk as mentioned previously.

Table 3.14 Activation parameters for the adsorption of alum-brazilein and alum-extracted dye dyeing on silk

	Temp (°C)	k_2 (g silk/mg second)	E_a (kJ/mol)	R^2	$\Delta H^\#$ (kJ/mol)	$\Delta S^\#$ (J/mol K)	$\Delta G^\#$ (kJ/mol)	R^2
alum-	30	3.73×10^{-3}					88.36	
brazilein	50	1.04×10^{-2}	41.57	0.99993	39.08	-162.54	91.61	0.99983
	70	2.54×10^{-2}					94.86	
alum-	30	1.73×10^{-4}					96.16	
ext. dye	50	2.75×10^{-4}	21.20	0.99840	18.91	-254.83	101.26	0.99757
	70	4.83×10^{-4}					106.36	

3.4.4.2 Comparison of thermodynamic parameters between

alum-brazilein and alum-extracted dye dyeing on silk

The thermodynamic parameters of alum-brazilein and alum-extracted dye adsorption onto silk are reported in Table 3.15. The negative values of ΔG° indicated that adsorption of dye onto silk was spontaneous in both cases. The negative value of ΔH° in each case confirmed that the adsorption of alum-brazilein and alum-extracted dye onto silk are exothermic processes, although a little more exothermic in the latter case. In addition, the negative values of ΔS° were consistent with the adsorbed alum-brazilein and alum-extracted dyes becoming more restrained within the silk fiber molecules than in the dyeing solutions.

Table 3.15 Thermodynamic parameters for the adsorption of alum-brazilein and alum-extracted dye dyeing on silk

	Temp (°C)	$\ln K_c$	ΔG° (kJ/mol)	ΔH° (kJ/mol)	ΔS° (J/mol K)	R^2
alum-brazilein	30	5.60	-14.11			
	50	4.92	-13.22	-25.32	-36.64	0.99745
	70	4.39	-12.52			
alum-extracted dye	30	7.23	-18.22			
	50	6.34	-17.03	-32.63	-47.87	0.99703
	70	5.66	-16.15			

3.5 Conclusion

Mordanting to fiber techniques such as pre-mordanting, simultaneous mordanting and post-mordanting were tested to find the best conditions for dyeing. It was found that the highest amount of dye adsorbed onto silk occurred with the simultaneous mordanting technique. The adsorption kinetics and isotherms of alum-brazilein dyeing onto silk with simultaneous alum mordanting were studied in this work. The most important parameters influencing the dyeing process including pH, the material to liquor ratio (MLR), the initial dye concentration and temperature were investigated. It was found that the adsorption capacity was dependent on the pH of the dye solution and optimal uptake on silk occurred at pH 4.0. The initial dye adsorption rate of alum-brazilein dye on silk yarn was very fast with an increase in adsorption rate observed with an increase in temperature. Before equilibrium was reached, an increase in temperature led to an increase in the initial dye adsorption rate which pointed to a kinetically controlled process. A pseudo second-order kinetic model was

indicated with an activation energy of 41.57 kJ/mol. This suggested that the overall rate of alum-brazilein dye adsorption is likely to be controlled by the chemical process. The values of the enthalpy (ΔH^\ddagger) and entropy of activation (ΔS^\ddagger) were 39.08 kJ/mol and -162.54 J/mol K respectively. The free energy of activation (ΔG^\ddagger) at 30°C was 88.36 kJ/mol. The free energy (ΔG°), enthalpy (ΔH°), and entropy (ΔS°) terms for alum-brazilein dyeing were also determined, and the negative values of ΔG° and ΔH° obtained indicated that the alum-brazilein dye adsorption process is a spontaneous and an exothermic one. The experimental data fitted well to the Langmuir and Freundlich isotherms with a high correlation coefficient (R^2) in each case.

The adsorption kinetics and isotherm of alum-extracted dye adsorption (with simultaneous alum mordanting) onto silk were also studied. The main dye component of the extract was brazilein. The adsorption capacities are significantly affected by the material to liquor ratio (MLR), the initial dye concentration, and temperature. It was found that the results showed similar trends to those seen with alum-brazilein dyeing onto silk. The dye uptake increased at higher initial dye concentration of alum-extracted dye and was influenced by the material to liquor ratio (MLR). In addition, the initial dye adsorption rates (h_i) onto silk before equilibrium time increased at higher dyeing temperatures. The adsorption kinetics of alum-extracted dye on silk was also found to follow the pseudo second-order kinetic model. The activation energy for the adsorption of alum-extracted dye on silk was evaluated using the pseudo second-order rate constants. The free energy (ΔG°), enthalpy (ΔH°), and entropy (ΔS°) terms for alum-extracted dyeing showed similar results to those with alum-brazilein dye

adsorption process, although there was some evidence that other components in the extracted dye did have an effect on this process and on the desorption of the dye.

3.6 References

- Aksu, Z., (2002). Determination of the equilibrium, kinetic and thermodynamic parameters of the batch biosorption of nickel(II) ions onto *Chlorella vulgaris*. **Process Biochemistry** 38: 89-99.
- Al-Ghouti, M. A., Khraisheh, M. A. M., Allen, S. J., and Ahmad, M. N. (2005). Thermodynamic behaviour and the effect of temperature on the removal of dye from aqueous solution using modified diatomite: a kinetic study. **Colloid and Interface Science** 287: 6-13.
- Anirudhan, T. S. and Radhakrishnan, P. G. (2008). Thermodynamics and kinetics of adsorption of Cu(II) from aqueous solutions onto a new cation exchanger derived from tamarind fruit shell. **Journal Chemistry Thermodynamic** 40: 702-709.
- Bhattacharyya, K. G. and Sarma, A. (2003). Adsorption characteristics of the dye, Brilliant Green, on Neem leaf powder. **Dyes and Pigments** 57: 211-222.
- Bruce, R. L. and Broadwood, N. V. (2000). Kinetics of wool dyeing with acid dyes. **Textile Research Journal** 70: 525-531.
- Bulut, E., Özacar, M., and Şengil, I. A. (2008). Adsorption of malachite green onto bentonite: Equilibrium and kinetic studies and process design. **Microporous and Mesoporous Materials** 115: 234-246.
- Carr, C. M. (1995). **Chemistry of the textiles industry**. Glasgow: Blackie Academic & Professional.

- Chairat, M. (2004). **Extraction and characterization of lac dye from Thai stick lac and development of lac dyeing on silk and cotton.** Ph.D. Thesis, Suranaree University of Technology.
- Chairat, M., Rattanaphani, S., Bremner, J. B., and Rattanaphani, V. (2005). An adsorption and kinetic study of lac dyeing on silk. **Dyes and Pigments** 64: 231-241.
- Chairat, M., Rattanaphani, S., Bremner, J. B., and Rattanaphani, V. (2008). Adsorption kinetic study of lac dyeing on cotton. **Dyes and Pigments** 76: 435-439.
- Chiou, M. S. and Li, H. Y. (2002). Equilibrium and kinetic modeling of adsorption of reactive dye on cross-linked chitosan beads. **Journal of Hazardous Materials** 93: 233-248.
- Chiou, M. S. and Li, H. Y. (2003). Adsorption behavior of reactive dye in aqueous solution on chemical cross-linked chitosan bead. **Chemosphere** 50: 1095-1105.
- Christie, R. M., Mather, M. M., and Wardman, R. H. (2000). **The Chemistry of Colour Application.** Oxford: Blackwell Science.
- Cristea, D. and Vilarem, G. (2006). Improving light fastness of natural dyes on cotton yarn. **Dyes and Pigments** 70: 238-245.
- Doménech-Carbó, A., Doménech-Carbó, M.T., and Sauf-Peris, M.C. (2005). Electrochemical identification of flavonoid dyes in solid work of art samples by abrasive voltammetry at paraffin-impregnated graphite electrodes. **Talanta** 66: 769-782.

- Ferreira, E. S. B., Hulme, A. N., McNab, H., and Quye, A. (2004). The natural constituents of historical textile dyes. **Chemical Society Reviews** 33: 329-336.
- Hall, K. R., Eagleton, L. C., Acrivos, A., and Vermeulen, T. (1966). Pore- and solid-diffusion kinetics in fixed-bed adsorption under constant pattern conditions. **Industrial Engineering Chemistry Fundamental** 5: 212-223.
- Hameed, B. H. and Daud, F. B. M. (2008). Adsorption studies of basic dye on activated carbon derived from agricultural waste: *Hevea brasiliensis* seed coat. **Chemical Engineering Journal** 139: 48-55.
- Hameed, B. H. and El-Khaiary, M. I. (2008). Sorption kinetics and isotherm studies of a cationic dye using agricultural waste: Broad bean peels. **Journal of Hazardous Materials** 154: 639-648.
- Harborne, J. B., Baxter, H., and Moss, G. P. (1999). **Phytochemical dictionary a handbook of bioactive compounds from plants** (2nd ed.). United Kingdom. Taylor & Francis.
- Ho, Y. S. and McKay, G. (1999). Pseudo-second model for sorption process. **Process Biochemistry** 34: 451-465.
- Hojo, N. (2000). **Structure of silk yarn. Part A: Biological and physical aspects.** Enfield: Science publishers.
- Horrocks, A. R. and Anand, S. C. (2000). **Handbook of Technical Textiles.** Cambridge: Woodhead.
- House, J. E. (1997). **Principles of chemical kinetics.** Dubuque, IA: Wm. C. Brown Publishers.

- Hulme, A. N., McNab, H., Peggie, D. A., and Quye, A. (2005). Negative ion electrospray mass spectrometry of neoflavonoids. **Phytochemistry** 66: 2766-2770.
- In-Kyung, B., Hye-Young, M., Ah-Reum, H., Eun-Kyoung, S., and Sang Kook, L. (2005). Suppression of lipopolysaccharide-induced expression of inducible nitric oxide synthase by brazilin in RAW 264.7 macrophage cells. **European Journal of Pharmacology** 513: 237-242.
- Kaplan, D., Adam, W. W., Farmer, B., and Viney, C. (1994). **Silk polymers: Materials science and Biotechnology**. Washington: American Chemical Society.
- Kavitha, D. and Namasivayam, C. (2008). Capacity of activated carbon in the removal of acid brilliant blue: Determination of equilibrium and kinetic model parameters. **Chemical Engineering Journal** 139: 453-461.
- Khan, Md. M. R, Morikawa, H., Gotoh, Y., Miura, M., Ming, Z., Sato, Y., and Iwasa, M. (2008). Structural characteristics and properties of *Bombyx mori* silk fiber obtained by different artificial forcibly silking speeds. **International Journal of Biological Macromolecules** 42: 264-270.
- Kim, D. S., Baek, N. I., Oh, S. R., Jung, K. Y., Lee, I. S., and Lee, H. K. (1997). NMR assignment of brazilein. **Phytochemistry** 46(1): 177-178.
- Kim, T. K., Son, Y. A., and Lim, Y. J. (2005). Thermodynamic parameters of disperse dyeing on several polyester fibers having different molecular structure. **Dyes and Pigments** 67: 229-234.
- Kongkachuichay, P., Shitangkoon, A., and Chinwongamorn, N. (2002). Thermodynamics of adsorption of laccic acid on silk. **Dyes and Pigments** 53: 179-185.

- Laidler, K. J., Meiser, J. H., and Sanctuary, B. C. (2003). **Physical Chemistry**. Boston: Houghton Mifflin.
- Lemmens, R. H. M. J. and Wulijarni-Soetjpto, N. (1992). **Plant resources of South-East Asia³: Dye and tannin-producing plants**. Prosea, Bogor Indonesia, p. 60-62.
- Nuhoglu, Y. and Malkoc, E. (2009). Thermodynamic and kinetic studies for environmentally friendly Ni(II) biosorption using waste pomace of olive oil factory. **Bioresource Technology** 100: 2375-2380.
- Ofomaja, A. E. (2007). Sorption dynamics and isotherm studies of methylene blue uptake on to palm kernel fibre. **Chemical Engineering Journal** doi:10.1016/j.cej.2006.08.022.
- Önal, Y. (2006). Kinetic of adsorption of dyes from aqueous solution using activated carbon prepared from waste apricot. **Journal of Hazardous Materials B** 137: 1719-1728.
- Özcan, A. S. and Özcan, A. (2005). Adsorption behavior of a disperse dye on polyester in supercritical carbon dioxide. **Journal of Supercritical Fluids** 35: 133-139.
- Perkins, W. S. (1996). **Textile coloration and finishing**. North Carolina: Carolina Academic Press.
- Purkait, M.K., DasGupta, S., and De, S. (2005). Adsorption of eosin dye on activated carbon and its surfactant based desorption. **Journal of Environmental Management** 76: 135-142.
- Raisanen, R., Nousiainen, P., and Hynninen, P. H. (2001). Emodin and dermocybin natural anthraquinones as mordant dyes for wool and polyamide. **Textile Research Journal** 71: 1016-1022.

- Rattanaphani, S., Chairat, M., Bremner, J. B., and Rattanaphani, V. (2007). An adsorption and thermodynamic study of lac dyeing on cotton pretreated with chitosan. **Dyes and Pigments** 72: 88-96.
- Septhum, C. (2006). **Adsorption and related studies on some flavonoid dyes from *Maclura cochinchinensis* (Lour.) Corner and silk dyeing**. Ph.D. Thesis, Suranaree University of Technology.
- Septhum, C., Rattanaphani, S., Bremner, J. B., and Rattanaphani, V. (2007). An adsorption study of Al(III) ions onto chitosan. **Journal of Hazardous Materials** 148: 185-191.
- Shanker, R. and Vankar, P. S. (2006). Dyeing cotton, wool and silk with *Hibiscus mutabilis* (Gulzuba). **Dyes and Pigments** xx: 1-6.
- Tan, I. A. W., Ahmad, A. L., and Hameed, B. H. (2008). Adsorption of basic dye using activated carbon prepared from oil palm shell: batch and fixed bed studies. **Desalination** 225: 13-28.
- Tan, I. A. W., Hameed, B. H., and Ahmad, A. L. (2007). Equilibrium and kinetic studies on basic dye adsorption by oil palm fibre activated carbon. **Chemical Engineering Journal** 127: 111-119.
- Thinakaran, N., Baskaralingam, P., Pulikesi, M., Panneerselvam, P., and Sivanesan, S. (2008). Removal of Acid Violet 17 from aqueous solutions by adsorption onto activated carbon prepared from sunflower seed hull. **Journal of Hazardous Materials** 151: 316-322.
- Treigien, R. and Musnickas, J. (2003). Influence of nonionic surfactant on wool fiber dyeing thermodynamics and kinetics parameters. **Chemija (Vilnius)** 14(3): 145-150.

- Ucun, H., Bayhan, Y. K., and Kaya, Y. (2008). Kinetic and thermodynamic studies of the biosorption of Cr(VI) by *Pinus sylvestris* Linn. **Journal of Hazardous Materials** 153: 52-59.
- Vankar, P. S., Shanker, R., Dixit, S., Mahanta, D., and Tiwari, S. C. (2008). Sonicator dyeing of modified cotton, wool and silk with *Mahonia napaulensis* DC. and identification of the colorant in *Mahonia*. **Industrial Crops and Products** 27: 371-379.
- Vankar, P. S., Shanker, R., and Verma, A. (2006). Enzymatic natural dyeing of cotton and silk fabrics without metal mordant. **Journal of Cleaner Production** xx: 1-10.
- Vasanth Kumar, K. and Sivanesan, S. (2007). Isotherms for malachite green onto rubber wood (*Hevea brasiliensis*) sawdust: comparison of linear and non-linear methods. **Dyes and Pigments** 72: 124-129.
- Ye, M., Xie, W-d., Lei, F., Meng, Z., Zhao, Y-n., Su, S., and Du, L-j. (2006). Brazilein, an important immunosuppressive component from *Caesalpinia sappan* L. **International Immunopharmacology** 6: 426-432.
- Zhao, Y. N., Pan, Y., Tao, J. L., Xing, D. M., and Du, L. J. (2006). Study on cardioactive effects of brazilein. **Pharmacology** 76: 76-83 (Chem. Abstr., 2006, 144, 225980)
- Zollinger, H. (1991). **Colour Chemistry**. (2nd ed.) Weinheim. Wiley-VCH.
- Zollinger, H. (2003). **Colour Chemistry**. Weinheim. Wiley-VCH.

CHAPTER IV

TREATMENT OF DYE EFFLUENT USING ACTIVATED CARBONS

4.1 Abstract

In this part of the study, coconut shell- and wood-based activated carbons with different surface chemistry and porous texture were used to remove residual dye from real silk dyeing effluent. This crude dye was extracted from the heartwood of *Ceasalpinia sappan* Linn. and reacted with alum to form a dye complex $[Al(Brazilein)_2]^+$. The surface chemical property of activated carbon in terms of content and type of surface oxygen functional groups was characterized using Boehm titration, Fourier transform infrared spectrophotometer (FT-IR) and pH at the point of zero charge (pH_{pzc}). The carbon porous texture in terms of surface area and porosity was determined using N_2 adsorption at $-196^\circ C$. Oxidation and heat treatment changed the content and type of surface oxygen functional groups on activated carbons. Oxidation treatment introduced carboxylic acid groups in the highest content as compared with the other two acidic groups (lactonic and phenolic groups). The higher content of surface oxygen functional groups enhanced the dye adsorption by the electrostatic interaction mechanism. Different activation methods and different precursors produced activated carbons with different porous textures. Chemically activated carbon contained more mesopore volume than the physically activated

carbon. The greater proportion of mesoporosity in activated carbon could be obtained when a higher chemical ratio of activating agent and precursor was used. The activated carbon with higher mesopore volume significantly enhanced the dye uptake by π - π dispersion interaction. It was concluded that for achieving the highest efficiency of dye removal, the microporous activated carbon required oxidation treatment, whereas the activated carbon specially prepared to have highly developed mesoporosity, can be directly used without surface treatment.

4.2 Surface modification of activated carbon

Generally, activated carbon is a non-polar solid, and thus is not nearly as effective at removing metal ions and polar inorganic pollutants as it is in adsorbing organic compounds. Therefore, modification of the activated carbon with suitable chemical agents, such as oxidation of a carbon surface to obtain a more hydrophilic surface structure with a relatively large number of oxygen-containing surface chemical groups is needed (Shim, Park, and Ryu, 2001; Monser and Adhoum, 2002). A wide range of oxidizing agents such as HNO_3 , H_2SO_4 , H_2O_2 , HClO_4 , NaOCl , $(\text{NH}_4)_2\text{S}_2\text{O}_8$, KIO_4 , and KMnO_4 have been used in the liquid phase, while air, O_2 , and O_3 have been used in the gas phase (Pradhan and Sandle, 1999; Moreno-Castilla *et al.*, 2000; Shim *et al.*, 2001; El-Hendawy, 2003; Rios, Alves, Dalmázio, Fernando, Bento, Donnici, and Lago, 2003; Chen and Wu, 2004; Santiago, Stüber, Fortuny, Fabregat, and Font, 2005). As mentioned previously, the oxidation treatment produces two types of surface oxides: acidic and basic groups, which are usually polar in nature. The oxidation treatment can also affect the surface area and pore texture of the activated carbon (Moreno-Castilla, Ferro-García, Joly, Bautista-Toledo, Carrasco-

Marín, and Rivera-Utrilla, 1995). Many researchers have shown that the introduced surface functional groups are dependant on the oxidation conditions such as the type and concentration of oxidizing agent, the pH of the oxidizing solution, oxidation time and oxidation temperature (Bandosz, Jagiello, and Schwarz, 1996; Tamon and Okazaki, 1996; Carrasco-Marín, Mueden, Centeno, Stoeckli, and Moreno-Castilla, Carrasco-Marín, and Mueden, 1997; Pradhan and Sandle, 1999; Salame and Bandosz, 1999; Jia and Thomas, 2000; Moreno-Castilla *et al.*, 2000; Pereira *et al.*, 2003; Rios *et al.*, 2003; Rivera-Utrilla and Sánchez-Polo, 2003; Chen and Wu, 2004; Jaramillo, Gómez-Serrano, and Álvarez, 2008; Stavropoulos, Samaras, and Sakellaropoulos, 2008; Tao and Xiaoqin, 2008).

Fixation of the acidic groups such as carboxylic, phenolic, and lactonic groups on the surface of activated carbon makes it more hydrophilic and increases the negative surface charge density. The changes in the surface chemistry of activated carbon induced by the formation of acidic oxygen functional groups will significantly affect the adsorptive behavior of the activated carbons when they are used as an adsorbent. For example, such groups enhance the adsorption of aqueous metal cation species such as Pb^{2+} (El-Hendawy, 2003; Xiao and Thomas, 2005), Cu^{2+} (Biniak *et al.*, 1999; Goyal, Rattan, Aggarwal, and Bansal, 2001; Chen, Wu, and Chong, 2003), Cd^{2+} (Jia and Thomas, 2000; Park, Lee, Ryu, and Kim, 2002), with ion exchange playing an important role in the adsorption process. The acidic functional groups on the activated carbon surface can also increase the adsorption capacities of dyes with cationic characteristics such as basic dyes (basic red 14) (Soundping, 2002) and aniline dyes (Radovic *et al.*, 1997; Soundping, 2002) by enhancing electrostatic interaction.

Thermal treatment of activated carbon in an inert atmosphere at high temperature can selectively remove some of surface oxygen functional groups depending on their thermal instability. Consequently, activated carbon exhibits more hydrophobic character after high temperature heat treatment in an inert atmosphere and thus the heat-treated carbons enhance the adsorption capacities of organic compounds such as phenol (Ania, Parra, and Pis, 2002; Nevskaia, Castillejos-Lopez, Guerrero-Ruiz, and Muñoz, 2004), benzene (Wibowo, N., Setyadi, Wibowo, D., Setiawan, and Ismadji, 2007), toluene (Wibowo *et al.*, 2007), and dye with anionic characteristics such as reactive red 198 (Pereira *et al.*, 2003), direct yellow 106 (Pereira *et al.*, 2003), and acid red 73 (Attia, Rashwan, and Khedr, 2006). The adsorption of these adsorbates is generally determined by π - π dispersion interaction between the electrons in the activated carbon surface and the aromatic ring of the adsorbates. In the case of dyes with their large molecular sizes, adsorption is obstructed by the high fraction of micropores of most activated carbons. Therefore, the use of mesopore-activated carbon or modification of pore size is generally required for effective dye adsorption.

4.3 The treatment of dye effluent using activated carbons

Activated carbons have been proven to be effective adsorbents due to their well developed internal pore structure, surface area and the presence of a wide spectrum of surface functional groups (Chingombe *et al.*, 2005). For organic compounds (such as aromatics and dyes), it has been postulated that organic compounds adsorb through a π - π dispersion interaction mechanism (Haydar, Ferro-Garcia, Rivera-Utrilla, and Joly, 2003). This mechanism assumes the interaction of

the π -electrons of the aromatic species with the π -electrons in the basal planes of the carbon. However, some experimental data suggest that the sorption of organic species may be due to an electron donor-acceptor mechanism. This involves the formation of a complex between the adsorbed molecule and the carboxyl group on the acidic surface of the activated carbon. Pinto and co-workers (Franz, Arafat, and Pinto, 2000) have also proposed a mechanism that involves a combination of hydrogen bonding between aromatics and the carboxylic groups on the acidic surface of the activated carbon and the π - π dispersion interaction.

The removal of dyes before the effluent is discharged into rivers and lakes is generally required by environmental regulations. Activated carbon adsorption is one such method that has a potential for the removal of dyes from wastewater. Consequently, a considerable amount of research on dye removal has been carried out in this direction.

Dyes used in dyeing are normally classified into anionic dyes and cationic dyes. Examples of anionic dyes include reactive, direct, and acid dyes, whereas basic dyes are classified as cationic dyes. Their removal from wastewater depends both on the nature of the dyes and the activated carbon. For dyes, their molecular size, types of functional groups and polarity are primarily concerned with adsorption effectiveness. For activated carbons, their surface area, microporous character and surface chemistry determine the adsorption capacity for dye removal.

The adsorption of dyes on activated carbons was studied by Pereira *et al.* (Pereira *et al.*, 2003; Faria *et al.*, 2004) and Órfão *et al.* (Órfão, Silva, Pereira, J. C. V., Barata, Fonseca, Faria, and Pereira, M. F. R., 2006). They prepared a series of activated carbons with different acidic and basic surface chemistry. It was found that

the surface chemistry of activated carbon plays a key role in dye adsorption performance. The activated carbon was oxidized with nitric acid and thermally treated to obtain basic surface carbon which had the best adsorption capacity for anionic dyes such as reactive red 198, reactive yellow 3, reactive blue 5, direct red 80, direct yellow 106, direct blue 78, acid red 151, acid yellow 49, and acid blue 113 (Pereira *et al.*, 2003), reactive red 241, acid blue 113 (Faria *et al.*, 2004), reactive red 241 (Órfão *et al.*, 2006), acid red 73 and acid yellow 23 (Attia *et al.*, 2006). The interaction of anionic dyes and the activated carbon surface occurs between the delocalized π electrons of the oxygen-free Lewis basic sites and the free electrons of the dye molecule present in the aromatic rings and multiple bonds. These authors reported evidence for the protonation of basal plane sites on basic carbon. They stated that oxygen-free carbon sites can adsorb protons from solution, conferring a positive charged surface to the carbon. Thus, it is possible that negatively charged ions of the dyes also interact with these sites.

For cationic dyes such as basic red 14 (Pereira *et al.*, 2003; Faria *et al.*, 2004), basic yellow 21, and basic blue 41 (Pereira *et al.*, 2003), the acid oxygen-containing surface groups (acidic surface carbon) have a positive effect on the adsorption, but thermally treated samples (basic surface carbon) still elicit a better performance, showing the existence of two adsorption mechanisms involving electrostatic and dispersive interactions. The latter interaction plays a dominant role in the adsorption mechanism. These investigators therefore concluded that basic carbons were the most efficient sorbent for the removal of both cationic and anionic dyes. Wang *et al.* (Wang *et al.*, 2005) investigated the removal of methylene blue (basic dye or cationic dye) from aqueous solution using modified activated carbons. They also found that the

acidic functional groups on the surface of carbon are not favorable for basic dye adsorption.

In Thailand, the aqueous extracts from the heartwood of *Ceasalpinia sappan* Linn. are generally used for the dyeing of silk, especially in the Northeast (Moeyes, 1993). The extracted dyes, which are mainly composed of brazilin and brazilein (see Figure 4.1), give a beautiful red or pink color to silk. However, this natural dye has poor fastness properties, and in order to try and overcome this metal ion-based mordants are used (Lemmens and Wulijarni-Soetjipto, 1992; Yan *et al.*, 2005). One such mordant generally used by villagers in Northeast Thailand is alum, which provides a source of Al(III) ions. The dye used in this study was extracted from the heartwood of *C. sappan* and reacted with alum to form the dye complex, $[Al(\text{brazilein})_2]^+$, as shown in Figure 4.2. However, effluent from the silk dyeing is highly colored. As this can cause a problem in the environment, dye removal by an adsorption process was investigated.

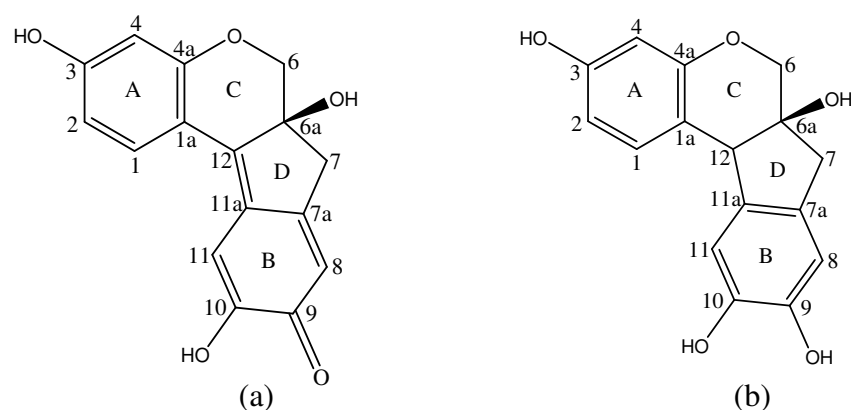


Figure 4.1 Chemical structure of (a) brazilein and (b) brazilin (Wongsooksin *et al.*, 2008).

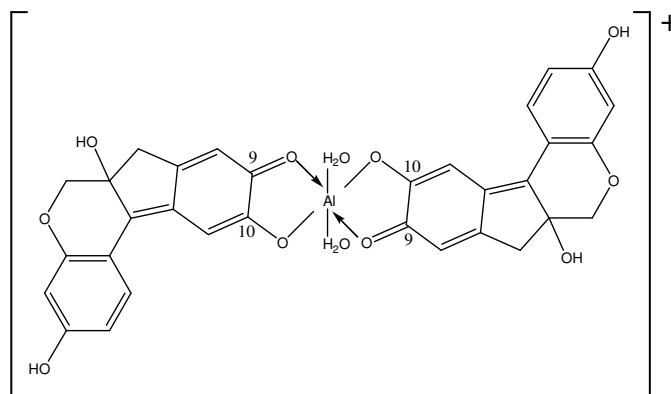


Figure 4.2 The proposed structure of the $[Al(\text{brazilein})_2]^+$ complex (Wongsooksin *et al.*, 2008).

In the present study, a commercial coconut-based activated carbon was chosen as an adsorbent for the adsorption of the above mentioned cationic dye from real effluent. The activated carbon adsorbent was prepared by the physical activation method using steam, and it had a highly microporous and hydrophobic property. Therefore the carbon was modified using nitric acid and thermal treatments in order to change its surface chemistry. Chemical surface properties for the carbon samples including surface acidity, surface basicity, existence of surface functional groups as well as the point of zero charge (pH_{pzc}) were measured and compared. Then the adsorption of activated carbon before and after surface treatment was examined to test its efficiency for purifying real effluent containing dyes, and to gain an understanding of the electrostatic interactions between the surface functional groups of the activated carbon and the cationic dyes. Apart from investigation of the electrostatic interaction, the coconut shell based-activated carbon, and a wood based-activated carbon prepared by chemical activation which had a different surface porous texture, was also tested for dye adsorption in order to investigate the role of porosity in the adsorption process

as well as π - π dispersion interactions. The chemically activated carbon was also modified and tested for its efficiency for dye removal.

4.4 Experimental

4.4.1 Materials and chemicals

- (a) Activated carbon, C. Gigantic Carbon Co., Ltd., Nakhon Ratchasima, Thailand.
- (b) Coconut shell, Suranakhon market, Nakhon Ratchasima, Thailand.
- (c) Nitric acid 69.5% (w/v), HNO₃, Carlo erba
- (d) Hydrochloric acid 37% (w/v), Carlo erba
- (e) Zinc chloride, ZnCl₂, Unilab
- (f) Silver nitrate, AgNO₃, Merck
- (g) Sodium hydroxide, NaOH, Aldrich
- (h) Sodium carbonate, Na₂CO₃, Carlo erba
- (i) Sodium bicarbonate, NaHCO₃, Carlo erba
- (j) Potassium hydrogen phthalate, KH(C₈H₄O₄), Carlo erba
- (k) Potassium bromide, KBr
- (l) Sodium chloride, NaCl, Carlo erba
- (m) Phenolphthalein indicator
- (n) Methyl orange indicator
- (o) Al-extracted dye complex solution (after dyeing onto silk)

(p) Nitrogen gas (industrial grade with 99.9% purity for chemical activation and ultra high purity grade with 99.999% purity for physical activation, supplied by Thai Industrial Gases Public Company Limited)

(q) Carbon dioxide (high purity grade with 99.95% purity, supplied by Thai Industrial Gases Public Company Limited)

4.4.2 Instruments

(a) Horizontal steel tube furnace (VC TF4 with 4.5 cm diameter and 140 cm, Vecstar)

(b) Automated adsorption apparatus (ASAP 2010, Micromeritics)

(c) Fourier Transform Infrared spectrophotometer (FT-IR), (Model spectrum GX, Perkin-Elmer)

(d) UV-Vis spectrophotometer (Agilent 8453)

(e) pH meter (Laboratory pH Meter CG 842, SCHOTT)

(f) Themostatted shaker bath (Type SBD-50, HetoHolten A/S, Denmark)

(g) Sieves (ASTM11, Retsch) and sieve shaker (analysette, FRITSCH)

(h) Rotor beater mill (BB1, Retsch)

(i) Oven hot air (600, Memmert)

(j) Analytical balance (BP221S, Sartorius)

(k) Peristaltic pump (101F/R, Watson marlow)

4.4.3 Methods

Coconut shell based-activated carbon (sample code C) was supplied by C. Gigantic Carbon Co., Ltd., Nakhon Ratchasima, Thailand. It was produced by physical activation using steam and was used in form of granular with particle size 8

x 16 mesh. Sample C was modified using 7.5 M HNO₃ as an oxidizing agent to enhance the hydrophilic characteristic. Then the study of equilibrium adsorption of dye in the spent dye bath of aqueous extract from the wood of *C. sappan* was performed to investigate the role of surface functional groups of activated carbon. The modified activated carbon was also subjected to heat treatment in order to remove some of the existing surface functional groups. Then, the adsorption of activated carbons before and after surface treatment was compared to test their efficiency for purifying real effluent containing dyes. In addition, another coconut shell based-activated carbon was prepared by chemical activation using ZnCl₂ and this was also tested for dye uptake. Moreover, one carbon sample with a high micropore fraction and another carbon sample with a high fraction of mesopore were also tested for comparison with the oxidized samples.

4.4.3.1 Surface modification of activated carbon

Oxidation treatment of activated carbon (sample C) using 7.5 M HNO₃ as an oxidizing agent for incorporating oxygen functional groups was performed as follows :

(a) The sample C was washed with distilled water by using the reflux method for 1 h to remove water soluble materials present in the as received sample. Then the sample was dried in an oven at 110°C for 24 hours.

(b) The cleaned sample C was modified with 7.5 M HNO₃ solution (ratio 1:10 w/v) by heating at reflux (boiling point temperatures ~ 80-90°C) for 1, 2, 4, 8, 16, 24, and 48 hours. After oxidation, the oxidized activated carbon was washed several times with hot water, followed by boiling with water in a reflux condenser to remove residual HNO₃ and other soluble materials until the pH of the

water washings became constant. Finally, the washed activated carbon was dried at 110°C overnight.

(c) For thermal treatment, about 5 g of oxidized activated carbon (sample C4) was placed in a horizontal stainless steel tube furnace, heated to 700 or 900°C at 20°C min⁻¹ under a flow of N₂ (100 cm³ min⁻¹) and held for 4 hours. After cooling to room temperature under the same atmosphere, the sample was collected and stored in a desiccator.

4.4.3.2 Preparation of activated carbon by chemical activation and surface modification

(a) The coconut shell was milled by a rotor beater mill and sieved to obtain a size fraction of 8 x 16 mesh. Next, the coconut shell sample was dried at 110°C for 24 hours in an oven to remove excess moisture.

(b) The above sample was impregnated with a ZnCl₂ (60 wt%) solution using ratio of ZnCl₂/shell 3:1 w/w and dehydrated in an oven overnight at 110°C.

(c) About 5 g of the dehydrated sample was placed in horizontal tube furnace. The temperature was ramped from ambient temperature to 800°C at 20 °C/min and pyrolysed under a flow of N₂ (100 cm³ min⁻¹) at 800°C for 1 hour. After this, N₂ gas was replaced by CO₂ gas and the solid activated at 800°C for another hour.

(d) The activated product was cooled to room temperature under a flow of N₂ gas. The sample was transferred to a beaker containing 250 mL of 0.1 M HCl, stirred for 1 h, and washed with hot deionized H₂O until the washed solution

was free of zinc(II) and chloride ions and then dried at 110°C overnight. The code for this sample was CZ.

(e) The CZ sample was oxidized under the same conditions as for sample C4 (4.4.3.1).

(f) Eucalyptus wood from a local sawmill in the form of wood shavings was milled by a rotor beater mill and sieved to obtain a size fraction of 20 x 30 mesh. Next, the wood sample was dried at 110°C for 24 hours in an oven to remove excess moisture.

(g) The wood sample (7 g) was impregnated for 1 hour with 50 wt% H₃PO₄, prepared from 85 wt% H₃PO₄, using a 0.5:1 and 2:1 chemical weight ratio of H₃PO₄ solution and wood. Under this condition, the wood sample was completely soaked with acid solution.

(h) The mixture of wood and H₃PO₄ solution was loaded into a ceramic boat and placed in the heated zone of the tube furnace with N₂ flowing through at a constant rate of 100 cm³/min. The furnace was heated from room temperature to 400°C at a heating rate of 25°C/min and held at this temperature for 1 hour. After carbonization, the furnace was turned off and the activated carbon was allowed to cool down to room temperature under a flow of N₂.

(i) The activated carbon product was washed several times with distilled water to remove the remaining acid until the measured pH became constant. and the final suspension was filtered through a filter paper. The washed product was dried at 110°C in an oven. The codes of the samples were W1 and W2.

The preparation and oxidation conditions and sample codes are tabulated in Table 4.1 and 4.2.

Table 4.1 Preparation conditions and sample code used in prepared original activated carbons.

Precursor	Activating agent	Chemical weight ratio chemical:precursor	Carbonization	Code
Coconut shell	Steam	-	-	C
Coconut shell	ZnCl ₂ (60 wt% ZnCl ₂)	3:1	800°C (N ₂ 1 h and CO ₂ 1 h)	CZ
Eucalyptus wood	H ₃ PO ₄ (50 wt% H ₃ PO ₄)	0.5:1	400°C (1 h)	W1
Eucalyptus wood	H ₃ PO ₄ (50 wt% H ₃ PO ₄)	2:1	400°C (1 h)	W2

Table 4.2 The experimental conditions for liquid phase oxidation.

Sample	Oxidizing agent	Conditions			Sample code
		Method	Temperature	Treatment time (hour)	
C	HNO ₃ (7.5 M)	Reflux	Boiling point (~ 80-90°C)	1	C1
				2	C2
				4	C4
				8	C8
				16	C16
				24	C24
				48	C48
CZ	HNO ₃ (7.5 M)	Reflux	Boiling point	4	CZ4

4.4.3.3 Characterization of activated carbons

The original activated carbons and the oxidized activated carbons were characterized using several techniques including Boehm titration, FT-IR, and pH_{pzc} .

The Boehm titration experiment was performed by the following procedure: one gram of activated carbon was mixed with 100 mL of each of the 0.1 M solutions of HCl, NaOH, and NaHCO₃ and 0.05 M Na₂CO₃. Each vial was sealed, shaken for 24 hours and the suspensions filtered. 10 mL of the filtrate solutions of NaOH, Na₂CO₃, and NaHCO₃ were pipetted and titrated with 0.1 M HCl, while the filtrate solution of HCl was titrated with 0.1 M NaOH. The titrant volumes of the

various bases and acids were used to determine the amount of functional groups on the activated carbon surface.

An FT-IR spectrophotometer was used to measure the infrared spectrum of the activated carbons and to identify their chemical functionality. The activated carbon was mixed with KBr powder and the pellet formed by compressing at 10 tons for 2 min in a hydraulic press. Before measurement, the instrument was run to collect the background, which was automatically subtracted from the sample spectrum. The spectra were recorded from 4000 to 400 cm^{-1} at a scan rate of 0.2 cm^{-1} s^{-1} , and the number of interferograms at nominal resolution of 4 cm^{-1} was fixed at 25.

The determination of pH_{pzc} was done by adjusting the pH of 0.01 M NaCl (50 mL) to values between 1 to 10 obtained by adding either 0.1 M HCl or NaOH. About 0.15 g of activated carbon was added to each solution at room temperature and then shaken for 48 hours. The final pH was measured and plotted against the initial pH. The pH at which the plotted curve intersected the line of $\text{pH}(\text{final}) = \text{pH}(\text{initial})$ was taken as the pH_{pzc} of the activated carbon surface.

Porous properties of the activated carbons were determined using N_2 adsorption isotherm data at -196°C acquired by the automated adsorption apparatus. The activated carbon was first degassed at 300°C under vacuum ($< 50 \mu\text{mHg}$) for 12 hours to remove moisture and other volatiles. From the obtained isotherm data, the specific surface area, S_{BET} , was estimated by applying Brunauer-Emmett-Teller (BET) equation (Do, 1998). The micropore volume, V_{mic} , was calculated by using Dubinin-Radushkevich (DR) equation (Do, 1998). The total pore volume, V_{T} , was found from the amount of N_2 gas adsorbed at the relative pressure of 0.99 and then converted to the corresponding volume in the liquid state.

4.4.3.4 Batch adsorption experiments

The carbon samples C, C1, C2, C4, C4-700, C4-900, CZ, CZ4, W1, and W2 were used in the batch adsorption experiments to determine the amount of dye uptake. Since the maximum introduction of oxygen surface concentration had occurred with C4 which was oxidized for 4 hours, the samples from longer oxidation times, i.e., C8, C16, C24, and C48, were not investigated.

4.4.3.4.1 Preparation of natural dye extract and Al-extracted dye complex

The heartwood of *C. sappan* was obtained from a plantation area in Nakhon Ratchasima Province, Thailand. The dried heartwood was chopped into small pieces and extracted with boiling deionized water using the ratio of 1 gram of wood per 10 ml of water for one hour at 80-95°C. The aqueous extract was filtered and concentrated using a vacuum evaporator. Then it was dried in a vacuum freeze dryer, giving the dye extract in powdered form with 13% yield by weight.

The simultaneous-mordanting technique was used for dyeing of silk in this study. The dye solution containing the Al-complex dye was prepared from a 2:1 mole ratio of $\text{KAl}(\text{SO}_4)_2 \cdot 12\text{H}_2\text{O}$ and natural dye extract solution. This dye was present in the dye bath as a complex $[\text{Al}(\text{brazilein})_2]^+$ (Wongsooksin *et al.*, 2008). After dyeing onto silk, the dye solution was diluted to an initial concentration of 220 mg/L, and was simply called the dye solution and was kept for the batch adsorption experiments.

4.4.3.4.2 Batch contact time studies

Adsorption experiments were carried out by shaking the dye solution (25 mL) of initial concentration of 220 mg/L without adjusting the pH, in a conical flask (125 mL) with each 0.25 g of carbon samples (C, C4, and CZ) over a range of time of 24 to 120 hours. The temperature was controlled at 30°C by using a thermostatted shaker bath. The aqueous sample was filtered by filter paper and the dye concentration was determined at time zero and at time t using a UV-Visible spectrophotometer (Agilent 8453) and a calibration curve based on absorbance at λ_{\max} 507 nm versus dye concentration. The amount of dye adsorbed onto the carbon sample, q_t (mg/g AC), at time t was calculated by the mass balance relationship (equation (4.1)).

$$q_t = (C_0 - C_t) \frac{V}{W} \quad (4.1)$$

where C_0 (mg/L) and C_t (mg/L) are the concentrations in the solution at time zero and at time t , respectively, V is the volume of the solution (L), and W is the weight of activated carbon (g) used.

4.4.3.4.3 Batch pH studies

The pH of the dye solutions over a range of initial pH values from 2.0 to 4.5 was adjusted by using 0.1 M NaOH or 0.1 M HNO₃. Adsorption experiments were carried out by shaking the dye solution (25 mL) at an initial concentration of 220 mg/L in a conical flask (125 mL) with 0.25 g of carbon sample in a thermostatted shaker bath at 30°C for 72 hours. After equilibrium was

reached, the aqueous sample was filtered by filter paper and the dye concentration was determined using a UV-Visible spectrophotometer (Agilent 8453) and a calibration curve based on absorbance at λ_{\max} 507 nm versus dye concentration. The amount of adsorption at equilibrium, q_e (mg/g AC) was obtained by the mass balance relationship (equation (4.2)).

$$q_e = (C_0 - C_e) \frac{V}{W} \quad (4.2)$$

where C_0 (mg/L) and C_e (mg/L) are the concentrations in the solution at time zero and at equilibrium time t , respectively, V is the volume of the solution (L), and W is the weight of activated carbon (g) used.

4.4.3.4.4 Batch equilibrium studies

Batch equilibrium studies were performed by adding 0.05 to 1.00 g of activated carbon into a series of 125 mL conical flasks. Each flask was filled with 25 mL of dye solution at an initial concentration of 220 mg/L without adjusting the pH and the suspension shaken in a thermostatted shaker bath operated at 30°C for 72 hours. After equilibrium, the aqueous sample was filtered by filter paper and the dye concentration was determined as in 4.4.3.4.3.

The adsorption isotherms at 30°C of the dye effluent on the various activated carbons were analyzed using Langmuir isotherms (equations 4.3 and 4.4).

$$q_e = \frac{QbC_e}{1 + bC_e} \quad (4.3)$$

A linear form of this expression is:

$$\frac{C_e}{q_e} = \frac{1}{Qb} + \left(\frac{1}{Q}\right)C_e \quad (4.4)$$

In the above equation, Q is the maximum amount of the dye per unit weight of activated carbon to form a complete monolayer coverage on the surface bound at high equilibrium dye concentration C_e , q_e is the amount of dye adsorbed per units weight of activated carbon at equilibrium, and b the Langmuir constant related to the affinity of binding sites. The value of Q represents a practical limiting adsorption capacity when the surface is fully covered with dye molecules and it assists in the comparison of adsorption performance under different conditions.

4.5 Results and discussion

4.5.1 Characterization of porosity and surface chemistry of activated carbons

Tables 4.3 and 4.4 show the porous properties, amount and distribution of surface oxygen functional groups as well as pH_{pzc} for all samples used in this study. The original physically activated carbon (sample C) exhibited mainly microporosity (88%) with a Type I isotherm (see Figure 4.3). The chemically activated carbon (sample CZ) also contained mainly micropore (80%) but had more mesopore volume

than sample C. It was observed that the porous property of sample C decreased after oxidation. This could arise from the inaccessibility of N_2 molecule into the internal adsorption sites due to the presence of more functional groups at the pore entrance and possibly by the collapse of some thin pore walls caused by oxidizing agents during the oxidation treatment (Xiao, 2004; Moreno-Castella, Carrasco-Marín, and Mueden, 1997; Choma, Burakiewicz-Mortka, Jaroniec, and Klinik, 1999; Salame, Bagreev, and Bandosz, 1999). The lowering in the access amount of N_2 for the oxidized carbon is evident from the adsorption isotherm data of N_2 at -196°C , as shown in Figure 4.4. Porous properties of those samples which contain very high acidic functional groups such as C8, C16, and C48, could not be determined from the N_2 adsorption measurement. The heat treated samples (samples C4-700 and C4-900) had much higher surface areas and micropore volumes than those of the oxidized carbons. This is expected, since the thermal treatment of oxidized carbon at high temperatures in an inert atmosphere would cause the detachment of surface functional groups, giving rise to the restoration of its porous properties and even higher surface area than in the original activated carbon (sample C) (Figure 4.5).

The chemically activated carbons prepared from Eucalyptus wood using different chemical weight ratios of H_3PO_4 solution and wood of 0.5:1 and 2:1 (sample W1 and W2) showed different porous properties as shown in Table 4.3. The surface area and pore volume of activated carbon increased with an increase of chemical weight ratio from 0.5:1 to 2:1. Sample W1 exhibited mainly micropore (94.8%) and 5.2% of mesopores, whereas sample W2 contained a slightly higher proportion of mesopore (50.4%) than micropore (49.6%) volumes. Figure 4.6 compares the adsorption and desorption isotherms of N_2 between sample W1 and W2.

Sample W1 shows Type I isotherm, typical of microporous adsorbent. However, sample W2 gives type II isotherm with hysteresis, showing characteristic of mesoporous material. This increased mesopore volume appears to occur as more H_3PO_4 is incorporated into the raw wood material, presumably due to the increasing degree of dilation of the wood structure by the phosphate linkage group.

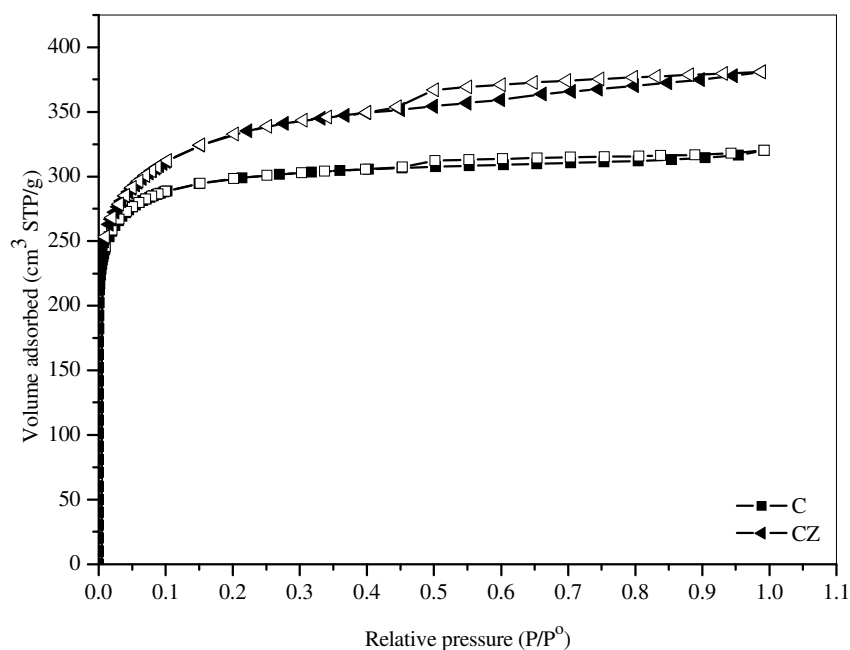


Figure 4.3 Adsorption (closed symbols) and desorption (open symbols) isotherms of N_2 at -196°C for physically activated carbon (sample C) and chemically activated carbon (sample CZ).

Table 4.3 Textural characteristics obtained from N₂ adsorption isotherm for various activated carbon (the value in the square bracket [] is the percentage changes with reference to the original carbon, where “+” denotes % increasing and “-” denotes % decreasing).

Sample	S_{BET} (m ² /g)	V_{mic} (cm ³ /g)	$V_{\text{meso+mac}}$ (cm ³ /g)	V_{T} (cm ³ /g)	D (nm)
C	977	0.44 (88%)	0.06 (12%)	0.50	2.03
C1	905 [- 7%]	0.40 (85%) [- 9%]	0.07 (15%) [+ 17%]	0.47 [- 6%]	2.09 [+ 3%]
C2	852 [- 13%]	0.37 (84%) [- 16%]	0.07 (16%) [+ 17%]	0.44 [- 12%]	2.08 [+ 2 %]
C4	581 [- 41%]	0.25 (83%) [- 43%]	0.05 (17%) [- 17%]	0.30 [- 40%]	2.08 [+ 2%]
C8	ND	ND	ND	ND	ND
C16	ND	ND	ND	ND	ND
C24	ND	ND	ND	ND	ND
C48	ND	ND	ND	ND	ND
C4-700	1140 [+ 96%]	0.51 (86%) [+ 104%]	0.08 (14%) [+ 60%]	0.59 [+ 97%]	2.05 [- 1%]
C4-900	1144 [+ 97%]	0.51 (88%) [+ 104%]	0.07 (12%) [+ 40%]	0.58 [+ 93%]	2.03 [- 2%]
CZ	1079	0.47 (80%)	0.12 (20%)	0.59	2.18
CZ4	525 [- 51%]	0.26 (79%) [- 45%]	0.07 (21%) [- 42%]	0.33 [- 44%]	2.09 [- 4%]
W1	1200	0.55 (95%)	0.03 (5%)	0.58	-
W2	1688	0.61 (50%)	0.62 (50%)	1.23	-

ND = Not Detectable

Table 4.4 Boehm titration results of original and oxidized activated carbons (the value in the square bracket [] is the percentage changes with reference to the original carbon, where “+” denotes % increasing and “-” denotes % decreasing).

Sample	Acidic group (mequiv/g)				Basic group (mequiv/g)	pH _{pzc}
	Carboxylic	Lactonic	Phenolic	Total		
C	0.78 (67%)	0.02 (2%)	0.37 (31%)	1.17	1.67	8.57
C1	2.13 (69%) [+ 173%]	0.20 (6%) [+ 900%]	0.76 (25%) [+ 108%]	3.10 [+ 165%]	1.48 [-11 %]	6.99
C2	2.69 (63%) [+ 244%]	0.44 (10%) [+ 2100%]	1.12(27%) [+ 203%]	4.25 [+ 263%]	1.29 [- 22 %]	6.87
C4	3.49 (67%) [+ 347%]	0.47 (9%) [+ 2250%]	1.28 (24%) [+ 246%]	5.24 [+ 348%]	1.11 [+ -34%]	5.48
C8	3.64 (67%) [+ 367%]	0.51 (9%) [+ 2450%]	1.28 (24%) [+ 246%]	5.43 [+ 364%]	0.93 [- 44 %]	-
C16	3.86 (67%) [+ 395%]	0.55 (9%) [+ 2650%]	1.37 (24%) [+ 270%]	5.78 [+ 394%]	0.92 [-45%]	-
C24	3.90 (67%) [+ 400%]	0.57 (10%) [+ 2750%]	1.38 (23%) [+ 273%]	5.85 [+ 400%]	0.86 [- 49 %]	-
C48	3.98 (67%) [+ 410%]	0.59 (10%) [+ 2850%]	1.38 (23%) [+ 273%]	5.95 [+ 409%]	0.86 [- 48%]	-
C4-700	0.59 (54%) [- 83%]	0.21 (9%) [- 55%]	0.30 (27%) [- 77%]	1.10 [-79 %]	1.74 [+ 57%]	8.65
C4-900	0.39 (43%) [- 89%]	0.22 (24%) [- 53 %]	0.30 (33%) [-76 %]	0.91 [- 83%]	2.34 [+ 75%]	8.98
CZ	1.10 (79%)	0.07 (5%)	0.24 (16%)	1.51	1.72	7.80
CZ4	2.82 (80%) [+ 135%]	0.20 (5%) [+ 186%]	0.52 (15%) [+ 117%]	3.54 [+ 134%]	1.12 [- 35%]	6.95
W1	0.06 (9%)	0.43 (65%)	0.17 (26%)	0.66	0.63	7.50
W2	0.67 (46%)	0.29 (20%)	0.49 (34%)	1.45	1.35	-

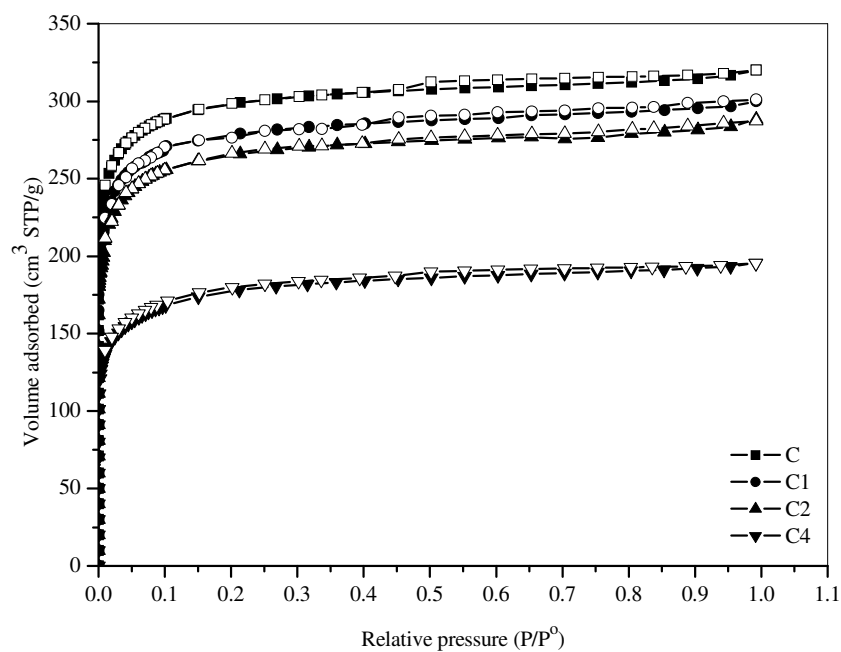


Figure 4.4 Adsorption (closed symbols) and desorption (open symbols) isotherms of N_2 at -196°C for physically activated carbon (sample C) and their oxidized activated carbons (sample C1, C2, and C4).

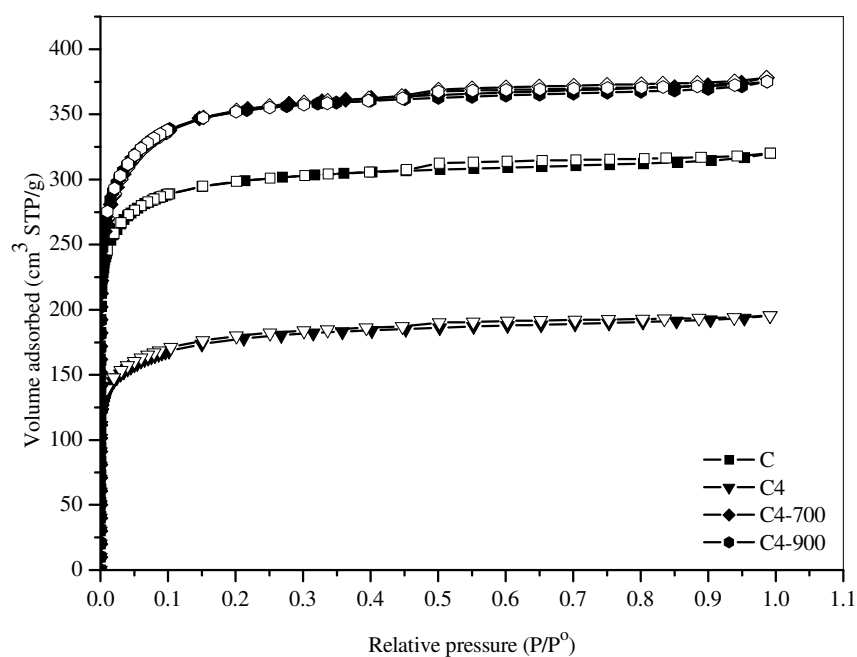


Figure 4.5 Adsorption (closed symbols) and desorption (open symbols) isotherms of N_2 at $-196^\circ C$ for physically activated carbon (sample C), oxidized activated carbon (sample C4) and heat treatment activated carbons (sample C4-700 and C4-900).

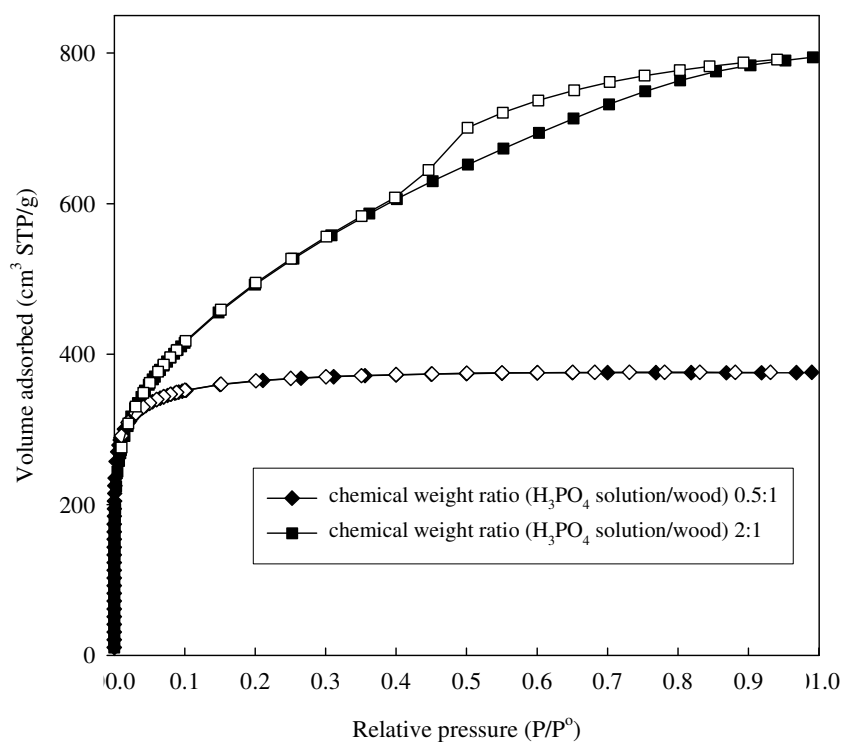


Figure 4.6 Adsorption (closed symbols) and desorption (open symbols) isotherms of N_2 at -196°C for wood based-activated carbons prepared from chemical activation (sample W1 and W2).

The amounts and distribution of oxygen acidic groups and basic sites on the activated carbon surfaces as determined from the Boehm titration are shown in Table 4.4 and Figure 4.7. From this figure, it is seen that the total acidic group increased after oxidation and increased with increasing oxidation time from 1 hour to 4 hours. After 4 hours it became almost constant, therefore the sample C4 which was fully oxidized, was used in the study of dye adsorption. The HNO_3 oxidation of all samples gave of the following functional groups in the relative amount order of: carboxylic acid > phenolic > lactonic groups. It is noted that the carboxylic group content of the oxidized carbon (sample C4) was increased by 4.5 times when compared to the unoxidized carbon (sample C). Other researchers also reported that

HNO₃ gave the highest proportion of carboxylic acid on the oxidized carbon surfaces (Jia and Thomas, 2000; Xiao and Thomas, 2005). When compared to the original carbon, the basic group content decreased after the HNO₃ treatment and there was a tendency to further decreases with increasing oxidation times (see Table 4.4 and Figure 4.7). This result is consistent with other reported results (Moreno-Castilla *et al.*, 2000; Domingo-García, López-Garzón, and Pérez-Mendoza, 2000). The decrease of basic group content may arise from the conversion of ketones to carboxylic acid and lactone functionalities (Lebedev, 1984; Denisov and Afanas'ev, 2005; Smith and March, 2007). This may partly explain the observed highest content of carboxylic acid groups and the increase in lactonic group content in these oxidized carbons.

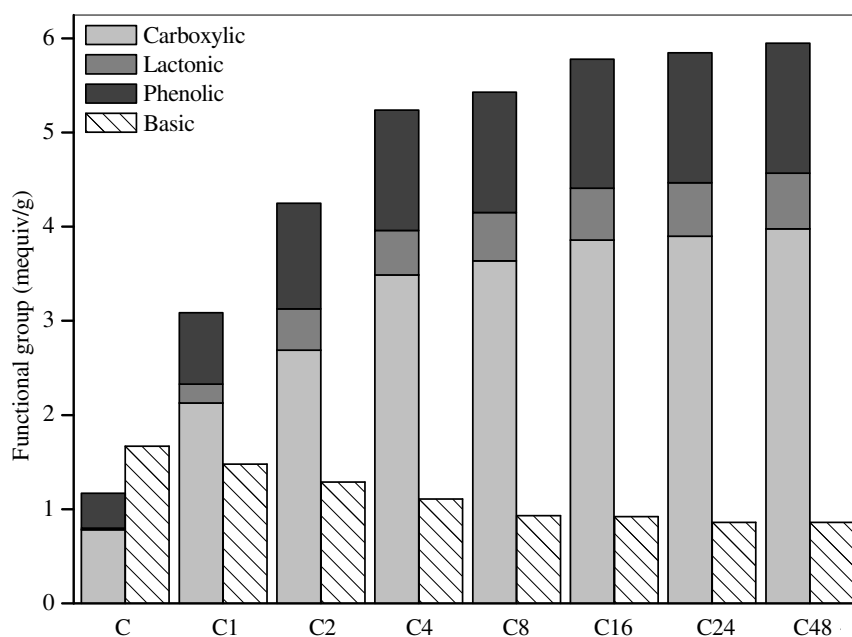


Figure 4.7 Content of surface functional groups of the physically activated carbon (sample C) and their oxidized activated carbons (sample C1, C2, C4, C8, C16, C24, and C48).

In order to further study the effect of surface chemistry on the dye adsorption, the oxidized sample was heat-treated to selectively remove some of the surface oxygen functional groups. The heat treatment process reduced the amount of acidic functional groups present as indicated in Table 4.4 and Figure 4.8 (see sample C4 compared with sample C4-700 and C4-900). Also from this data, the carboxylic acid groups are most sensitive to heat treatment, i.e. this group content decreased by the largest amount at both treatment temperatures, as compared to the other two acidic groups (lactonic and phenolic groups). Furthermore, the thermal treatment developed more of the basic groups on the carbon surface. This could be due to the transformation of some acidic groups into Bronsted basic groups at the high treatment temperature or to an increase in Lewis basic content. The latter effect probably comes from the fact that heat treatment removed some of the electron withdrawing groups (carboxylic acid and lactonic groups) and consequently the Lewis basic sites which are associated with π electron density within the carbon basal plane is increased.

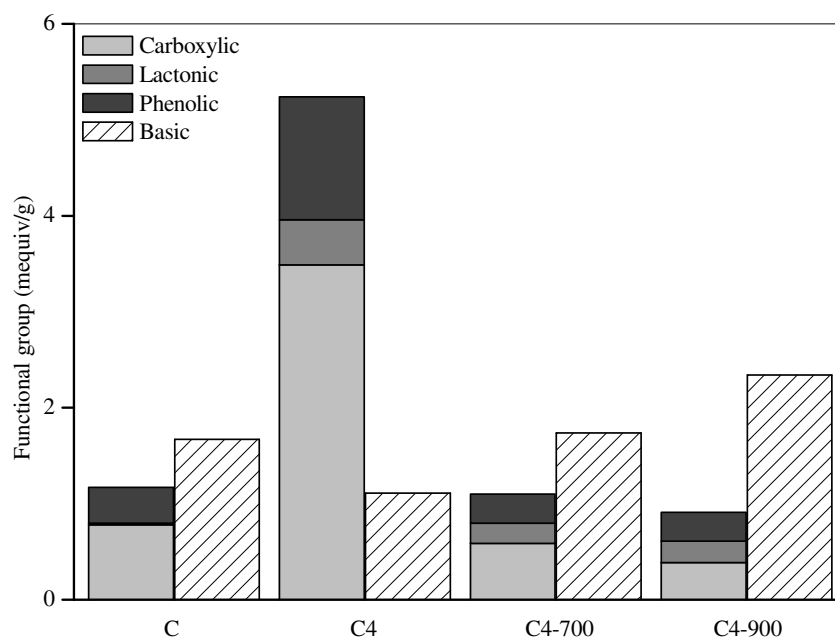


Figure 4.8 Content of surface functional groups of the physically activated carbon (sample C), oxidized activated carbon (sample C4) and heat treatment activated carbons (sample C4-700 and C4-900).

The content and types of surface oxygen functional groups of the chemically activated carbons are tabulated also in Table 4.4 and Figure 4.9. The chemically activated carbon (ZnCl_2 ; sample CZ) prepared from coconut shell material contained a higher total content but the same distribution of surface oxygen functional groups as for the physically activated carbon (sample C). However, when sample CZ was oxidized under the same conditions as sample C4, a lower content of surface oxygen functional groups was observed (shown in Table as CZ4 compared with C4). It is probable that the physically activated carbon could contain greater surface defects due to the higher activation temperature, thus allowing the physically

activated carbon to be more susceptible to oxidation compared to the chemically activated carbon and hence producing a larger number of surface oxygen functional groups.

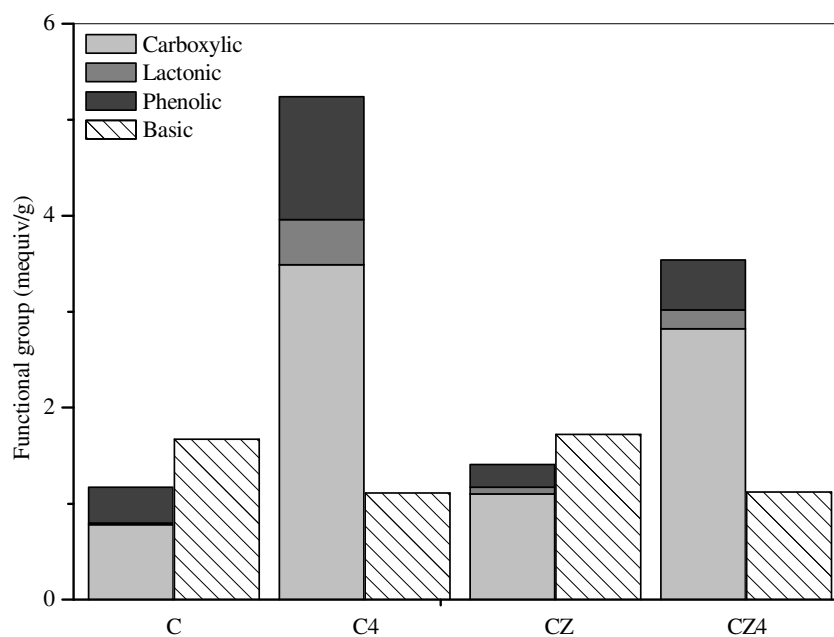


Figure 4.9 Content of surface functional groups of the physically activated carbon (sample C), chemically activated carbon and their oxidized activated carbons (sample C4 and CZ4).

For H_3PO_4 chemically activated carbon prepared from Eucalyptus wood, the surface oxygen functional group content introduced depended on the chemical weight ratio of H_3PO_4 /wood. The higher ratio of H_3PO_4 used exhibited higher surface oxygen functional group content. This can be observed from the content of surface oxygen functional groups in sample W1 and W2 as shown in Table

4.4 and Figure 4.10. This observation had been also previously observed by some other authors.

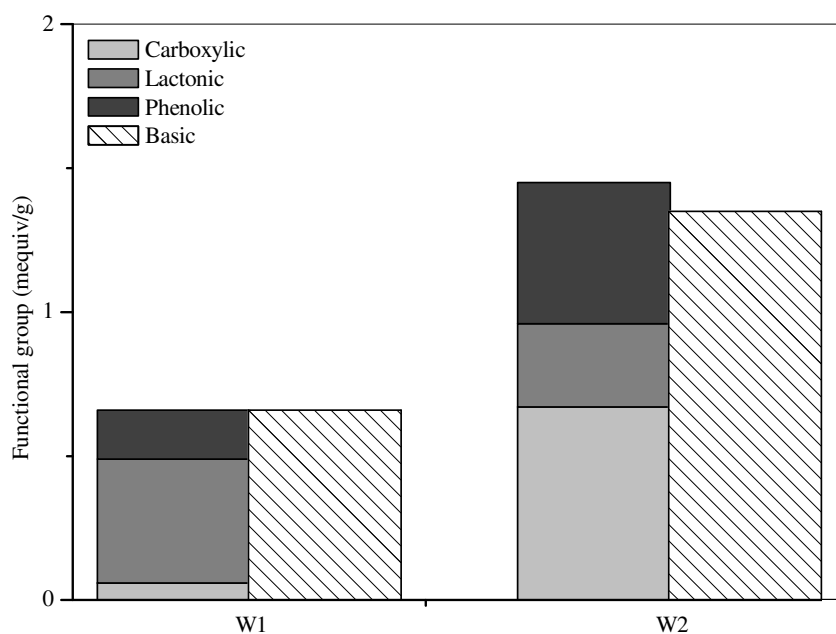


Figure 4.10 Content of surface functional groups of the wood based-activated carbons prepared from chemical activation (sample W1 and W2).

Table 4.4 also summarizes the pH_{pzc} values. As seen from the table, the oxidized carbons exhibit lower pH_{pzc} values than that of the original activated carbon. The order of the pH_{pzc} values is in agreement with the amount of acidic functional groups from Boehm titration i.e. the higher content of acidic functional groups, the lower the pH_{pzc} .

The FT-IR transmission spectra of original and oxidized activated carbons are presented in Figure 4.11 and 4.12. From these data, it was shown that the differences of FT-IR spectra between the original and oxidized activated carbons are

mainly due to the formation of oxygen surface functional groups. For the original activated carbon, the band around 1606 cm^{-1} is a characteristic peak for activated carbon materials and is probably ascribable to carbonyl groups which are highly conjugated in the graphene layer such as quinones and/or ionoradical structures; this is also consistent with the basic nature of the activated carbon. For both the original and oxidized activated carbons, a strong broad band was observed around 3400 cm^{-1} and this was assigned to the carboxylic group O-H stretching. The oxidized as well as the original sample spectra have an extended broad band between $1000\text{-}1250\text{ cm}^{-1}$ associated with C-O stretching and O-H bending modes of the lactone, phenol, and carboxylic acid groups. For oxidized activated carbons, the most characteristic changes are observed within two additional bands around 1580 cm^{-1} and 1710 cm^{-1} . The band observed around 1580 cm^{-1} is assigned to aromatic ring stretching coupled to highly conjugated carbonyl groups (C=O). The band observed around 1710 cm^{-1} is assigned to the stretching vibrations of carboxyl groups on the edges of graphitic layer planes or to conjugated carbonyl groups (C=O in carboxylic acid and lactone groups). These results indicated that HNO_3 treatment gave rise to a greater increase in C=O bonds in carboxylic acid and lactone groups. In both regions, the band intensities increase with increasing oxidation time.

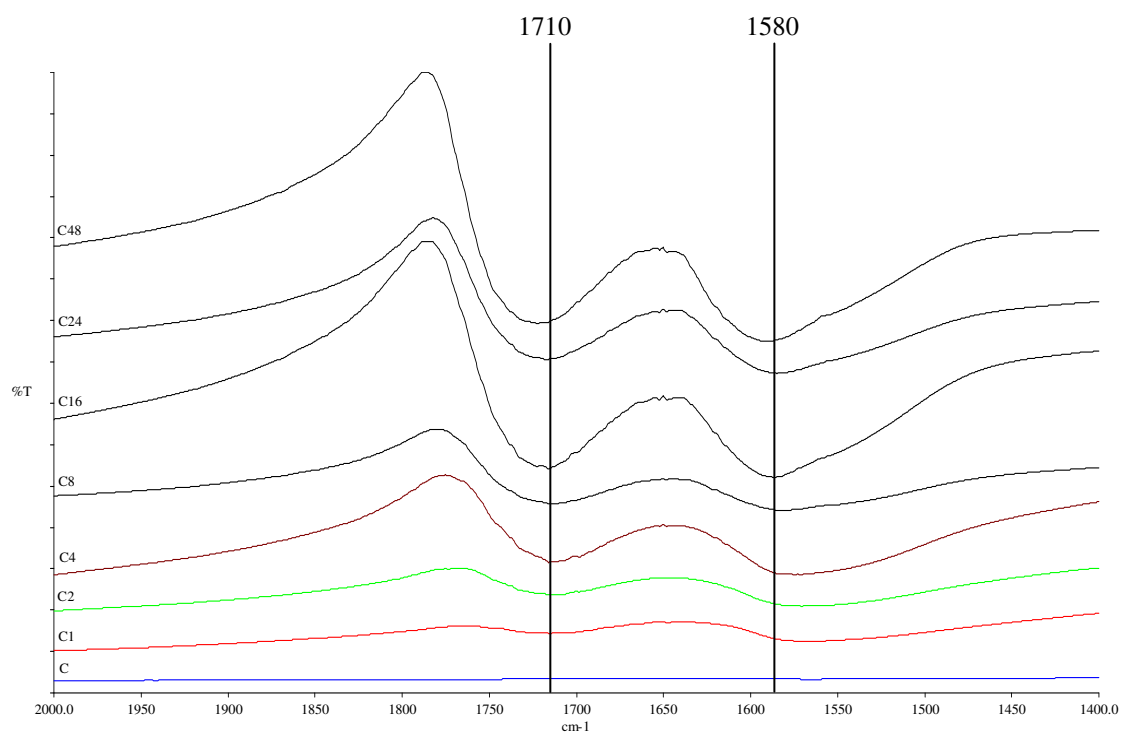


Figure 4.11 FT-IR spectra of the physically activated carbon (sample C) and their oxidized activated carbons (sample C1, C2, C4, C8, C16, C24, and C48).

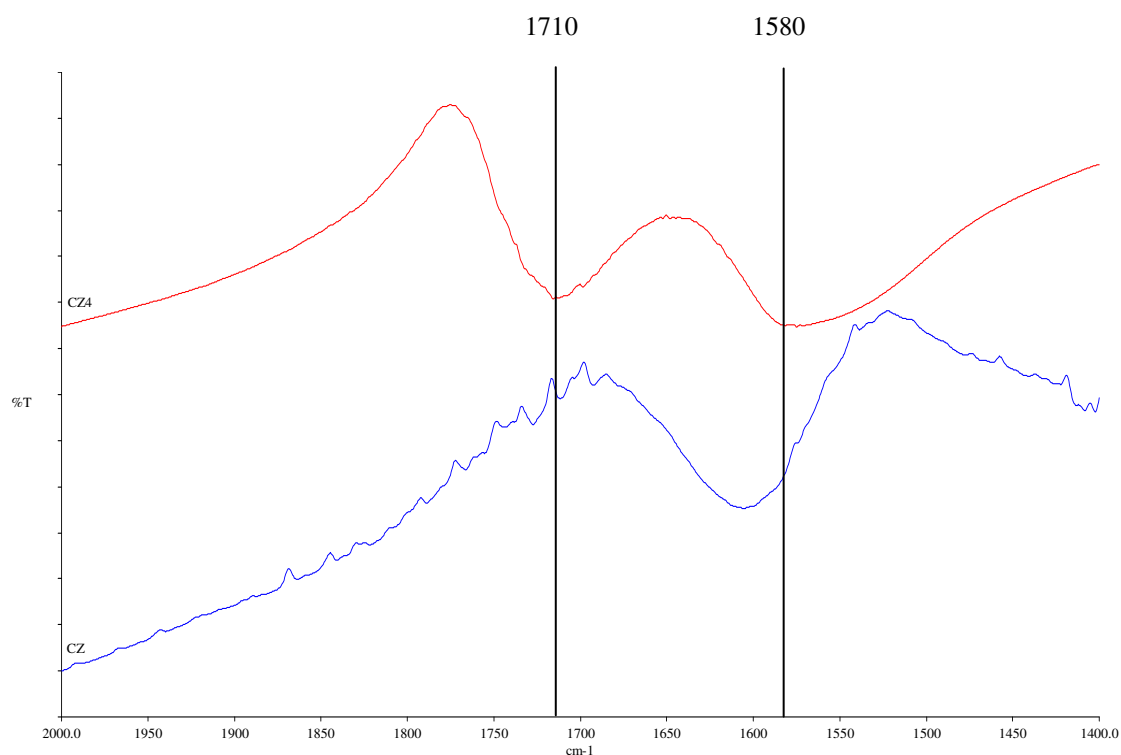


Figure 4.12 FT-IR spectra of the chemically activated carbon (sample CZ) and oxidized activated carbon (sample CZ4).

The changes in the FTIR spectra of oxidized activated carbon C4 after the heat treatment process are shown in Figure 4.13. It is apparent that the reduction of the band intensities in the 1580 cm^{-1} band with heat treatment at 700 and 900°C occurred and this suggests that considerable decomposition of phenolic and quinone groups had taken place. Heat treatment at 700 and 900°C resulted in loss of the band around 1710 cm^{-1} , due to the expected thermal decarboxylation of the carboxylic acid group (Figueiredo, Pereira, Freitas, and Órfão, 1999).

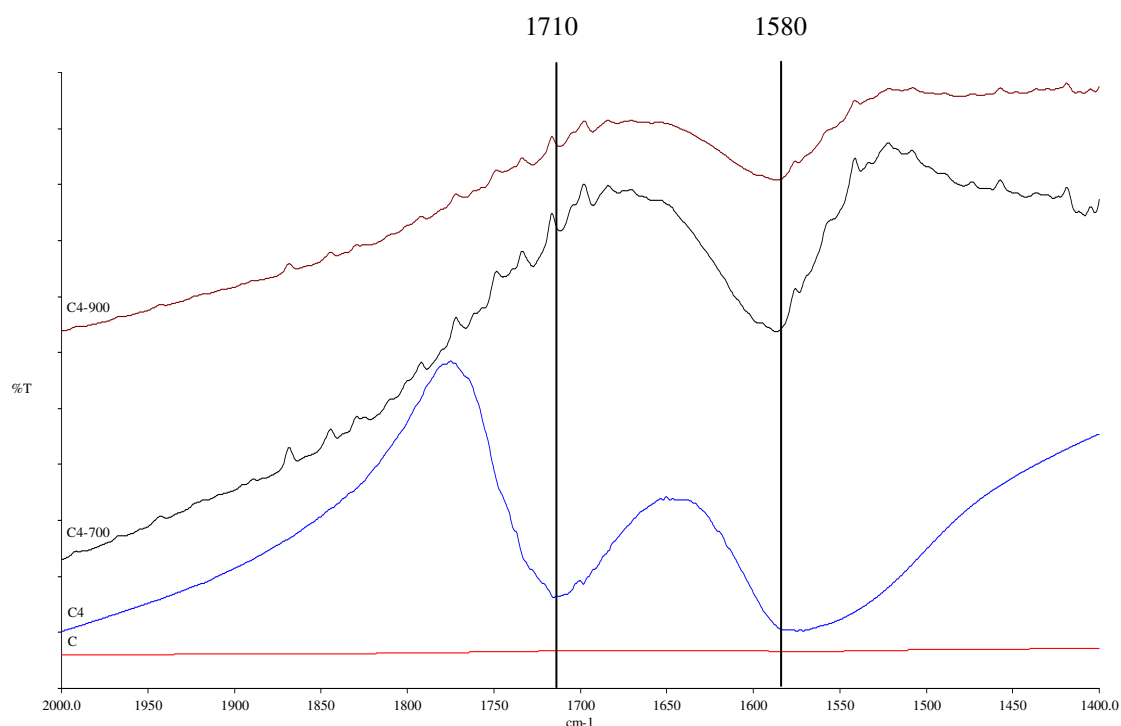


Figure 4.13 FT-IR spectra of the physically activated carbon (sample C), oxidized activated carbon (sample C4) and heat treatment activated carbons (sample C4-700 and C4-900).

4.5.2 Adsorption studies

4.5.2.1 Equilibrium adsorption time

The adsorption kinetic of dye solution by the original samples and oxidized carbon (C, CZ, C4) was studied and the results are shown plotted in Figure 4.14. A difference in percent adsorption between these samples was noticed but their adsorption characteristics followed a common trend. That is the dye adsorption process increased with time and attained equilibrium within about 72

hours. This equilibrium time of 72 hour was then used for the adsorption studies throughout this investigation.

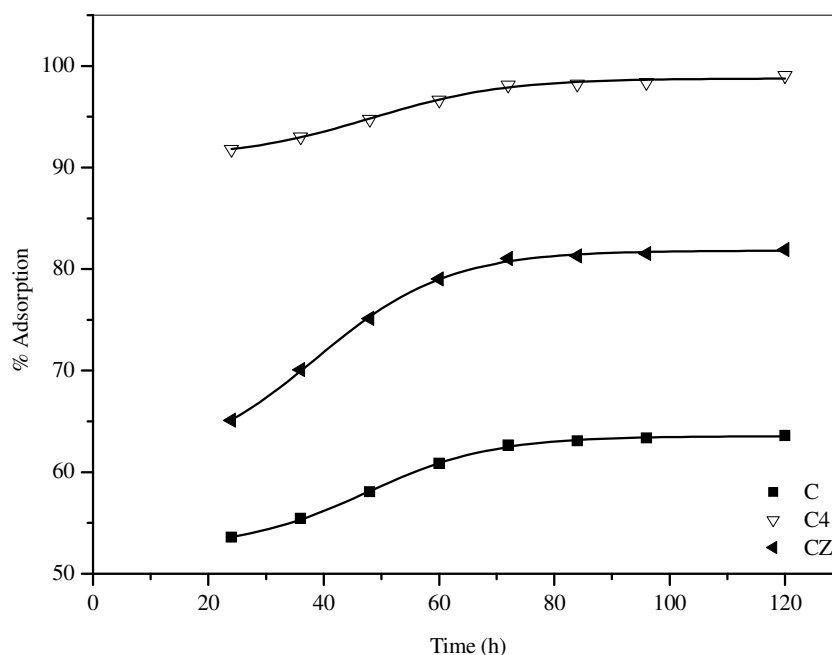


Figure 4.14 Effect of the contact time on the adsorption of dye effluent on unoxidized physically activated carbon (sample C), oxidized activated carbon (sample C4) and unoxidized chemically activated carbon (sample CZ).

4.5.2.2 Effect of pH

The effect of solution pH on the adsorption of dye solution by carbon sample C4 is illustrated in Figure 4.15. The amount of dye uptake first increased sharply with increasing pH followed by a slower increase before attaining a plateau for pH values in the range 3.5-4.5. It was found experimentally that dye adsorption was not possible at a pH greater than about 5 since the precipitation of Al(OH)_3 started to occur in the system. The low adsorption of cationic dye molecules

at low solution pH results from the lower number of negatively charged active sites of proton-donating functional groups on the carbon surface at this low pH. Similar reasoning can be applied to explain the increased amount of dye adsorbed as the pH is increased, that is, increasing electrostatic attraction between the more negatively charged surface of the carbon and the cationic dye. From these results, the pH of 4 was considered to be suitable for maximum adsorption of cationic dye in this study. Since the pH range of dye solution after silk dyeing is 3.8-4.0, the dye solution was used throughout the adsorption experiment in this work without adjusting the pH.

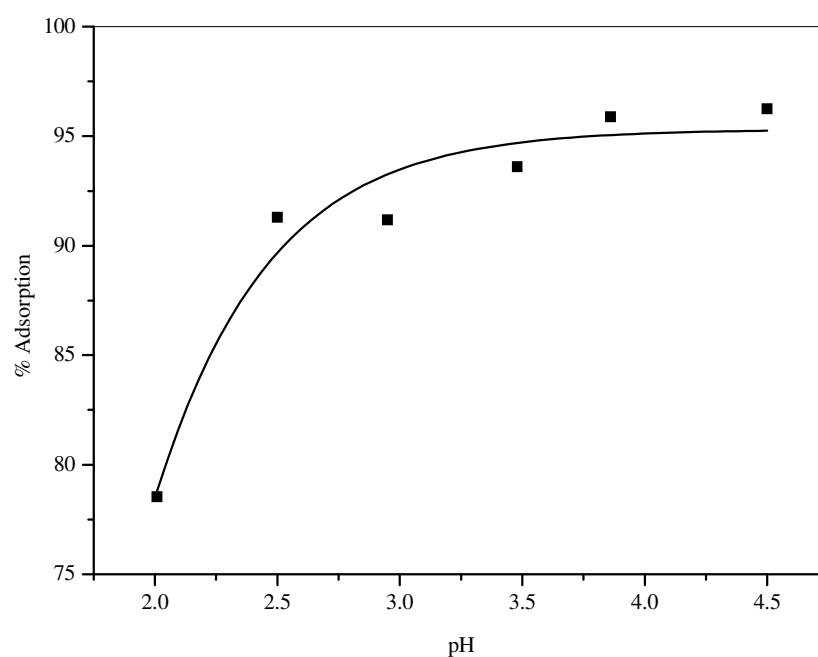


Figure 4.15 Effect of pH on the adsorption of dye effluent on oxidized activated carbon (sample C4).

4.5.2.3 Effect of adsorbent dosage

Figure 4.16 shows the effect of adsorbent dosage (sample C4) on the percent adsorption of the dye uptake. Increasing the adsorbent dosage at fixed dye concentration provided more available adsorption sites for the dye and thus increased the percent adsorption. While the adsorbent dosage increased from 0.05 to 0.2 gram, the percent adsorption increased rapidly from 45% to 98%. The very high increase of percent adsorption (almost 100%) indicated the very high adsorption capacity of the oxidized carbon (sample C4) in this study. The stable value for percent adsorption in the higher dosage (> 0.2) suggests that all dye species in the solution have been used up and no dye species were available for further adsorption.

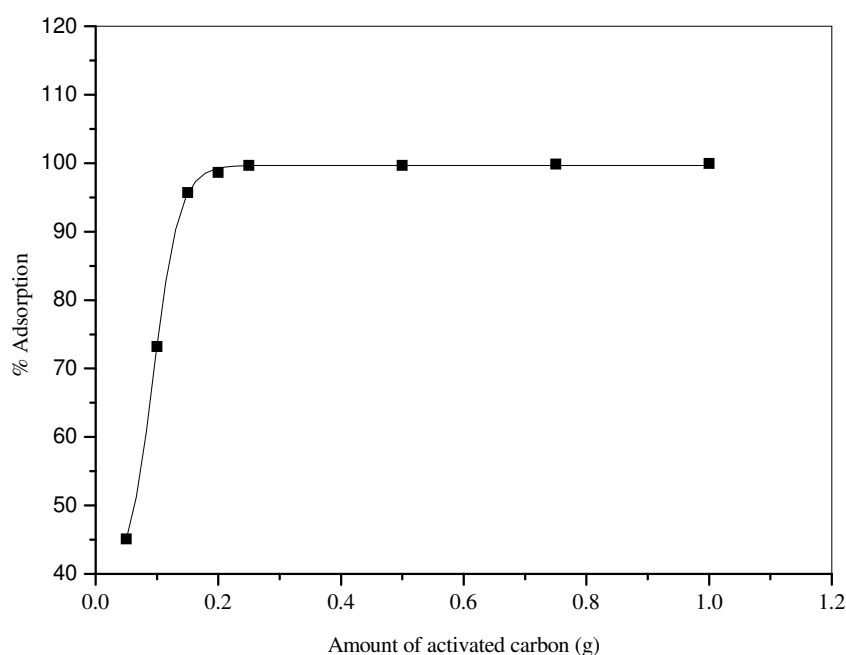


Figure 4.16 Effect of amount of activated carbon on the adsorption of dye effluent on oxidized activated carbon (sample C4).

4.5.2.4 Dependence of adsorption capacity of cationic dye on different surface characteristics of activated carbon

Figure 4.17 shows adsorption isotherms of dye on C, C1, C2, and C4 samples. The different adsorption capacities of these adsorbent samples were clearly seen. The adsorption capacity was increased in the following order: $C < C1 < C2 < C4$. Although the unoxidized carbon (sample C) has the highest surface area, it contains mainly micropores that are not fully accessible to the large dye-Al(III) complex and thus sample C had low adsorption capacity. This indicates that a suitable porous structure of carbon is important in the adsorption of dye in this study. It is apparent from the figure that the adsorption capacities of dye were greatly enhanced after the original carbon was oxidized with HNO_3 . The increasing adsorption capacity follows the same order of increasing acidic group content that is, $C4 > C2 > C1$. The higher amount of acid functional groups which provide more negative sites may be the main reason for the higher adsorption capacity by enhancing the electrostatic interactions. Therefore the surface functional groups play an important role in the adsorption of dye by these carbons.

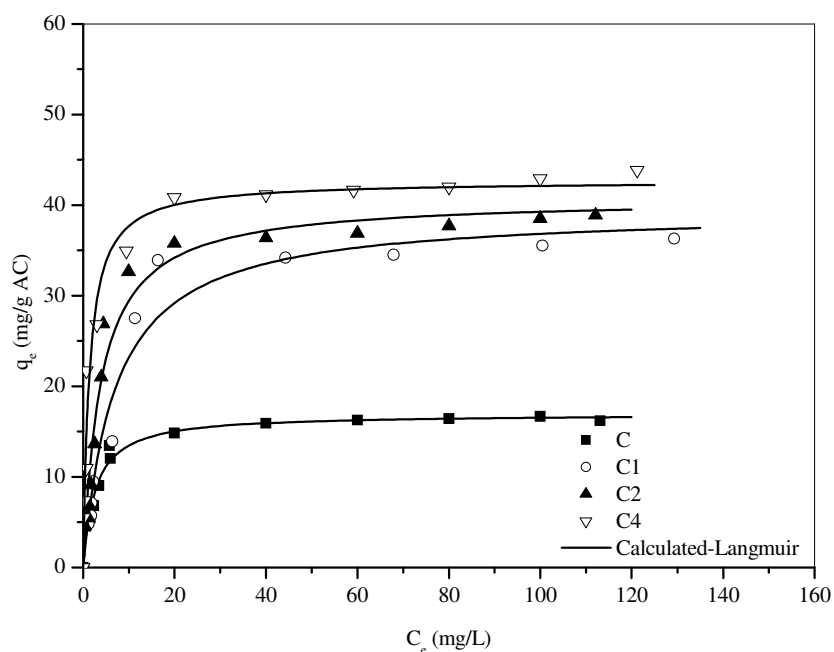


Figure 4.17 Adsorption isotherms at 30°C of dye effluent on physically activated carbon (sample C) and their oxidized activated carbons (sample C1, C2, and C4).

After the sample C4 was subjected to decomposition of surface oxygen functional groups by heat treatment at two elevated temperatures (samples C4-700 and C4-900), the adsorption capacity of dye on the carbon was reduced significantly (see Figure 4.18). The result from Boehm titration indicated that the heat treated carbon contains less acidic functional groups on the carbon. Since the carboxylic acid functional group is the most sensitive to the heat treatment (Puente, Pis, Menéndez, and Grange, 1997), its amount was more reduced by the thermal action than the other functional groups (83% reduction for C4-700 and 89% reduction for C4-900). Therefore, the lower amount of dye uptake was due primarily to the lower amount of

carboxylic acid group functionality. When compared to the unoxidized sample C, these two heat-treated carbons showed higher dye adsorption although they contain comparatively lower amounts of surface functional groups. It is possible that these two carbons may have a textural structure of the surface with more reactive sites for dye adsorption. This surface character could result from the effect of high heat treatment under an inert atmosphere.

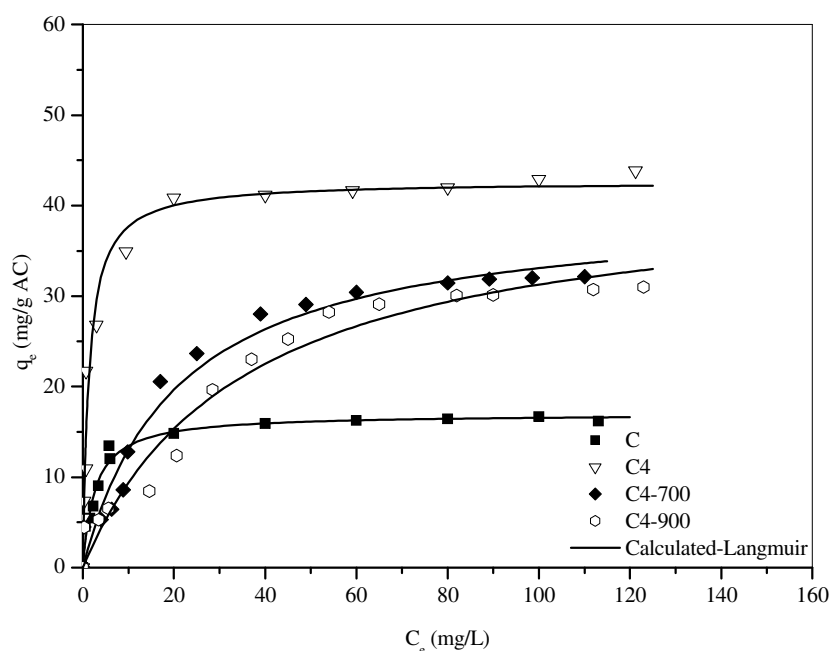


Figure 4.18 Adsorption isotherms at 30°C of dye effluent on physically activated carbon (sample C), oxidized activated carbon (sample C4) and heat treatment activated carbons (sample C4-700 and C4-900).

Figure 4.19 illustrates the similarity in adsorption behavior between the heat-treated sample (samples C4-700, C4-900) and the chemically activated carbon (CZ sample). The adsorption isotherms of dye on sample C4 are also compared in this

Figure. This comparison is to demonstrate that the adsorption of dye depends on both porous structure and surface functional groups, but to different degrees. As compared to sample C4, the amount of dye uptake with the CZ sample as well as with C4-900 was initially lower and slowly increased as the equilibrium concentration was further increased until at 100 mg/L the uptake approached that for the C4 oxidized sample. This evidence indicated that the dye occurred by physical adsorption on the CZ carbon, C4-700, and C4-900, whereas an electrostatic interaction is involved on the C4 carbon when the surface functional groups are available. After the CZ was oxidized under the same conditions as for sample C, this oxidized carbon (sample CZ4) showed a more rapid dye adsorption (see Figure 4.20). This was probably due to the extra binding through oxygen functional groups being added to the physical adsorption.

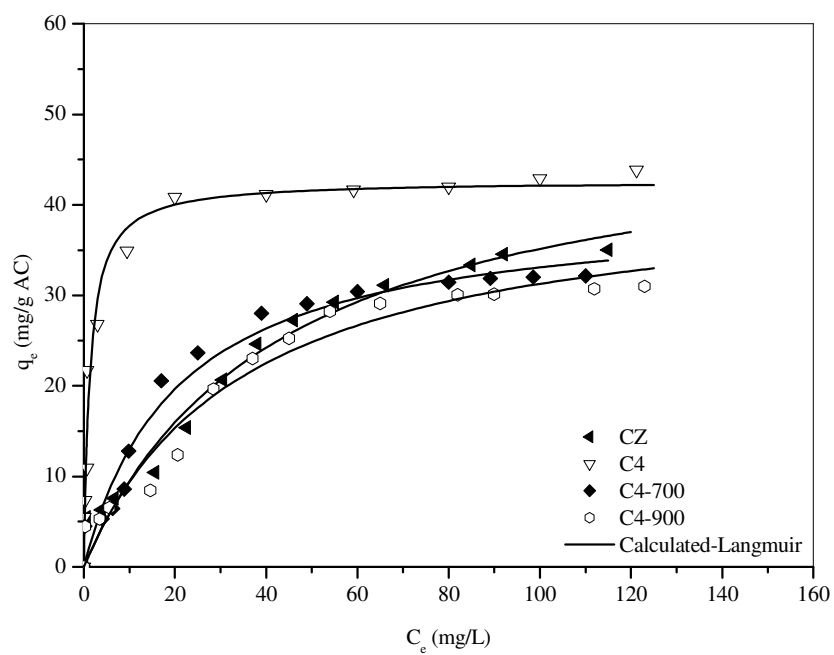


Figure 4.19 Adsorption isotherms at 30°C of dye effluent on unoxidized chemically activated carbon (sample CZ), oxidized physically activated carbon (sample C4) and heat treated activated carbons (sample C4-700 and C4-900).

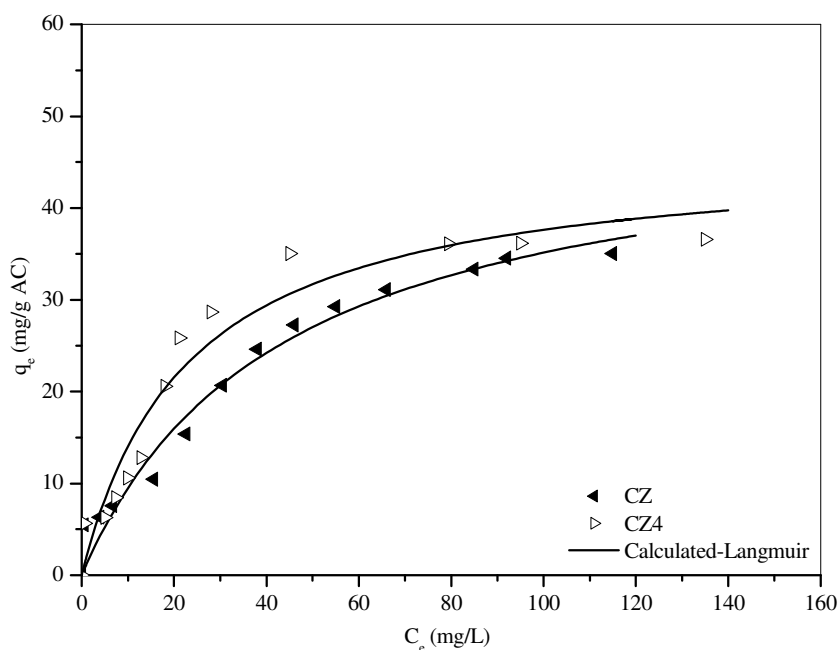


Figure 4.20 Adsorption isotherms at 30°C of dye effluent on chemically activated carbon (sample CZ) and oxidized activated carbon (sample CZ4).

4.5.2.5 Adsorption of dye on mesoporous activated carbon

As there was a low uptake of dye on sample C, which was mainly microporous, the adsorption of dye on mesoporous activated carbon was then investigated. It was expected that the wider pores should allow greater accessibility of adsorptive molecules and thus give a higher adsorption capacity. Since the coconut shell material produced activated carbon with mainly micropores but the Eucalyptus wood prepared in our laboratory produced activated carbon with a wider range of pores covering micropores and a higher proportion of mesopores, the latter was chosen to run the adsorption tests for comparison purposes. Two samples of activated carbon from wood with different surface area and porosity were obtained from

chemical activation using H_3PO_4 . Sample W1 had a surface area of $1200 \text{ m}^2/\text{g}$ with pore volumes of 94.8% microporosity and 5.2% mesoporosity (total pore volume of $0.58 \text{ cm}^3/\text{g}$), whereas sample W2 had a surface area of $1688 \text{ m}^2/\text{g}$ with 49.6% microporosity and 50.4% mesoporosity (total pore volume of $1.23 \text{ cm}^3/\text{g}$). As expected, the highest dye uptake was observed with sample W2 as compared to sample W1 (Figure 4.21) and oxidized carbon (sample C4). This dye uptake by sample W2 was the highest noted for any carbon sample in this study. The higher dye uptake is primarily due to the role of physical adsorption. The dye adsorption of this carbon is determined by π - π dispersion interactions between the π electrons of the activated carbon surface and the π electrons in the aromatic rings of the dye complex (physical adsorption). In addition, this mesoporous activated carbon contains some surface functional groups created from the chemical activation process which could augment the adsorption of this cationic dye.

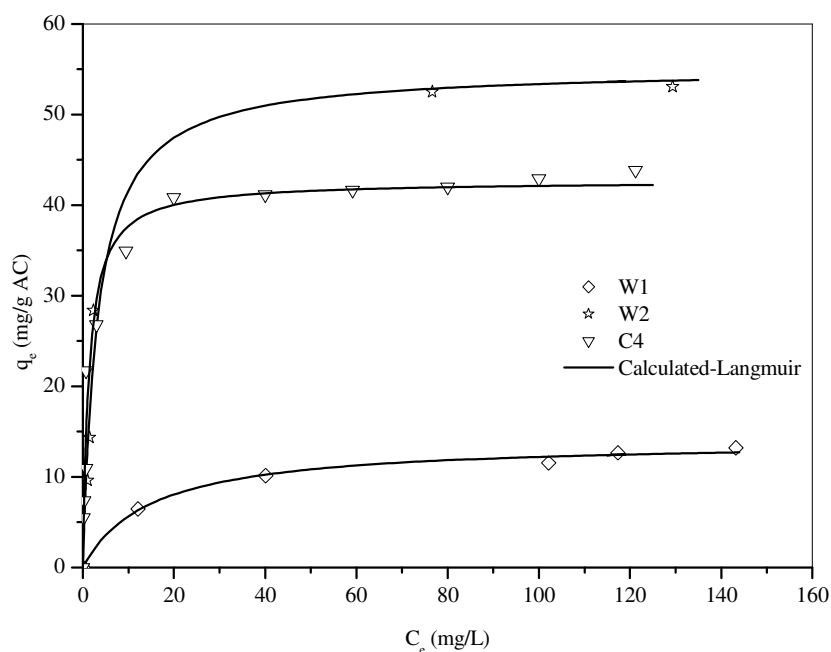


Figure 4.21 Adsorption isotherms at 30°C of dye effluent on chemically activated carbons prepared from wood (sample W1 micropore and W2 mesopore) and oxidized activated carbon (sample C4).

4.6 Conclusion

The adsorption of dye effluent from *C. sappan* wood using activated carbons was investigated as a function of surface chemical properties in terms of the content and type of surface functional groups, and surface texture with respect to surface area and porosity. Modifications of the surface chemistry of activated carbon were performed by oxidation with HNO_3 and heat treatment and these activated carbons were used to study the effect of surface chemistry on dye removal. The activated carbons prepared by different activation methods and different precursors were tested to study the effect of porous texture on dye removal.

Oxidation treatment to introduce oxygen functional groups onto the surface of coconut shell-based activated carbon led to a large increase of acidic group content but a small decrease in the content of basic sites. Carboxylic acid showed the largest content as compared with the other two acidic groups (lactonic and phenolic groups). The heat treatment reduced most of the acidic groups, in particularly the most thermally sensitive carboxylic acid group, whereas the basic sites showed a small increase. These results were consistent with other previous reported results. The lower content of acidic oxygen functional groups in the oxidized chemically activated carbon as compared with the oxidized physically activated carbon, indicated that the preparation method had a direct effect on the amount of oxygen functional groups.

The different adsorption characteristics of dye uptake were clearly seen both in the activated carbons with different surface chemistry and porous texture. The higher amounts of surface oxygen functional groups significantly enhanced the dye uptake. The important finding from this work is the demonstration that for the physically activated carbon prepared from coconut shell, which contains mainly micropores, the modification by oxidation treatment to increase the oxygen functional groups led to a greater adsorption capacity for the dye uptake. This is due to the enhancement in hydrophilicity in the oxidized activated carbon which lead to an increase in electrostatic interactions between the negatively charged activated carbon and the positively charged dye-complex molecules in this study. On the other hand, for the chemically activated carbon prepared from coconut shell, which contains a higher mesopore volume than the physically activated carbon, the oxidation treatment gave a lower increase in surface functional groups. Hence, the physical adsorption via π - π dispersion is the main interaction for dye uptake in these carbons. The

mesoporous chemically activated carbon prepared from Eucalyptus wood exhibited the highest dye uptake via predominantly π - π dispersion interaction and electrostatic interaction due to its high proportion of mesoporosity and additional surface oxygen functional groups.

In conclusion, the efficient removal of the relatively large dye molecular species from solution by adsorption depends strongly on the initial porous nature of the adsorbent. Microporous adsorbents, such as physically activated carbon prepared from coconut shell in this study, required a surface oxidation treatment to utilize the role of introduced oxygen functional groups in adsorption, but highly developed mesoporous activated carbon prepared from Eucalyptus wood can be directly applied without surface treatment.

4.7 References

- Ania, C. O., Parra, J. B., and Pis, J. J. (2002). Influence of oxygen-containing functional groups on active carbon adsorption of selected organic compounds. **Fuel Processing Technology** 79: 265-271.
- Attia, A. A., Rashwan, W. E., and Khedr, S. A. (2006). Capacity of activated carbon in the removal of acid dyes subsequent to its thermal treatment. **Dyes Pigments** 69: 128-136.
- Bandosz, T. J., Jagiello, J., and Schwarz, J. A. (1996). Effect of surface chemistry on sorption of water and methanol on activated carbons. **Langmuir** 12: 6480-6486.

- Biniak, S., Pakula, M., Szymański, G.S., and Świątkowski, A. (1999). Effect of activated carbon surface oxygen-and/or nitrogen-containing groups on adsorption of copper (II) ions from aqueous solution. **Langmuir** 15: 6117-6122.
- Carrasco-Marin, F., Mueden, A., Centeno, T. A., Stoeckli, F., and Moreno-Castilla, C. (1997). Water adsorption on activated carbons with different degrees of oxidation. **Journal of the Chemical Society, Faraday Transactions** 93: 2211-2215.
- Chen, J. P. and Wu, S. (2004). Acid/base-treated activated carbons: characterization of functional groups and metal adsorptive properties. **Langmuir** 20: 2233-2242.
- Chen, J. P., Wu, S., and Chong, K.-H. (2003). Surface modification of a granular activated carbon by citric acid for enhancement of copper adsorption. **Carbon** 41: 1979-1986.
- Chingombe, P., Saha, B., and Wakeman, R. J. (2005). Surface modification and characterization of a coal-based activated carbon. **Carbon** 43: 3132-3143.
- Choma, J., Burakiewicz-Mortka, W., Jaroniec, M., Li, Z., and Klinik, J. (1999). Monitoring changes in surface and structural properties of porous carbons modified by different oxidizing agents. **Journal of Colloid and Interface Science** 214: 438-446.
- Denisov, E. T. and Afanas'ev, I. B. (2005). **Oxidation and Antioxidations in Organic Chemistry and Biology**. CRC Press.
- Do, D. D. (1998). **Adsorption analysis: Equilibria and Kinetics**. Singapore: Imperial College Press.

- Domingo-García, M., López-Garzón, F. J., and Pérez-Mendoza, M. (2000). Effect of some oxidation treatments on the textural characteristics and surface chemical nature of an activated carbon. **Journal of Colloid and Interface Science** 222: 233-240.
- El-Hendawy, A. N. A. (2003). Influence of HNO₃ oxidation on the structure and adsorptive properties of corncob-based activated carbon. **Carbon** 41: 713-722.
- Faria, P. C. C., Orfao, J. J. M., and Pereira, M. F. R. (2004). Adsorption of anionic and cationic dyes on activated carbons with different surface chemistries. **Water Research** 38: 2043-2052.
- Figueiredo, J. A., Pereira, M. F. R., Freitas, M. M. A., and Órfão, J. J. M. (1999). Modification of the surface chemistry of activated carbons. **Carbon** 37: 1379-1389.
- Franz, M., Arafat, H.A., and Pinto, N.G. (2000). Effect of chemical surface heterogeneity on the adsorption mechanism of dissolved aromatics on activated carbon. **Carbon** 38: 1807-1819.
- Goyal, M., Rattan, V. K., Aggarwal, D., and Bansal, R. C. (2001). Removal of copper from aqueous solutions by adsorption on activated carbons. **Colloids and Surfaces A: Physicochemical and Engineering Aspects** 190: 229-238.
- Haydar, S., Ferro-Garcia, M. A., Rivera-Utrilla, J., and Joly, J. P. (2003). Adsorption of *p*-nitrophenol on an activated carbon with different oxidations. **Carbon** 41: 387-395.
- Jaramillo, J., Gómez-Serrano, V., and Álvarez, P. M. (2008). Enhanced adsorption of metal ions onto functionalized granular activated carbons prepared from cherry stones. **Journal of Hazardous Materials, In Press, Corrected Proof.**

- Jia, Y. F. and Thomas, K. M. (2000). Adsorption of cadmium ions on oxygen surface sites in activated carbon. **Langmuir** 16: 1114-1122.
- Lebedev, N. N. (1984). **Chemistry and Technology of Basic Organic and Petrochemical Synthesis**. Moscow: MIR Publishers.
- Lemmens, R. H. M. J. and Wulijarni-Soetjipto, N. (1992). **Plant resources of South-East Asia³: Dye and tannin-producing plants**. Prosea, Bogor Indonesia, p. 60-62.
- Moeyse, M. (1993). **Natural dyeing in Thailand**. Bangkok: White Lotus.
- Monser, L. and Adhoum, N. (2002). Modified activated carbon for the removal of copper, zinc, chromium and cyanide from wastewater. **Separation and Purification Technology** 26: 137-146.
- Moreno-Castilla, C., Ferro-García, M. A., Joly, J. P., Bautista-Toledo, I., Carrasco-Marín, F., and Rivera-Utrilla, J. (1995). Activated carbon surface modifications by nitric acid, hydrogen peroxide, and ammonium peroxydisulfate treatments. **Langmuir** 11: 4386-4392.
- Moreno-Castilla, C., Carrasco-Marín, F., and Mueden, A. (1997). The creation of acid carbon surface by treatment with $(\text{NH}_4)_2\text{S}_2\text{O}_8$. **Carbon** 35: 1619-1626.
- Moreno-Castilla, C., López-Ramón, M. V., and Carrasco-Marín, F. (2000). Changes in surface chemistry of activated carbons by wet oxidation. **Carbon** 38: 1995-2001.
- Nevskaia, D. M., Castillejos-Lopez, E., Guerrero-Ruiz, A., and Muñoz, V. (2004). Effects of the surface chemistry of carbon materials on the adsorption of phenol-aniline mixtures from water. **Carbon** 42: 653-665.

- Órfão, J. J. M., Silva, A. I., M., Pereira, J. C. V., Barata, S. A., Fonseca, I. M., Faria, P. C. C., and Pereira, M. F. R. (2006). Adsorption of a reactive dye on chemically modified activated carbons-influence of pH. **Journal of Colloid and Interface Science** 296: 480-489.
- Park, G. I., Lee, J. K., Ryu, S. K., and Kim, J. H. (2002). Effect of two-step surface modification of activated carbon on the adsorption characteristics of metal ions in wastewater I. Equilibrium and batch adsorptions. **Carbon Science** 3: 219-225.
- Pereira, M. F. R., Soares, S. F., Órfão, J. J. M., and Figueiredo, J. L. (2003). Adsorption of dyes on activated carbons: influence of surface chemical groups. **Carbon** 41: 811-821.
- Pradhan, B. K. and Sandle, N. K. (1999). Effect of different oxidizing agent treatments on the surface properties of activated carbons. **Carbon** 37: 1323-1332.
- Puente, G. de la, Pis, J. J., Menéndez, J. A., and Grange, P. (1997). Thermal stability of oxygenated functions in activated carbons. **Journal of Analytical and Applied Pyrolysis** 43: 125-138.
- Radovic, L. R., Silva, I. F., Ume, J. I., Menéndez, J. A., Leon, Y., Leon, C. A., and Scaroni, A. W. (1997). An experimental and theoretical study of the adsorption of aromatics possessing electron-withdrawing and electron-donating functional groups by chemically modified activated carbons. **Carbon** 35: 1339-1348.

- Rios, R. R. V. A., Alves, D. E., Dalmázio, I., Fernando, S., Bento, V., Donnici, C. L., and Lago, R. M. (2003). Tailoring activated carbon by surface chemical modification with O, S, and N containing molecules. **Materials Research** 6(2): 129-135.
- Rivera-Utrilla, J. and Sánchez-Polo, M. (2003). Adsorption of Cr(III) on ozonised activated carbon: importance of C π -cation interactions. **Water Research** 37: 3335-3340.
- Salame, I. I., Bagreev, A., and Bandosz, T. J. (1999). Revisiting the effect of surface chemistry on adsorption of water on activated carbons. **Journal of Physical Chemistry B** 103: 3877-3884.
- Salame, I. I. and Bandosz, T. J. (1999). Study of water adsorption on activated carbons with different degrees of surface oxidation. **Journal of Colloid and Interface Science** 210: 367-374.
- Santiago, M. S., Stüber, F., Fortuny, A., Fabregat, A., and Font, J. (2005). Modified activated carbons for catalytic wet air oxidation of phenol. **Carbon** 43: 2134-2145.
- Shim, J. W., Park, S. J., and Ryu, S. K. (2001). Effect of modification with HNO₃ and NaOH on metal adsorption by pitch-based activated carbon fibers. **Carbon** 39: 1635-1642.
- Smith, M. B. and March, J. (2007). **March's Advanced Organic Chemistry: Reactions, Mechanisms, and Structure**. John Wiley & Sons, Inc.
- Soundping, C. (2002). **Surface modification of activated carbon by oxidation reaction for adsorption capacity study of aniline, dyes and chromium(III) ion**. M. thesis, King Mongkut's University of Technology Thonburi, Thailand.

- Stavropoulos, G. G., Samaras, P., and Sakellaropoulos, G. P. (2008). Effect of activated carbons modification on porosity, surface structure and phenol adsorption. **Journal of Hazardous Materials** 151: 414-421.
- Tamon, H. and Okazaki, M. (1996). Influence of acidic surface oxides of activated carbon on gas adsorption characteristics. **Carbon** 34: 741-746.
- Tao, X. and Xiaoqin, L. (2008). Peanut shell activated carbon: characterization, surface modification and adsorption of Pb^{2+} from aqueous solution. **Chinese Journal of Chemical Engineering** 16(3): 401-406.
- Wang, S., Zhu, Z. H., Coomes, A., Haghseresht, F., and Lu, G. Q. (2005). The physical and surface chemical characteristics of activated carbons and the adsorption of methylene blue from wastewater. **Journal of Colloid and Interface Science** 284: 440-446.
- Wibowo, N., Setyadhi, L., Wibowo, D., Setiawan, J., and Ismadji, S. (2007). Adsorption of benzene and toluene from aqueous solutions onto activated carbon and its acid and heat treated forms: Influence of surface chemistry on adsorption. **Journal of Hazardous Materials** 146: 237-242.
- Wongsooksin, K., Rattanaphani, S., Tangsathitkulchai, M., Rattanaphani, V., and Bremner, J. (2008). Study of an Al(III) complex with the plant dye brazilin from *Ceasalpinia sappan* Linn. **Suranaree Journal of Science and Technology** 15(2): 159-165.
- Xiao, B. (2004). **Characterisation of functionalised nanoporous carbon materials & adsorption of aqueous metal ions**. Ph.D. thesis, University of Newcastle upon Tyne, United Kingdom.

- Xiao, B. and Thomas, K. M. (2005). Adsorption of aqueous metal ions on oxygen and nitrogen functionalized nanoporous activated carbons. **Langmuir** 21: 3892-3902.
- Yan, X., Wang, W., Xing, D., Zhao, Y., and Du, L. (2005). Development and optimization of a method for the analysis of brazilein by HPLC with electrochemical detection. **Journal of Chromatography A** 1077: 44-48.

CHAPTER V

CONCLUSION

The primary purpose of this study was to overcome the poor fastness properties of silk dyed using extracted dye from *C. sappan*. In this task, the interaction of brazilein (BE) as well as extracted dye with some metal ions and an amino acid derivative were investigated. The study of kinetics and thermodynamics of dye adsorption onto silk were performed. The study to remove the residual dye left after the silk dyeing process was also carried out. To achieve the highest dye removal capacity, the activated carbons were prepared and modified to have different porous texture and surface chemistry and then used for dye removal by adsorption. The following conclusions can be drawn.

From the molar ratio and Job's methods, it was found that the interaction of brazilein with Al(III) ion in aqueous solution gave a 1:2 complex i.e., $[\text{Al}(\text{BE})_2]^+$. The 1:2 complex was verified by using electrospray ionization mass spectra. Similar 1:2 complexes were formed between brazilein with other related metal ions (Ga(III) and In(III)). In the interaction between brazilein with metal ions and an amino acid derivative, it was found that the complexes formed with 1:1:1 stoichiometry for $[\text{SerMBE}]^+$, $M = \text{Al(III)}, \text{Ga(III)}, \text{and In(III)}$. The negative heat of formation of these complexes calculated from computational modeling (semiempirical PM3) provided the possible stable structure. These proposed interaction structures indicated that serine in the silk protein could be involved in binding of the complex with the silk.

From the view point of using the lowest Al content and the highest amount of dye adsorption, simultaneous mordanting was found to be the most suitable method for dyeing of brazilin/brazilein dyes onto silk.

The important parameters influencing the dyeing process include pH of the dye solution, the material to liquor ratio (MLR), contact time, the initial dye concentration and temperature. The best conditions of these parameters found in this study were: pH = 4.0, MLR = 1:100, contact time 120 min and an initial dye concentration of 14 mg/L.

The adsorption kinetic study of dye onto silk revealed that before equilibrium, the rate of dye adsorption increased with the increase in temperature, indicating a kinetically controlled process. In addition, the pseudo second-order kinetic model with an activation energy (E_a) of 41.57 kJ/mol confirmed that the overall rate of dye adsorption onto silk was controlled by the chemical process.

The results from the dye equilibrium adsorption study indicated that the process is an exothermic one since the amount of dye adsorbed decreased with increasing temperature. The negative values of the thermodynamic parameters (ΔG° , ΔH°) confirmed the dye adsorption as being a spontaneous and an exothermic process. All experimental data fitted well to the Langmuir isotherms with a high correlation coefficient (R^2).

All the results from alum-extracted dye adsorption onto silk showed similar trends to those obtained from the alum-brazilein adsorption.

Activated carbon having different porous texture was successfully prepared using a number of activation methods and precursors. The chemical activation method produced coconut shell based-activated carbon with higher mesopore volumes than

the physically activated carbon. For the wood precursor, the chemical weight ratio of H_3PO_4 and wood determined the proportion of mesoporosity in the activated carbon.

Modification of surface chemical properties of activated carbon was achieved either by introducing oxygen functional groups by HNO_3 -oxidation treatment or by removing oxygen functional groups by thermal treatment. The oxidation treatment led to a significant increase of acidic group content with carboxylic acid groups having the largest content. The carboxylic acid groups were found to be the most thermally-sensitive functional groups as compared to other acidic groups (lactonic and phenolic groups).

Different adsorption characteristics of dye uptake were clearly seen in the activated carbons with different porous structure and surface chemistry. The activated carbon with the higher content of surface functional groups significantly enhanced the dye uptake by electrostatic interaction between the negatively charged surface of the activated carbon and the positively charged dye. On the other hand, the activated carbon with higher mesopore volume was found to enhance the dye uptake by π - π dispersion interaction between the π electrons of the activated carbon and the π electrons in the aromatic ring of the dye molecule.

With coconut shell-based activated carbon, removal of dye from relatively high concentrations of dye solution should be performed first with chemically activated carbon containing a high proportion of mesoporosity to take advantage of its large pore volume structure. The remaining solution may then be treated further with surface-modified microporous carbon which is effective in removing dye in the low range concentration.

To achieve high efficiency of cationic dye removal using microporous coconut shell based-activated carbon prepared by the physical activation method, modification by oxidation treatment to increase the oxygen functional group density is necessary. On the other hand, the wood based-chemically activated carbon which has a high degree of mesoporosity, can be directly used for large dye removal without surface treatment and should provide a viable means for brazilein dye waste water treatment.

CURRICULUM VITAE

KAMONCHANOK WONGSOOKSIN

E-mail: wongsooksin@hotmail.com

Born: 3 March, 1972 in Nakhon Ratchasima, Thailand

Citizenship: Thailand

Nationality: Thai

Education:

1990-1994 B.Sc. (Chemistry), Ubon Teachers College, Ubonrajthani, Thailand

1994-1997 M.Sc. (Chemistry), Khon Kaen University, Khon Kaen, Thailand

Experiences:

1997-present Lecturer, Nakhon Ratchasima Rajabhat University,
Nakhon Ratchasima, Thailand

2006 Ph.D. research at University of Wollongong, Australia

Publications:

Wongsooksin, K., Rattanaphani, S., Tangsathitkulchai, M., Rattanaphani, V., and
Bremner, J. (2008). Study of an Al(III) complex with the plant dye brazilein
from *Ceasalpinia sappan* Linn. **Suranaree Journal of Science and
Technology** 15(2): 159-165.